THE DIELECTRIC PROPERTIES AND CONDUCTIVITY OF GLASSES IN THE As - S AND As - Se SYSTEMS

BY

RICHARD BRIAN SOUTH

A thesis submitted for the degree of Doctor of Philosophy.

University of Edinburgh.

January, 1974.

This thesis has been composed by myself.

Apart from preparation and chemical analysis of the materials, the work is my own. Discussions with my supervisor, Dr. A.E. Owen, have helped to form some of the conclusions. Where appropriate, reference to other investigators' results or techniques has been acknowledged.

Acknowledgements.

I am very much indebted to Dr. A.E. Owen for his guidance and encouragement throughout the course of this work.

I would like to thank my colleagues in the department of Electrical Engineering for many stimulating discussions, and assistance: in particular Dr. C. Main, Dr. J.M. Marshall and Dr. J.M. Robertson.

This work could not have been so extensive without the assistance of the Technical staff of the department, particularly that of Mr. D. Reynolds for the glass preparation and chemical analyses.

Finally, I am grateful to my mother for typing the text and my wife for her constant encouragement and assistance with the diagrams.

CONTENTS

List of commonly used symbols

A	constant; area
a	radius of localised wave function
C	capacitance; constant
c	velocity of light in vacuo
D	diffusion coefficient
E	activation energy; electric field
E_F	Fermi energy
e	electronic charge
f	frequency
$f(t)$	response function
$G(\tau)$	density of relaxation times
G	conductance
H	magnetic field
h	substrate thickness; Planck's constant
$\hbar$	$h/2\pi$
i	$\sqrt{-1}$
k	Boltzmann's constant
L	inductance
l	sample thickness
N	number of particles
$N(E_F)$	density of states at the Fermi energy
N_s	density of localised states
N_c	density of charge carriers
N_q	density of charged states
n	number of pairs of states; integer

P	power; polarisation
Q	Q factor
q	charge
R	resistance
r	distance
r_ω	most probable hopping distance
r_s	average separation of localised states
T	temperature
T_g	glass transformation temperature
t	time; conductor thickness
U	barrier height
W	energy
Z	impedance
α	optical absorption coefficient; attenuation; polarisability.
α_L	thermal expansion coefficient
γ	temperature coefficient of the activation energy; propagation constant
δ	skin depth; loss angle
ϵ_o	permittivity of free space
ϵ_r^*	complex relative permittivity
ϵ_r'	dielectric constant
ϵ_r''	dielectric loss
λ	wavelength
μ	mobility; dipole moment
μ_o	permeability of free space

ν_e electronic frequency

σ conductivity

τ relaxation time

τ_o reciprocal phonon frequency; constant

Φ potential

χ electric susceptibility

ω angular frequency

ω_o phonon frequency; constant

Summary

The dielectric properties in the frequency ranges 7.10^2 to 10^5Hz and 10^9 to $1{\cdot}2.10^{10}$Hz and the d.c. conductivities have been investigated for amorphous semiconductors of compositions close to stoichiometry in the As - S and As - Se systems.

In the audio frequency range the results are consistent with a thermally assisted electron hopping model showing an almost linear frequency dependence and weak temperature of the conductivity. As the compositions were changed the a.c. and d.c. conductivities of the As - S system showed a minimum close to the stoichiometric material, whereas the As - Se system proved to have a maximum at the corresponding composition. This is interpreted as providing evidence that the conduction mechanisms are fundamentally different: conduction in the As - S system is by hopping in the localised states and that in the As - Se system is by a trap limited process in the extended states.

A technique for making microwave dielectric measurements over a wide frequency range (1 to 12·5GHz) has been developed using the microstrip techniques of modern microwave technology. The technique has been proved useful for measurements of reasonable accuracy and was easily adaptable for a wide range of measurement temperatures (90 to 400 K).

Using this technique the conductivities of $As_2 S_3$ and $As_2 Se_3$ were measured and have been interpreted as showing the existence of a low frequency tail to the phonon absorption region.

CHAPTER 1

Introduction

1.1 Physical Properties.

Vitreous solids are those which have been cooled from the liquid phase sufficiently rapidly to prevent crystallisation. The contrast between vitreous and crystalline materials is mainly one of long range order. In both forms the symmetry of nearest neighbour atoms is similar: i.e. short range order is preserved. Glass is also an unstable thermodynamic state.

The terms "vitreous", "glassy" and "amorphous" in this work will be used synonomously, though there is a tendency to reserve "amorphous" for materials prepared by vacuum evaporation or some similar technique.

The degree of disorder can be determined by X-ray diffraction techniques. The results are converted into a radial distribution function which gives the probability of finding an atom at a particular distance from a given atom. Figure (1.1) illustrates the radial distribution function for bulk arsenic sulphide ($As_2 S_3$) after Hopkins et al[1]. At small distances the function is close to the corresponding crystalline form but the similarity extends only as far as two or three interatomic distances.

When a liquid is cooled to form a glass the

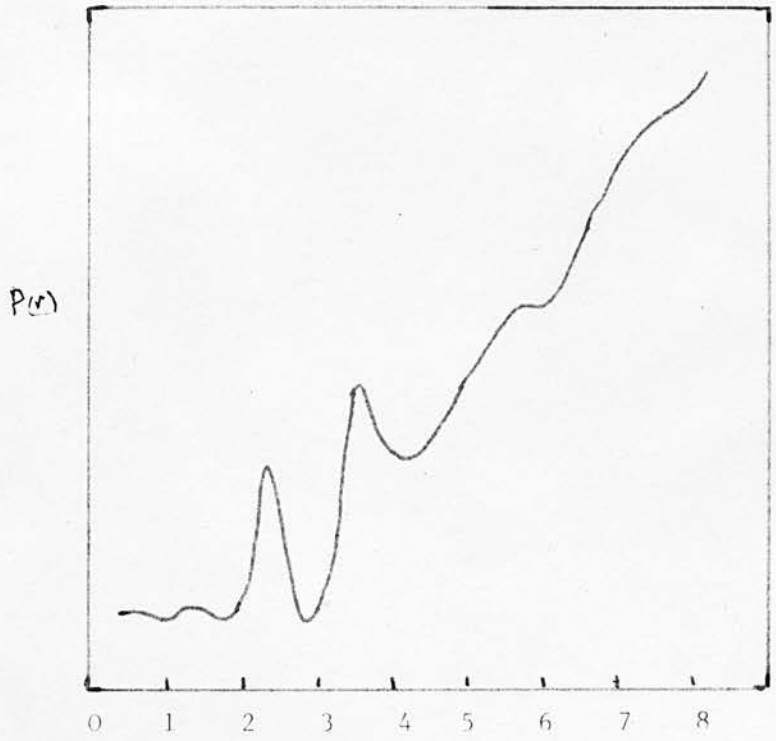

Figure (1.1)

Radial distribution curve for As_2S_3 after Hopkins et al [1]

material becomes rigid as the viscosity rises. The temperature at which this happens is called the glass transformation temperature, T_g. T_g is not well defined but depends on the rate of cooling; it is therefore not unique for a particular composition. However, information about the structure of a glass can be obtained from the variation of T_g with composition[2].

1.2 The Chalcogenide Glasses.

The Chalcogenide glasses are composed of one or more of the elements S, Se and Te, often compounded with other elements such as As, Si, Ge, P, Sb and Tl. Two of the most widely studied glasses are arsenic selenide ($As_2 Se_3$) and arsenic sulphide ($As_2 S_3$).

For a given group of elements there is a limited region of compositions which will form vitreous materials on cooling from the melt. Figure (1.2) shows the glass forming region of the As-S-Se system.

The basic unit of $As_2 S_3$ glass is (as in the crystalline form) a pyramid of $As S_{3/2}$. The linking is at the S atoms and the layer structure is partially broken to form rings or chains of differing sizes.[2]

Away from stoichiometry in the As-S system either S_n rings or chains exist (excess S) or $As_4 S_4$ units are formed (excess As).[3] The As-Se system is similar[2] but

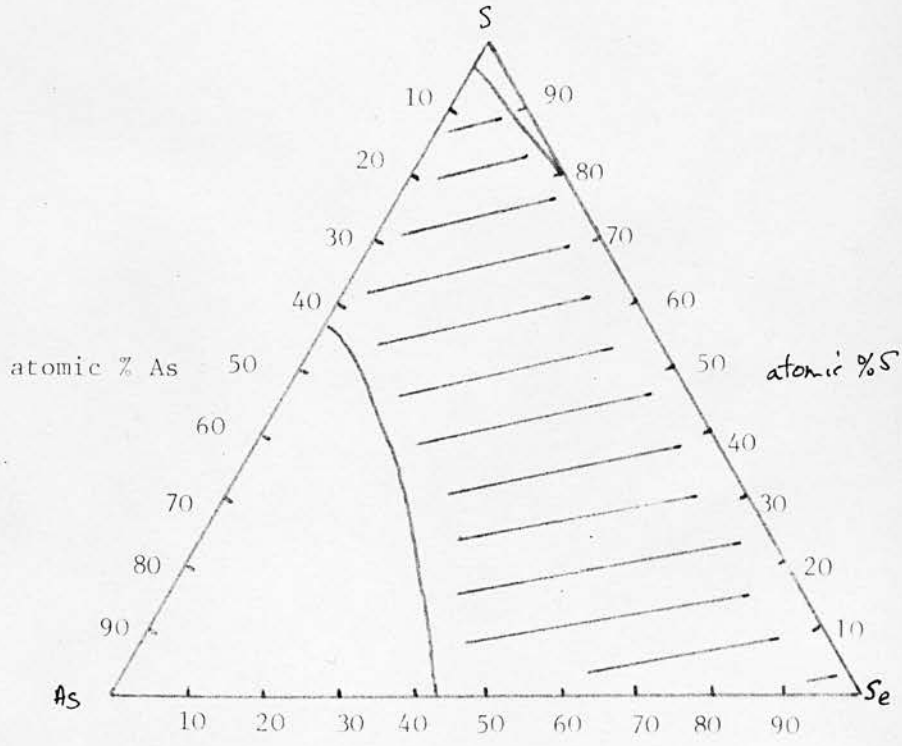

Figure (1.2)

Glass forming region of the As-S-Se system after Myers and Felty[2]

this does not necessarily imply similar electrical properties

1.3 Basic Electrical Properties.

The electrical conductivity of the chalcogenide glasses varies from about 10^{-16} ohm^{-1} cm^{-1} ($As_2 S_3$) to 10^{-3} ohm^{-1} cm^{-1} ($Tl_2 Se \cdot As_2 Te_3$).[4,5] This range is from the semi-insulating to the semiconducting.

Experimental evidence[4] has shown that the chalcogenide glasses are electronic conductors. The more "conventional" oxide based glasses are usually ionic conductors.[6]

The lack of long range order introduces large densities of traps in the energy gap between the valence and conduction bands. These traps affect the behaviour of the charge carriers in the solid and electrical measurements can be used to determine their density and distribution. Dielectric measurements are among these techniques.

In the electronic conducting glasses it is of interest to know whether the a.c. conduction is by a band or hopping process. Pollak[7] has derived the form of the conductivity for both processes. The frequency dependences are different and hence dielectric measurements can be used to eliminate one or both processes.

There may be other processes which have similar frequency dependences and are equally possible in an amorphous solid. It was hoped that measurements over large frequency and temperature ranges would distinguish between the possible mechanisms.

CHAPTER 2

Electrical Properties and Band Structure

2.1 Introduction.

In a perfect crystalline solid the allowed energies of the electrons form definite bands where the density of states function, N(E), is continuous and non-zero. The electrical characteristics of the solid are determined by the positions of the valence and conduction bands and their occupancy by electrons. The electrons occupy extended states in the allowed bands and if the band is neither empty nor completely full their motion becomes impeded only by some scattering process. Scattering results from the presence of impurities (taken here to include imperfections in the structure and phonons) and restricts the electrons to a finite mean free path.

An important effect of impurities is the creation of energy levels within the "forbidden" gap. Amorphous materials have a high degree of disorder and this results in the establishment of a large number of localised energy levels in the gap, affecting the electrical properties of the material. Most of the theoretical and experimental work on non-crystalline solids aims towards an understanding of the distribution and origin of these localised energy levels, whether the transition from localised to delocalised at the band edges is discontinuous or not,[8],[9] and their effect on the conductivity, mobility and optical and other properties.

2.2 Band Models,

The existence of an energy gap between the extended states of the valence and conduction bands is implied by the variation of d.c. conductivity with temperature and the existence of an optical absorption edge. Simple models have been deduced by Mott[10],[15] and Cohen, Fritsche and Ovshinsky[11] to cover the range from amorphous elements to amorphous alloys.

The models are shown in figure (2.1a,b). The model (2.1a) is thought applicable to the simpler glasses containing one or two elements. Mott[12] argues that there must exist energies E_C and E_V where there is a sharp transition from extended to localised states. The range of the localised states (i.e. $E_C - E_A$ or $E_B - E_V$) is estimated to be about 0·1 to 0·2 eV.[12] An important feature of the model is that the mobility of the charge carriers decreases sharply at E_C and E_V. The change of mobility may be by a factor $\sim$ 1000.[13] The energies at these points define the energy gap but it is better described as a mobility gap. (Fig. (2.1c))

If some specific defect exists in the material Davis and Mott[14] propose that a narrow band of localised states may be formed in the gap which pins the Fermi energy. This is shown in figure (2.1d).

The model more applicable to amorphous alloys,

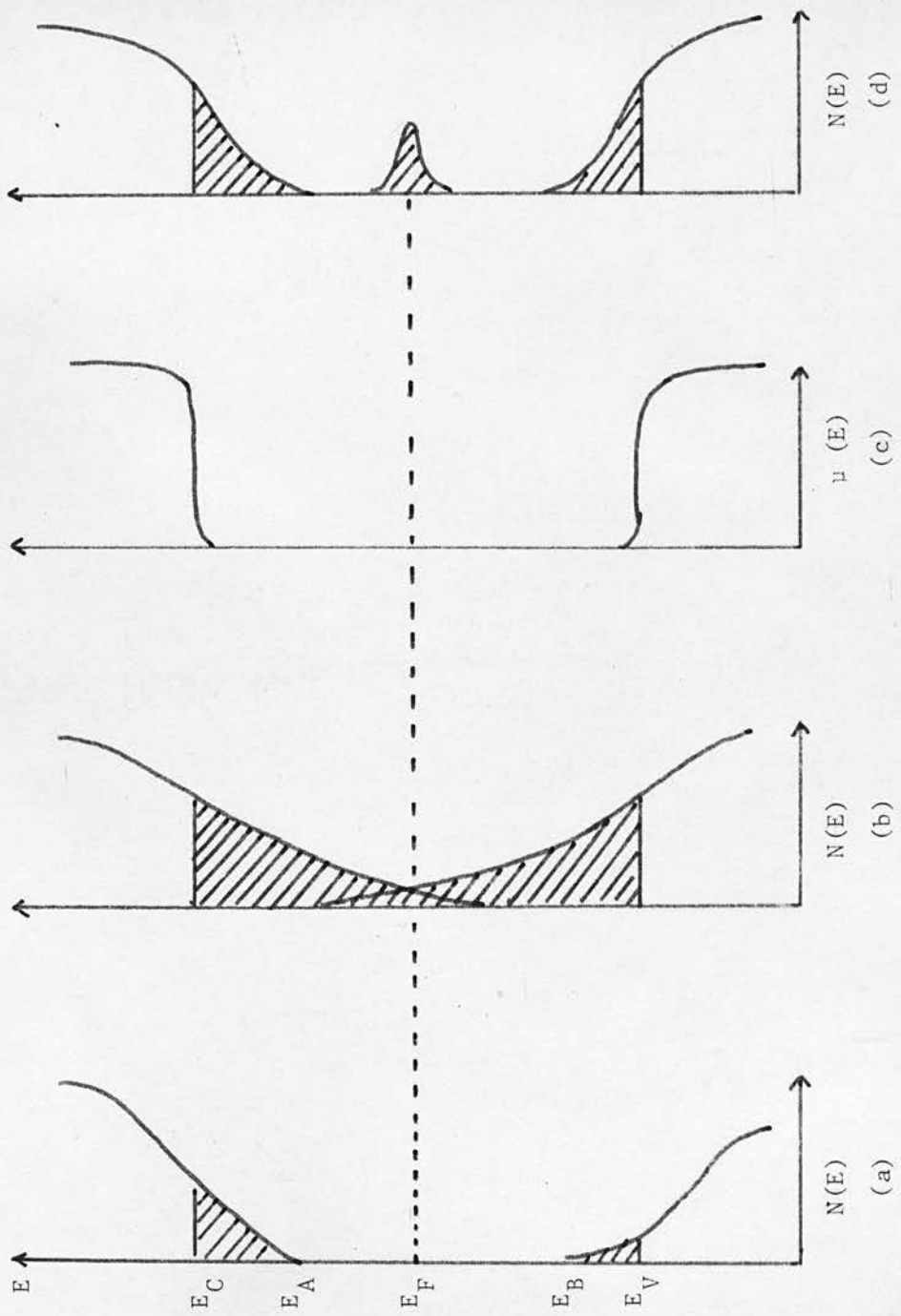

Figure (2.1)

Possible band models for amorphous semiconductors

where compositional disorder may be greater, is that of Cohen, Fritsche and Ovshinsky shown in figure (2.1b). The main feature is the much greater extent of the localised states resulting in an overlap near the centre of the gap. The overlap ensures a transfer of electrons from the top of the valence band states to the bottom of the conduction band states keeping the Fermi energy in the region of the overlap.

These models form a basis for further work. For a particular amorphous semiconductor there may be several "bands" of localised states in the mobility gap corresponding to particular defects; or combinations of the various models might apply.

2.3 Charge Transport.

Transport of electrons (or holes) in an amorphous semiconductor is possible in the region of the extended states or in the localised states. In the localised region the motion of the carriers is a thermally activated process usually referred to as hopping. Transport in this region is of particular importance to gather information on the distributions, densities and electrical characteristics of the localised states.

2. 3. 1 D.C. Conductivity.

D.C. conduction is possible by three mechanisms:[13]

(a) Carriers thermally excited from the extended

states below E_V to those above E_C. This leads to a conductivity of the form (for electrons):

$$\sigma = \sigma_0 \exp\left[-(E_c - E_F)/kT\right] \tag{2.1}$$

$E_C - E_F$ is constant and usually roughly half the energy of the optical absorption edge. σ_0 can be calculated from theory with fair accuracy[12],[14] and is in the range 200 to 500 $ohm^{-1} \cdot cm^{-1}$.

If the activation energy varies with temperature as

$$E_c - E_F = E - \gamma T \tag{2.2}$$

then

$$\sigma = \sigma_0 \exp\frac{\gamma}{k} \exp -\frac{E}{kT} \tag{2.3}$$

and a plot of $\log\sigma$ verses $\frac{1}{T}$ will still give a straight line. The temperature coefficient, γ is expected to be roughly half that of the optical energy gap.

(b) Carriers can be excited from the non-localised states to the localised states. In this case the conductivity (again for electrons) has the form:

$$\sigma = \sigma_1 \exp\left[-(E_n - E_F + \Delta W_1)/kT\right] \tag{2.4}$$

where ΔW_1 is an average activation energy for hopping. The constant σ_1 is expected to be approximately $10^{-3}\ \sigma_0$ [14].

(c) Hopping of electrons with energies near the Fermi energy. For a defect band of localised states, as proposed by Davis and Mott[14], of width $2\Delta W_2$, the conductivity is

$$\sigma = \sigma_2 \exp[-(\Delta W_2)/kT] \qquad (2.5)$$

with $\sigma_2 << \sigma_1$.

Plots of $\log\sigma$ versus $\frac{1}{T}$ are expected to give three different activation energies as the temperature is decreased.

It should be noted that the third mode of conduction will only give a unique energy ΔW_2 if the carriers hop to their nearest neighbours[15]. If the temperature is lowered so that it is energetically more likely for the carriers to tunnel to distant sites, then the expected form is[15]

$$\sigma \propto \exp(A/T^{\frac{1}{4}}) \qquad (2.6)$$

2.3.2 Mobility.

In the region of localised states the mobility is of the form[15]

$$\mu = \mu_0 \exp(-W/kT) \qquad (2.7)$$

with

$$\mu_o = \frac{\nu_o e a^2}{kT} \exp(-2\alpha a) \qquad (2.8)$$

ν_o is a phonon frequency ($\sim 10^{12}$ sec^{-1}) and a is the distance between localised states. The factor exp (- 2 α a) is a measure of the overlap of the wave functions when the localised states are far apart.

Where the states are non-localised the mobility will be much greater but in amorphous semiconductors the existence of large densities of localised states ensures that the effective mobility is trap limited. The mobility is then a function of the densities of free and trapped electrons (n_o and n_t) so that

$$\mu_D = \mu_o \frac{n_o}{n_o + n_t} \qquad (2.9)$$

If the density of localised states at the band edges is a linear function of energy for a range ΔE then(16)

$$\mu_D = \mu_o \frac{\Delta E}{kT} \exp\left(-\frac{\Delta E}{kT}\right) \qquad (2.10)$$

The range of localised states at the mobility edges can therefore be determined if this simple relationship holds.

Equation (2.10) may be compared with the mobility limited by a discrete level of traps at energy ΔE below the conduction band. If N_c is the density of states in the conduction band and Nt the density of traps, then

$$\mu_D = \mu_o \left[1 + \frac{N_t}{N_c} \exp\left(\frac{\Delta E}{kT}\right)\right]^{-1} \qquad (2.11)$$

At low temperatures this approximates to

$$\mu_D = \mu_o \frac{N_c}{N_t} \exp\left(-\frac{\Delta E}{kT}\right) \qquad (2.12)$$

2.3.3 The Mobility Shoulder.

At the energies E_C and E_V the mobility (at $T = 0$ K) falls from a finite value (above E_C and below E_V) to zero or a very small value. This point is discussed by Cohen[9]. In this change the mean free path of the electrons decreases rapidly from greater than to the order of the electron wavelength. Just above E_C the wavelength is comparable to the interatomic spacing and the motion of the electrons is best described as diffusive[9]. In this case the mobility is

$$\mu = \frac{eD}{kT} = \frac{\nu_e e a^2}{kT} \qquad (2.13)$$

Where D is the diffusion coefficient and ν_e is an electronic frequency ($\sim 10^{14}$ sec^{-1}).

This description allows for a continuous transition in the mobility as the states change their nature at the mobility edges.

2.4 Optical Absorption.

The variation of the optical absorption coefficient, α, with photon energy found in amorphous semiconductors (and in other materials) usually shows an initial exponential increase leading to a variation of the form

$$\alpha\hbar\omega \propto (\hbar\omega - E_o)^n \qquad (2.14)$$

The exponential section obeys the "Urbach rule".

$$\alpha = \alpha_o \exp(A\hbar\omega/kT) \qquad (2.15)$$

In the region described by (2.14) the exponent n is usually 2 but may vary depending on the transitions involved[13]. The relation forms a way of defining the optical energy gap as E_0. E_0 is not, in general, twice the conductivity activation energy.

CHAPTER 3

Dielectric Properties and A. C. Conduction

3.1 Introduction.

The dielectric properties of a material are defined by the electric field strength $\underline{E}$, the electric displacement or flux density $\underline{D}$ and the polarisation $\underline{P}$. The relation between these quantities is

$$\underline{D} = \epsilon_0 \underline{E} + \underline{P} \qquad (3.1)$$

where ϵ_0 is the permittivity of free space. If the medium is linear then

$$\underline{D} = \epsilon_0 \epsilon_r \underline{E} \qquad (3.2)$$

and ϵ_r is the relative permittivity of the medium.

Equations (3.1) and (3.2) imply that

$$\underline{P} = \epsilon_0 (\epsilon_r - 1) \underline{E} = \epsilon_0 \chi \underline{E} \qquad (3.3)$$

where χ is defined as the electric susceptibility.

If the dielectric medium is placed in an alternating electric field $E_0 e^{i\omega t}$ the polarisation and displacement may lag in phase behind E, the applied field. To include this let

$$D = D_0 \exp i(\omega t - \delta) \qquad (3.4)$$

Using equation (3.2)

$$D_0 \exp i(\omega t - \delta) = \epsilon_0 \epsilon_r^* E_0 \exp i\omega t \qquad (3.5)$$

or
$$\epsilon_0 \epsilon_r^* = \frac{D_0}{E_0}(\cos\delta - i \sin\delta) \qquad (3.6)$$

In general, therefore, the permittivity may be complex and is written

$$\epsilon_r^* = \epsilon_r' - i\epsilon_r'' \qquad (3.7)$$

ϵ_r' and ϵ_r'' are the relative dielectric constant and dielectric loss respectively.

An important quantity is the loss tangent defined as

$$\tan\delta = \frac{\epsilon_0 \epsilon_r''}{\epsilon_0 \epsilon_r'} = \frac{\epsilon_r''}{\epsilon_r'} \qquad (3.8)$$

ϵ_r^* (and thus $\tan\delta$) are related to the loss of energy in the dielectric.

It can be shown that the dielectric loss is equivalent to a conductivity, σ where

$$\sigma = \omega \epsilon_0 \epsilon_r'' \qquad (3.9)$$

The dielectric properties of a material can equally be described in terms of the complex quantities σ^* , χ^* and ϵ^* ; these are related by

$$\sigma^* = i\omega\epsilon^* \tag{3.10}$$

$$\chi^* = \epsilon_r^* - 1 \tag{3.11}$$

The most physically meaningful quantity is the polarisation. The total polarisation can be considered as the sum of polarisation of individual mechanisms: e.g. displacements of electrons, ions and molecules possessing an electric dipole moment. Particular mechanisms are usually dominant at different frequencies.

3.2 Dielectric Response.

If an electric field is applied to a solid at time $t = t_0$ polarisation will result. The response of the electric charges in the solid may not be instantaneous and the growth of the polarisation with time can be represented qualitatively as shown in figure (3.1). The "instantaneous" polarisation P_∞ and the polarisation represented by the section $P_s - P_\infty$ may be accounted for by different mechanisms.

Let

$$P(t) = P_\infty + (P_s - P_\infty) f(t - t_0) \tag{3.12}$$

where $f(t-t_0)$ is a response function such that $f(0) = 0$ and $f(\infty) = 1$.

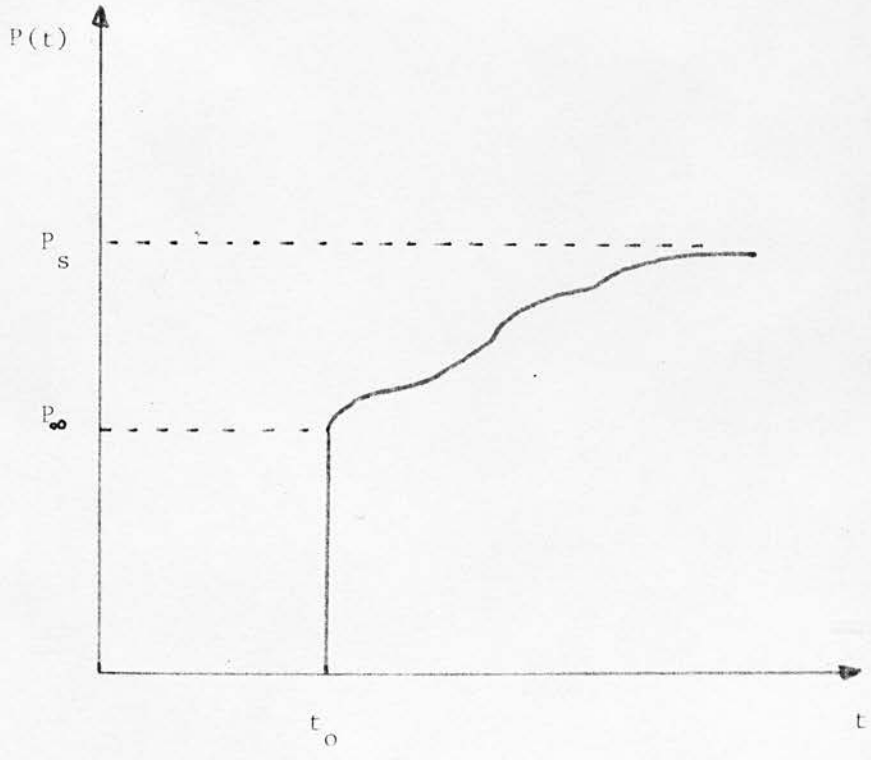

Figure (3.1)

Dielectric polarisation for electric field applied at time t_o

Following the treatment of Gevers[17] the application of a periodic field at $t = -\infty$ results in a contribution to the polarisation of

$$\Delta P(t) = \epsilon_0(\chi_s - \chi_\infty)E_0 \int_{-\infty}^{t} \exp(i\omega t').\frac{df}{dt'}(t-t').dt' \qquad (3.13)$$

which (using (3.12) and (3.3)) gives

$$\epsilon_r^* = \epsilon_\infty + (\epsilon_s - \epsilon_\infty)\int_0^\infty \frac{df}{dt}(t).\exp(-i\omega t).dt \qquad (3.14)$$

having components

$$\epsilon_r' = \epsilon_\infty + (\epsilon_s - \epsilon_\infty)\int_0^\infty \frac{df}{dt}(t).\cos\omega t.dt \qquad (3.15)$$

$$\epsilon_r'' = (\epsilon_s - \epsilon_\infty)\int_0^\infty \frac{df}{dt}(t).\sin\omega t.dt \qquad (3.16)$$

ϵ_s and ϵ_∞ are the dielectric constants corresponding to zero and "infinite" frequencies.

Equations (3.15) and (3.16) are completely general and the only assumption made in their derivation is the validity of the principle of superposition. Particular mechanisms will determine the response function $f(t)$.

If the response function has the form

$$f(t) = 1 + \exp\left(\frac{-t}{\tau}\right) \qquad (3.17)$$

i.e. equivalent to an exponential rise or decay, then

$$\epsilon_r' - \epsilon_\infty = (\epsilon_s - \epsilon_\infty) \cdot \frac{1}{1 + \omega^2 \tau^2} \qquad (3.18)$$

$$\epsilon_r'' = (\epsilon_s - \epsilon_\infty) \cdot \frac{\omega\tau}{1 + \omega^2 \tau^2} \qquad (3.19)$$

These equations were originally derived by Debye[18] and are known as the Debye equations.

The loss tangent is

$$\tan\delta = (\epsilon_s - \epsilon_\infty) \cdot \frac{\omega\tau}{\epsilon_s + \epsilon_\infty \omega^2 \tau^2} \qquad (3.20)$$

The time constant, or relaxation time, τ defines the rate of growth or decay of the polarisation.

Figure (3.2) illustrates the behaviour of the Debye equations.

A response function $f(t) \propto \exp\left(\frac{-t}{\tau}\right) \cdot \cos \omega_o t$ results in a complex permittivity of the form[19]

$$\epsilon_r^* - \epsilon_\infty = \frac{\epsilon_1 - \epsilon_\infty}{2} \cdot \left[\frac{1 - i\omega_o\tau}{1 - i(\omega_o + \omega)\tau} + \frac{1 + i\omega_o\tau}{1 + i(\omega_o + \omega)\tau}\right] \qquad (3.21)$$

where ω_o is a natural resonance frequency. In this

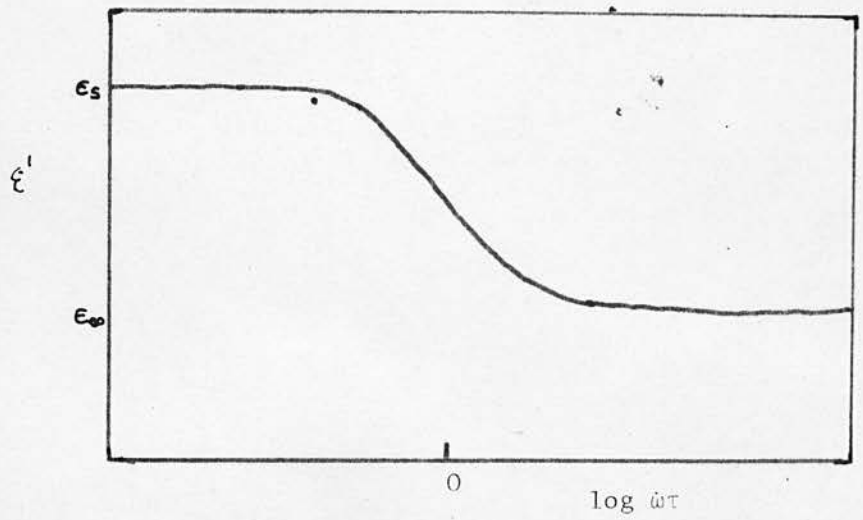

Dielectric constant

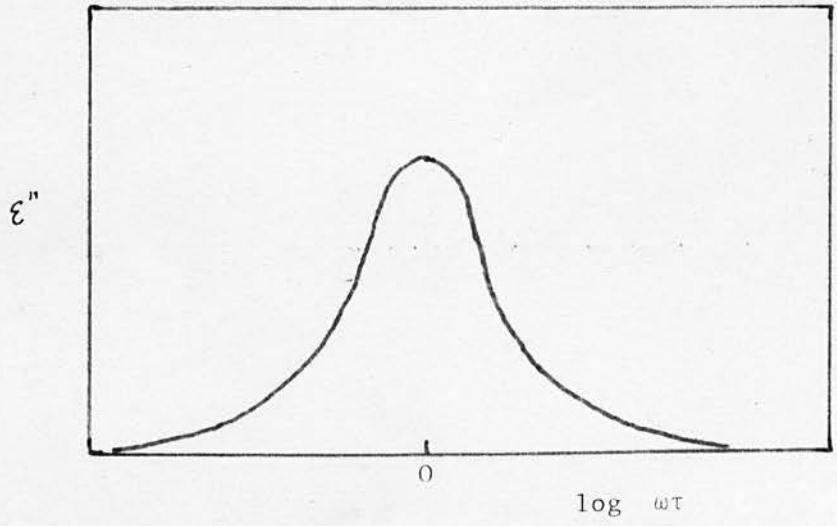

Dielectric loss

Figure (3.2)

The Debye equations

equation ϵ_1 is the " ϵ_∞ " of the Debye equations and ϵ_∞ is the dielectric constant at a higher frequency ($\gg \omega_0$). Equation (3.21) describes resonance absorption processes. These usually occur at high frequencies (from microwave to optical frequencies).

Purely exponential decay functions are expected if the system has no preferred configuration or more than one stable equilibrium position. One stable configuration results in resonance behaviour[19].

3.3 Models for Relaxation.

The most useful simple model for relaxation is that described by Debye[19] and Frohlich[20].

Consider a dielectric with N charged particles each of which has two equilibrium positions separated by a potential barrier of height U . Interaction between the particles is assumed negligible.

If the positions of a pair of particles are called 1 and 2 as shown in figure (3.3), the occupation probabilities with no external field are equal, i.e.

$$p_1 = p_2 = \frac{1}{2} \qquad (3.22)$$

As a simplification the "no-field" potential of each well is assumed the same.

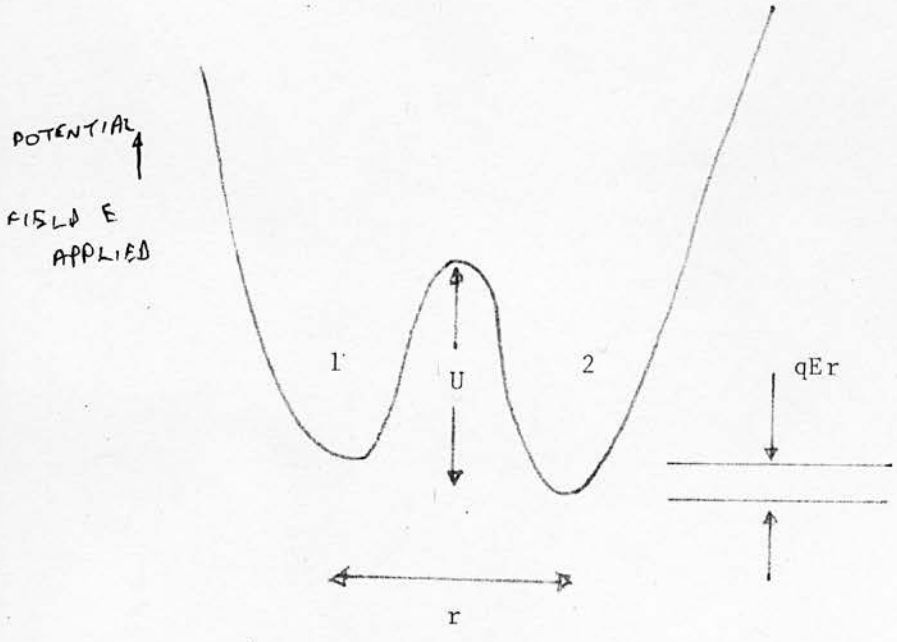

Figure (3.3)

Frohlich two-site model for dielectric relaxation

Over the whole solid the number of particles in sites 1 and 2 is the same and

$$2N_1 = 2N_2 = N \tag{3.23}$$

If an electric field, $\underline{E}$ is applied at time $t = 0$ the difference in the potentials of the wells will be

$$\Phi_1 - \Phi_2 = q\,\underline{r}\cdot\underline{E} \tag{3.24}$$

for a charge q and distance apart $\underline{r}$.

At temperature T the probability of occupation of the wells becomes

$$p_1 = \frac{\exp - \phi_1}{\exp - \phi_1 + \exp - \phi_2} \tag{3.25}$$

and

$$p_2 = \frac{\exp - \phi_2}{\exp - \phi_1 + \exp - \phi_2} \tag{3.26}$$

where $\phi_i = \Phi_i / kT \qquad i = 1,2$

The two sites will be in contact with a thermal reservoir and transitions between them will occur. The transition rates are

$$\omega_{12} = A \exp - (u - \Delta) \tag{3.27}$$

$$\omega_{21} = A \exp - (u + \Delta) \tag{3.28}$$

where $u = U/kT$ and $\Delta = (\phi_1 - \phi_2)/2$.

In general for low fields $\Delta << 1$ i.e.

$\Phi_1 - \Phi_2 << kT$ and so

$$\omega_{12} \approx A \exp -u.\,[1-\Delta] = B\,[1-\Delta] \tag{3.29}$$

$$\omega_{21} \approx A \exp -u.\,[1+\Delta] = B\,[1+\Delta] \tag{3.30}$$

The average rates of change of N_1 and N_2 are

$$\frac{dN_1}{dt} = -N_1\omega_{12} + N_2\omega_{21} \tag{3.31}$$

$$\frac{dN_2}{dt} = N_1\omega_{12} - N_2\omega_{21} \tag{3.32}$$

i.e.

$$\frac{d}{dt}(N_2 - N_1) = 2B\left[-(N_2 - N_1) + N\Delta\right] \tag{3.33}$$

and the solution to this equation is

$$N_2 - N_1 = N\Delta(1 - \exp -2Bt) \tag{3.34}$$

The polarisation $P = (N_2 - N_1)\mu$ for dipole moment μ and therefore

$$P = N\Delta\mu\,(1 - \exp -2Bt) \tag{3.35}$$

The polarisation has an exponential decay and thus this model

leads to the Debye equations with relaxation time $1/2B$

i.e. $$\tau = \frac{1}{2A} \cdot \exp \frac{U}{kT} = \tau_0 \exp \frac{U}{kT} \qquad (3.36)$$

As $\Delta = \mu E/kT$ and assuming μ and E are parallel, equation (3.35) becomes

$$P = \frac{N\mu^2 E}{kT}\left(1 - \exp -\frac{t}{\tau}\right) \qquad (3.37)$$

The above treatment is only valid when the collision time with the surrounding medium is short compared with τ (the average time a particle spends in a well) and the period of the external field[20]. If there is interaction between particles the transition probabilities will not be constant but will depend on the positions of neighbouring charges. This results in non-linear equations for N_1 and N_2.

An important result of this treatment is the relation between τ , U and T given by equation (3.36).

A more general case of the model is when the well potentials are not equal in the absence of an external field and μ and E are not parallel. For a zero-field energy difference ΔW , averaging over all angles results in a contribution to the polarisation[21],[22].

$$P = \frac{N\mu^2 E}{3kT} \operatorname{sech}^2 \left(\frac{\Delta W}{2kT}\right).\left(1 - \exp -\frac{t}{\tau}\right) \qquad (3.38)$$

In this case the relaxation time is

$$\tau = \frac{1}{\omega_{12} + \omega_{21}} \qquad (3.39)$$

Equation (3.38) still has an exponential decay and will lead to the Debye equations.

In an amorphous solid the dielectric properties would result from averaging over the differences between pairs of localised states, assuming that this is the appropriate conduction mechanism. The most obvious variables are the differences in energy, ΔW , the relaxation times, τ and the distances between states, r .

3. 4 The Relaxation Time.

3. 4. 1 Single relaxation times.

The assumption of a single relaxation time for a description of the dielectric properties of a material results in the Debye equations as was shown in section (3.2). However, experimental results show that in general loss peaks are usually wider than the Debye case, asymmetric, or no loss peak is found over a wide frequency range. This implies that many relaxation times may exist in a material.

3.4.2 Distributions of Relaxation Times.

In 1907 von Schweidler[23] introduced the idea that the response function $f(t)$ consisted of an infinite

number of different relaxation times, τ_i , coupled with a density function, $G(\tau_i)$. defined so that

$$\sum_{i=0}^{\infty} G(\tau_i) = 1 \tag{3.40}$$

and $$f(t) = \sum_{i=0}^{\infty} G(\tau_i) f_i(t) \tag{3.41}$$

here $f_i(t)$ is a function of τ_i , possibly with the form of equation (3.17).

Using this gives a dielectric constant and loss:

$$\epsilon_r' = \epsilon_\infty + (\epsilon_s - \epsilon_\infty) \sum_{i=0}^{\infty} \frac{G(\tau_i)}{1 + \omega^2 \tau_i^2} \tag{3.42}$$

$$\epsilon_r'' = (\epsilon_s - \epsilon_\infty) \sum_{i=0}^{\infty} \frac{G(\tau_i)\, \omega \tau_i}{1 + \omega^2 \tau_i^2} \tag{3.43}$$

Generalising these equations results in

$$\epsilon_r' = \epsilon_\infty + (\epsilon_s - \epsilon_\infty) \int_0^{\infty} \frac{G(\tau).\, d\tau}{1 + \omega^2 \tau^2} \tag{3.44}$$

$$\epsilon_r'' = (\epsilon_s - \epsilon_\infty) \int_0^{\infty} \frac{G(\tau)\, \omega \tau .\, d\tau}{1 + \omega^2 \tau^2} \tag{3.45}$$

with the condition

$$\int_0^{\infty} G(\tau).\, d\tau = 1 \tag{3.46}$$

$G(\tau)$ is now the distribution of relaxation times and

$G(\tau)d\tau$ is the fraction of relaxation times in the range τ to $\tau + d\tau$.

The effect of a distribution of relaxation times is to widen the loss peak and decrease the dispersion of the dielectric constant. The distribution can be deduced from experimental results but relating $G(\tau)$ to physical processes remains one of the most difficult problems in the study of dielectric behaviour.

Possible insight into the processes involved may be gained from the Frohlich two-site model where

$$\tau = \tau_0 \exp U/kT \qquad (3.36)$$

A distribution in relaxation times is equivalent to a distribution in barrier heights. Gevers[17] and Gevers and Du Pré[24] adopt this approach.

As ϵ_r' and ϵ_r'' are functions of the same distribution function, in principle one quantity can be calculated from the other. The resulting equations are called the Kramers-Kronig relations and are expressed as

$$\epsilon_r'(\omega) = \epsilon_\infty + \int_0^\infty \frac{u\epsilon_r''(u)}{u^2 - \omega^2} \, . \, du \qquad (3.47)$$

$$\epsilon_r''(\omega) = -\int_0^\infty \frac{\epsilon_r'(u) - \epsilon_\infty}{u^2 - \omega^2} \, . \, du \qquad (3.48)$$

where u is the variable of integration.

There are a number of distribution functions which may be used to fit experimental results. The simplest was derived by Frohlich[20] from basic physical ideas. If it is assumed that there is a distribution of barrier heights, U such that the barriers are uniformly distributed over the range U_o to $U_o + u_o$ (i.e. $U = U_o + u$ with $0 \leq u \leq u_o$) then for N dipoles there are $N \frac{du}{u_o}$ barriers between $U_o + u$ and $U_o + u + du$. Neglecting interaction,

$$d\epsilon_s = \frac{\epsilon_s - \epsilon_\infty}{N} \cdot \frac{N\,du}{u_o} \tag{3.49}$$

which is the total contribution to ϵ_s by barriers close to $U_o + u$ But also

$$\epsilon_s - \epsilon_\infty = (\epsilon_s - \epsilon_\infty) \int_0^\infty G(\tau)\,.\,d\tau$$

$$= (\epsilon_s - \epsilon_\infty) \int_0^{u_o} G(\tau) \cdot \frac{d\tau}{du} \cdot du$$

$$= \frac{(\epsilon_s - \epsilon_\infty)}{kT} \int_0^{u_o} G(\tau)\,\tau\,.\,du \tag{3.50}$$

from (3.36). Thus $(\epsilon_s - \epsilon_\infty)\, G(\tau)\,\tau\, du/kT$ is the contribution to ϵ_s and by comparison with equation (3.49)

$$G(\tau) = \frac{kT}{u_o} \cdot \frac{1}{\tau} \tag{3.51}$$

for the range of τ defined by U . $G(\tau)$ is zero outside this range.

Provided $G(\tau)$ decreases rapidly outside the range the result is still valid and the resulting dielectric parameters are

$$\epsilon_r' = \epsilon_\infty + (\epsilon_s - \epsilon_\infty)\left[1 - \frac{kT}{2u_0} \ln\left(\frac{1+\omega^2\tau_2^2}{1+\omega^2\tau_1^2}\right)\right] \qquad (3.52)$$

$$\epsilon_r'' = (\epsilon_s - \epsilon_\infty)\frac{kT}{u_0}\left[\tan^{-1}\omega\tau_2 - \tan^{-1}\omega\tau_1\right] \qquad (3.53)$$

where τ_1 and τ_2 correspond to the limits $u = 0$ and $u = u_0$ respectively. For a very wide range of relaxation times

$$\epsilon_r'' \rightarrow \frac{\pi}{2}(\epsilon_s - \epsilon_\infty)\frac{kT}{u_0} \qquad (3.54)$$

In this case the dielectric loss is independent of frequency and proportional to temperature.

One of the simplest forms of distribution function is that which leads to a Gaussian distribution of relaxation times centred on a relaxation time τ_0 . This is

$$G(\tau)d\tau = \frac{b}{\sqrt{\pi}}\exp(-b^2s^2).ds \qquad (3.55)$$

where $s = \ln(\tau/\tau_0)$ The width of the resulting loss peak depends on the parameter b: when b is small the

dielectric loss is almost independent of frequency.

There are other functions which may be used to describe dielectric behaviour, but one of the most useful was formulated by Cole and Cole[25]. Expressed in its simplest form the complex dielectric constant is

$$\epsilon_r^* = \epsilon_\infty + \frac{\epsilon_s - \epsilon_\infty}{1 + (i\omega\tau_0)^{1-\alpha}} \qquad (3.56)$$

In this case the parameter α $(0 \leq \alpha < 1)$ defines the width of the distribution. Following from this a plot of the real component against the imaginary component of ϵ_r^* will produce an arc extending from ϵ_∞ to ϵ_s on the real axis. The parameter α defines where the centre of the circle producing the arc lies. The Debye case has $\alpha = 0$ and the centre lies on the real axis, whereas for $\alpha > 0$ the centre lies below the real axis. The usefulness of the Cole-Cole plot is greatest when there are perhaps two or three mechanisms over the whole frequency range where their mean relaxation times are quite different. In this case two or three arcs may be resolved.

3.5 Models for Relaxation in Amorphous Dielectrics.

3.5.1 General Models.

Gevers and Du Pré[17],[24] in an analysis of dielectric relaxation in materials with wide distributions of relaxation times assume a similar distribution of

barrier heights to Frohlich (see paragraph (3.4.2)). That is $G(U)$ is approximately constant over a wide range of U and tends to zero at $U = 0$ and at large U . They make no assumptions as to the specific shape of the distribution. In their treatment $\omega\tau$ is replaced by $\exp \frac{(U - U_0)}{kT}$ where U_0 is defined as the barrier height needed for $\omega\tau$ to equal unity. i.e.

$$\omega\tau = \omega\tau_0 \exp U_0/kT = 1 \qquad (3.57)$$

The general expression for the dielectric constant (equation (3.44)) involves the function $(1 + \omega^2\tau^2)^{-1}$ which is equal to unity except where $\omega\tau \gtrsim 1$ when it decreases to zero. Using this the dielectric constant can be written as

$$\epsilon_r' \approx \epsilon_\infty + (\epsilon_s - \epsilon_\infty) \int_0^{U_0} G(U) \cdot dU \qquad (3.58)$$

Similarly the function $\omega\tau/(1 + \omega^2\tau^2)$ is narrow compared with $G(U)$ and centred about $\omega\tau = 1$ (or $U = U_0$) Then

$$\epsilon_s \approx (\epsilon_s - \epsilon_\infty)\, G(U_0) \int_0^\infty \frac{\omega\tau}{1 + \omega^2\tau^2} \cdot dU \qquad (3.59)$$

giving

$$\epsilon_r' \approx (\epsilon_s - \epsilon_\infty)\, G(U_0)\, kT \left[\frac{\pi}{2} - \tan^{-1}(\exp - U_0/kT)\right] \qquad (3.60)$$

For $U_0 \gg kT$ this simplifies to

$$\epsilon_r'' \approx \frac{\pi}{2}(\epsilon_s - \epsilon_\infty) G(U_o) kT \qquad (3.61)$$

which is similar to equation (3.54). In both equations the temperature dependence arises from the use of similar expressions for the relaxation time (equation (3.36)).

Expressions for the variation of dielectric constant with frequency and temperature can be derived from equations (3.57), (3.58) and (3.61); they are

$$\frac{1}{\epsilon_r'} \frac{\partial \epsilon_r'}{\partial \omega} \approx -\frac{2}{\pi} \tan\delta \qquad (3.62)$$

and

$$\frac{1}{\epsilon_r'} \frac{\partial (\epsilon_r' - \epsilon_\infty)}{\partial T} \approx \frac{2}{\pi T} \ln\left(\frac{1}{\omega \tau_o}\right) . \tan\delta \qquad (3.63)$$

or

$$\frac{1}{\epsilon_r'} \frac{\partial \epsilon_r'}{\partial T} \approx A \tan\delta - \alpha_l \left(1 + \epsilon_\infty - \frac{2}{\epsilon_\infty}\right) \qquad (3.64)$$

where α_l is the coefficient of linear thermal expansion.

The quantity $A \left(= \frac{2}{\pi T} \ln \frac{1}{\omega \tau_o}\right)$ is approximately constant for a wide variety of amorphous materials at a fixed temperature. At 300 K it has a value of about 0·06[24].

Gevers and Du Pré interpret these equations ((3.58) and (3.61)) to mean that only charged particles with

activation energies less than or equal to U_0 contribute significantly to the dielectric constant. That is, when the relaxation times are smaller than $1/\omega$. On the other hand the major contribution to the dielectric losses originates in particles with activation energies close to U_0, and in this case, relaxation times are approximately $1/\omega$. (This is analagous to the pair separation for hopping conductivity, r_ω - see paragraph (3.5.2)).

It should be noted that a wide flat distribution of activation energies is equivalent to a distribution of relaxation times

$$G(\tau) \propto \frac{1}{\tau} \tag{3.65}$$

which also gives a frequency independent dielectric loss[26].

A different approach was used by Garton[26] who considered a combination of deep permanent wells and shallow temporary wells as a model for an amorphous material. He assumed that the shallow wells, due to thermal fluctuations, were distributed in depth as

$$\delta N \propto \exp -\frac{v}{kT} \cdot \frac{\delta v}{kT} \tag{3.66}$$

where v is the depth of a thermal well. This description implies the existence of two time constants τ and τ_0 where.

$$\tau = A \exp \frac{v}{kT} \tag{3.67}$$

$$\tau_o = A_o \exp \frac{U}{kT} \qquad (3.68)$$

U is the depth of the large well. Further assumptions are that $\tau + \tau_o$ is much smaller than the time that the temporary well exists and that $\tau + \tau_o << 1/\omega$
The resulting dielectric loss is

$$\epsilon_r'' = (\epsilon_s - \epsilon_\infty)\frac{(\pi - 1)}{A_o} \cdot \frac{\exp(-v_o/kT)}{2kT} \qquad (3.69)$$

which is completely independent of frequency. The temperature dependence is different from that of Gevers and Du Pré (equation (3.61)).

Descriptions of dielectric relaxation in terms of barrier heights are more "physically obvious" than in terms of relaxation times. However in spite of the exponential relaxation between τ and U a very broad range of barrier heights is needed to explain the independence of dielectric loss over a wide range of frequency, as is observed in many amorphous materials; assuming that the loss mechanism is the same over the whole range.

Jonscher[27] has formulated a qualitative theory for the frequency dependence of the a.c. conductivity resulting from a stochastic hopping of charge carriers. Each hop provides a current pulse which contributes to the conductivity through the Fourier transform of the response function. The total pulse is the sum of random hops

occuring at random times. The application of a step function electric field perturbs the random processes by superimposing a sequence of ordered events. The amplitudes of the ordered hops will be in the field direction but the times of the events are still random, though they become more widely spaced as time increases and "difficult" hops are encountered. Jonscher uses the sequence of ordered amplitudes to derive the dielectric constant and loss. The form of the a.c. conductivity depends on the particular sequence of events. If each event occurs at time t_m then in general for

$$t_m = am^k \qquad k \geq 1 \tag{3.70}$$

the conductivity has the form

$$\sigma(\omega) \propto \omega^{1-1/k} \tag{3.71}$$

The value $k = \infty$ also corresponds to the sequence $t_m = a.\exp(bm)$. (m is integer)

Jonscher's theory results in a frequency dependence for the conductivity in agreement with the experimental results but leaves the problem of a fundamental physical treatment no nearer solution.

3.5.2 Electronic Processes.

So far the description has been in fairly general terms and no specific charged particle was needed to describe

a particular behaviour. A possible mechanism for the a.c. conductivity with relevance to non-crystalline semiconductors could involve electrons in the region of localised states in the mobility gap.

Frohlich, Machlupp and Mitra[28] have shown that if the mobility of a solid is low the electrons can be described classically and may be localised. In this case the electrons exhibit Debye losses. Sussman[29] has also shown that a trapped electron may give rise to an electric dipole and again Debye losses would result.

A theoretical treatment of thermally activated hopping motion in solids was provided by Sewell[30]. Sewell considers the motion of a particle confined to a set of localised states and moving either by tunneling or by thermally activated hopping. The former process does not involve phonons and can be described by quantum mechanics whereas the latter process does. For one mechanism to predominate the temperature plays an important part. The probability that a particle known to be on one site at time $t = 0$ is at another at time t is

$$p(t) = \frac{1}{2}\left(1 - \exp(-\gamma t).\cos \Omega t\right) \qquad (3.72)$$

γ and Ω are constants representing the hopping and tunneling processes respectively. At low temperatures $\gamma \ll \Omega$ and the system will absorb energy at

frequency Ω .

The dielectric response function is

$$K(t) = -\frac{e^2 a^2}{kT} \cdot \frac{d}{dt}\left(\exp(-\gamma t)\cdot \cos \Omega t\right) \qquad (3.73)$$

where a is the hopping or tunneling distance. For thermally activated hopping $\Omega \ll \gamma$ and the response function reduces to

$$K(t) = \frac{e^2 a^2 \gamma}{kT} \cdot \exp(-\gamma t) \qquad (3.74)$$

The exponential decay leads to Debye type losses.

In amorphous semiconductors it is possible that the a.c. conduction occurs either by electrons in the non-localised or in the localised states. The d.c. conductivity behaves as that for intrinsic conduction in semiconductors and involves electrons in the extended states. It is reasonable to assume that this process may account for at least part of the measured a.c. conductivity.

Pollak[7] has shown that the two conduction processes can be distinguished by their differing frequency dependences. For n electrons and field E the conductivities behave as

$$\sigma_b = \frac{ne}{E} \sum_i \langle v_i \rangle \Delta f_i(t=\infty) \cdot \frac{1}{1+\omega^2 \tau_i^2} \qquad (3.75)$$

for the extended states and

$$\sigma_h = \frac{ne}{E} \sum_i \langle x_i \rangle \Delta f_i \ (t = \infty) \cdot \frac{1}{\tau_i} \cdot \frac{\omega^2 \tau_i^2}{1 + \omega^2 \tau_i^2} \tag{3.76}$$

for hopping in between localised states.

The reason for the difference arises from the basic equation regarding the current carried. This is, for all states

$$j = ne \sum_i \frac{d}{dt}(x_i f_i) \tag{3.77}$$

where x_i is the coordinate of the electron state and f_i its occupation probability. In the extended states x_i only will be a function of time, whereas in the localised states it is f_i that is a function of time. The result of this is

$$j = ne \sum_i \langle v_i \rangle f_i \tag{3.78}$$

for bands and

$$j = ne \sum_i \langle x_i \rangle \frac{df_i}{dt} \tag{3.79}$$

for the localised states. $\langle v_i \rangle$ and $\langle x_i \rangle$ are the velocity component and coordinate of state i. The application of an electric field changes the occupation probability from its equilibrium value by an amount

$$\Delta f_i = \Delta f_i (t = \infty) \left[1 - \exp - \frac{t}{\tau}\right] \tag{3.80}$$

The expression for band conduction is essentially the same as the Drude equation:

$$\sigma = \frac{Ne^2\tau}{m} \cdot \frac{1}{1+\omega^2\tau^2} \qquad (3.81)$$

which decreases with frequency. If the main contribution to the conductivity ~~comes from hops where~~ occurs when $\omega\tau_i \approx 1$ then σ_b is independent of frequency and σ_h is proportional to frequency.

All treatments of hopping between pairs of localised states reduce to a Debye-type behaviour which needs an appropriate distribution function for the relaxation time (or activation energy) for a complete description of the dielectric properties. It is necessary that the averaging used predicts the correct magnitude as well as the correct frequency and temperature dependences. Factors affecting the magnitude (for example densities of pairs of localised states) need to be determined by independent measurement rather than be deduced from a dielectric measurement.

Significant contributions to the theory of a.c. conduction in localised states have been made by Pollak.[31][21] Pollak begins with the general expression

$$\sigma(\omega) = \omega \int_a^b d\tau \int \alpha(\tau,[g]) \cdot n(\tau,[g]) \cdot d[g] \qquad (3.82)$$

where $n(\tau, [g])$ is the density of pairs of localised states, $\alpha(\tau, [g])$ the polarizability and $[g]$ represents any other variables (e.g. energy differences between the states of a pair (ΔW) or wave function radii). Equation (3.82) implies that the major contribution to the conductivity arises from values of τ between a and b where $\tau\omega \approx 1$.

Assuming that $[g] = \Delta W$ only, that is the localised wave functions have the same radius, and using the expressions

$$\alpha = \frac{e^2 r^2}{3kT} \cdot \frac{1}{4\cosh^2 \Delta W/2kT} \tag{3.83}$$

for the polarizability derived by Pollak and Geballe[21] and

$$\tau = \tau_0 \exp \frac{2r}{a} \tag{3.84}$$

for the dependence of the relaxation time on the hopping distance r, Pollak arrived at two expressions for the a.c. conductivity. These are

$$\sigma(\omega) = \frac{\pi^2}{4} \alpha\omega r_\omega^3 \epsilon N_c \tag{3.85}$$

and

$$\sigma(\omega) = \frac{\pi^3}{96} \left[N(E_F)\right]^2 kT e^2 \alpha\omega r_\omega^4 \tag{3.86}$$

r_ω is the distance given by $\alpha \ln\left(\frac{1}{\omega\tau_0}\right)$ and is the most

probable hopping distance at frequency ω ; N_c is the concentration of charge carriers; r_s is the average separation of localised states given by $\left(\frac{4\pi N_s}{3}\right)^{-\frac{1}{3}}$ for density of localised states N_s; and $N(E_F)$ is the density of states at the Fermi energy.

The derivation of equations (3.85) and (3.86) involves consideration of the probabilities of finding pairs of localised states separated by a distance r_ω and with energy difference ΔW . To make a hopping event possible such a pair of states must be singly occupied. This probability can be written

$$F = f(i)[1-f(j|i)] + f(j)[1-f(i|j)] \qquad (3.87)$$

where $f(i)$ is the probability that state i is occupied and $f(j|i)$ is the conditional probability that state j is occupied if state i is occupied.

There is an additional conditional probability $p(\Delta W|r_\omega)$ that the two states at distance r_ω have energy separation ΔW . The effect of these conditional probabilities is to separate two cases: that where $p(\Delta W|r_\omega)$ and $f(j|i)$ are important and that where they are not. This is a distinction between short and long hops. The longer the hopping distance the more likely the charge carrier is to find an unoccupied state. This can be expressed using a length r_q given by

$$r_q = \left(\frac{4\pi N_q}{3}\right)^{-\frac{1}{3}} \qquad (3.88)$$

where N_q is the concentration of charged states. For

$r_\omega \ll r_q$ equation (3.85) should be used and for

$r_\omega \gg r_q$ equation (3.86).

For chalcogenide glasses the second condition is usually satisfied if suitable assumptions are made regarding the values for a and τ_o $(= 1/\omega_o)$[31] (i.e. 3Å and 10^{-12} sec respectively). In full, equation (3.86) can be written

$$\sigma(\omega) = \frac{\pi^3}{96}\left[N(E_F)\right]^2 kT e^2 a^5 \omega \left[\ln \frac{\omega_o}{\omega}\right]^4 \qquad (3.89)$$

The important features of this equation are that hopping close to the Fermi energy is assumed; the conductivity is proportional to temperature; and the frequency dependence is almost linear. The equation suffers from depending on the quantities ω_o, a and $N(E_F)$ which are not known particularly accurately. This puts the magnitude of the predicted conductivity in some doubt.

Equations similar to (3.89) have been derived by Austin and Mott[32] and Mott and Davis[13].

In a recent review Pollak[33] summarises three possible mechanisms responsible for the a.c. conductivity in amorphous materials. They are:

(a) A phonon assisted tunnelling process (hopping)

(b) Charge transfer over a potential barrier, now referred to as "leaping".

(c) A combination of (a) and (b).

These processes can be distinguished by the forms of the relaxation time which are

$$\tau = \tau_0 \exp 2r/a \tag{3.90}$$

$$\tau = \tau_0 \exp U/kT \tag{3.91}$$

and

$$\tau = \tau_0 \exp(2r/a + U/kT) \tag{3.92}$$

The results depend to a large extent on the distribution of the random variables r and U but the frequency and temperature dependences vary slightly. Again correlation effects change the temperature dependence by a factor T, as for equations (3.85) and (3.86). An important point that Pollak makes is that the conductivity depends on a factor N which is $N_c N_s$ for strong correlation and $N(E_F) k T N_s$ for weak correlation. Between these extremes N must vary such that it approaches $N_c N_s$ at high frequencies where the hopping distance is short and $N(E_F) k T N_s$ at low frequencies. This implies that N is

an increasing function of frequency in the intermediate region. Representing the a.c. conductivity as

$$\sigma = A\omega^{s} \tag{3.93}$$

suggests that s is increasing. This effect should be coupled to a temperature dependence between T^{0} and T^{1} for hopping.

The relation between the index s and the phonon frequency ω_o can be stated as[34]

$$s = 1 - 4/\ln\frac{\omega_o}{\omega} \tag{3.94}$$

or

$$\omega_o = \omega \exp\left[4/(1-s)\right] \tag{3.95}$$

ω_o is expected to be close to 10^{12} sec^{-1} but if s is close to unity this will be impossible unless the frequency ω is very low.

The model used by Pike[34] is a leaping one with a probability function used to define nearest neighbour distances. This is expressed as the probability that a site has a neighbour at a distance between r and $r+dr$ or

$$P(r).dr = 4\pi N r^{2} \exp(-4\pi N r^{3}).dr \tag{3.96}$$

where N is the density of sites. This results in a

conductivity as given by equation (3.93) again with $s \approx 1$ but the quantity $s - 1$ is now $6\,kT/U_m$ where U_m is the maximum barrier height. The model predicts values of s close to unity at low temperatures and a decrease in s as the temperature increases.

3.6 Inhomogeneous Dielectrics.

The existence of boundaries separating regions of differing dielectric constants and losses within a solid produces an interfacial polarisation often called the Maxwell-Wagner effect. The existence of boundaries within an amorphous solid must be considered as a possible explanation for the measured dielectric properties. An extensive review of the subject is given by van Beek[35].

The simplest system is a two layer model with conductivity σ_i and dielectric constant ϵ_i for the i th layer. The resulting equations have the Debye form with

$$\epsilon_s = \frac{(d_1 + d_2)(\epsilon_1 d_1 \sigma_2^2 + \epsilon_2 d_2 \sigma_1^2)}{\sigma_1 d_2 + \sigma_2 d_1} \qquad (3.97)$$

$$\epsilon_\infty = (d_1 + d_2)\,\epsilon_1 \epsilon_2 / (\epsilon_1 d_2 + \epsilon_2 d_1) \qquad (3.98)$$

$$\tau = \epsilon_0 (\epsilon_1 d_2 + \epsilon_2 d_1) / (\sigma_1 d_2 + \sigma_2 d_1) \qquad (3.99)$$

where the thicknesses of the layers are d_1 and d_2.

There will be an additional conductivity term given by

$$\sigma = (d_1 + d_2)\,\sigma_1\,\sigma_2 / (\sigma_1 d_2 + \sigma_2 d_1) \qquad (3.100)$$

The dielectric parameters are thus functions of the individual dielectric constants and losses of the components as well as their thicknesses.

More generally, the components may consist of spheres or some other geometrical shape embedded in a different material.

Sillars[36] has shown that for a wide variety of shapes of material of higher conductivity dispersed in a low conductivity medium the resulting dielectric loss is independent of frequency over several decades and then decreases at high frequencies. This means that the conductivity saturates at a high frequency and therefore it may be possible to distinguish the conductivity mechanism by measurements in this region.

Maxwell-Wagner polarisation essentially provides a qualitative description as the various parameters can always be altered to fit the experimental results. To achieve a plausible outcome the structure of the solid needs to be studied to determine the proportions of differing components present (if any), and an estimation of their relative volumes made.

CHAPTER 4

Review of Electrical and Related Properties of some Chalcogenide Glasses

In the past few years much has been published on the a.c. and d.c. conductivity of the chalcogenide glasses. Most of the work has concentrated on low frequencies (between 10^2 and 10^6 Hz) but measurements have also been made in the microwave and far infra-red regions.

4.1 A.C. conductivity and dielectric properties.

The a.c. conductivity of the chalcogenide glasses is often found to obey the relation

$$\sigma = A\omega^s \qquad (4.1)$$

where $s \approx 1$. This is a common result of dielectric measurements on many materials. Gevers,[17] in a review of the frequency dependence of dielectric materials, points out that the dielectric losses ϵ'' ($= \sigma/\omega$) of many plastics and other non-crystalline materials are often constant over a wide range of frequencies. Equation (4.1) is not, therefore, limited to amorphous materials which conduct electronically.

An important point to consider is the variation in the magnitudes of the conductivity in the published

results. Mitchell, Bishop and Taylor[37] summarise the results of several investigations of $As_2 Se_3$, one of the most studied amorphous semiconductors. Figure (4.1) shows log σ against log f as taken from Mitchell et al[37]. The a.c. conductivity at 10^4 Hz varies from 10^{-9} ohm^{-1} cm^{-1} (Lakatos and Abkowitz[38]) to close to 10^{-12} ohm^{-1} cm^{-1} (Crevecoeur and de Wit[39]). Lakatos and Abkowitz' measurements were made on thin films as opposed to bulk material and this may explain some of the discrepancy, but even on bulk materials there can be a difference of an order of magnitude. Obviously the sample preparation, purity of the material and electrical contacts during measurement may all play a part in the results.

Coupled with a high a.c. conductivity for thin films a low dielectric constant is often found. Polanco, Roberts and Myers[40] find the thin film dielectric constant for $As_2 S_3$ to be 6·3 whereas the bulk value is closer to 10[16]. Street and Yoffe[41] show that annealing thin films changes their dielectric properties to agree more closely with the bulk material.

Interpretation of the a.c. conductivity where equation (4.1) is obeyed, is often made by assuming that a thermally activated electron hopping mechanism is dominant and the analyses of Pollak[31] or Austin and Mott[32] used to determine the density of states at the

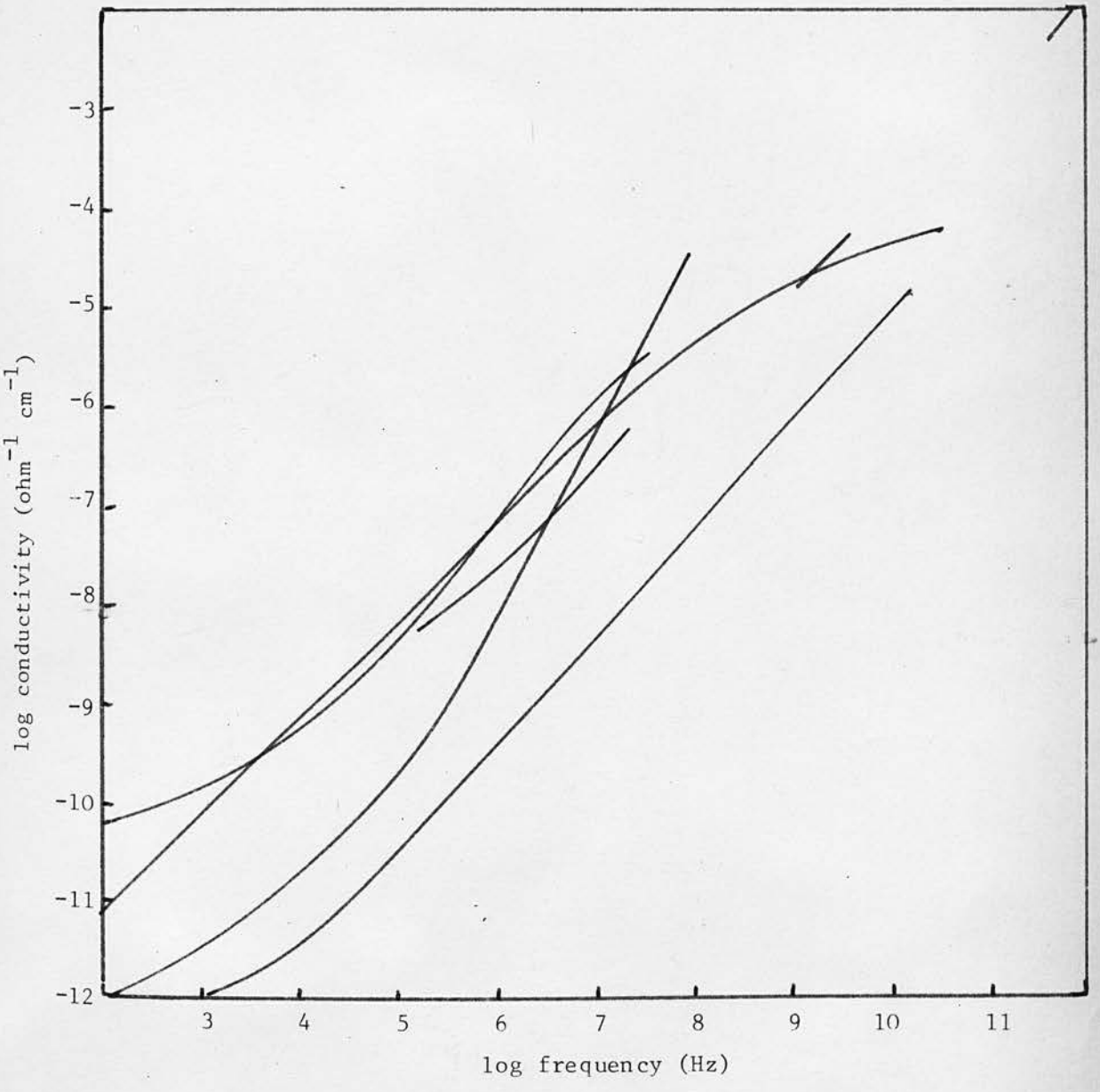

Figure (4.1)

Summary of a.c. conductivity of As_2Se_3
(from Mitchell et al[37])

Fermi energy (i.e. equation (3.89)). For $As_2 Se_3$ and $As_2 S_3$ $N(E_F)$ is close to 10^{18} cm^{-3} eV^{-1} (14). There are difficulties in this interpretation: firstly assumptions have to be made regarding the effective radius of the localised wave functions and the phonon frequency, and secondly, the predicted value for s is close to 0·8. Measured values for s vary from about 1·1 to zero. It has already been pointed out that large values for s lead to unphysically large phonon frequencies (see section 3.5.2 equation (3.95)). Similar doubts are expressed by Kitao(42) who argues that in $As_2 Se_3$ the conductivity at low frequencies is a result of Maxwell-Wagner polarisation caused by regions of differing conductivity in the solid.

Crevecoeur and de Wit(39) and others find that the magnitude of the conductivity is affected by the contacts to the glass which introduce additional losses. In this case measurements give a maximum value for the a.c. hopping conductivity enabling a maximum for the density of states at the Fermi level to be found.

Lakatos and Abkowitz(38) reject Maxwell-Wagner conduction because their glasses showed no microstructure. Their results are best described by the electron hopping model but they mention the possibility of trap controlled conduction. In this case the form of the frequency dependence of the conductivity (i.e. the magnitude of s)

would depend on the shape of the distribution of localised states with energy.

Rockstad[43] has measured the a.c. conductivity of glass films based on the elements As, Te, Si and Ge. At a frequency of 10^5 to 10^6 Hz he finds that the ratio of the a.c. component to the d.c. conductivity is approximately constant; a factor which leads him to propose that the dominant hopping conduction is at the mobility edges rather than at the Fermi energy.

The temperature dependence of the a.c. conductivity is weak[16],[38],[44] indicating that the form of Pollak's result (equation (3.89)) could be correct. The range of temperature covered is small and it is not possible to reach any firm conclusions about the exact behaviour. Hopping at the mobility edges would result in an exponential temperature dependence with an activation energy $(E_F - E_B)$[13]. In the temperature range covered this is not found in $As_2 Se_3$, $As_2 S_3$ or Se.

Several authors[16],[42],[45] have reported conductivities where the exponent s approaches two. The region where this occurs is usually between 10^6 and 10^9 Hz. The existence of this behaviour has been doubted and explained as resulting from small contact resistances which dominate the conductivity at high frequencies[38]. However some measurements (e.g. Hayatee[16]) have been performed by

slotted-line techniques which do not require contact with the sample. Kitao[42] fits his results at these frequencies to a Debye type response with a relaxation time of 9.10^{-10} seconds where the conduction arises from hopping between equivalent pairs of localised states. Kitao stresses that sample preparation may be the factor deciding how the conductivity varies with frequency. The apparent temperature independence of the conductivity in this region presents a problem. The relaxation time at least would be expected to be a function of temperature.

Few measurements have been made at microwave frequencies. In the region 10^9 to 10^{11} Hz differing conductivity mechanisms would be expected to show a variety of behaviour. As the frequency increases the hopping conductivity should saturate and decrease[37], Maxwell-Wagner conductivity should lose its frequency dependence or the conductivity may increase owing to some other mechanism.

Austin and Garbett[46] following Amrhein[47] suggest the possibility that the phonon absorption tail may extend well into the microwave region. In this case the conductivity will increase into the far infra-red region.

The measurements of Lakatos and Abkowitz[38] at 36 GHz on amorphous As_2Se_3, As_2S_3 and Se show the conductivity saturating at microwave frequencies. This is

not confirmed by Taylor, Bishop and Mitchell[48] at 1 to 6 G Hz and Austin and Garbett[46] for $As_2 Se_3$. Taylor et al. find that their results are too low to be a continuation of the ω^2 region and that the simplest explanation is that the conductivity has increased nearly proportionally to frequency from 10^3 to 10^{10} Hz. The ω^2 region is not inconsistent with Austin and Garbett's result.

To a large extent the relation between the audio and microwave frequency regions depends on whose low frequency results are chosen. Lakatos and Abkowitz[38] low frequency results are higher than average for $As_2 Se_3$ and their microwave conductivity is low, so it might be expected that together the results show an apparent saturation. The published a.c. conductivity data for $As_2 Se_3$ fall into a broad line which increases approximately as the first power of frequency and within this line some measurements deviate.

Lilja and Stubb[49] find that the conductivity of amorphous Se at 24 G Hz is below 10^{-5} ohm^{-1} cm^{-1} agreeing closely with Lakatos and Abkowitz[38] results. There is also good agreement on the microwave dielectric constant between these two sources and Gebbie and Kiely[50] and Klinger and Saker[51]. The agreement for amorphous Se may be a reflection of its being a one componant glass and thus forming a homogeneous system more easily.

The variation in conductivity of other glasses is

matched by that in the dielectric constant. Low frequency values vary from 9·7[16] to 6·3[40] for $As_2 S_3$ and 13·7[16] to 8·87[44] for $As_2 Se_3$. Unfortunately much data on the a.c. conductivity is published without reference to the dielectric constant.

Amorphous semiconductors show resonant vibrational features in the infra-red region[46],[52],[53],[37]. The absorption can be related to the local structure of the glass and the vibration of the atomic bonds[3],[54].

4.2 Variations from Stoichiometry.

There have been few investigations of the electrical conductivity as a function of composition.

Kolomiets[4] in a study of the d.c. conductivity of the $As_2 Se_3$ - $As_2 Te_3$ and $Tl_2 Se \cdot As_2 (Se,Te)_3$ systems found an increase in conductivity with the proportion of heavy components in the glass.

The d.c. conductivity As - S system has been investigated by Myuller, Baidov and Borisova[55] and Minami, Hattori, Nakamachi and Tanaka[56]. The conductivity is a minimum near stoichiometry and increases as the sulphur content rises. The variation can be attributed to changing pre-exponential constants (σ_o) or activation energies.

Edmond[57], Lezal, Srb and Dokoupil[58], Arai, Kuwahata, Namikawa and Saito[59] and Minami, Yoshida and Tanaka[60] have performed similar measurements on the As - Se system and find that the conductivity reaches a maximum at stoichiometry or just on the selenium rich side (Edmond). Edmond[57] finds that the variation is not all explained by a change in the activation energy and suggests that the conductivity is affected by barriers which are more effective in the non-stoichiometric material.

The optical absorption edge of the range of materials $As_2 S_3$ to $As_2 S_5$ is shown by Kosek and Tauc[61] to increase in energy with rising sulphur content, whereas Edmond[57] finds no change in the corresponding As - Se system. This may reflect differing effects of the range of localised states at the band edges or simply a change in band gap due to structural changes.

Some measurements of the dielectric properties of the As - S system have been made by Maruno[62]. The loss tangents show a minimum near stoichiometry for the four compositions studied (57·5, 64·3, 70·5 and 75·5 atomic % S), while the permittivities decreased with increasing sulphur content. Sutton[63] quotes results for ionic conducting glasses which show that the dielectric constant at low frequencies and the square of the refractive index are approximately proportional to the density of the material. Taking the data of Tanaka and Minami[64] and Tsuchihashi and

Kawamoto[3] for the density of As - S glasses, the results of Maruno[62] show a similar relation as does the variation of refractive index[3]. To help determine the structural changes with composition quantities such as the glass transformation temperature, T_g, hardness and expansion coefficient can be measured. In the As - S and As - Se glass systems T_g reaches a maximum at or near stoichiometry [2],[3],[65] but the shapes of the maxima are different. In the As - S system it is sharp and T_g is proportional up to As_2S_3 to the atomic percentage of sulphur, whereas in the As - Se system the maximum is rounded and the behaviour of T_g with composition more complex[2]. At stoichiometry the hardness has a maximum and the expansion coefficient possibly a minimum[3] in the As - S system though the latter was not found by Tanaka, Minami and Hattori[66].

In order to help clarify the situation in the As - S and As - Se systems, with regard to the various discrepancies in the magnitude and behaviour of the a.c. and d.c. conductivities, it was felt necessary to perform careful measurements on these materials. It seemed that an examination of the materials in a small range centred on As_2X_3 (X = S or Se) would provide most useful information.

In order to do this care was taken in the sample preparation and in the measurement techniques.

CHAPTER 5

Measurement of Dielectric Properties

Various techniques can be used to measure the dielectric properties of solids, the choice depends mainly on the frequency range to be covered and, to a lesser extent, the magnitudes of the dielectric constant and loss tangent.

The frequency ranges and techniques normally employed are:

(a) low frequencies ($<$ 1Hz) - time domain and bridge methods

(b) audio frequencies (1Hz to 10^7 Hz) - bridge methods

(c) radio frequencies (10^6 to 10^8Hz) - resonance methods

(d) high frequencies (10^8 to 10^9Hz) - waveguide methods

(e) Microwave frequencies (10^9 to 10^{11}Hz) - waveguide methods.

An essential difference between these methods is that in the first three the wavelength is long compared with the sample dimensions and the physical size of the components used.

In the present experiments measurements were made

in the ranges covered by sections (b) and (e) and so these will be described in more detail.

5.1 Bridge methods.

The general principle of bridge methods (and most other dielectric measurements) is the balancing of a known impedance against the unknown impedance of a capacitor containing the dielectric material. The known impedance is composed of a combination of resistors and capacitors. A variation of this is to balance the bridge, remove the specimen and rebalance; or substitute an impedance of similar value to that of the sample and rebalance to obtain the small difference. This method has the advantage that the specimen impedance is replaced by a known impedance eliminating the need to allow for stray impedances.

The most common bridge circuits used are the Schering and transformer ratio bridges.

The Schering bridge is an a.c. variation of the Wheatstone bridge used for d.c. resistance measurements. The arms consist of a capacitor holding the dielectric material and variable and fixed resistors and capacitors for the other three arms. An a.c. generator and null detector are needed and the variable components used to balance out both the in- and out-phase components of the signal. Similarly the transformer ratio bridge is an a.c. variety of

the Wheatstone bridge. In this case two of the arms consist of the two windings of a transformer. In this way any stray impedances across the winding on the specimen side also appear on the other side because the magnetic flux is common to both windings. These bridges are accurate for measuring low dielectric losses but care is needed in construction to keep strays to a minimum.

The bridge used in this work for the audio frequency measurements was one designed by Lynch[67] and shown in figure (5.1). This bridge is similar to the transformer bridge but it has several advantages over conventional transformer and Schering bridges. The transformer is used to give signals 180^{o} out of phase in the two sections and enables a common earth for the generator and detector to be used. Stray capacitances appear mainly across the source and detector, and thus have little effect on the measurement. The bridge covers a large frequency range (~ 10Hz to 10M Hz mainly depending on the transformer) and is most useful for small capacitances and conductances. It is a substitution bridge and the change in C_v and R_v (or C_3) give the capacitance and conductance of the sample. i.e.

$$C_s \cdot \Delta C_v \qquad (5.1)$$

and

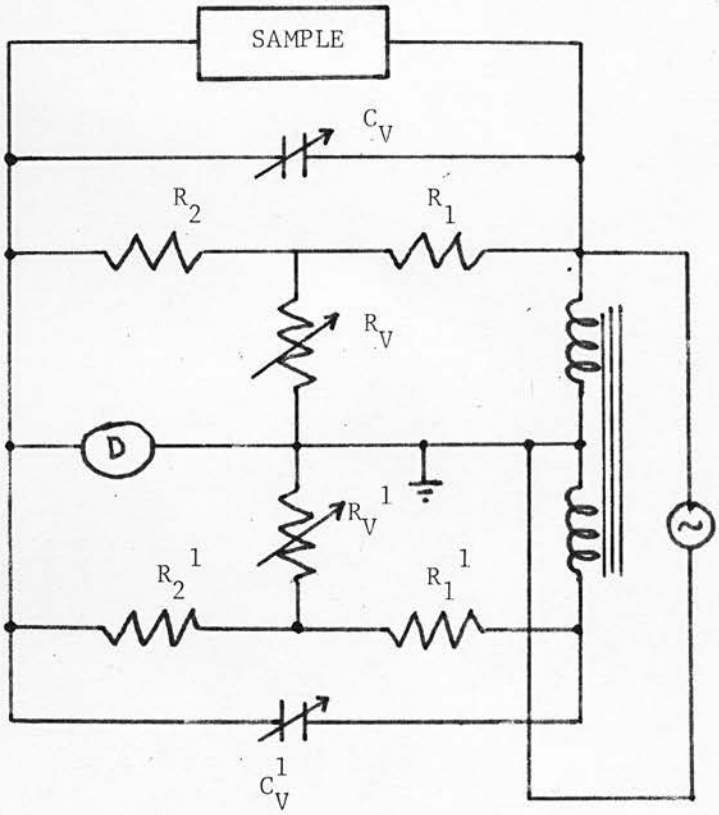

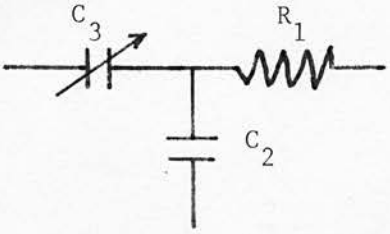

high frequency
modification replacing
R_1, R_2, R_V

Figure (5.1)

Lynch bridge circuit

$$G_s = \left[\frac{R_1 R_2}{\Delta R_v} + R_1 + R_2\right]^{-1}$$

$$\approx \frac{\Delta R_v}{R_1 R_2} \qquad \left(\text{or } \frac{\Delta C_3}{R_1 C_2}\right) \qquad (5.2)$$

For the materials used and typical sample dimensions $C_S \approx 3pF$ and $G_S \approx 10^{-11}$ ohm^{-1}.

5.2.1 Microwave methods (conventional)

Dielectric measurements at microwave frequencies are basically determinations of the wavelength of an electromagnetic wave in the dielectric and its attenuation on passing through the material. Techniques commonly employed are slotted lines, cavity resonators or cavity perturbation methods. Transmission and bridge methods are also used but are more difficult to apply with comparable accuracy and thus not so common[68]. The method utilised has to be chosen with regard to the probable magnitude of the dielectric constant and loss, the size and shape of the samples available and the comparative ease of mathematical analysis.

It will be useful to consider some of the techniques in more detail.

5.2.1.1 Slotted line methods.

The slotted line is a waveguide with a slot along

one wall through which a probe can detect the magnitude of the electric field along the length of the guide.

Any mismatching of the line impedance will create a standing wave and the impedance of the mismatch can be determined by the position of the nodes and standing wave ratio (i.e. the ratio of the magnitudes of the minima and maxima of the standing wave).

Dielectric measurements involve the use of a fixed or variable short circuit to create a standing wave. The basic apparatus is shown in figure (5.2). The standing wave ratio s is given by

$$s = E_{max} / E_{min} \qquad (5.3)$$

and the guide wavelength by

$$\lambda_g = 2|N_1 - N_2| \qquad (5.4)$$

for node positions N_1 and N_2 and maximum and minimum fields E_{max} and E_{min}.

The quantity s is a measure of the losses in the guide. The change in s when the sample is inserted depends on the additional losses (dielectric loss), and the change in a node position is caused by the decreased wavelength in the dielectric and thus the dielectric constant.

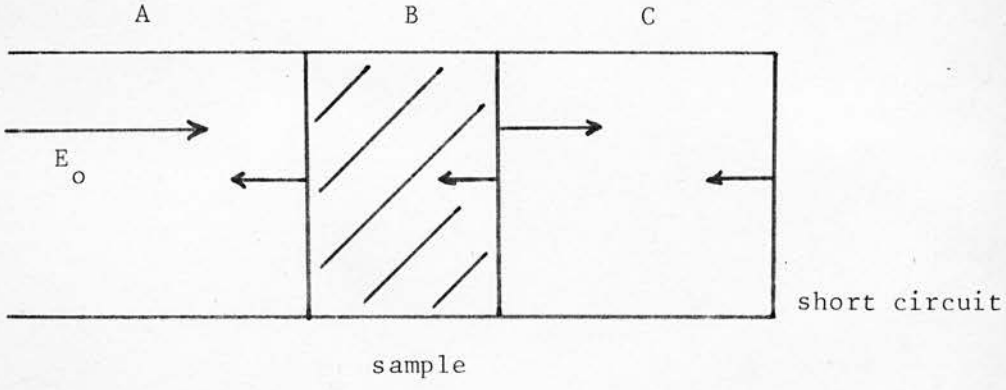

Figure (5.2)

Slotted line measurements showing
incident and reflected waves

In general there are three regions to consider: A, B and C as illustrated in figure (5.2). The incoming wave will be reflected at the interfaces AB and BC as well as at the short circuit. To determine the dielectric constant and loss of the sample the impedance at the interface AB, Z_{AB} and the propagation constant, γ, must be found[69]. Z_{AB} is found from the standing wave ratio and a node position N, and γ is determined by the thickness of the sample, l, Z_{AB} and λ_g. For a guide of impedance Z_0 (usually 50 ohms)

$$\frac{Z_{AB}}{Z_0} = \left(1/s - i \tan \frac{2\pi N}{\lambda_g}\right) \Big/ \left(1 - \frac{i}{s} \tan \frac{2\pi N}{\lambda_g}\right) \qquad (5.5)$$

where $i = \sqrt{-1}$

By varying the position of the short circuit relative to the dielectric the two most useful situations are:

(i) when the short circuit is in contact with the samples (or at distance $\lambda_g/2$ from it)

(ii) when the short circuit is at distance $\lambda_g/4$ from the sample - giving an effective open circuit at the sample interface BC.

If the impedance of the dielectric is Z_S (see equation (A.16)) then for condition (i)

$$Z_{AB} = Z_s \tanh \gamma l \tag{5.6}$$

and for condition (ii)

$$Z_{AB} = Z_s \coth \gamma l \tag{5.7}$$

Consider only the short circuit case:

$$\left(\frac{Z_{AB}}{Z_o}\right)_{(i)} = \frac{Z_s}{Z_o} \tanh \gamma l \tag{5.8}$$

As $Z_o = i\omega \mu_o / \gamma_o$ (equation(A.17)) (5.9)

$$\frac{Z_s}{Z_o} = \frac{\gamma_o}{\gamma} \tag{5.10}$$

giving $$\left(\frac{Z_{AB}}{Z_o}\right)_{(i)} = \frac{\gamma_o}{\gamma} \tanh \gamma l$$

or $$\frac{\tanh \gamma l}{\gamma l} = \frac{1}{\gamma_o l} \left(\frac{Z_{AB}}{Z_o}\right)_{(i)} \tag{5.11}$$

Usually the losses in the air-filled section of the guide can be neglected and in this case

$$\gamma_o = \frac{2\pi i}{\lambda_g} \tag{5.12}$$

Using equation (5.5), equation (5.11) can be solved[69]. Although many solutions are possible this presents little difficulty if approximate values of ϵ_r' and ϵ_r'' are known. The ambiguity can be removed by making

both open- and short-circuit measurements on the same sample and using the product of equation (5.11) and its open circuit equivalent to eliminate the hyperbolic functions.
This gives

$$\gamma^2 = \gamma_o^2 \Big/ \left[\left(\frac{Z_{AB}}{Z_o} \right)_{(i)} \cdot \left(\frac{Z_{AB}}{Z_o} \right)_{(ii)} \right] \qquad (5.13)$$

The dielectric parameters can be found from

$$\gamma = i\omega \sqrt{\mu_o \epsilon^*} \qquad (5.14)$$

The equations can be simplified if the dielectric losses are low (i.e. $\epsilon_r'' << \epsilon_r'$)

Slotted line techniques suffer from two main difficulties. Firstly the stability of the signal source and secondly the preparation of the samples. Frequency stability is necessary to enable the node positions of the standing wave and the standing wave ratio to be found accurately. This is particularly important for dielectrics with low losses. The fit of the sample on the waveguide affects the accuracy of the measurements but it is usually satisfactory to have a slide fit. It is particularly important that the dielectric occupies that part of the guide where the electric field is greatest. For the dominant mode in a rectangular guide (TE_{10}) the electric field vanishes at the smaller side walls so a good fit is needed along the broad side[68]. With a coaxial waveguide it is

the fit at the centre conductor which is more critical. These errors are greatest for materials with medium and high dielectric constants. The faces of the specimen should be as smooth as possible and square. The calculations are simplified if the sample length is an integral multiple of quarter wavelengths in the dielectric (69). The dielectric losses also affect the optimum length since the sample needs to be long enough to have a measurable attenuation but also short enough so that the simplified equations can be used (i.e. the losses are still low).

As an indication of the sample sizes involved consider a coaxial line at a frequency of 1 GHz and a material of dielectric constant 9.

$$\lambda_g = 30 \text{ cm}$$

and thus the wavelength in the dielectric is

$$\lambda_s = 30/\sqrt{9} = 10 \text{ cm}$$

giving $\lambda_s/4 = 2{\cdot}5 \text{ cm}$

This length is a minimum for accurate and fairly straight forward measurements. To cover a wide range of frequencies with the same sample may require a sample of several times this size. The problem of preparing an accurate sample of this size may be formidable. There are however methods employing slotted lines and small samples

which may give fairly precise results[69].

At higher frequencies rectangular waveguides are often used and thus separate samples would be needed for each wave-band covered.

5.2.1.2 Cavity methods.

If a microwave cavity contains electromagnetic radiation the solutions to the wave equations will depend on the physical dimensions of the cavity and the dielectric medium contained within its walls. Standing waves will be set up at particular frequencies (the resonant frequencies).

If the cavity resonates at frequency f_o when airfilled then

$$f_o = v/\lambda_g \qquad (5.15)$$

where v is the phase velocity, λ_g is the wavelength in the cavity, then, when filled with dielectric with relative permittivity greater than one, the new resonant frequency for the same wavelength is

$$f = v/(\lambda_g \sqrt{\epsilon_r'}) \qquad (5.16)$$

giving

$$\epsilon_r' = (f_o/f)^2 \qquad (5.17)$$

If the walls of the cavity are perfect conductors, the oscillations at the resonant frequencies will be maintained indefinitely but, in practice, energy is lost by their finite conductivity. These losses are expressed by the "Q" of the cavity, defined as

$$Q = 2\pi \frac{\text{energy stored in the cavity}}{\text{energy lost per cycle}} \qquad (5.18)$$

Dielectric losses should be included if the cavity contains a lossy material.

The usual method of defining the "sharpness" of the resonance is to take the frequencies at energies equal to half that stored at the resonant frequency. Let these be ω_1 and ω_2, then

$$Q = \omega_0 / |\omega_1 - \omega_2| \qquad (5.19)$$

As the resonant frequency of a particular mode in a cavity depends on the dimensions of the cavity there are two ways of measuring its Q: keeping the dimensions fixed and varying the frequency or keeping the frequency constant and varying the cavity dimensions.

When the cavity is filled with a lossy dielectric the additional losses can be expressed by a dielectric Q factor, Q_D. The resulting Q, Q_L is given by

$$\frac{1}{Q_L} = \frac{1}{Q_o} + \frac{1}{Q_o} \qquad (5.20)$$

where Q_L is the loaded Q factor and Q_O the unloaded Q .

In the dielectric the rate of energy dissipation per unit volume is σE^2 for conductivity σ and field E . The energy loss per unit volume in one cycle is

$$\delta U_D = \sigma E^2 \frac{2\pi}{\omega} \qquad (5.21)$$

The total energy stored in unit volume is

$$\delta U = \frac{1}{2} \epsilon_r' \epsilon_o E^2 + \frac{1}{2} \mu_o H^2$$

$$= \epsilon_r' \epsilon_o E^2 \qquad (5.22)$$

at some instant during a cycle. For a volume V

$$Q_D = 2\pi \frac{\int_V \delta U \cdot dV}{\int_V \delta U_o \cdot dV} \qquad (5.23)$$

or

$$Q_D = \frac{\omega_o \epsilon_r' \epsilon_o}{\sigma} = 1/\tan\delta \qquad (5.24)$$

Equations (5.17) and (5.24) may be used when the dielectric fills the cavity.

In a practical situation it may be impossible

however to completely fill the cavity for two reasons. Firstly, the preparation of a suitable sample is often difficult and the same conditions about fit and surface finish as were described for the slotted line also apply. Secondly, there is a large change in the resonant frequency when the dielectric is inserted into the cavity. From equation (5.17) the new resonant frequency is $f = f_0/\sqrt{\epsilon_r'}$ so that if $\epsilon_r' \gtrsim 2$ the new resonant frequency will be appreciably different from f_0 . The limits of equipment operating at X-band are 8 to 12·4 GHz, so the maximum dielectric constant in this case (i.e. to change from 12·4 GHz to close to 8 GHz) would be about 2·4. Total filling is therefore impracticable. On the other hand, most gases and liquids have low dielectric constants and in these cases this method is often used.

A more practical solution is to use a disc or rod of dielectric which is positioned in the cavity where the electric field is greatest. Unfortunately the simple expressions for ϵ_r' and $\tan\delta$ (equations (5.17) and (5.24)) will not be valid and the mathematical analysis becomes difficult.

As an example, consider a cylindrical cavity operating in the TE_{01n} mode and containing a dielectric disc. This particular arrangement can be used if the frequency or the cavity dimensions are variable and is most practicable at wavelengths of about 1 to 3 cm.

In cylindrical coordinates the components of the fields for the TE_{01n} mode are H_r, H_z and E_ϕ. The derivation of these components of the magnetic and electric field is given in appendix A1, equations (A.33), (A.34) and (A.35). A full analysis is given by Horner, Taylor, Dunsmuir, Lamb and Jackson[70].

For a dielectric of thickness l, filling one end of the cavity

$$\epsilon_r' = (\beta_1^2 + k_c^2)/(\beta_0^2 + k_c^2) \qquad (5.25)$$

where k_c is a wave number, $\beta_0 = 2\pi/\lambda_{g0}$ (λ_{g0} is the wavelength in the air-filled part of the cavity) and β_1 is found from

$$\frac{\tan \beta_1 l}{\beta_1} = \frac{-\tan[\beta_0(L-l)]}{\beta_0} \qquad (5.26)$$

for a cavity of total length L.

The loss tangent is

$$\tan\delta = \frac{\left[p(2l-s) + \frac{2(L-l)-q}{\epsilon_r'}\right]}{p(2l-s)} \cdot \left[\frac{1}{Q_L} - \frac{1}{Q_0'}\right] \qquad (5.27)$$

where $p = \sin^2[\beta_0(L-l)]/\sin^2\beta_1 l$

$q = \sin[2\beta_0(L-l)]/\beta_0$

$s = \dfrac{\sin 2\beta_1 l}{\beta_1}$

Q_0' is the Q derived from the measured value when the cavity is air-filled.

The measurement procedure is:

(i) Find λ_{g0} when the resonator is empty

(ii) Find Q_0'

(iii) Find L when the specimen is present

(iv) Find Q_L

Cavity measurements, if carefully performed, provide a very accurate determination of dielectric constants and losses. Typical errors are $< 1\%$ and $< 10\%$ respectively. Their main disadvantages are: sample preparation, frequency stability, cavity construction and fairly complex mathematics. The frequency range of these techniques is very limited for a particular cavity.

5.2.2 Microstrip transmission lines.

A recent development in microwave technology is the use of microstrip or stripline transmission lines for integrated circuits. The transmission lines covering the broadest frequency range are coaxial. This is because the dominant propagation mode, transverse electro-magnetic (TEM), has a zero cut-off frequency. Microstrip is a development of the coaxial line and its evolution is shown in figure (5.3). In its most convenient form it consists of two conductors separated by a uniform solid dielectric. A conducting

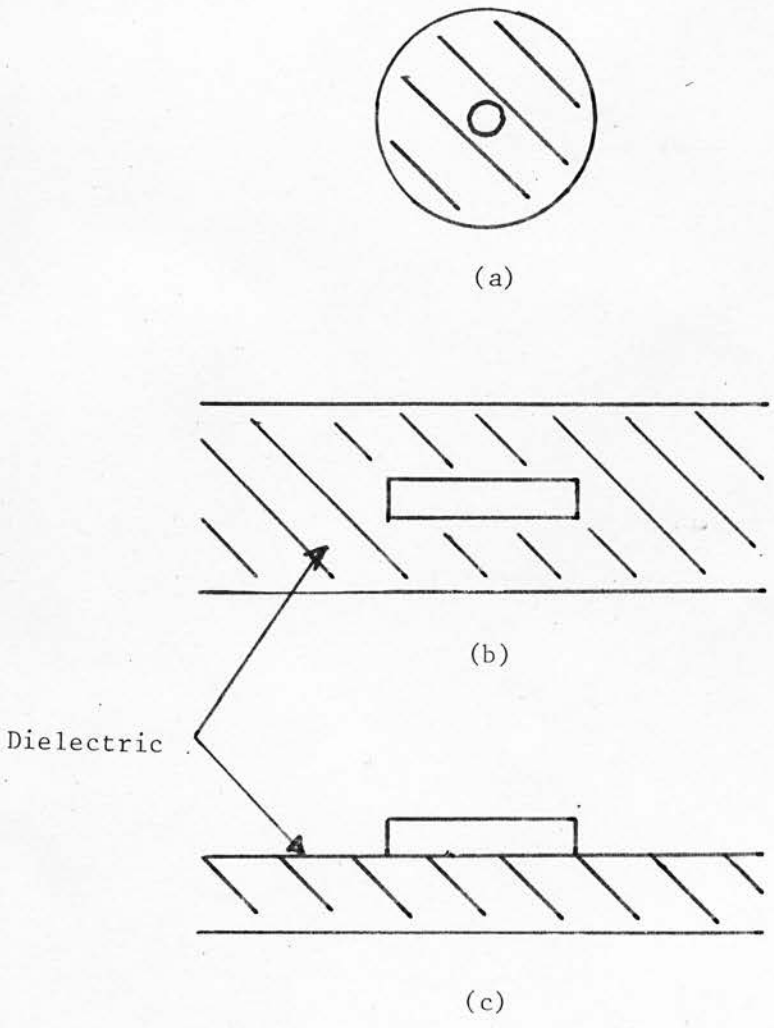

Figure (5.3)
Evolution of microstrip (c) from coaxial line (a)

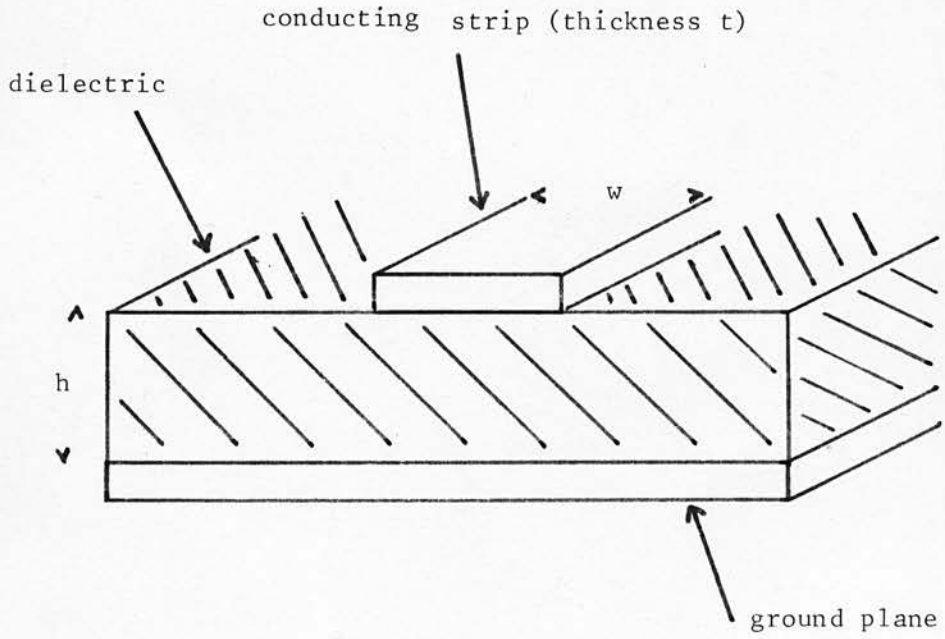

Figure (5.4)

Microstrip line

ground plane supports the dielectric and upper conducting strip (figure (5.4)). The geometrical parameters h , w and t (defined in the figure), the permittivity of the substrate and the conductivities of the dielectric and metal conductors define the impedance and attenuation of the line.

Microstrip lines and their possible use for making dielectric measurements are described in detail in the following chapter.

CHAPTER 6

Microstrip Transmission Lines and their use for Dielectric Measurements

6.1 Dielectric parameters and TEM mode transmission.

The propagation of a transverse electromagnetic (TEM) mode along a coaxial transmission line depends on the dielectric between the conductors. The line parameters for a dielectric with $\epsilon_r' \neq 1$ are related to those of free space so that:

impedance $$Z = Z_0 / \sqrt{\epsilon_r'} \qquad (6.1)$$

wavelength $$\lambda = \lambda_0 / \sqrt{\epsilon_r'} \qquad (6.2)$$

attenuation constant $$\alpha = \alpha_0 \sqrt{\epsilon_r'} \qquad (6.3)$$

the subscript zero refers to transmission in vacuo.

The mode of transmission in a microstrip line is close to TEM so by analogy the transmission parameters are defined in a similar way:

$$Z = Z_0 / \sqrt{\epsilon_e'} \qquad (6.4)$$

$$\lambda = \lambda_0 / \sqrt{\epsilon_e'} \qquad (6.5)$$

$$\alpha = \alpha_0 \sqrt{\epsilon_e'} \qquad (6.6)$$

The quantity ϵ_e' is the effective relative permittivity.

The dielectric losses are related to the Q factor of the dielectric in the line. Similarly to equation (5.24)

$$\frac{1}{Q_D} = (\tan \delta)_e = \frac{\epsilon''_e}{\epsilon'_e} \qquad (6.7)$$

where again the subscript e refers to an effective quantity, that is the quantities measured by assuming TEM propagation. The dielectric losses will be additional to any other losses.

The attenuation is related to the unloaded Q factor by

$$Q_o = \frac{20\pi}{\ln 10} \cdot \frac{1}{\alpha_o \lambda_o} \qquad (6.8)$$

The factor $20\pi/\ln 10$ is a conversion from $\alpha_o \lambda_o$ (decibels) to $\alpha_o \lambda_o$ (nepers).

The quantities Z_0, α_o and ϵ'_e are functions of the geometry of the microstrip, usually expressed in terms of w/h and t, the ratio strip width to dielectric thickness and thickness of the conductor.

Most analyses of microstrip lines are based on the conformal mapping treatment of Wheeler[71]. Useful expressions for the impedance, attenuation and effective dielectric constant have been derived by Schneider[72].

6.2 The impedance.

For dielectric measurements the impedance of the line is not of much importance but it is used in the calculation of the attenuation caused by the conductor losses, α_o .

Schneider[72] derives expressions for Z_0 from the equations

$$Z_o = \frac{1}{2\pi}\sqrt{\frac{\mu_o}{\epsilon_o}} \cdot \ln\left[\sum_{n=1}^{\infty} a_n \left(\frac{h}{w}\right)^n\right] \qquad \text{for } w/h \leq 1 \quad (6.9)$$

and

$$Z_o = \sqrt{\frac{\mu_o}{\epsilon_o}} \Big/ \sum_{n=1}^{\infty} b_n \left(\frac{w}{h}\right)^n \qquad \text{for } w/h \geq 1 \quad (6.10)$$

where a_n and b_n are constants. These equations are generalisations of

$$Z_o = \frac{1}{2\pi}\sqrt{\frac{\mu_o}{\epsilon_o}} \cdot \ln\frac{8h}{w} \qquad \text{for } w \ll h$$

and $$Z_o = \sqrt{\frac{\mu_o}{\epsilon_o}} \cdot \frac{h}{w} \qquad \text{for } w \gg h$$

Equations (6.9) and (6.10) can be approximated to give fairly accurate values ($\pm$ 0.25%[73]) for the range $0 \leq w/h \leq 10$. For most applications $w/h \approx 1$.

The resulting equations for the impedance are

$$Z_o = \frac{1}{2\pi}\sqrt{\frac{\mu_o}{\epsilon_o}}\ln\left(\frac{8h}{w} + \frac{w}{4h}\right) \qquad \text{for } w/h \leq 1 \qquad (6.11)$$

and

$$Z_o = \sqrt{\frac{\mu_o}{\epsilon_o}}\Big/\left[\frac{w}{h} + 2{\cdot}42 - 0{\cdot}44\frac{h}{w} + \left(1-\frac{h}{w}\right)^6\right] \qquad \text{for } w/h \geq 1 \qquad (6.12)$$

6.3 The effective dielectric constant.

6.3.1 Static derivation.

The results of Wheeler[71] can be approximated to give a relation between ϵ'_e and ϵ'_r. This is

$$\epsilon'_e = \frac{\epsilon'_r + 1}{2} + \frac{\epsilon'_r - 1}{2} \cdot F\left(\epsilon'_r, \frac{w}{h}\right) \qquad (6.13)$$

A suitable approximate function for F is[73]

$$F\left(\epsilon'_r, \frac{w}{h}\right) = \left(1 + 10\frac{h}{w}\right)^{-\frac{1}{2}} \qquad (6.14)$$

and so

$$\epsilon'_e = \frac{\epsilon'_r + 1}{2} + \frac{\epsilon'_r - 1}{2} \cdot \left(1 + 10\frac{h}{w}\right)^{-\frac{1}{2}} \qquad (6.15)$$

This expression has an accuracy of about $\pm$ 2%[72].

Equation (6.15) was derived from static conditions and measurements of the effective dielectric constant over a range of frequencies show that ϵ'_e is an increasing function

of frequency[73],[74],[75],[76]. Over the range 1 to 12 GHz the dispersion increases to about 10% depending on Z_0 and h.

6.3.2 Dispersive relations for the effective dielectric constant.

Various empirical equations have been derived to account for the dispersion. For example

Arnold:[77]

$$\frac{1}{\sqrt{\epsilon'_e}} = \frac{1}{\sqrt{\epsilon'_{eo}}} - \left[1{\cdot}15\left(\frac{W}{h}\right)^{0{\cdot}211}\left(\epsilon'_{eo}\right)^{2{\cdot}04} f_{GHz} \cdot 10^{-5}\right] \qquad (6.16)$$

ϵ'_{eo} is ϵ'_e calculated from equation (6.15) and f_{GHz} is the frequency in gigahertz.

Chudobiak, Jain and Makios:[78]

$$\epsilon'_e = 3.10^{-6}\left(\epsilon'_m + 1\right)\left(\epsilon'_m - 1\right)h\left[Z_o \frac{W'}{h}\right]^{\frac{1}{2}}\left(f_{GHz} - f_o\right) + \epsilon'_{eo} \qquad (6.17)$$

where $$W' = W + \frac{t}{\pi}\left(1 + \ln\frac{2h}{t}\right)$$

$$f_o = \frac{6{\cdot}0}{\left(\epsilon'_r - 1\right)^{\frac{1}{2}}}\sqrt{\frac{Z_o}{h}}$$

and ϵ'_m is the measured effective dielectric constant below $f_{GHz} = f_0$.

and Schneider:[79]

$$\frac{1}{\sqrt{\epsilon'_e}} = \frac{\frac{1}{\sqrt{\epsilon'_r}} \cdot \left(\frac{f}{f_c}\right)^2 + \frac{1}{\sqrt{\epsilon'_{eo}}}}{\left(\frac{f}{f_c}\right)^2 + 1} \qquad (6.18)$$

where $f_c = \frac{c}{4h\sqrt{\epsilon'_r - 1}}$ = the cut off frequency of the lowest order TE surface wave, and f is the frequency of the measurement.

Jain, Makios and Chudobiak[75] have deduced a dispersion equation based on coupling between the microstrip TEM mode and the lowest order TM mode. The lowest order TM mode (TM_0) has no lower cut-off frequency for an infinitely wide substrate[80] and coupling is likely as the field components of the TM_0 mode coincide with those of the quasi TEM mode.

The resulting expression for the effective dielectric constant is

$$\epsilon'_{e_{1,2}} = \left[\frac{\sqrt{\epsilon'_{eo}} + \sqrt{\epsilon'_{TM}}}{2} \pm \sqrt{\left(\frac{\epsilon_{12}}{\xi} \cdot \frac{\epsilon_{21}}{\xi} \cdot (\xi)^2 + \left[\frac{\sqrt{\epsilon'_{eo}} - \sqrt{\epsilon'_{TM}}}{2}\right]^2\right)}\right]^2 \qquad (6.19)$$

where ϵ'_{TM} is the effective dielectric constant for the TM_0 mode, $\frac{\epsilon_{12}}{\xi} = \frac{\epsilon_{21}}{\xi}$ is the coupling coefficient between the modes and the other quantities are given by

$$\xi^2 = (\epsilon'_{eo}\ \epsilon'_{TM})^{\frac{1}{2}}$$

$$\epsilon^2_{12} = 0.22\,(\sqrt{\epsilon'_r} - 1)^2 \left(\frac{w}{h}\right)^{\frac{3}{4}} \left(\frac{f}{f_L}\right)^{\frac{1}{3}}$$

and

$$f_1 = \frac{c}{2\pi h}\left(\frac{2}{\epsilon'_r - 1}\right)^{\frac{1}{2}} \cdot \frac{\tan^{-1}\left[\epsilon'_r \cdot \dfrac{1+\left(1+\frac{10h}{W}\right)^{-\frac{1}{2}}}{1-\left(1+\frac{10h}{W}\right)^{-\frac{1}{2}}}\right]^{\frac{1}{2}}}{\left[1-\left(1+\frac{10h}{W}\right)^{-\frac{1}{2}}\right]^{\frac{1}{2}}}$$

f_1 is the frequency at which the phase velocity of the TEM mode equals that of the TM_0 mode.

Equation (6.19) predicts two solutions for the effective dielectric constant. At frequencies less than $f_1/2$ ϵ'_{e2} is less than unity and thus at these frequencies only one solution will be found.

The derivation of the dispersion equation is not wholly theoretical and comparison with experiment was needed in order to derive the form of some of the relations. However, the equation represents a considerable advance over previous expressions.

In using equation (6.19) to determine the dielectric constant an approximation has to be made for the value of ϵ'_{TM} which is given by

$$\epsilon'_{TM} = 1 + p^2/k_o^2 \qquad (6.20)$$

p is the wave number for the TM_0 mode and k_0 is the free space wave number $\left(\frac{2\pi f}{c}\right)$. p can be calculated as shown by Collin[81]. Approximation is needed because the

equations defining p are difficult to solve, but this has little effect on the accuracy as ϵ'_{TM} will not be greater than 2 or 3 and the square roots only are involved.

Equation (6.19) is valid over a wide range of dielectric constants ($2 \leq \epsilon'_r \leq 104$), substrate thicknesses (0·6 to 3 mm) and a not so wide range of w/h ratios (0·9 to 6)[75]. The accuracy is estimated to be about $\pm$ 2%.

6.4 Losses in microstrip.

The losses in microstrip lines have three sources:

(i) conductor losses
(ii) radiation losses
(iii) dielectric losses

These losses can be related to Q factors (Q_C, Q_R and Q_D) each inversely proportional to the particular loss. The total loss is the sum of the components and in terms of Q factors is given by

$$\frac{1}{Q} = \frac{1}{Q_c} + \frac{1}{Q_R} + \frac{1}{Q_D} \qquad (6.21)$$

To find the dielectric loss the conductor and radiation losses have to be calculated and subtracted from the total measured.

6.4.1 Conductor losses.

Losses in the conducting strip and ground plane depend on the resistivity of the metal ρ, the frequency, f, and the geometry of the microstrip. The current is concentrated approximately in a thickness δ, the skin depth, given by

$$\delta = \left(\frac{\rho}{\pi f \mu_0}\right)^{\frac{1}{2}} \qquad (6.22)$$

A related quantity is the skin resistance,

$$R_s = \rho/\delta = (\pi \mu_0 f \rho)^{\frac{1}{2}} \qquad (6.23)$$

Expressions for the conductor attenuation have been deduced by Pucel, Hartwig and Masse[82], Schneider[72], and Caulton, Hughes and Sobol[83].

The simplest way of treating the problem is to assume that the current is uniformly distributed across the strip width, w, and also concentrated in a width w in the ground plane. This is known as the "wide strip" approximation as it can be derived by assuming that $w/h \gg 1$. The resulting conductor attenuation is[84]

$$\alpha_c = R_s/Z_0 w \qquad (6.24)$$

Pucel et al[83] and Schneider[73] use a different method to determine α_c. If the dimensions of the

conductors are shrunk by a small distance δn and the corresponding increase in inductance is δL, then the radio frequency resistance is

$$R = \frac{R_s}{\mu_o} \cdot \frac{\delta L}{\delta n} \tag{6.25}$$

For a TEM mode

$$L = \sqrt{\epsilon_o \mu_o} \cdot Z_o \tag{6.26}$$

and

$$\alpha_c = \frac{R}{2Z_o} \tag{6.27}$$

giving

$$\alpha_c = \sqrt{\frac{\epsilon_o}{\mu_o}} \cdot \frac{R_s}{2Z_o} \cdot \frac{\delta Z_o}{\delta n} \tag{6.28}$$

Equations (6.11) and (6.12) for Z_0 are used in this equation.

The shrinkage δn will have contributions from the ground plane (δh), the bottom of the strip (δh), the edges of the strip ($-\delta w$), and the top and bottom of the strip ($-\delta t$), giving

$$\alpha_c = \sqrt{\frac{\epsilon_o}{\mu_o}} \cdot \frac{R_s}{2Z_o} \left[\frac{\partial Z_o}{\partial h} - 2\frac{\partial Z_o}{\partial w} - 2\frac{\partial Z_o}{\partial t} + \frac{\partial Z_o}{\partial h} \right] \tag{6.29}$$

To simplify this expression into practical terms

use has to be made of

$$\frac{\partial Z_o}{\partial h} = -\frac{w}{h^2} \cdot \frac{\partial Z_o}{\partial w/h}$$

$$\frac{\partial Z_o}{\partial w} = \frac{1}{h} \cdot \frac{\partial Z_o}{\partial w/h}$$

$$\frac{\partial Z_o}{\partial t} = \frac{\partial Z_o}{\partial w} \cdot \frac{\partial w}{\partial t} = \frac{1}{h} \cdot \frac{\partial Z_o}{\partial w/h} \cdot \frac{\partial w}{\partial t}$$

to give

$$\alpha_c = -\sqrt{\frac{\epsilon_o}{\mu_o}} \cdot R_s \cdot \frac{\partial Z_o}{\partial w/h} \cdot \frac{1 + \frac{w}{h} + \frac{\partial w}{\partial t}}{h Z_o} \qquad (6.30)$$

To include the effects of the strip thickness, t, Wheeler's[84] correction to the actual width is used i.e.

$$\Delta w = \frac{t}{\pi}\left(1 + \ln \frac{4\pi w}{t}\right) \qquad (6.31)$$

for $w/h \leq \frac{1}{2\pi}$

$$\Delta w = \frac{t}{\pi}\left(1 + \ln \frac{2h}{t}\right) \qquad (6.32)$$

for $w/h \geq \frac{1}{2\pi}$

the qualifications for the use of these expressions are that $t \ll h$ and $t < w/2$; these are usually satisfied in practical situations.

The width w in the equations above should be the

effective width, w', given by

$$w' = w + \Delta w \tag{6.33}$$

thus taking the thickness of the strip into account.

The final results for the attenuation are

$$\alpha_c = 60\sqrt{\frac{\epsilon_0}{\mu_0}} \cdot \frac{R_s\left(\frac{8h}{w} - \frac{w}{4h}\right)\left(1 + \frac{h}{w} + \frac{h}{w}\cdot\frac{\partial w'}{\partial t}\right)}{h Z_0 \exp(Z_0/60)} \tag{6.34}$$

for $w/h \leq 1$

and

$$\alpha_c = \frac{\epsilon_0}{\mu_0}\cdot\frac{R_s Z_0}{h}\left[1 + 0{\cdot}44\left(\frac{h}{w}\right)^2 + 6\left(\frac{h}{w}\right)^2\left(1-\frac{h}{w}\right)^5\right]\left[1 + \frac{w}{h} + \frac{\partial w'}{\partial t}\right] \tag{6.35}$$

for $w/h \geq 1$

The effective width w' has not been used except in the expression $\frac{\partial w'}{\partial t}$: this is because w' is not very different from the true width except for very thin strips. In all the analyses the strips are assumed to be several skin depths thick and so the approximation will have little effect.

Pucel et al[82] treat the conductor attenuation so that the resulting equations are valid for three ranges

of the ratio w/h. The most practical range is the middle one where $\frac{1}{2\pi} \leq w/h \leq 2$ and the attenuation is

$$\alpha_c = \frac{R_s}{2\pi h Z_o}\left[1-\left(\frac{w}{4h}\right)^2\right]\left[1+\frac{h}{w}+\frac{h}{w}\cdot\frac{\partial w'}{\partial t}-\frac{t}{\pi w}\right] \qquad (6.36)$$

The difference between equations (6.34), (6.35) and (6.36) at $w/h = 1$ is small and can be neglected as far as practical measurements are concerned.

6.4.1.1 Thin conductors.

It may not be practical to construct microstrip lines with conductors having sufficient thickness to satisfy the equations derived for the conductor attenuation. (i.e. where it was assumed that t was at least a few skin depths). This may be particularly true at the lower frequencies (i.e. near 1 G Hz) where the skin depth is greatest. To compensate for this the skin resistance, R_s, can be modified. Welch and Pratt[85] quote the expression

$$R_s' = R_s \frac{\sinh\left(\frac{2t}{\delta}\right)+\sin\left(\frac{2t}{\delta}\right)}{\cosh\left(\frac{2t}{\delta}\right)-\cos\left(\frac{2t}{\delta}\right)} \qquad (6.37)$$

which has the form shown in figure (6.1). More recently Horton, Easter and Gopinath[86] found a similar result for the variation of the attenuation with t/δ. As the attenuation is proportional to the skin resistance the two results are equivalent. The effect of this correction is to increase the conductor attenuation by about 20% above the

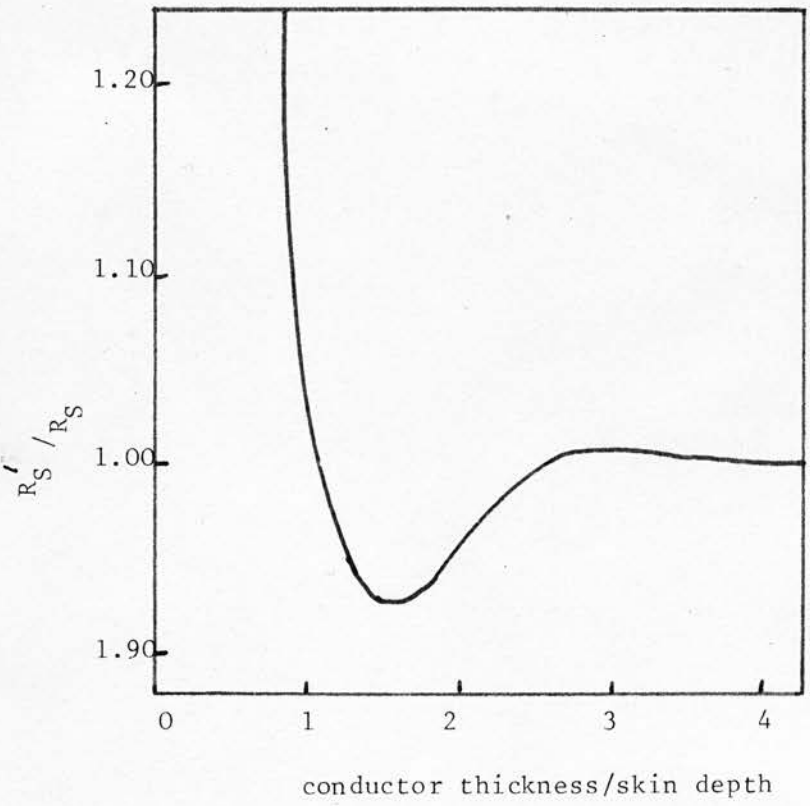

Figure (6.1)

Effective resistance for thin conductors
(from Welch and Pratt [85])

value for thick strips, when the strip thickness is equal to one skin depth.

6.4.1.2 Surface roughness.

The surface of the dielectric can affect the apparant resistance of the conductors[82],[87]. If the ratio of the root mean square surface roughness to the skin depth is greater than 3 or 4 the increase in skin resistance can be as much as 60%[87].

6.4.2 Radiation losses.

Radiation losses in microstrip are difficult to estimate with any certainty. Little quantitative work has been published on radiation from the strip though some details of radiation from discontinuities have appeared. The most important work was done by Lewin[88] who deduced that the fractional power radiated from a particular discontinuity has the form

$$\frac{P_r}{P_o} = 2\pi \sqrt{\frac{\epsilon_o}{\mu_o}} \left(\frac{h}{\lambda_o}\right)^2 \cdot \frac{F(\epsilon'_e)}{Z'} \qquad (6.38)$$

where $F(\epsilon'_e)$ is a function of the effective dielectric constant depending on the form of the discontinuity.

For an open circuit (possibly applicable to a

resonator)

$$F(\epsilon'_e) = \frac{\epsilon'_e + 1}{\epsilon'_e} - \frac{(\epsilon'_e - 1)^2}{2\epsilon'_e \sqrt{\epsilon'_e}} \cdot \ln\left[\frac{\sqrt{\epsilon'_e} + 1}{\sqrt{\epsilon'_e} - 1}\right] \qquad (6.39)$$

Denlinger[89] has shown that equation (6.38) agrees fairly closely with experiment.

Particular resonators will each emit different amounts of radiation depending on their geometry and several are discussed by Roberts and Easter[90]. In particular they give details of the radiation from a ring resonator. Their graph providing the radiation Q is reproduced in figure (6.2). In general the higher the dielectric constant and the smaller the dielectric thickness, the lower will the radiation be.

6.4.3 Dielectric losses.

The quantity related to dielectric losses that can be deduced from measurements is the dielectric Q factor, Q_D. The relation between Q_D and the effective dielectric constants was given in equation (6.7) (i.e. $1/Q_D = (\tan\delta)_e = \frac{\epsilon''_e}{\epsilon'_e}$).

Schneider[91] shows that

$$(\tan\delta)_e = \frac{\epsilon'_r}{\epsilon'_e} \cdot \frac{\partial \epsilon'_e}{\partial \epsilon'_r} \cdot \tan\delta \qquad (6.40)$$

and using equation (6.15) for the relation between the true

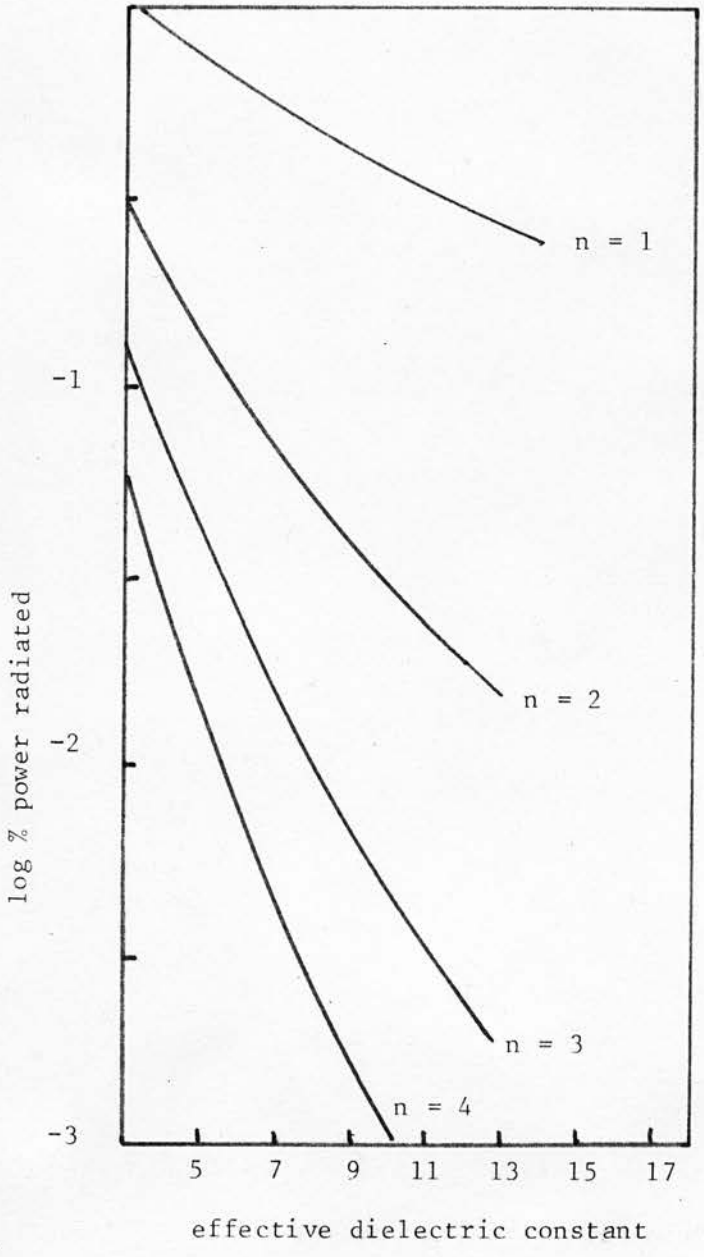

Figure (6.2)

Radiation from ring resonators (from Roberts and Easter[90])

(n = order of resonance)

f = 10GHz, Z_o = 50 ohm, h = 25 mm

% power radiated = $(2\pi/Q_r) \times 100$

and effective dielectric constants results in

$$(\tan\delta)_e = \frac{\epsilon'_r}{\epsilon'_e} \cdot \frac{\epsilon'_e - 1}{\epsilon'_r - 1} \cdot \tan\delta \qquad (6.41)$$

which enables $\tan\delta$ to be found from measurements of Q_D and ϵ'_e .

The frequency dependent form for the effective dielectric constant (equation (6.19)) should be used in equation (6.41) rather than the static solution (equation (6.15)) in order to reduce errors for frequencies above about 2 or 3 G Hz.

6.5 Microstrip resonators.

The simplest way of determining dielectric parameters using a microstrip technique is to measure the resonant frequency and Q factor of a resonator. Since the size of a microstrip resonator cannot be altered the frequency must be varied, to determine these quantities. In general a resonance will occur when the dimensions of the resonator are an integral number of half wavelengths in the dielectric. Two forms of resonator are shown in figure (6.3).

The conditions for resonance are:

line resonator $$\frac{n\lambda_g}{2} = l \qquad (6.42)$$

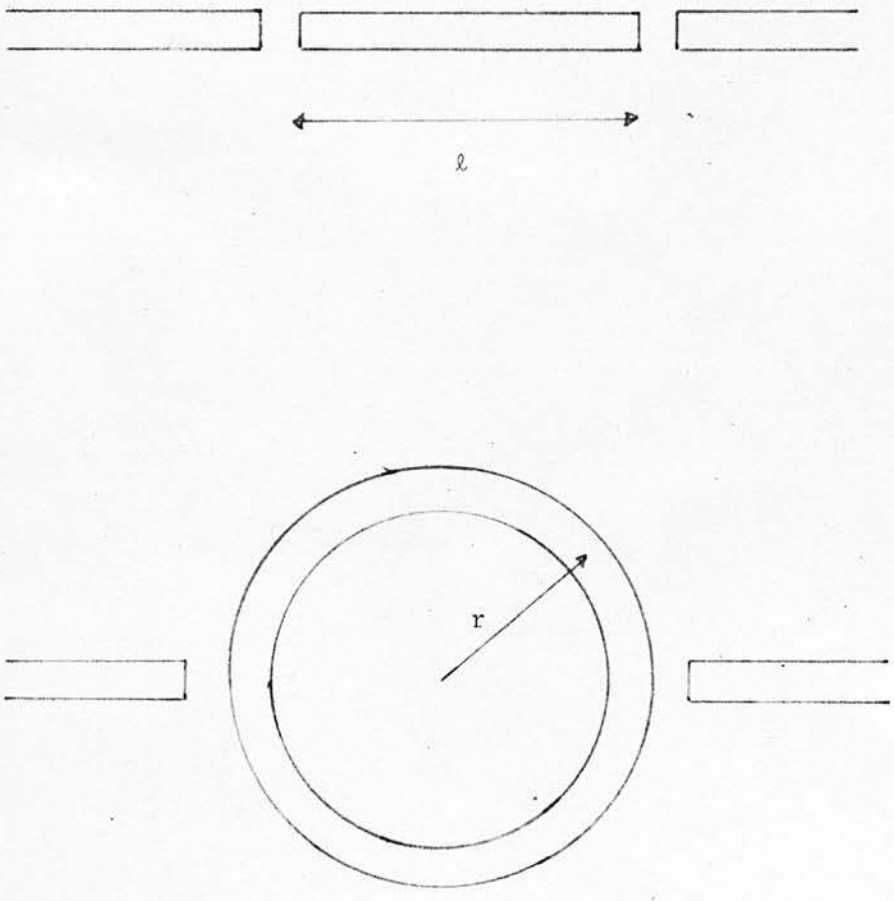

Figure (6.3)

Microstrip line and ring resonators

ring resonator[73]

$$\frac{n\lambda_g}{2} = \pi r \qquad (6.43)$$

n is an integer and l and r are defined in the figure. In the case of the ring the radius used is the arithmetic mean of the two radii of the annulus.

Although the straight line resonator appears at first sight to be simpler in so far as construction and calculation are concerned (e.g. the length l can be measured exactly, whereas the radius of the ring is not so well defined), a fringing field at the ends extends the apparent length, causing an error in the dielectric constant measurement. The problem can be overcome if measurements are made on substrates of the same thickness but with differing lengths, l. This allows the correction to be deduced[92].

The ring resonator is free from this effect and, in addition, a similar size of substrate has a longer resonant length.

The effective dielectric constant is found from equation (6.43):

$$\frac{n\lambda_g}{2} = \frac{n\lambda_o}{2\sqrt{\epsilon'_e}} = \pi r \qquad (6.44)$$

or

$$\sqrt{\epsilon'_e} = \frac{nc}{2\pi r f_o} \qquad (6.45)$$

for resonant frequency f_o.

Over a range of frequencies there will be several resonances depending on the radius of the ring. The unknown integer n in equation (6.45) can be determined by a knowledge of the approximate effective dielectric constant. Over a series of resonances any errors in the choice of n are easy to detect as the resulting dielectric constant should not change much from resonance to resonance.

The dielectric losses are calculated from measurements of the total Q factor at each resonance.

6.5.1 Ring resonator theory.

The ring resonator can be considered as an annular cavity with the fields confined between the conductors and the radii of the ring. The general solution of Maxwell's equations in cylindrical coordinates for the quasi-TEM mode is

$$E_z = [A J_n(kr) + B Y_n(kr)] \cos n\phi \qquad (6.46)$$

$$H_r = \frac{n}{i\omega\mu_o r} [A J_n(kr) + B Y_n(kr)] \sin n\phi \qquad (6.47)$$

$$H_\phi = \frac{k}{i\omega\mu_o} [A J'_n(kr) + B Y'_n(kr)] \cos n\phi \qquad (6.48)$$

J_n and Y_n are Bessel functions of the first and second kinds of order n, k is the wave number and the primes refer to differentiation with respect to kr. As $k = 2\pi/\lambda_g$,

for the microstrip case use of the effective dielectric constant is needed giving

$$k = \frac{2\pi f}{c} \cdot \sqrt{\epsilon'_e} \qquad (6.49)$$

The conditions for resonance follow from application of the boundary conditions and solution of the resulting equation. At the radii r_1 and r_2 of the inner and outer edges of the ring the magnetic field will have a radial component only so equation (6.48) gives (on eliminating the constants A and B)

$$\frac{J'_n(kr_1)}{J'_n(kr_2)} - \frac{Y'_n(kr_1)}{Y'_n(kr_2)} = 0 \qquad (6.50)$$

Equation (6.50) still has two unknowns, the frequency and the effective dielectric constant, but in an experiment the resonant frequency can be measured accurately and so the dielectric constant can be determined.

The purpose of performing this calculation is to determine whether the use of the arithmetic mean radius (equation (6.45)) is sufficiently accurate. Wolf and Knoppik[93] have shown that provided the curvature of the ring is not too great and the strip width is small compared with the wavelength in the dielectric, then use of the mean radius is correct.

A computer programme has been written (appendix A.2)

which solves equation (6.50) for the effective dielectric constant when the size of the resonator, resonant frequencies and integer n associated with each resonance are known.

6.6. Limitations of microstrip.

In spite of being useful over a wide frequency range where the quasi-TEM mode is dominant the existence of other modes must be considered. Mention has already been made of the TM_0 mode and its result on the effective dielectric constant (section (5.3)). Other modes impose a limit on the upper frequency for microstrip propagation: this limit is the cut-off frequency for the lowest order TE surface mode and is also the frequency for strong coupling to the lowest order TM mode[80]. The limit is

$$f_c = \frac{c}{4h\sqrt{\epsilon'_r - 1}} \qquad (6.51)$$

which is also used in the dispersion equations for the dielectric constant (e.g. eqn. (6.18)).

For a typical microstrip with $h = 1$ mm and $\epsilon'_r = 10$, f_c is about 25 G Hz.

There is also the possibility that transverse modes may exist when the strip width is too great (i.e. $\omega \approx \lambda_g/2$), but these modes occur at high frequencies

for narrow microstrips. For dielectric measurements a width of about 1·5 mm is practical and even if ϵ'_e is 9 the frequency limit is about 33 G Hz.

CHAPTER 7

Microstrip Measurement Technique

The technique for making microwave measurements proved simple to operate but difficult to interpret in terms of dielectric parameters. There was, therefore, a need to check the results and it was decided to make some measurements on an alumina substrate of known dielectric constant and loss. Alumina has a dielectric constant close to the probable value for $As_2 S_3$ and $As_2 Se_3$ and a low dielectric loss. The purpose in these measurements was not to provide an "absolute" standard but merely to obtain an indication of the accuracy of the theoretical equations for dispersion and dielectric loss that are described in Chapter 6. The dielectric properties of alumina depend on the purity and grain size and therefore the microwave properties were not known with extreme accuracy. The manufacturers quoted variations of $\pm$ 5% in dielectric constant and a result within this range could be considered satisfactory. The low dielectric loss was useful for indicating the sensitivity of the technique. The alumina resonators provided a useful method for comparison with the measurements on amorphous semiconductors.

7.1 Experimental equipment and procedure.

A block diagram of the apparatus is shown in figure (7.1). The microwave signal was provided by an

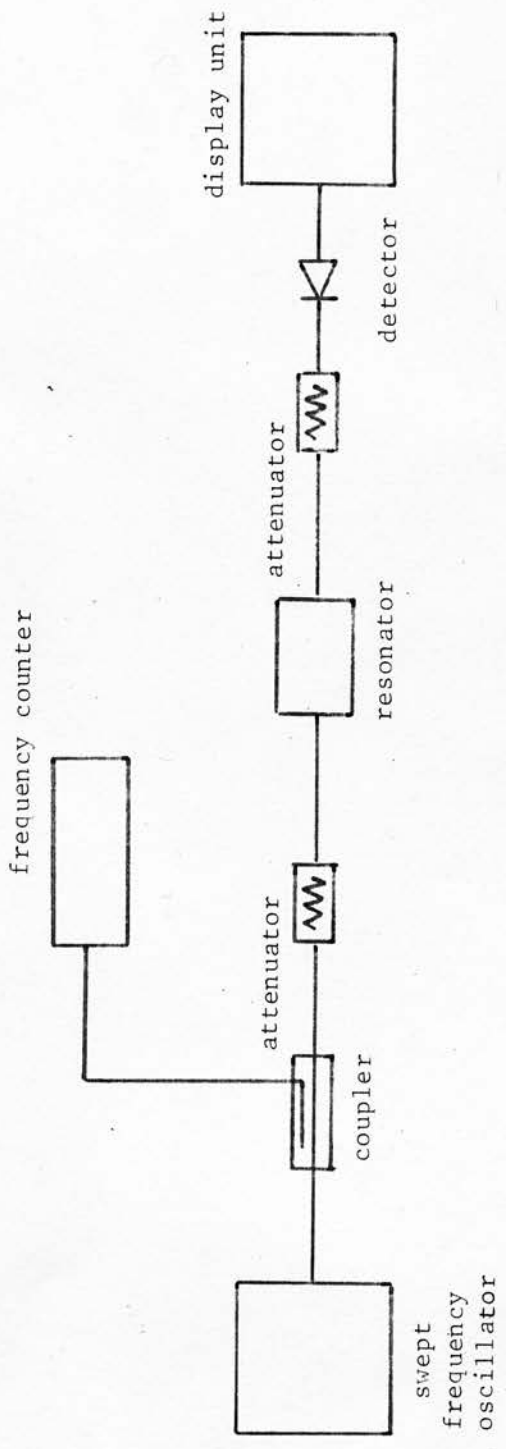

Figure (7.1)

Microstrip experimental arrangement

M.E.S.L. type M1000 swept oscillator and suitable plug-in units or an M.E.S.L. type MX882 oscillator (for 8 to 12·4 GHz only). The whole range from 1·8 to 12·4 GHz was covered. In order to dampen the effect of reflections due to the connectors in the line, two attenuators (OSM type 20600, 6 and 10 db) were placed on either side of the resonator. The detected signal was displayed on an M.E.S.L. microwave display unit type M2100 which was calibrated in decibels greatly simplifying measurements of resonator Q factors. The oscillators had the facility for automatic frequency sweeping over a complete band (e.g. 8 to 12·4 GHz) or over a limited portion of the band at variable rates. Manual frequency changing was also possible and this was used when accurate resonant frequency and Q measurements were made. The frequency was read from an E.I.P. autohet frequency counter type 351A which was connected to the oscillator via a 10 db directional coupler. The counter was only used when the frequency was changed manually. The display unit gave a visual indication of the resonances and allowed a rapid assessment of the approximate resonant frequencies.

To make the measurements the procedure was:

(a) Use the oscillator on as wide a sweep as possible, with a fast sweep rate. This allows the resonances to be found and any spurious responses resulting from loose connectors or the microstrip not being held correctly by the sample holder and thus making bad contacts with the rest of

the circuit.

(b) Once the resonant frequencies had been determined roughly using the frequency markers generated by the oscillator and all other responses had been reduced so that they were small compared with the transmitted power at resonance then the frequency sweep was narrowed so that the manual sweep could be used to determine accurately the resonant frequency.

(c) At the resonant frequency the signal on the display was reduced by 3 db. (i.e. to half power) by means of the calibrated y shift of the display unit and one of the three cursors on the display screen adjusted to coincide with this level.

(d) The power was increased to its original level and the manual control used to vary the frequency to find the half power points. The frequency at these points (i.e. where the signal coincided with the cursor) was measured on the counter. The Q factor was calculated from

$$Q = \frac{f_o}{f_2 - f_1} \qquad (7.1)$$

for resonant frequency f_o and half power width $f_2 - f_1$.

7.2 Microstrip sample holder.

7.2.1 Design

The microstrip resonators should be held firmly in place during measurements and a sample holder was required

to do this, as well as be used with resonators of various thicknesses and widths.

The sample holder is shown in figure (7.2) Adjustments for differing thicknesses were made at the connector supports and at the clamps. The clamps were used to give support to either OSM to type N coaxial adaptors or to the fixed attenuators in the circuit. The slots in the support blocks provided for any changes in resonator area. For each size of substrate a brass plate was cut to just under the substrate width and its faces ground flat. This supplied a good base for the resonator giving adequate contact between the ground plane and the outer conductor of the coaxial line. The electrical connection to the microstrip was made by adjusting the connector supports to give a pressure contact between the tab of the OSM to microstrip adaptor and the microstrip. Adequate coupling to the resonator (i.e. providing a measurable output signal) could often be achieved with no "physical" contact between the microstrip and the tab. In this case the gap between the two could be of the order of 1 mm.

7.2.2 Temperature variation.

Temperature variation of the resonator proved fairly simple. A Montford Mini A Mk.2 temperature control unit was used, and the resonator and its holder were heated and cooled together. An asbestos door was made to prevent the radiated microwave power from resonating in the metal

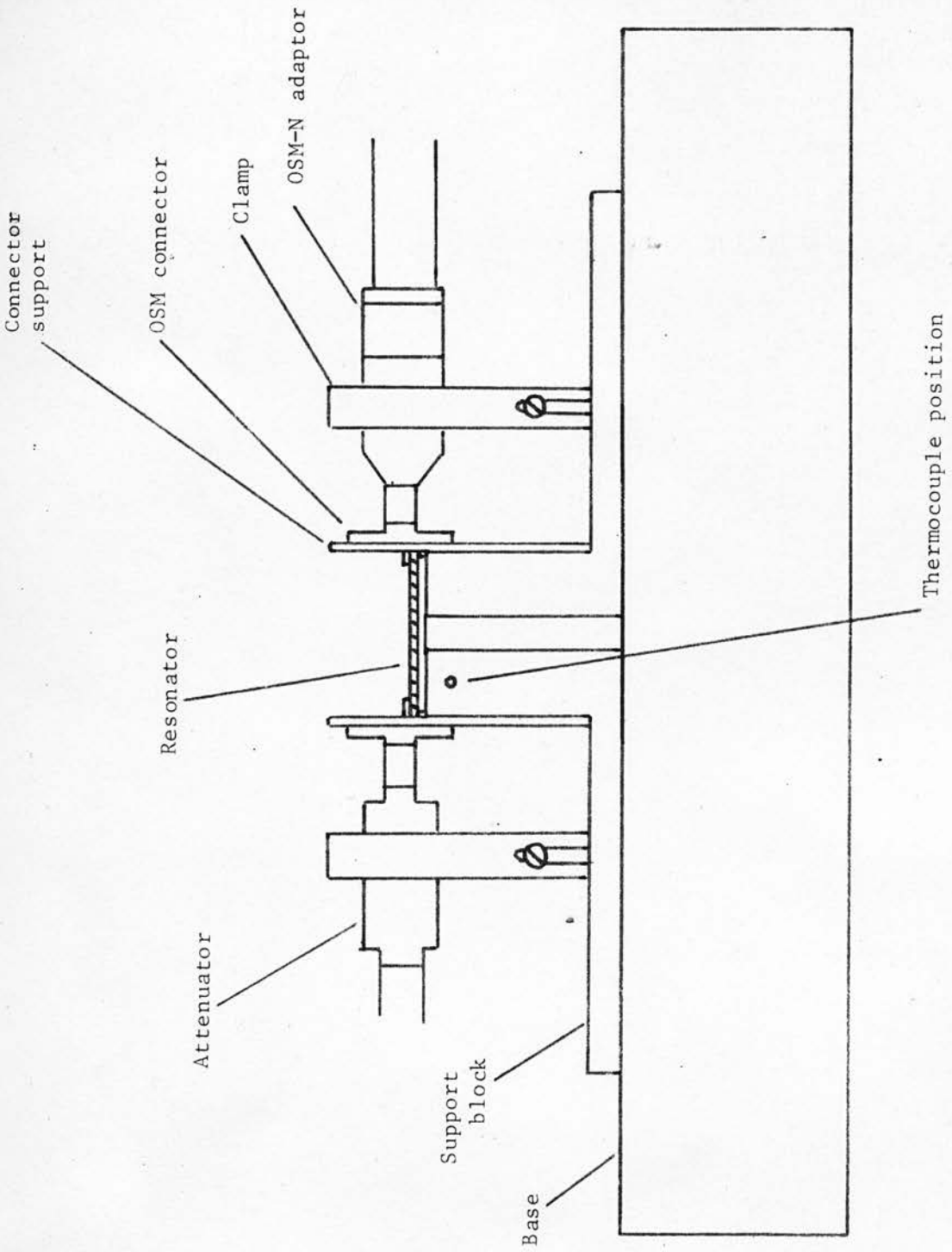

Figure (7.2)

Microstrip sample holder

chamber and a hole was cut in the door to allow access to the resonator. Semi-rigid 0·141 inch diameter coaxial cables were used to and from the resonator so that the attenuators and detector could be positioned outside the chamber and not be subjected to much temperature variation.

Liquid nitrogen was used as the coolant and in practice the temperature range proved to be 90 to 380 K.

The temperature was measured using a chromel-alumel thermocouple positioned in the supporting block just below the substrate. To allow for any temperature lag between the substrate and the metal support the system was left for 20 minutes at a particular temperature before a measurement was made. There was no difference between measurements taken as the temperature was falling or rising.

The resonator did not ice up at low temperatures. This was discovered by opening the chamber when the whole system was at about a temperature of 100 K.

7.3 Resonator preparation.

The alumina substrates had one face polished and therefore no initial preparation was needed before the conductor deposition.

7.3.1 Electrode deposition.

For proper microstrip transmission (i.e. satisfying the theoretical equations) conductors are required with a thickness greater than two skin depths[85]. At two gigahertz the skin depth for gold is about 3·6 μm so for a thickness of less than 7 μm a correction as described in section (6.4.1.1) has to be made to the skin resistance.

The metal chosen for the conductors was gold as this has a low resistivity, does not oxidise and is easily deposited in thick layers. In order to ensure that there was good adhesion between the gold and the dielectric a very thin (i.e. just visible on the glass bell jar of the evaporator) layer of nichrome was initially deposited on the surface in an electron beam evaporator. To avoid overheating the dielectric the gold was deposited in thin layers with a sufficient time between evaporations for the substrate to cool (about 20 minutes). This procedure was not necessary when alumina was used but As_2S_3 and As_2Se_3 have low melting points and can crack easily if subjected to thermal stress. In the majority of cases the adhesion of the gold was good.

An important point in the procedure was to ensure that the substrate was clean and free from dust before evaporation. The sample was cleaned several times in trichloroethylene in an ultrasonic cleaner and before it was mounted above the electron gun it was held face downwards in

the cleaning fluid and kept this way when removed, dried and mounted in the evaporator. The substrate was supported, about 6 inches from the electron gun, by an aluminium plate with a suitable hole cut in it.

7.3.2 The photo-etching process.

To achieve the correct conductor pattern on the dielectric it was decided that it would be best to use a photo-etching process.

Photographic masks were prepared of two ring resonators of mean radii 9·67 mm and 16·4 mm and conductor widths 1·5 and 2·0 mm respectively. Straight line resonator masks of lengths 17, 14 and 18 mm and widths 2·0, 1·5 and 2·0 mm respectively were also made. The coupling gaps were either 0·5 or 1·0 mm.

When the gold had been deposited on the polished surface, the sample was cleaned, dried and then a few c.c.s of Shipley AZ positive photo-resist were applied to the surface with a syringe. To provide an even film of resist the substrate was spun at 3000 r.p.m. for 30 seconds. Drying was carried out for 15 minutes at room temperature and 30 minutes at 50° C. When dry the mask was carefully positioned on the resist-covered side of the sample and then exposed to ultra-violet light for 30 seconds. The next stage was to develop the exposed surface using Shipley AZ

developer and etch the unwanted gold and nichrome. After the developing, and between each stage of etching, the sample was washed thoroughly in distilled water; when etching was complete the remaining photo-resist was removed with acetone.

At this stage the thickness of the gold film was measured on the "Talysurf".

7.3.3 Final preparation.

The last step in the fabrication of the resonator was the deposition of the ground plane. The gold was evaporated in the manner described in section (7.3.1). The upper side of the sample was covered with aluminium foil to prevent any metallic vapour condensing on the prepared resonator.

Finally the edges at the resonator input and output were ground down to eliminate any possible short circuits between the strip and ground plane caused by gold deposited on the sides of the substrate during evaporation.

7.4 Alumina measurements.

The alumina used was type Deranox 975 obtained from Andermann and Ryder. The substrates had one face polished and were one inch square and one millimetre thick. The dielectric properties quoted by the manufacturer were:

$$\epsilon'_r = 9.49$$

and $\tan\delta = 4{\cdot}3 \cdot 10^{-4}$

both at 25° C and a frequency of 9·368 GHz. The possible variation between samples was quoted as $\pm$ 5% for the dielectric constant.

The ring resonator was prepared with gold conductors and its parameters were:

strip width, $w = 1{\cdot}50$ mm

dielectric thickness, $h = 1{\cdot}00$ mm

conductor thickness, $t = 1{\cdot}78$ micron

mean resonator radius, $r = 9{\cdot}67$ mm

7.4.1 Results.

The measurements at room temperature, gave six resonances over the frequency range 1·8 to 12·4 GHz and a typical example (the resonance at 3·81 GHz) is shown in figure (7.3). Following the procedure detailed in section (7.1) each resonance provided a measurement of the effective dielectric constant and Q factor. The effective dielectric constant, calculated from

$$\sqrt{\epsilon'_e} = \frac{nc}{2\pi r f_o}$$

(equation (6.45)) as a function of frequency is plotted in figure (7.4). Also included in the figure is the theoretical

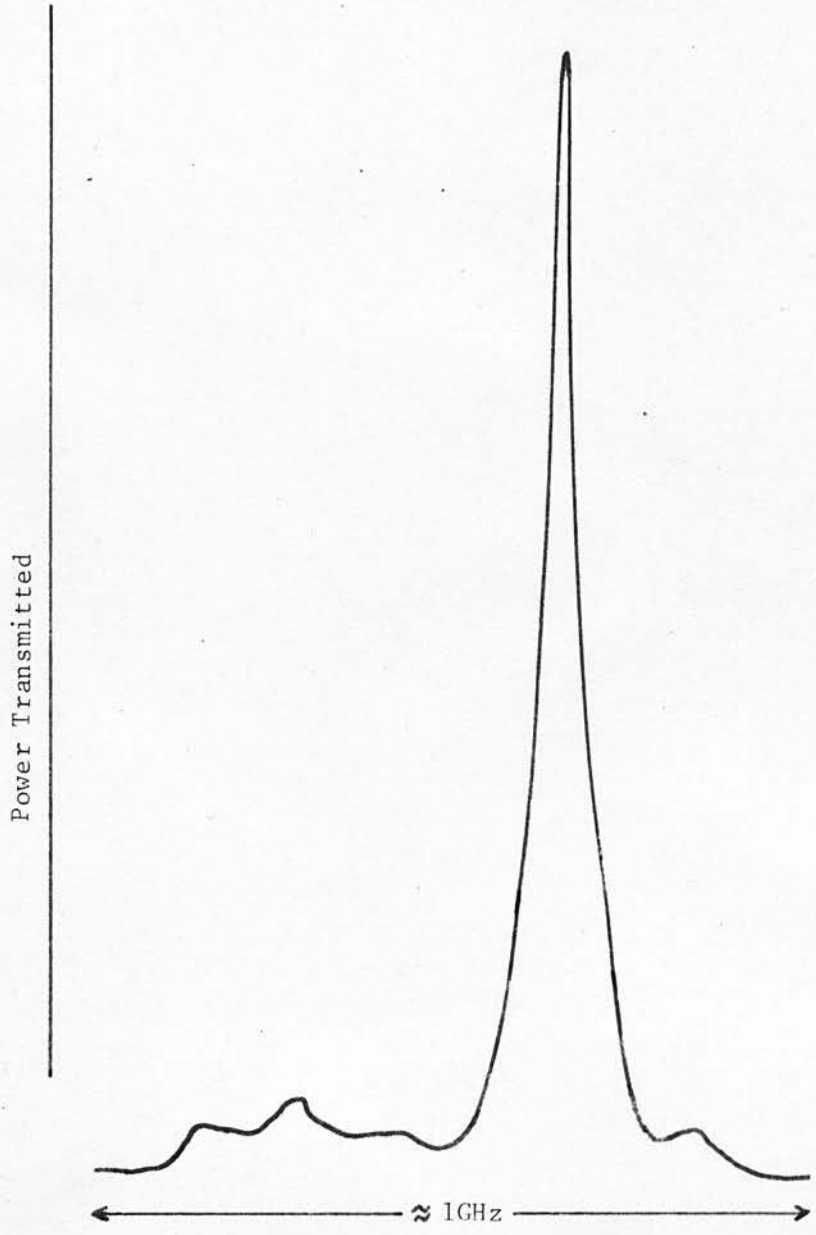

Figure (7.3)

3.81 GHz resonance of the alumina resonator

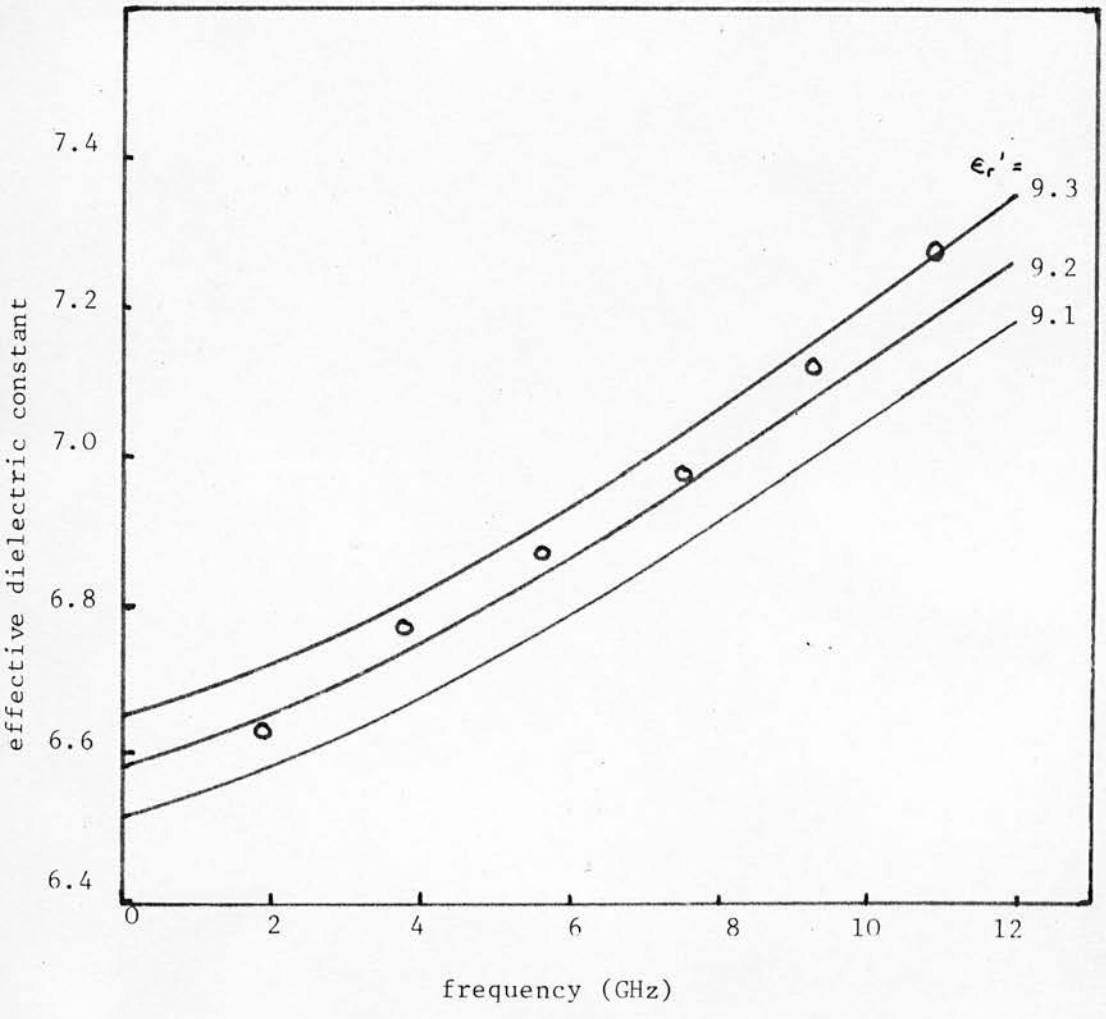

Figure (7.4)

Effective dielectric constant of alumina resonator

effective dielectric constant obtained from equation (6.19) for the geometrical parameters of the ring resonator (i.e. width, w and thickness, h) and for true dielectric constants between 9·0 and 9·4 . The figure shows that the true dielectric constant for the alumina is close to 9·25 over most of the frequency range.

Measurements of the dielectric loss were complicated by the numerous corrections to be made. The measured Q factor, Q_m, is an indication of the total losses in the system: conductor, radiation, dielectric and losses caused by the coupling of the resonator to the external circuit. The coupling can be accounted for by the equation[94]

$$Q_u = \frac{Q_m}{1-\sqrt{T}} \qquad (7.2)$$

Q_u is the unloaded Q factor and T is the ratio of transmitted to incident power at the resonant frequency. The unloaded Q factors varied from 172 at 1·91 GHz to 438 at 10.97 GHz.

There is evidence that the effective resistivity of the conductors is higher at microwave frequencies than at d.c.[95],[96],[97]. Patel[96] and Corkhill and O'Donnell[97] find that the effective resistivity is about four times the d.c. value over the whole range from one to twelve gigahertz. The present measurements, however, do not agree with this

as in most cases the correction is too drastic and negative loss tangents result. The method of deposition of the gold conductors used by these authors (screen printing instead of evaporation) may explain this. It is often found that the wide strip approximation for the attenuation (equation (6.24)) gives good results in practice[95], though strictly not valid for microstrip transmission lines. The reason for this is that the errors involved (i.e. neglecting fringing fields at the edge of the strip and the apparent increase in conductor resistivity) tend to cancel. The resulting loss tangents using equations (6.34) and (6.35) from Schneider[72] and the wide strip equation (6.24) are:

frequency	(loss tangent) . 10^3	
GHz	equation: Schneider	Wide strip
1·91	1·43	1·10
3·81	2·40	1·65
5·65	1·20	0·81
7·47	1·61	0·82
9·25	1·27	0·57
10·97	1·15	0·50

The manufacturers' quoted value is 0·43 . 10^{-3} at 9·368 GHz.

7.4.2 Comparison with expected results.

7.4.2.1 Dielectric constant.

The value of 9·25 for the relative permittivity (see figure (7.4)) is in good agreement with the manufacturers' quoted value (9·49), and it can be concluded that the theoretical equations give a sufficiently accurate description of the dielectric constant. There is a little deviation from theory at the higher frequencies ($\approx$ 10 GHz) but this is within the $\pm$ 2% accuracy of the equations used.

7.4.2.2 Dielectric loss

The measured values of the loss tangent are all higher than the quoted value. Figure (7.5) shows the loss tangent versus frequency for the two different calculations (Schneider and wide strip) of section (7.4.1).

The wide strip approximation shows fairly good agreement with the manufacturers' value, especially at high frequencies.

The dielectric Q factor for an alumina resonator is probably greater than 2000 ($\approx 1/\tan\delta$) and so these losses are dominated by the conductor losses (Q_c is about 200 to 800 depending on frequency, for the size of resonator used) and are even comparable with the theoretical radiation losses at low frequencies ($\approx$ 2 GHz). Bearing this in mind it is not surprising that the loss tangent appears too great by a factor of two or even three. The errors are smallest in the X-band region and these results should be

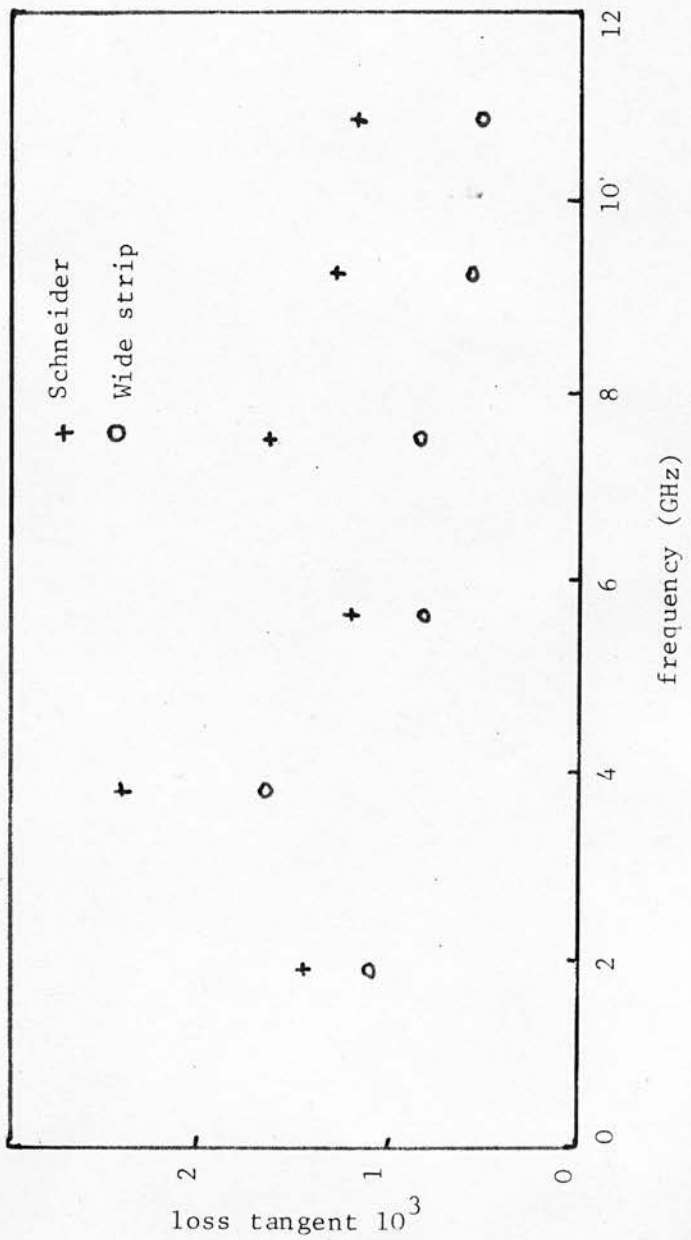

Figure (7.5)

Loss tangent of alumina

regarded as more reliable.

7.4.3 Conclusions.

It was considered that these results showed that the technique was useful for dielectric measurements of reasonable accuracy over a wide frequency range. The interpretation of dielectric properties, especially in amorphous solids, requires results over many decades of frequency and thus the inaccuracy in determinging the dielectric losses is not of major importance.

The results for the alumina resonator can be considered as a reference. If similar resonators are constructed (i.e. having similar physical dimensions and similar dielectric constants) a comparison of the Q values will show variations in the dielectric losses assuming all other losses are much the same.

7.5 Calculation and interpretation of the measured parameters.

The fairly complex and lengthy calculations that are needed to arrive at the dielectric constant and conductivity of the substrate material from the measurement of the physical dimensions of the resonator, its resonant frequency and Q factor were incorporated in a computer program. Most of the equations of chapter 6 were included,

but the essential parts were the determination of the effective dielectric constant and its transformation into the true dielectric constant (equations (6.45), (6.15) and (6.19)) and the derivation of the conductivity from the measured Q factor via equations (6.21), (6.34), (6.35) and (6.40) and also taking losses due to radiation into account.

The computer program is reproduced in appendix (A.2).

CHAPTER 8

Experimental Results

The aim of the measurements was to investigate the behaviour of the dielectric and electrical conduction properties of a range of simple glasses as a function of frequency and temperature. It was decided that the most useful information would come from microwave measurements and a low frequency study of materials based on the As - S and As - Se systems, as vitreous As_2S_3 and As_2Se_3 are regarded as "prototype" chalcogenide glasses.

8.1 Audio frequencies.

In order to perform accurate a.c. measurements it was decided to rebuild the existing Lynch bridge paying special attention to screening the leads. A new sample holder was designed and made that was capable of operating over a wide range of temperatures.

8.1.1 Coaxial sample holder.

A sample holder was needed which enabled measurements to be made on small discs of amorphous material. Also, as dielectric measurements involve two measuring operations - with the sample in the system and with the sample removed - the sample in the holder had to be switched in and out of the circuit at all temperatures. To eliminate as much as possible of the impedance of the sample holder, the switch

was positioned close to the sample.

It was decided to make the holder coaxial so that measurements were possible to high frequencies.

The sample holder is shown in cross-section in figure (8.1). The method of switching the sample in or out of the bridge circuit was to use a dry reed switch operated by a coil between the inner and outer conductors. To withstand high temperatures the coil was wound of aluminium oxide coated wire on a P.T.F.E. former. The reed switch could be operated by applying a few volts to the coil. The sample was held in place by a small spring making the lower end of the central conductor. This also ensured that the disc of material made good contact with the brass electrodes. To eliminate air-gaps between the sample and the electrodes, the electrodes were ground flat and polished. The electrode diameters were 12 mm.

The whole assembly was encased in a stainless steel tube for screening and to keep the conduction of heat to a minimum. To prevent ice forming round the sample at low temperatures the sample holder could be evacuated.

The temperature was measured by a chromel-alumel thermocouple placed near the sample.

8.1.2 Lynch bridge measurements.

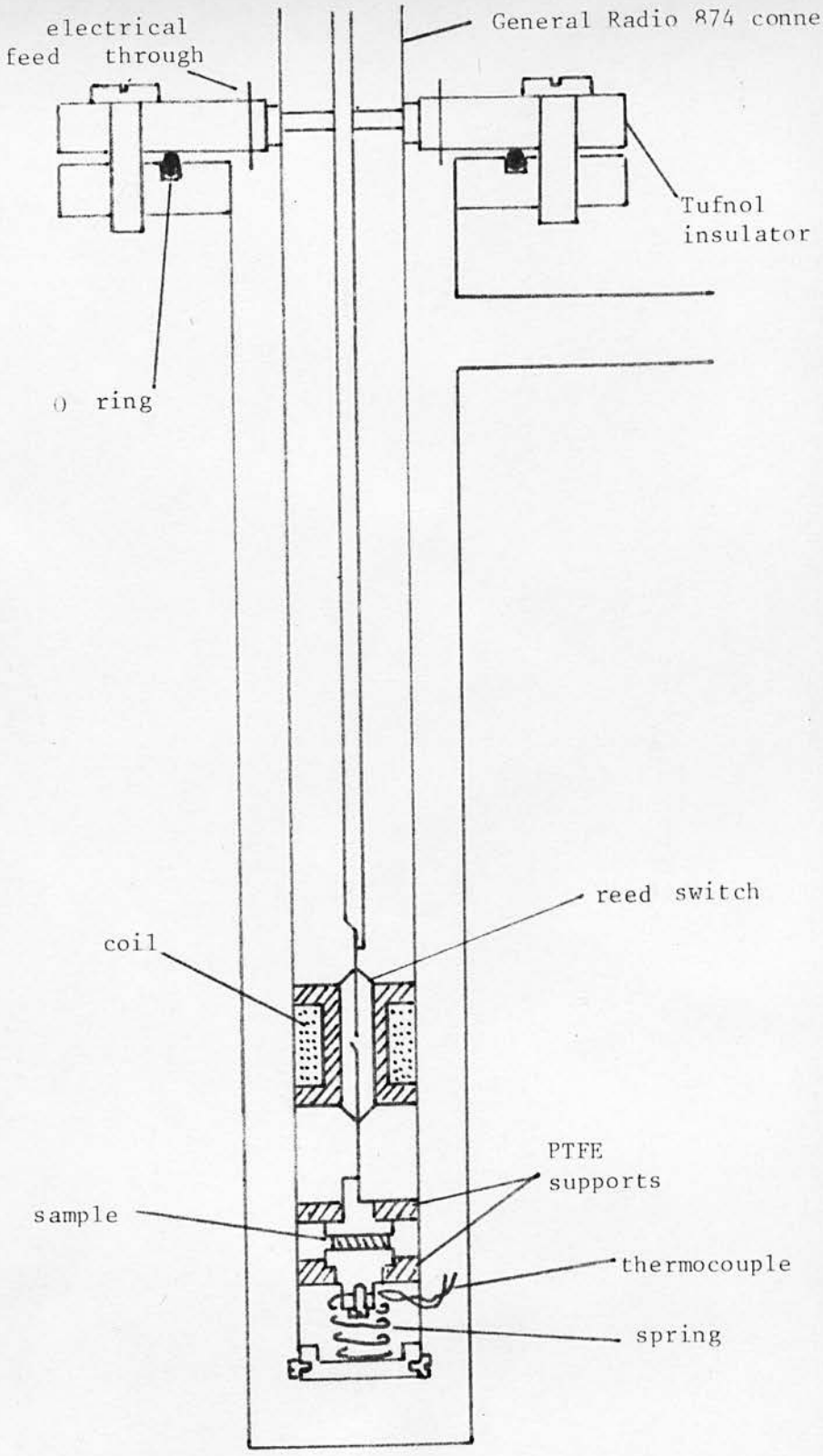

Figure (8.1)

Coaxial sample holder

The circuit of the Lynch bridge has been described in section (5.1). High stability carbon resistors were used for R_1 , R_2 , R_1' and R_2' , R_V and R_V' were non-inductive resistance boxes and C_V and C_V' precision air-spaced variable capacitors. A Hewlett-Packard type 3300A function generator was used as the source and the signal to be detected was amplified by a Brookdeal low noise amplifier type 450 before being detected by a General Radio type 1232-A tuned amplifier and null detector.

The bridge could measure conductances down to less than 10^{-11} ohm^{-1} and capacitances as small as one or two picofarads. The frequency range was restricted to a lower limit of 200 Hz by mains frequency pickup and an upper limit of 100 K Hz by the inductive behaviour of the bridge components. In practice the conductances of the materials measured were too small to be determined accurately below 700 Hz.

The temperature of the sample was varied by putting the sample holder to a depth of about 8 inches in the side opening of a Montford Mini A Mk 2 oven. In this way the sample temperature could be increased to 370 K. The sample temperature was measured by the thermocouple and a Computing Techniques type DM2-1 digital voltmeter. The cold junction was kept in a mixture of ice and water. As the thermocouple was not in contact with the sample the apparatus was left for about 20 minutes after the thermocouple reached the

required temperature so that the holder could reach equilibrium.

The bridge was checked for errors by removing the lower electrode and measuring the impedance of the holder between the reed switch and upper electrode and the outer conductor. It was found that there was a residual capacitance of 1·55 pF but the conductance was too small to measure. The capacitance would appear in parallel with a sample and could easily be subtracted from the total capacitance measured. The additional capacitance was independent of frequency. Measurements on high value resistors were generally a few per cent higher than their marked values but as the results are usually plotted on a logarithmic scale this error is not very significant.

8.1.3 Three terminal measurements.

Accurate dielectric measurements on low loss materials are often made using a guard ring electrode to eliminate the fringing of the electric field at the edges of the electrode and sample. The possibility of using such an arrangement was investigated with reference to a paper by Garton[99].

Garton considers the various geometrical factors (radius of the electrodes, width of the guard-ring gap and the thickness of the sample), the measurement frequency and

surface conductivity of the sample, and concludes that unless the ring gap is very much less than the thickness of the sample spurious loss tangents may result. The maximum error occurs when the surface resistivity is

$$r = \frac{2}{\omega C g^2} \qquad (8.1)$$

for capacitance per unit area, C, guard-ring gap, 2g and frequency ω . The maximum error in loss tangent is of the order of, or less than the ratio of guard-ring gap to the diameter of the ring. The losses originate in the distributed resistance and capacitance that exists across the gap. These factors are easily affected by the surface conditions of the sample and may be reduced by keeping the sample clean and dry thus raising the surface resistivity.

In the present case the maximum error that could be tolerated in the loss tangent was 10^{-4} and the electrode radius was limited to 4 mm. Applying Garton's work to the required frequency range and probable values for the dielectric constant and loss tangent of the materials to be studied, the results indicated that the guard-ring gap needed to be approximately 50 μm. To construct a system with a gap this small would have been difficult, but a design based on photo-etching techniques was made. The design is shown in figure (8.2). Each electrode consists of a polished disc of quartz with a tungsten rod in the centre and a thick layer of gold on one surface. The final electrode patterns could be

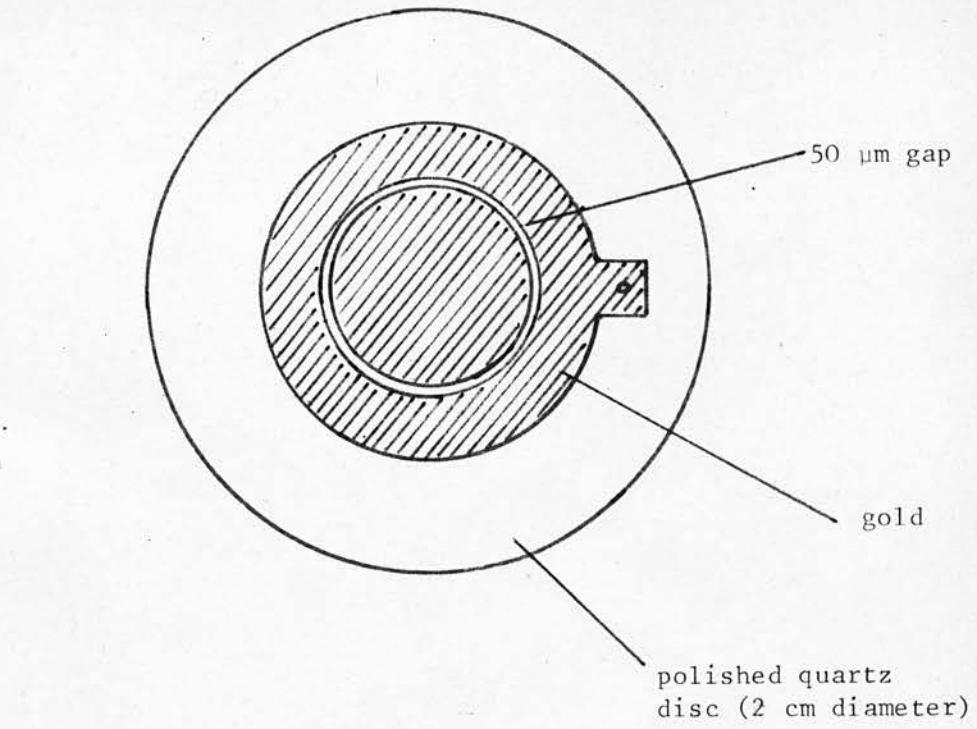

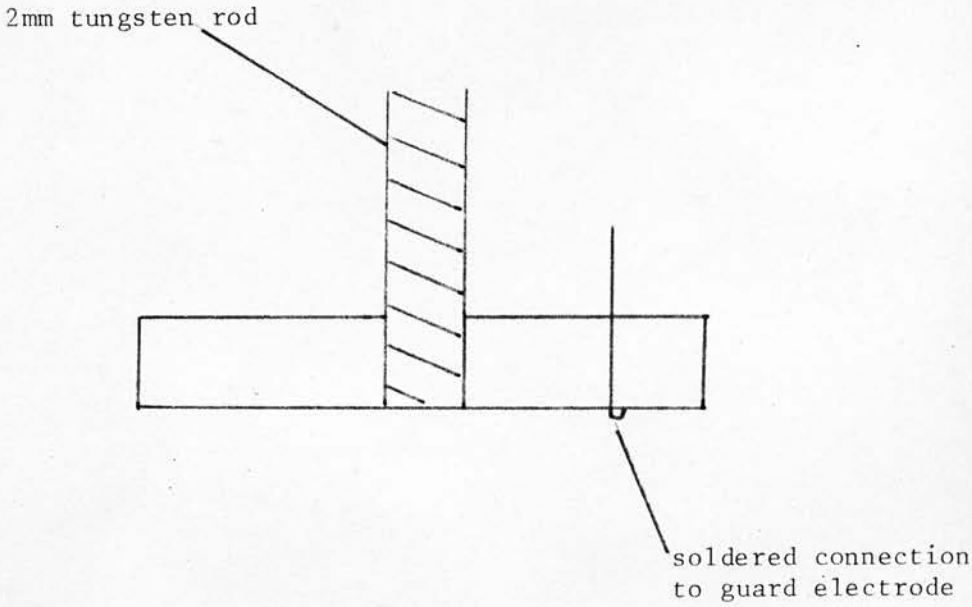

Figure (8.2)

Design for guard ring electrode
for small samples

etched in the gold after using the photographic mask, also shown in figure (8.2). The connection to the guard-ring was to be made by a small hole near the edge of the quartz disc. Suitable dimensions for this would be 2 cm diameter by 5 mm thick and 2 mm diameter tungsten rods. Although the mask was made, the arrangement was not tried through lack of time.

8.1.4 Contact problems.

The type and quality of the contact to a material can affect the result of an electrical measurement. The large variation in the published values of the a.c. conductivities and dielectric constants of nominally the same material (e.g. $As_2 Se_3$ - see Mitchell, Bishop and Taylor[37]) may in part be due to the differing quality of the contacts. Gold is considered to make an ohmic contact with the chalcogenide glasses, while aluminium makes a blocking contact with some. For the measurements described here there is evidence that both these metals make good contacts on $As_2 S_3$ but aluminium is blocking on $As_2 Se_3$[100][38].

Measurements were made on $As_2 S_3$ using both gold and aluminium as electrodes and varying the thickness of the sample. Decreasing the sample thickness is equivalent to increasing the applied electric field. A plot of resistance versus sample thickness should give a straight line passing through the origin if the contact is "good". A "good" contact can be defined as one that introduces no additional impedance

into the measurement.

Moisture on the contacts caused by a humid atmosphere can also affect the measurements, and to avoid this all measurements were made at temperatures of 315 K and above.

Capacitance measurements can also be affected by the contacts and the simplest case is when air gaps exist between the electrodes and sample. The apparent dielectric constant can be as little as 85% of the true value for gaps of a few percent of the sample thickness,

Lynch[101] has devised a technique for measuring the permittivity without making contact to the specimen. Using a sample holder with an adjustable separation between the electrodes, the specimen is placed in the holder and the bridge balanced; then the specimen is removed and the bridge rebalanced by decreasing the electrode separation. The dielectric constant of the material is then given by

$$\epsilon_r' = l/(l - \Delta l) \qquad (8.2)$$

where l is the sample thickness and Δl the decrease in the electrode spacing. In principle the technique has a high accuracy and the errors arise from measurement of l and Δl, and the faces of the sample not being parallel. Loss measurements can also be made by adjusting the resistive components of the bridge.

A sample holder based on Lynch's description was constructed but it was found not to be suitable for the small samples available.

8.2 D. C. Conductivity

Measurements of the d.c. conductivity were made using a sample holder with two brass electrodes, the upper one being attached to a spring to ensure firm contact with the sample. The conductivity was deduced from the specimen dimensions and the conductance measured by an Ecko vibrating reed electrometer type N616 B. The sample holder was placed in a Montford Mini K Mk 2 oven which enabled the temperature of the specimen to be easily varied. To avoid pick-up of static electricity the leads to the sample were screened.

The apparatus was able to measure conductances as small as 10^{-14} ohm^{-1} which corresponds to conductivities of about 10^{-15} ohm^{-1} cm^{-1} for the samples used.

Temperatures were determined in the same way as for the audio frequency measurements (section 8.1.1). Measurements were made with the sample cooling to avoid the possibility of moisture on the electrodes. Initially measurements were made while both heating and cooling but it was found that the conductivity appeared higher on initial heating (room temperature to about 320 K) than on cooling in the same temperature range. This effect was repeatable on the same

sample provided there was a time interval between cycles and thus it was not due to a change in the glass (e.g. annealing).

8.3 Preparation of Samples

8.3.1 Bulk glasses

The glasses were prepared by weighing out the components (for example $As_2 S_3$ and excess As) and placing them in clean quartz tubes of internal diameter about 10mm, and sealed at one end. Usually 10 to 15gm of material were prepared at a time. The tube and its contents were then dried in an oven and a quartz plug placed over a constriction at the tube's mid-point. The tube was then evacuated using a rotary pump and sealed at the plug using an oxy-propane torch. The sealed tube was placed on a rocking furnace and heated to 1000° C where it was left for 24 hours. The tube was then left to cool in the oven, or in air or quenched in cold water. The exact method of cooling depended on the glass: e.g. $As_2 S_3$ will form a vitreous material even when cooled very slowly.

8.3.2 Preparation for measurement

The quartz tube was cut open with a diamond saw and the cylinder of vitreous material removed. The cylinder was next cut into thin slices, usually less than 2mm thick. Liquid paraffin was used as the lubricant.

After the samples had been cut their faces were

ground flat on a glass plate with 10 μm alumina powder as an abrasive. Again liquid paraffin was used as the lubricant. Water is absorbed slightly into the chalcogenide glasses and so had to be avoided.

The sample was next cleaned in trichloroethylene using an ultrasonic cleaner to remove any remaining alumina particles and liquid paraffin. The thickness and diameter of the specimens were measured with a micrometer when the material had dried.

Before electrodes were deposited on the surface the sample was again cleaned and the circumference covered with "Sellotape" to prevent any metal adhering to the sides. The electrode metals were deposited under vacuum using a heated filament. For all samples the conditions of evaporation were similar; the distance from the filament and the amount of metal used was approximately the same. In this way it was expected that the electrodes on the samples would be similar and any variation from specimen to specimen was likely to have resulted from the glass itself. The electrodes were made fairly thick, approximately $\frac{1}{2}$ μm.

8.3.3 Microwave samples

The microwave measurements required larger samples than the other frequency ranges. Slices about 3 cm square and one to two millimetres thick were cut from large blocks

with a diamond saw and both faces were then ground flat on a glass plate, using 27 and then 10 μm alumina powder as the abrasive.

To polish one side the specimen was mounted on a polishing machine. It was found that the best finish could be achieved using an adhesive polishing pad and a little 10 μm alumina powder sprayed lightly with liquid paraffin. This procedure enabled all the polishing to be done in one stage (i.e. elimination of coarse pits to final polishing). The total polishing time was usually four to five hours. This method resulted in a surface which, though not optically perfect, was sufficiently smooth for microwave measurements. The surface roughness was measured using a "Talysurf" machine and was generally less than 0.04 μm. The finished plate was checked for uniformity of thickness with a micrometer. Typical variations were less than 5%. This was not expected to affect the measurement accuracy much.

The above technique was used for samples of $As_2 S_3$ and $As_2 Se_3$. Larger microstrip substrates enable more resonances in a given frequency range to be measured and so some large resonators of $As_2 S_3$ were made. The glass plates were prepared by melting lumps of material in an inert atmosphere (nitrogen) on a horizontal polished pyrex disc three inches in diameter. To keep the plate between 1 and 2 mm thick the melting had to be done slowly so that the $As_2 S_3$ did not

become too fluid. The upper surface of the resulting specimen was sufficiently smooth not to need polishing (it was in fact better than the polished specimens). The only flaws were occasional bubbles at the lower surface.

The evaporation of the electrodes and photo-etching was done as described for the alumina resonator (section (7.3)).

8.4 Materials studied

The work concentrated on materials in the As - S and As - Se systems.

8.4.1 Stoichiometric glasses

The major portion of the work was the determination of conductivity (a.c. and d.c.) of $As_2 S_3$ as a function of frequency, temperature, electrode material and sample thickness. In addition, the effect of annealing $As_2 S_3$ on the conductivity was determined.

The work on $As_2 Se_3$ was confined to measurement of the variation of conductivity with frequency and temperature as part of the study of the As - Se system.

In the microwave region $As_2 S_3$ proved the easier material with which to construct resonators, being less prone to fracture than $As_2 Se_3$ under the conditions of electrode

evaporation. (These are described in section (7.3.1)). Several resonators were made on $As_2 S_3$ but only two partially successful samples of $As_2 Se_3$ were prepared.

8.4.2 As - S and As - Se systems

The d.c. and low frequency a.c. conduction properties of the As - S and As - Se systems were measured for compositions near stoichiometry. It was attempted to prepare materials in the range $As_2 S_{2.6}$ ($Se_{2.6}$) to $As_2 S_{3.4}$ ($Se_{3.4}$).

8.4.3 Analyses and electron microscope studies of the samples

The electrical measurements were supplemented by chemical analyses to determine the As to S (Se) ratios of the compounds studied and by a scanning electron microscope investigation of fracture surfaces of the samples to determine the extent of any phase separation.

The compositions of the glasses were:

	nominal S (Se) content $As_2 S_x$ (Se_x)	Actual S (Se) content	Atomic % S (Se)
	x = 2·6	x = 2·48	55·3
	2·7	2·69	57·4
	2·8	2·73	57·8
As - S system	3·0	3·00	60·0
	3·2	3·20	61·5
	3·4	3·38	62·8
	2·6	2·55	56·2
	2·8	2·85	58·8
As-Se system	3·0	2·98	59·8
	3·2	3·18	61·4
	3·4	3·41	63·0

The analysis errors in x were estimated to be $\pm$ 0·03 or about 0·2 atomic %.

It was found impossible to prepare a sample of composition $As_2 S_{2.6}$ that was not phase separated.

The electron micrographs (figures (8.3 a,b)) were

$As_2S_{2.48}$ (1900X)

$As_2S_{2.73}$ (18200X)

$As_2S_{3.00}$ (16800X)

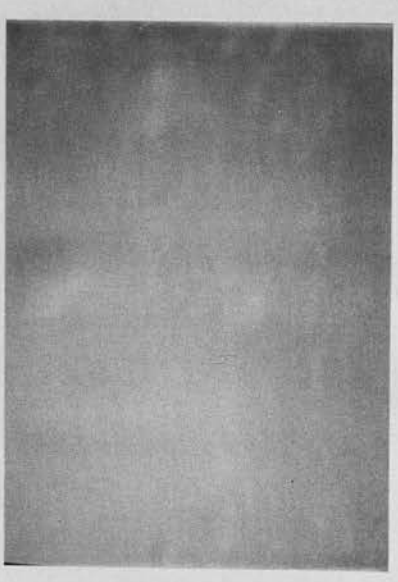

$As_2S_{3.20}$ (18200X)

$As_2S_{3.38}$ (23800X)

Figure (8.3a). Scanning electron micrographs of the As-S system

$As_2Se_{2.55}$ (1820OX)

$As_2Se_{2.85}$ (1960OX)

$As_2Se_{2.98}$ (1680OX)

$As_2Se_{3.18}$ (1820OX)

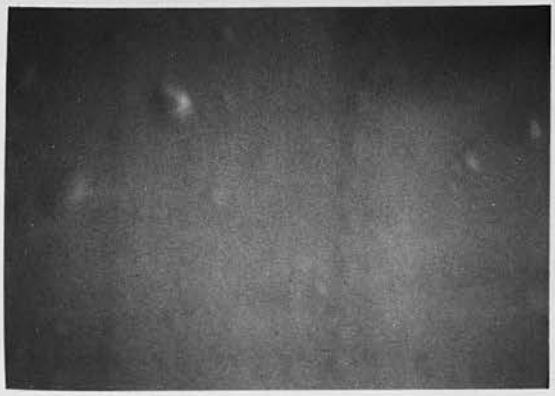

$As_2Se_{3.41}$ (1680OX)

Figure (8.3b). Scanning electron micrographs of the As-Se system

made on fractured surfaces covered with a very thin layer of evaporated gold. Micrographs were made of all samples except $As_2 S_{2.7}$ and, apart from $As_2 S_{2.6}$ show little evidence of phase separation at the greatest magnifications possible: about 20,000 times. Surface features greater than $0.1\mu m$ could be resolved.

Of the As - S system only $As_2 S_{2.6}$ and $As_2 S_{2.8}$ showed any phase separation and it is likely that $As_2 S_{2.7}$ would also show some as these compositions are close to the edge of the glass forming region. The features in figure (8.3) that appear on all photographs were necessary to ensure that the microscope was focussed.

The As - Se system appeared to have more surface irregularity than the As - S system. In some cases these may be surface dust or small voids but it is evidence that the material prepared for the As - Se system was not as homogeneous as the As - S system. This may have a bearing on the results of electrical measurements.

8.5 D.c. and low frequency experimental results

In the following sections reference to a particular material will be made using its nominal composition: e.g. $As_2 S_{2.8}$ instead of $As_2 S_{2.73}$. The true compositions are, of course, used in plotting experimental results.

8.5.1 Electrode/thickness dependence

Measurements of the a.c. resistance and capacitance were made on the same sample of $As_2 S_3$ using evaporated gold and aluminium electrodes. As new electrodes were put on the specimen it was ground down from about 2 mm to 0·44 mm thick. The grinding was done carefully to keep the faces as closely parallel as possible. The electrode metals alternated so that the resistance and capacitance could be plotted as a function of sample thickness. Figures (8.4) and (8.5) show the resistance at 1 k Hz and 10 k Hz for gold and aluminium electrodes. For both types of electrodes an equation of the form

$$R = l/\sigma A \qquad (8.3)$$

is obeyed for resistance R and thickness l . The constant of proportionality (σ A) is the product of the conductivity and cross-sectional area of the sample. The results show that the contact resistance (defined by the zero thickness resistance) is negligible compared with the sample resistance at these frequencies. Figure (8.6) shows the conductivity as a function of frequency deduced from the slopes of figures (8.4) and (8.5) and equation (8.3). There is a difference in the magnitudes of the conductivity with values for aluminium electrodes being about a factor of 1·5 smaller than those for gold.

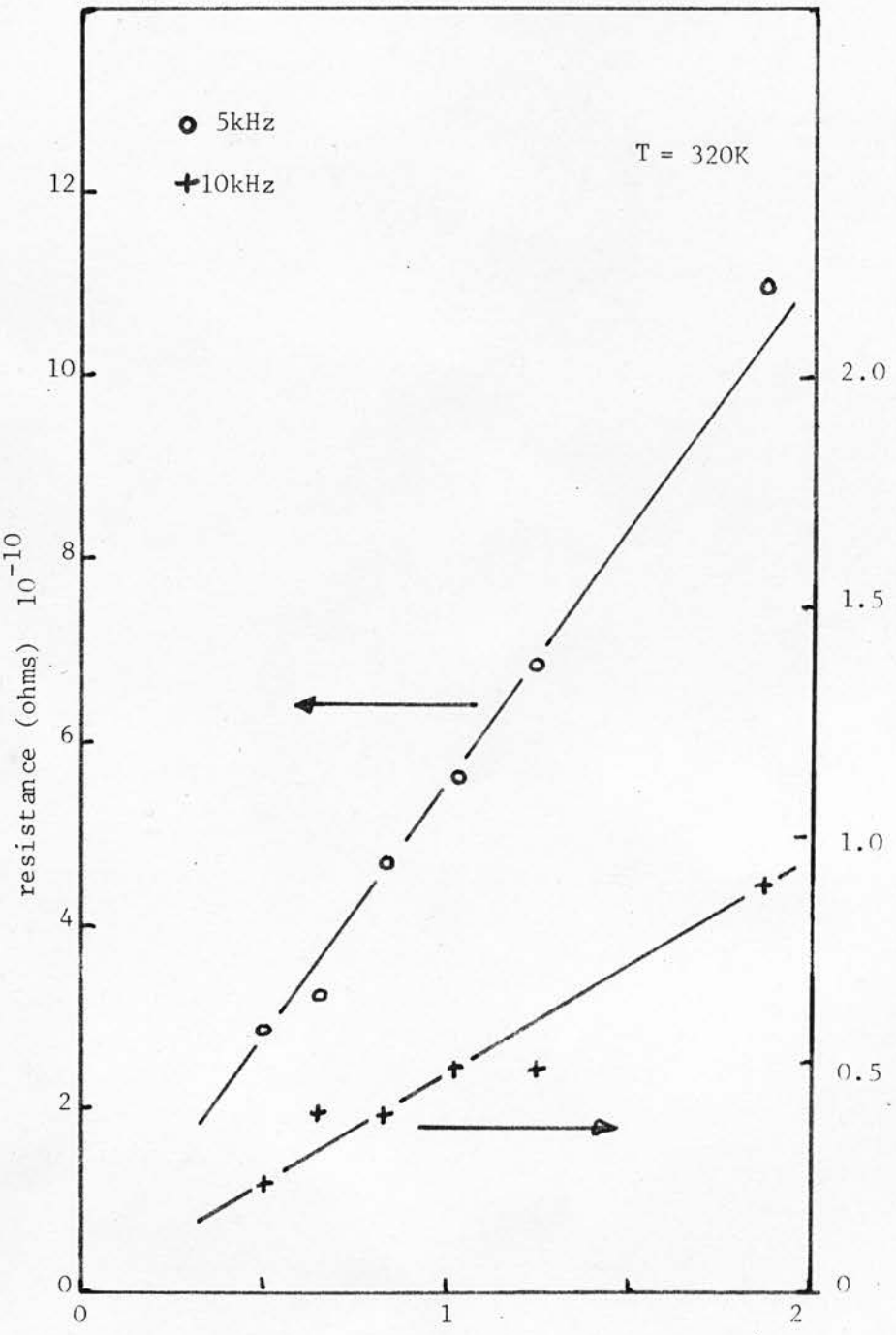

Figure (8.4)

Thickness dependence of As_2S_3 (gold electrodes)

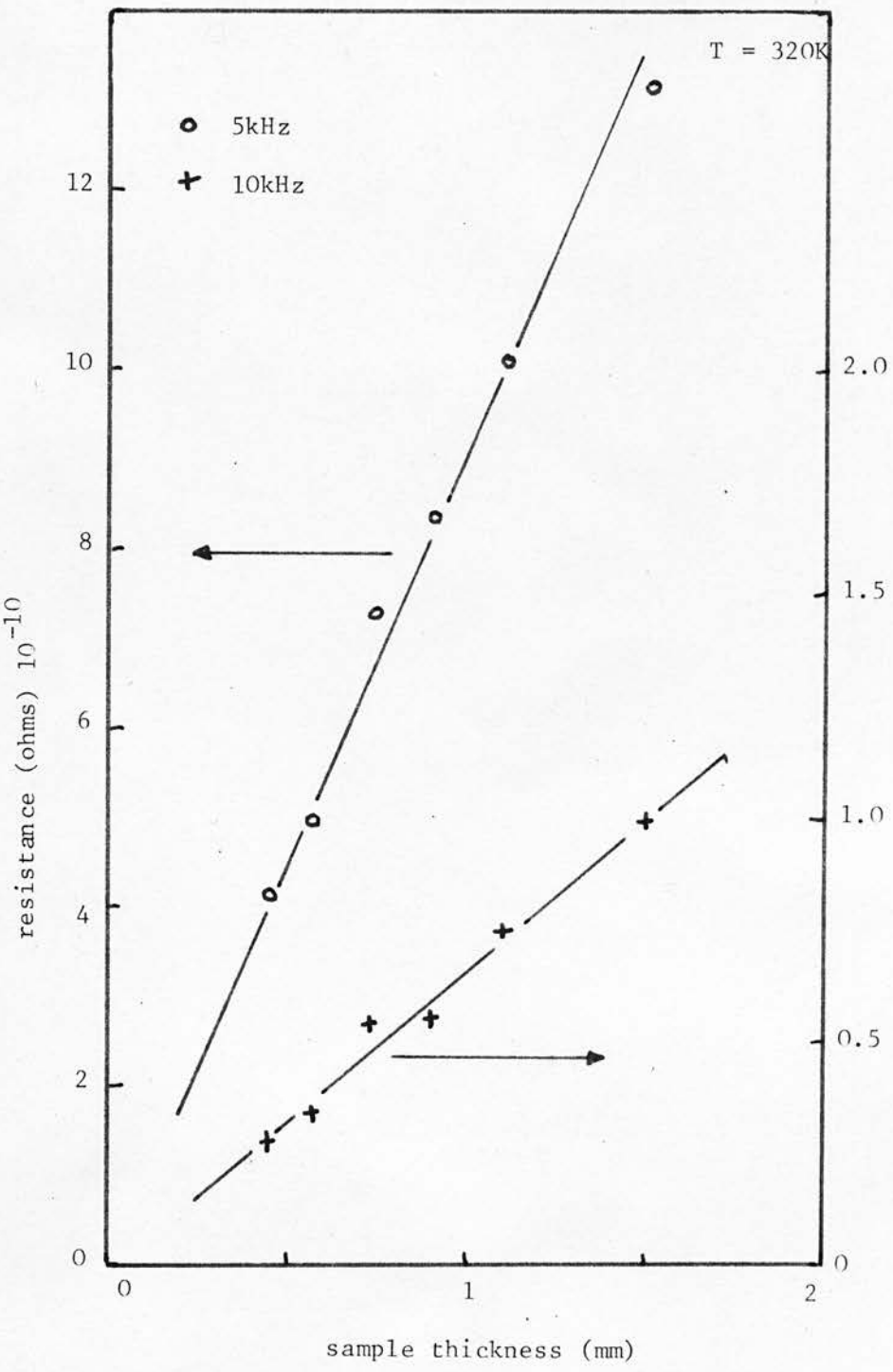

Figure (8.5)

Thickness dependence of As_2S_3 (aluminium electrodes)

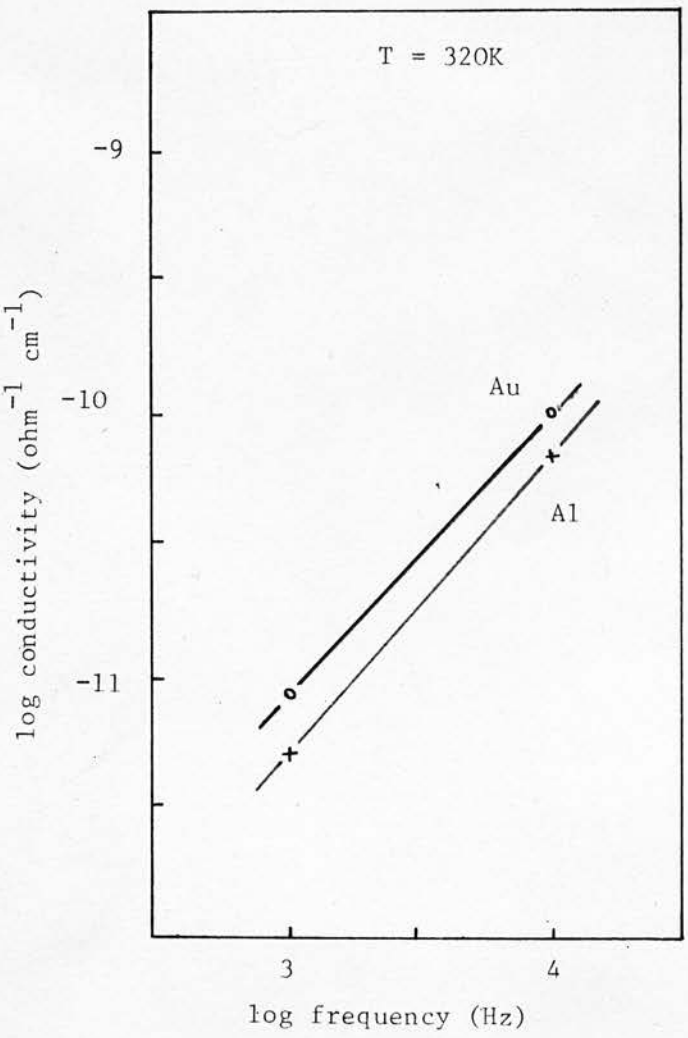

Figure (8.6)

Electrode dependence of conductivity for As_2S_3

Another difference occurs in the slopes of the log σ versus log f plots of figure (8.6). The slopes are 1·06 and 1·13 for gold and aluminium contacts respectively.

The sample capacitance as a function of reciprocal thickness is shown in figure (8.7) for a frequency of 5 k Hz. There was no measureable difference between the gold or aluminium electrodes. The slope of the line gives a dielectric constant of 8·51 from the relation

$$C = \epsilon_0 \epsilon_r' \frac{A}{l} \qquad (8.4)$$

The conversion factor from the arbitrary capacitance units in the figure is 0·689 to give picofarads.

8.5.2 Annealing

The a.c. conductivity of a sample of $As_2 S_3$ was measured and then its gold electrodes ground off. The sample was next placed in an oven at 180° C for four hours. The electrodes were removed to prevent any diffusion of the gold into the surface of the glass. When the sample was removed from the oven the surfaces were again ground to remove any surface oxidation and then the a.c. conductivity was re-measured after new electrodes had been deposited. The results of these measurements are shown in figure (8.8).

The annealing lowered the conductivity particularly

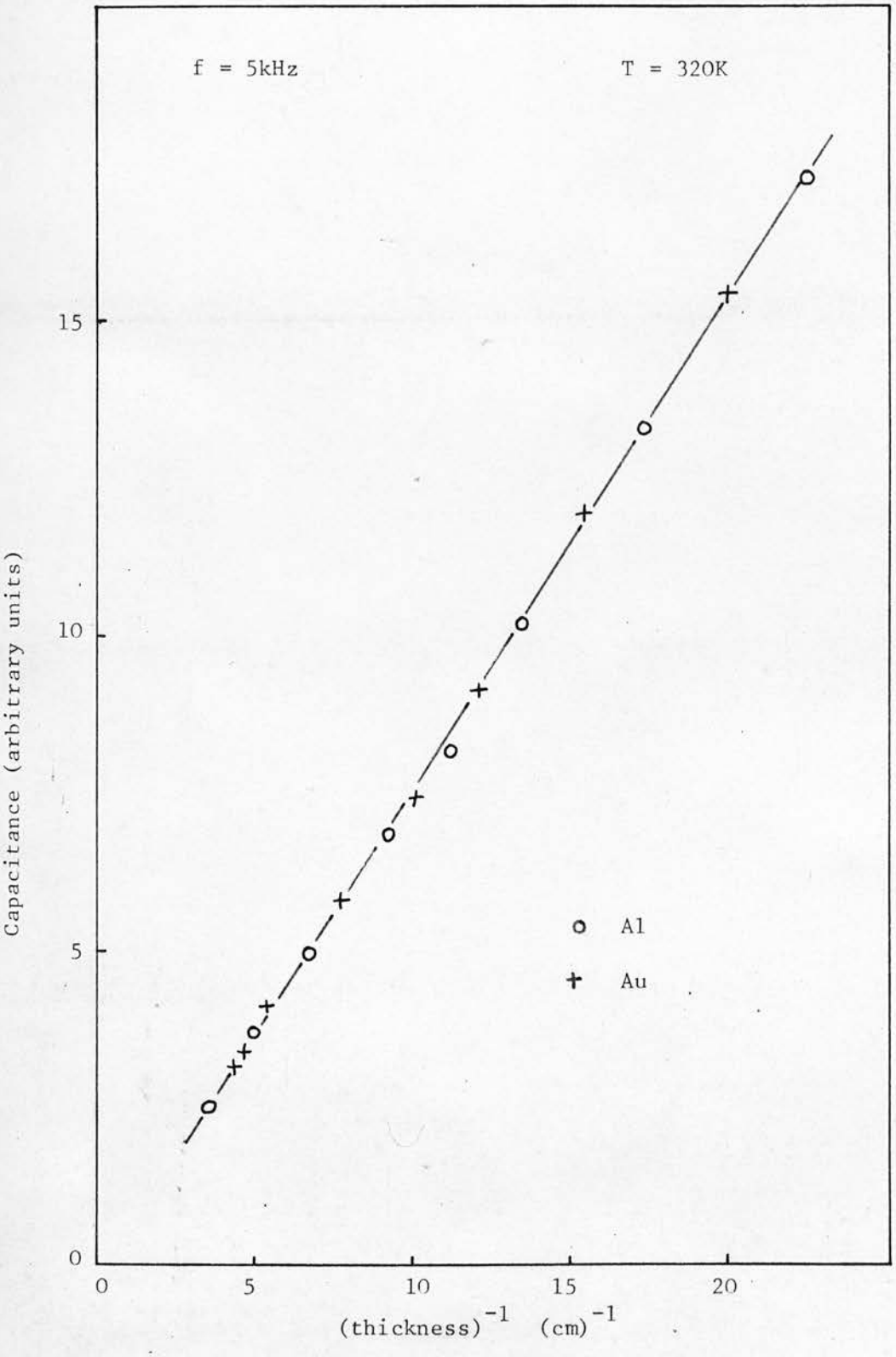

Figure (8.7)

Electrode dependence of capacitance for As_2S_3

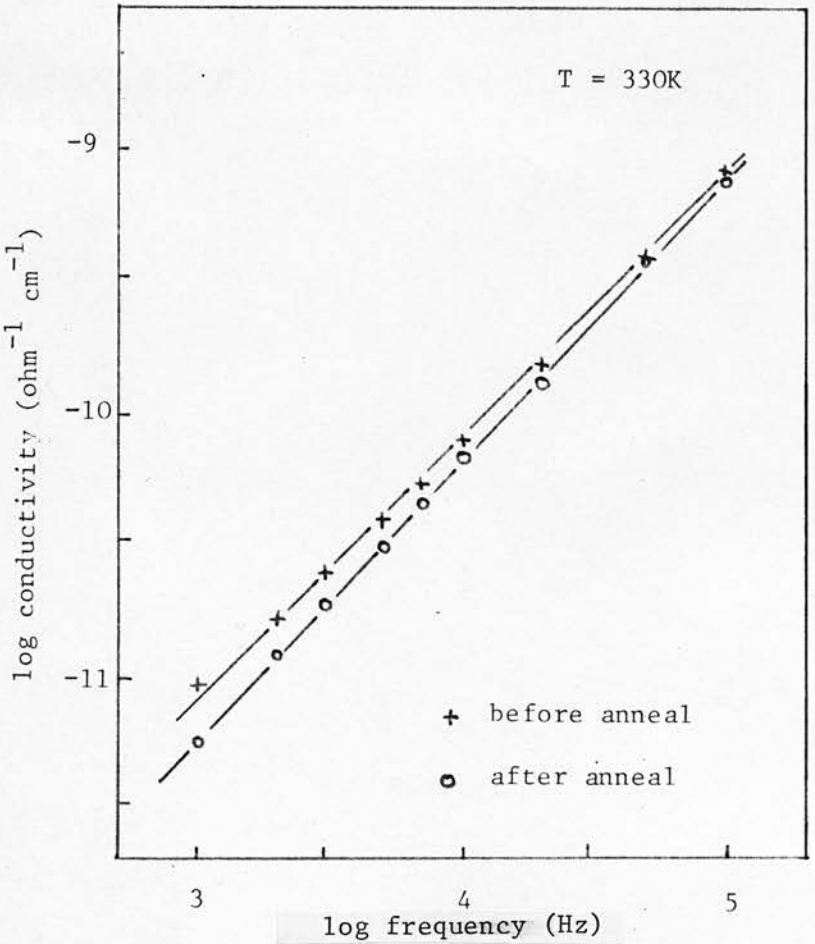

Figure (8.8)

Annealing of As_2S_3 at

180^{o}C for 4 hours

at lower frequencies, increasing the slope of the log σ versus log f graph. The gradients are 0·98 and 1·06. Further heat treatment (180°C for another 4 hours) had no measureable additional effect. The dielectric constant was unaffected by the heat treatment. It was noticed, however, that the colour of the $As_2 S_3$ was changed slightly to a brighter, more transparent red.

8.5.3 The As - S system

In all measurements on this system evaporated gold electrodes were used.

8.5.3.1 D.C. conductivity

The temperature dependence of the d.c. conductivity of all the compositions is shown in figure (8.9). In all cases the conductivity obeys a relation

$$\sigma = C \exp(-E/kT) \qquad (8.5)$$

The temperature range is 80°C to 150°C ; the upper limit being chosen to avoid approaching the glass transition temperature (about 190°C) too closely because this may have resulted in some annealing or partial crystallisation and thus altered the electrical properties of the glass. The lower limit was determined by the sensitivity of the electrometer.

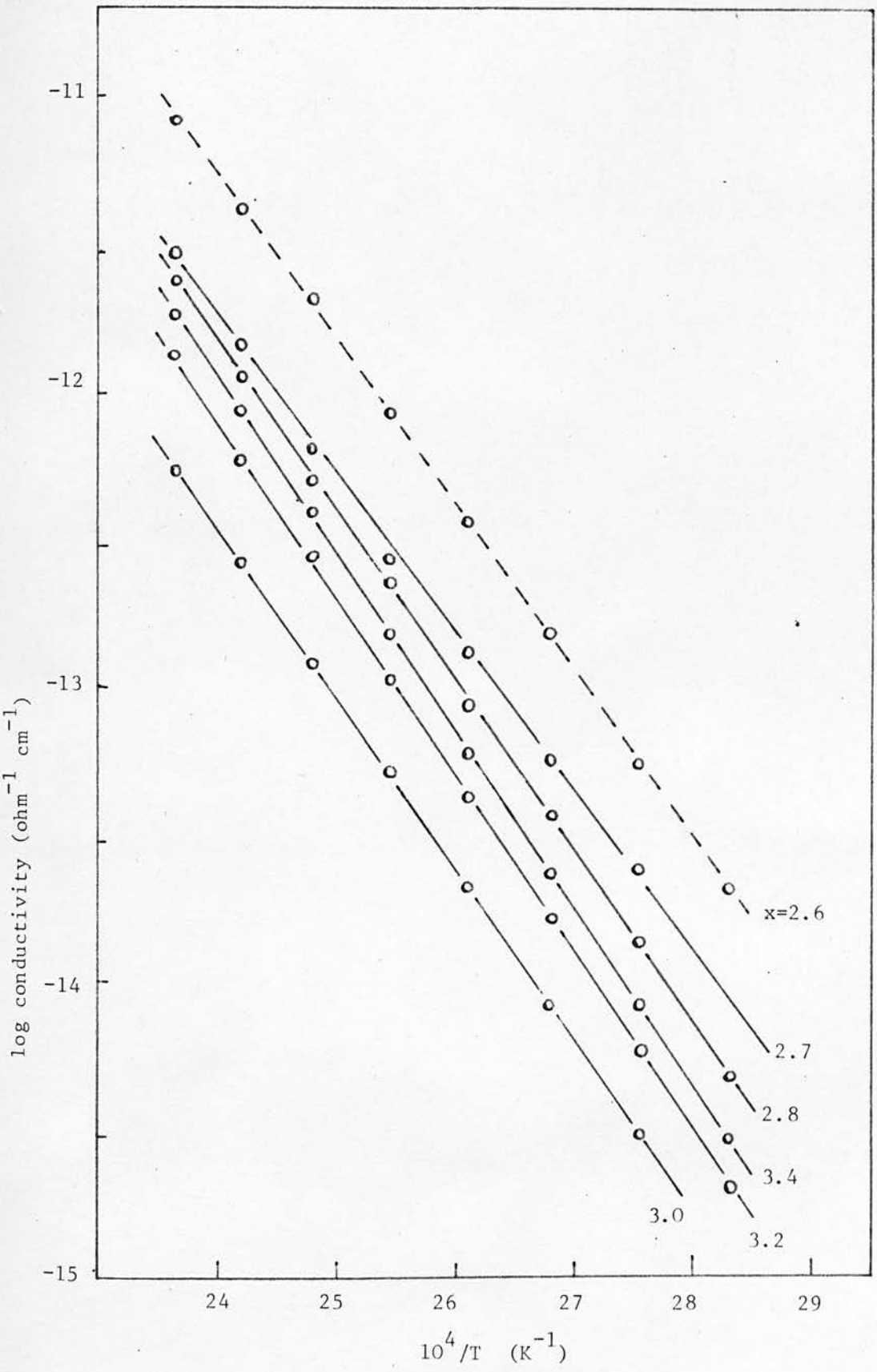

Figure (8.9)

Temperature dependence of d.c. conductivity of As_2S_x

The activation energies E and pre-exponential constants, C are:

nominal S content $As_2 S_x$	E eV	C $ohm^{-1}\ cm^{-1}$
x = 2·7	1·14 *	135
2·8	1·14 *	100
3·0	1·15	28·2
3·2	1·19	200
3·4	1·20	372

These data show that the activation energy is increasing slightly with sulphur content and that there is a minimum in the value of C at the stoichiometric composition. The minimum in C is shown in figure (8.10) where log C is plotted against the atomic % of sulphur. Figure (8.11) shows the conductivity at three different temperatures and reflects the behaviour of C.

8.5.3.2 A.C. conductivity

The a.c. conductivity as a function of frequency is shown in figure (8.12) for the temperature 350 K. Generally in this frequency range (i.e. 10^2 to 10^5 Hz) the a.c. conductivity can be described by

$$\sigma = A\omega^s \qquad (8.6)$$

* drawn incorrectly in fig (8.9)

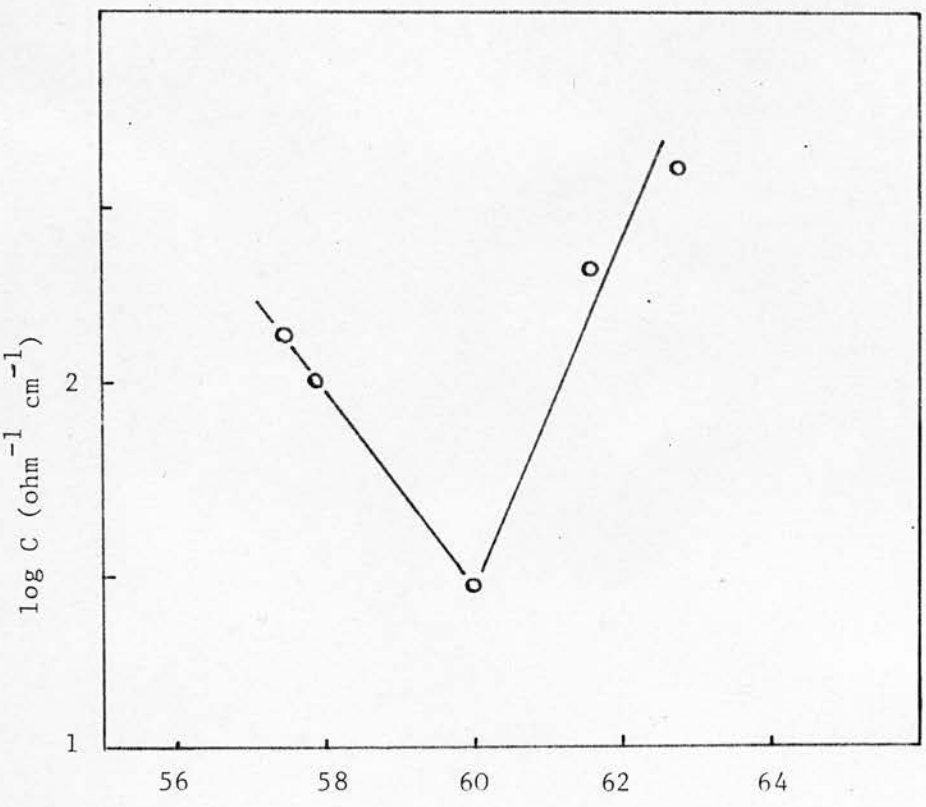

Figure (8.10)

Pre-exponential constant (C) of the As-S system

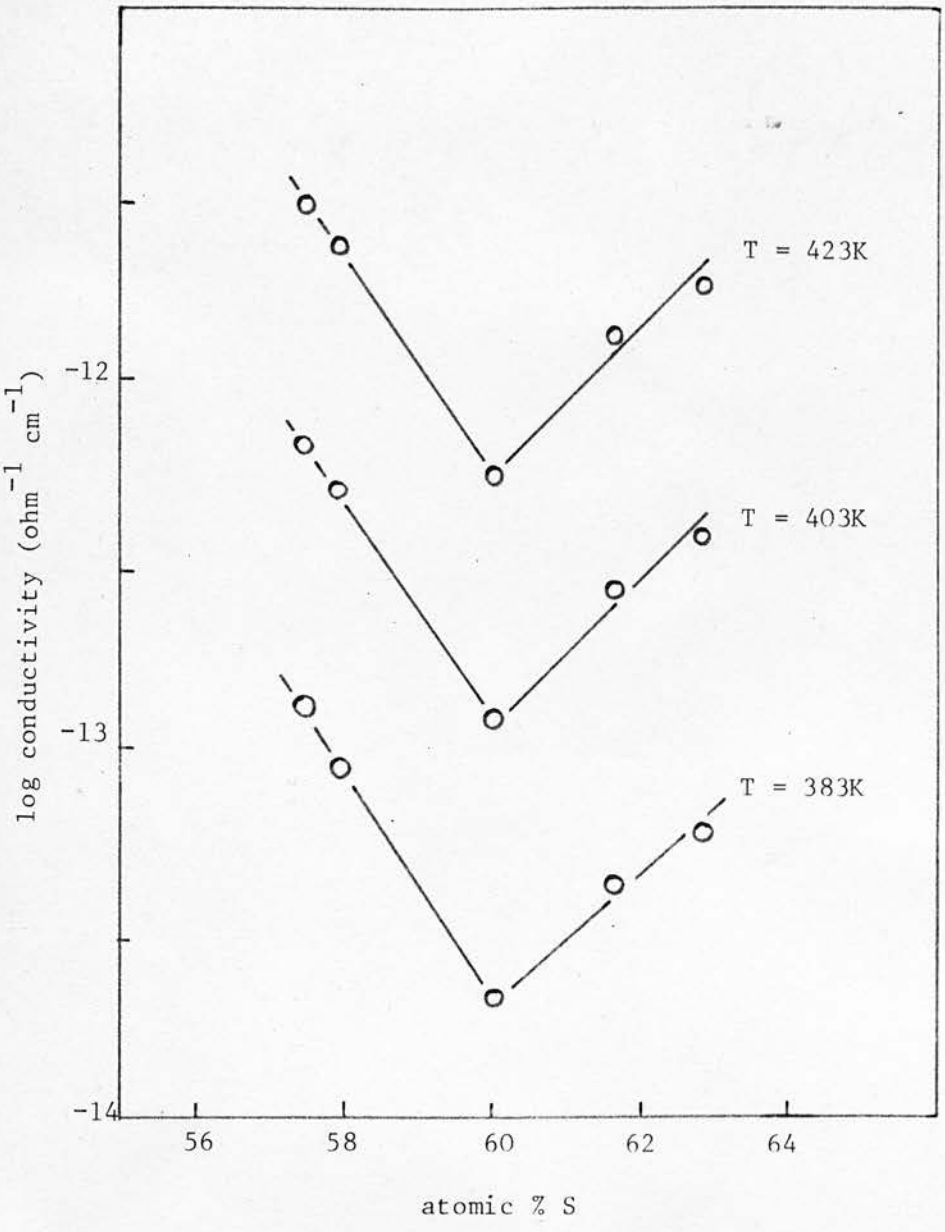

Figure (8.11)

D.c. conductivity of the As-S system

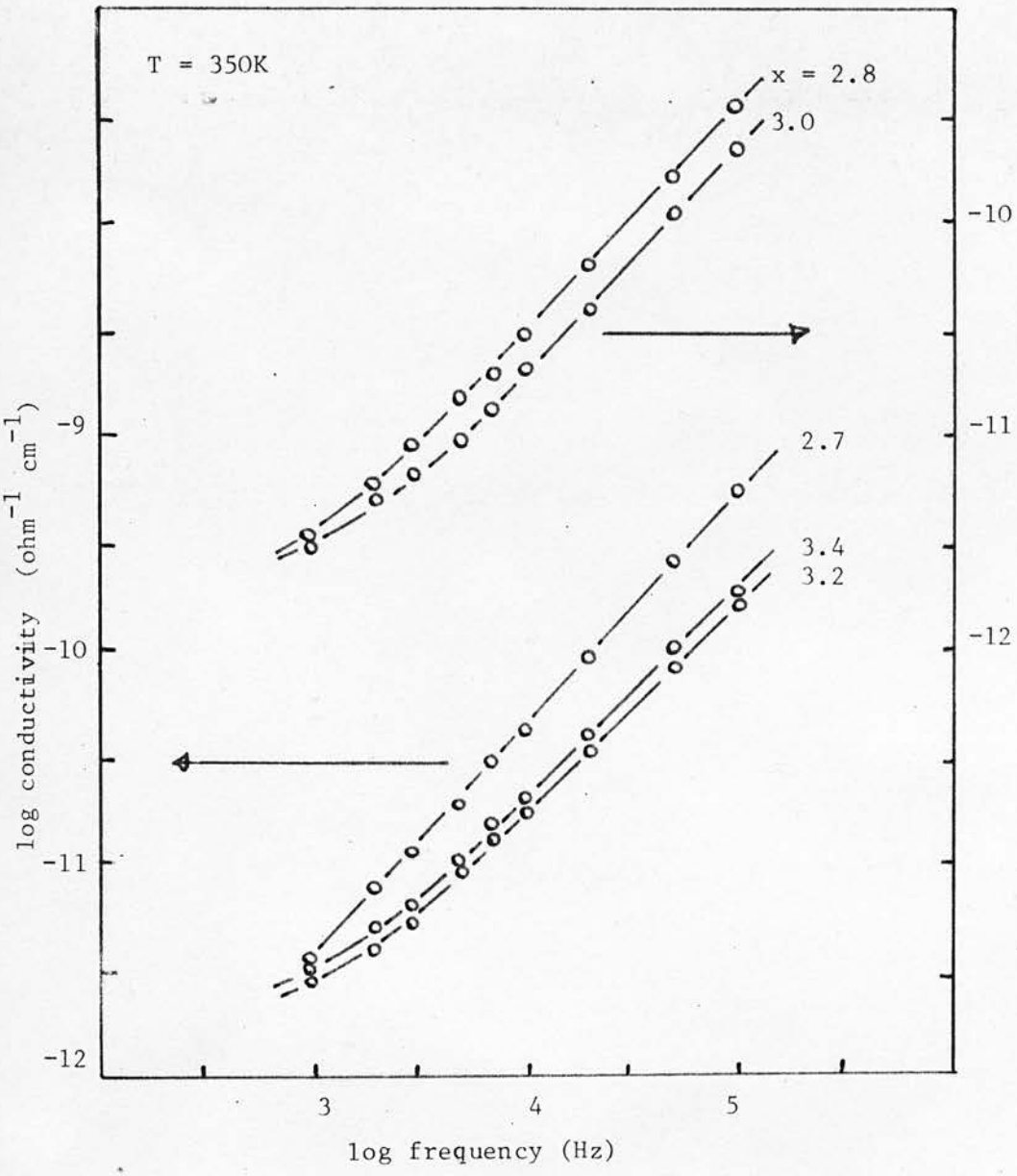

Figure (8.12)

A.c. conductivity of As_2S_x

where A is a constant and $s \approx 1$. This is typical of many amorphous materials.

The temperature variation of the conductivity is very small but there is an indication that the variation is greater in materials with excess sulphur (figure (8.13)). Figures (8.14) and (8.15) show the difference between $As_2 S_{2.7}$ and $As_2 S_{3.4}$ and also indicate that the temperature dependence diminishes as the frequency increases. It is not possible to distinguish with any reliability whether the conductivity is directly proportional to temperature or not for the temperature range used.

The dependence of conductivity on composition and frequency for three different temperatures is shown in figures (8.16) to (8.18). Important points to note are that the minima in conductivity do not, in general, coincide with the stoichiometric composition and the position of the minimum varies with frequency and temperature. At frequencies below 5 k Hz extrapolations from the straight portions of the $\log\sigma$ versus $\log f$ graphs were used as this was considered to be the correct continuation of the conductivity resulting from a mechanism described by equation (8.6).

For the different compositions and temperatures the exponents s (defined in equation (8.6)) are:

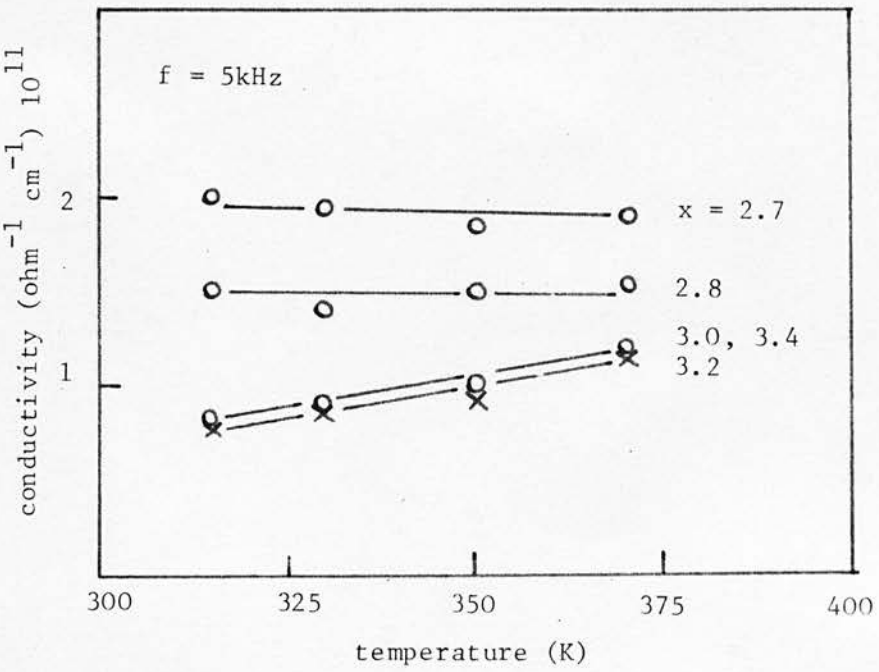

Figure (8.13)

A.c. conductivity of As_2S_x

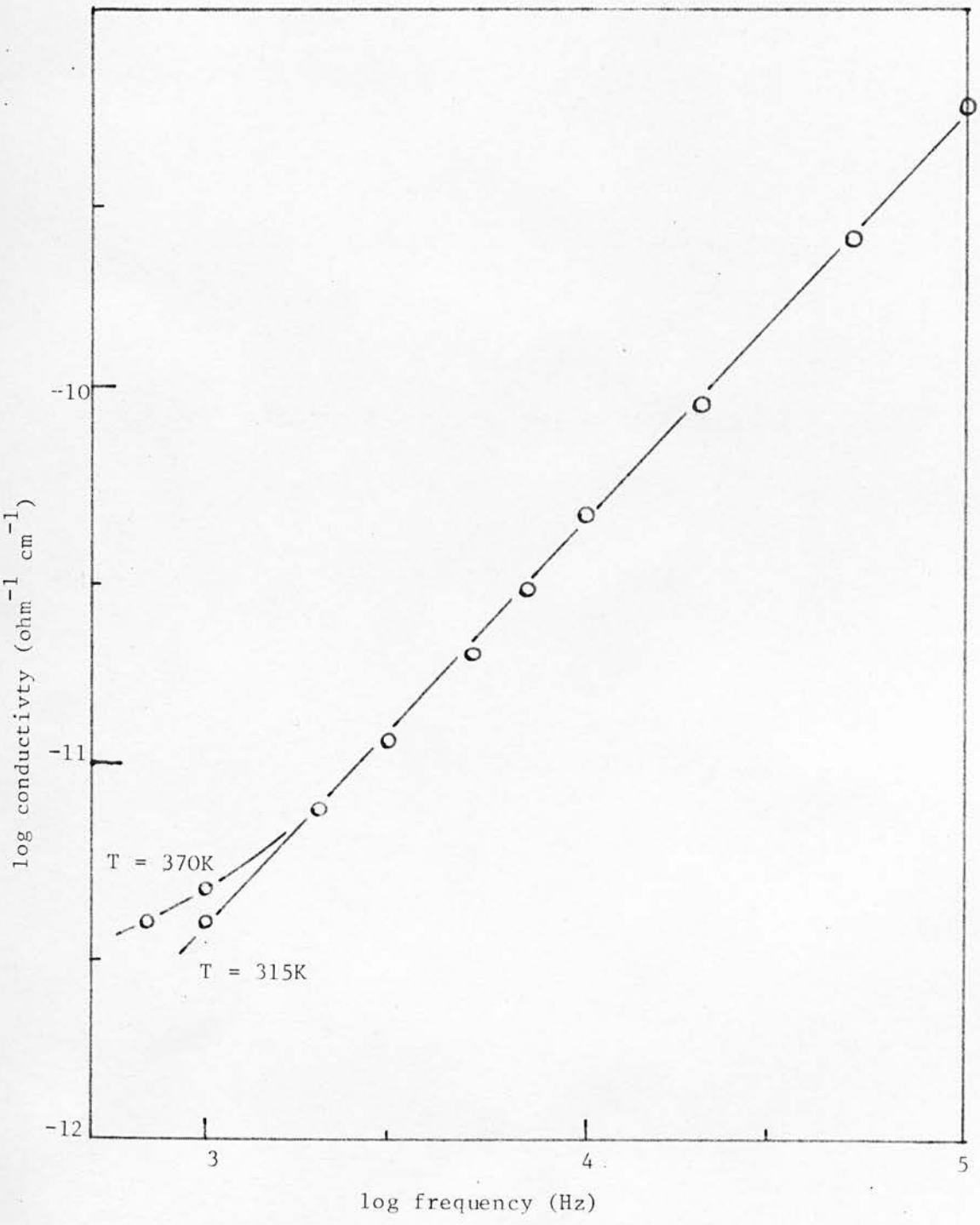

Figure (8.14) ·

A.c. conductivity of $As_2S_{2.7}$

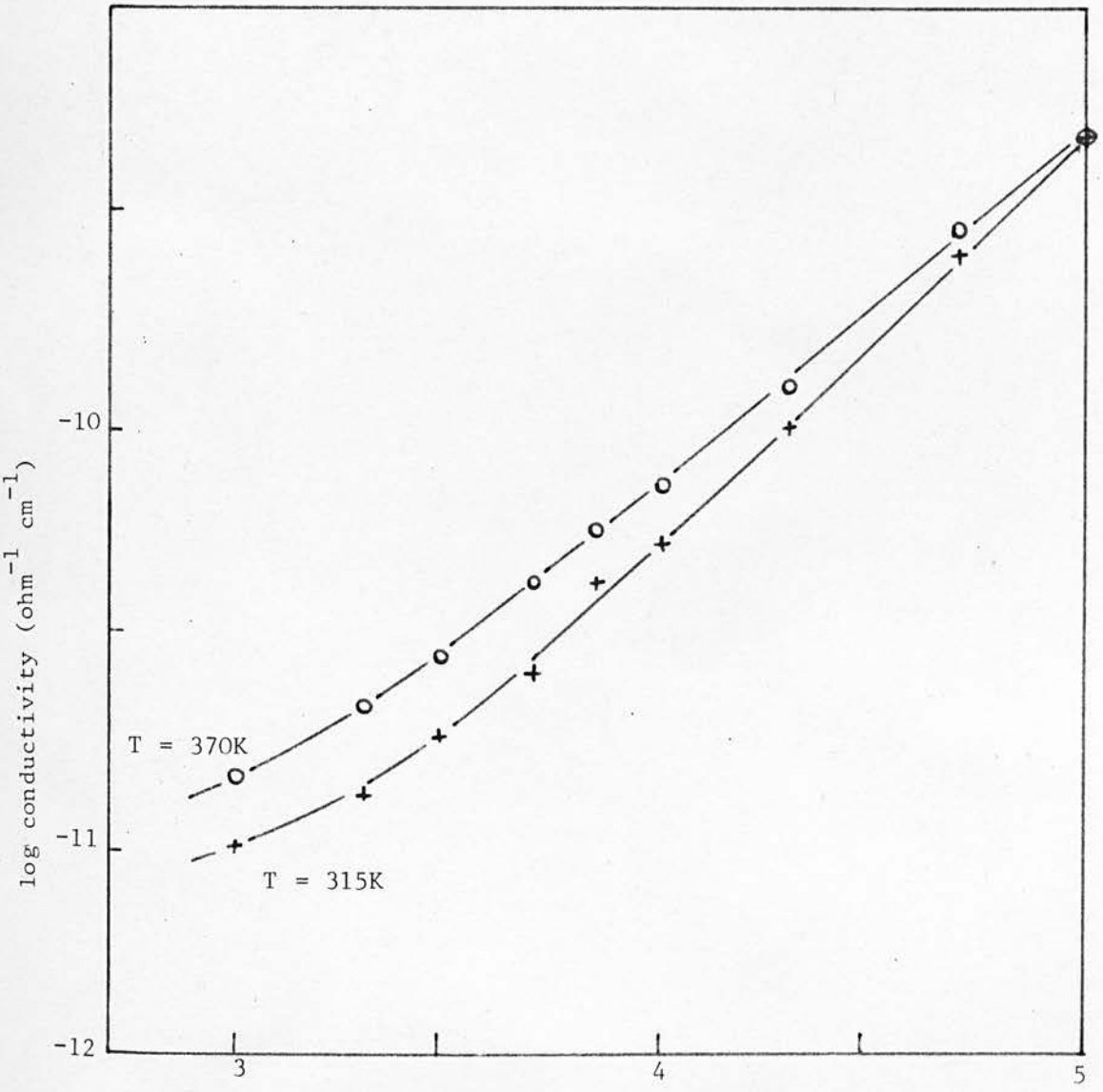

Figure (8.15)

A.c. conductivity of $As_2S_{3.4}$

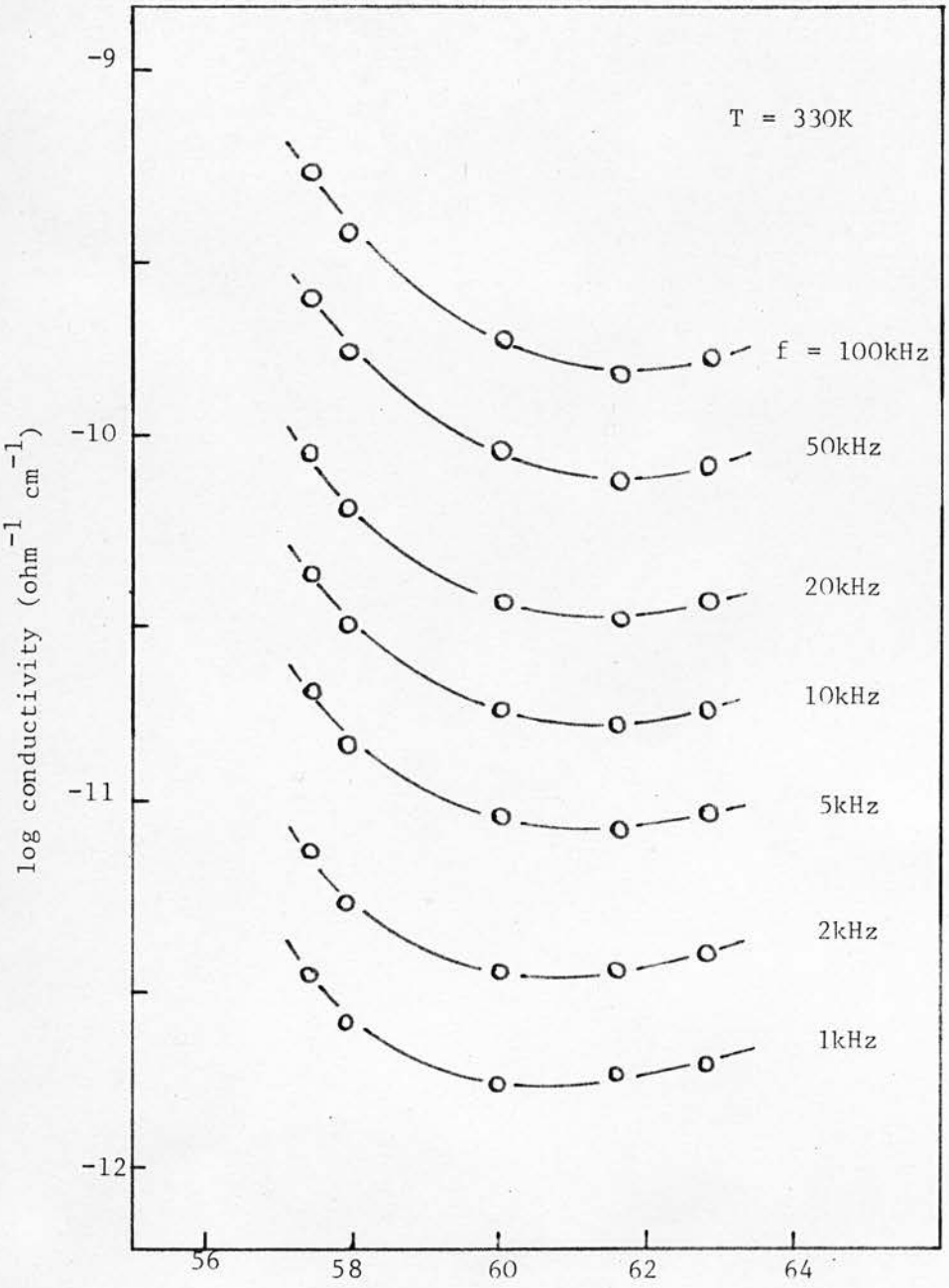

Figure (8.16)

A.c. conductivity of the As-S system (T=330K)

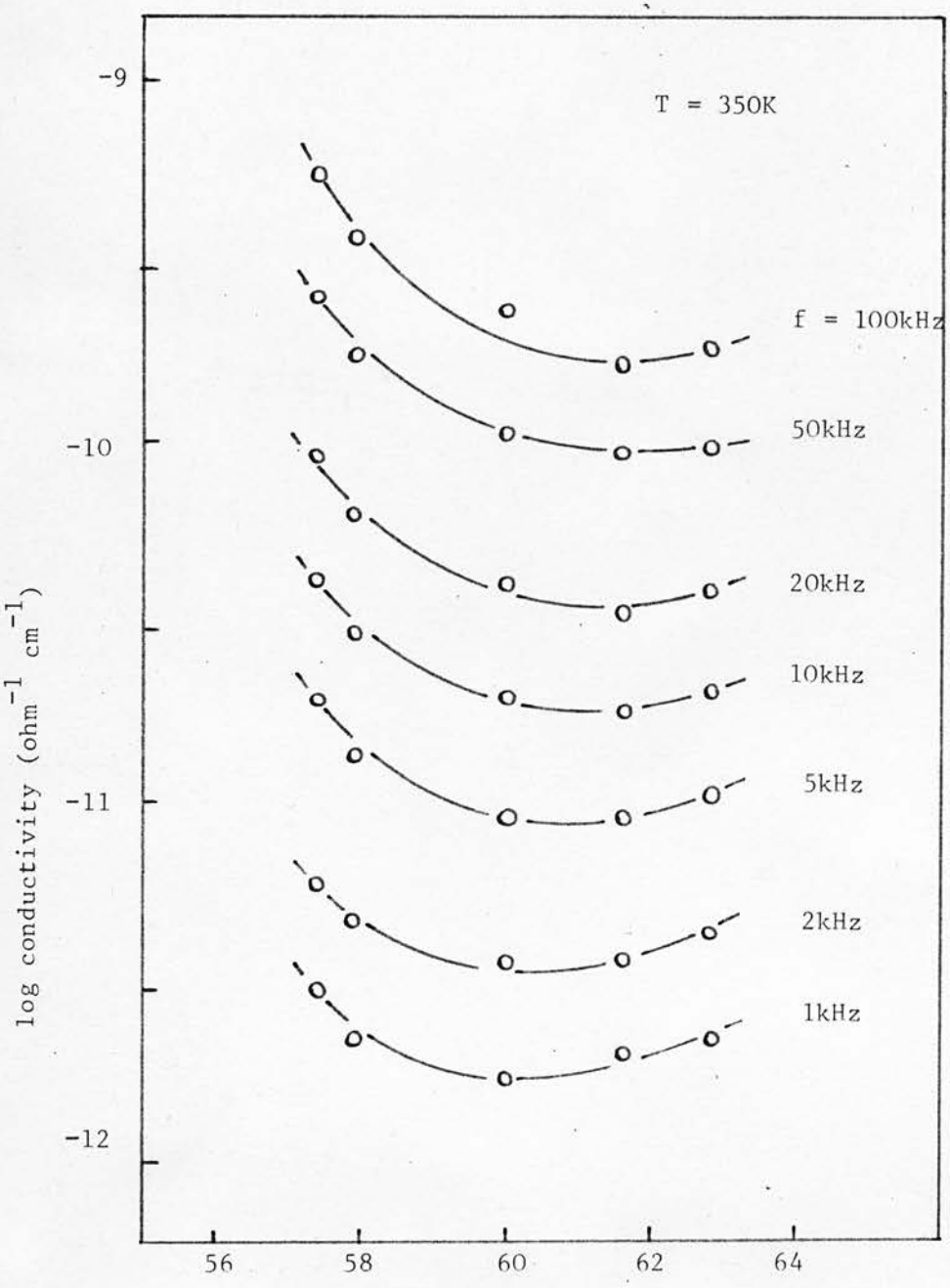

Figure (8.17)

A.c. conductivity of the As-S system (T=350K)

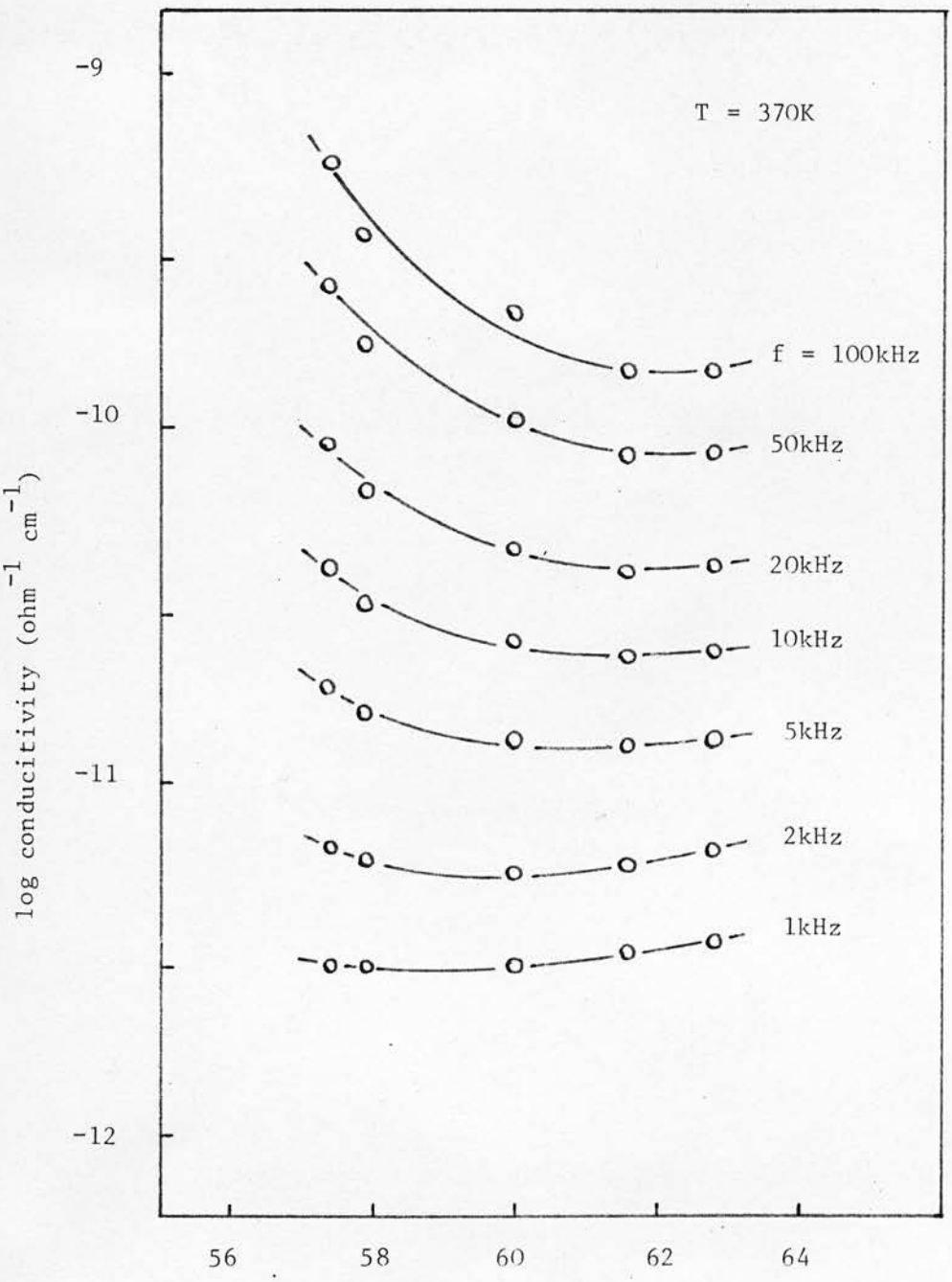

Figure (8.18)

A.c. conducitivity of the As-S system (T=370K)

Nominal S content $As_2 S_x$	Slope s of $\log \sigma$ - log f plot T = 315K	T = 330K	T= 350K	T= 370K
x = 2·7	1·11	1·11	1·10	1·10
2·8	1·12	1·10	1·05	1·04
3·0	1·09	1·01	1·03	0·92
3·2	1·00	1·01	0·96	0·82
3·4	0·97	0·97	0·95	0·81

The errors in these slopes are probably about ± 0·05. The slopes show a tendency to decrease with increasing temperature and increasing sulphur content.

The dielectric constants have a maximum at stoichiometry (figure (8.19)). The results of measurements on the phase separated material $As_2 S_{2.6}$ are included in the figure as they appear consistent with the other results. This may not be significant because there is no compatibility between the conductivities of the $As_2 S_{2.6}$ and the other materials in the As - S system. The variation of ϵ'_r with frequency is shown in figure (8.20). In most cases there was no measureable change in the dielectric constant when the temperature was increased, but there was a slight rise with $As_2 S_{3.4}$ (6·80 at 315 K to 6·87 at 370 K).

8.5.4 The As - Se system

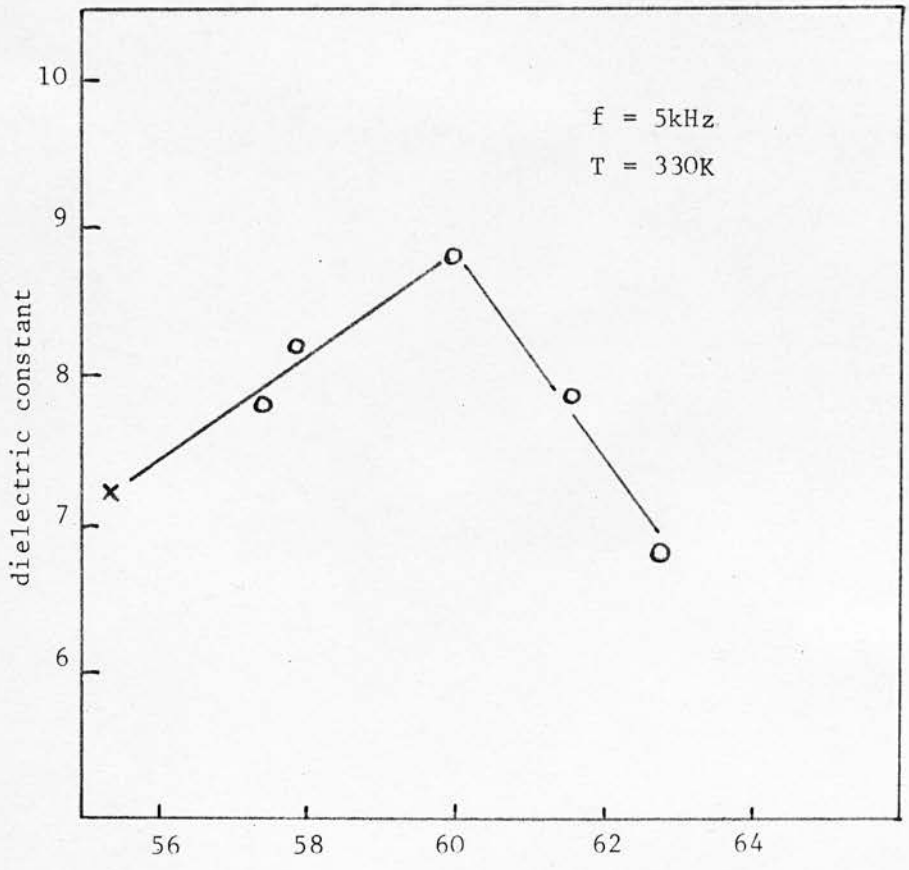

Figure (8.19)

Dielectric constant of the As-S system

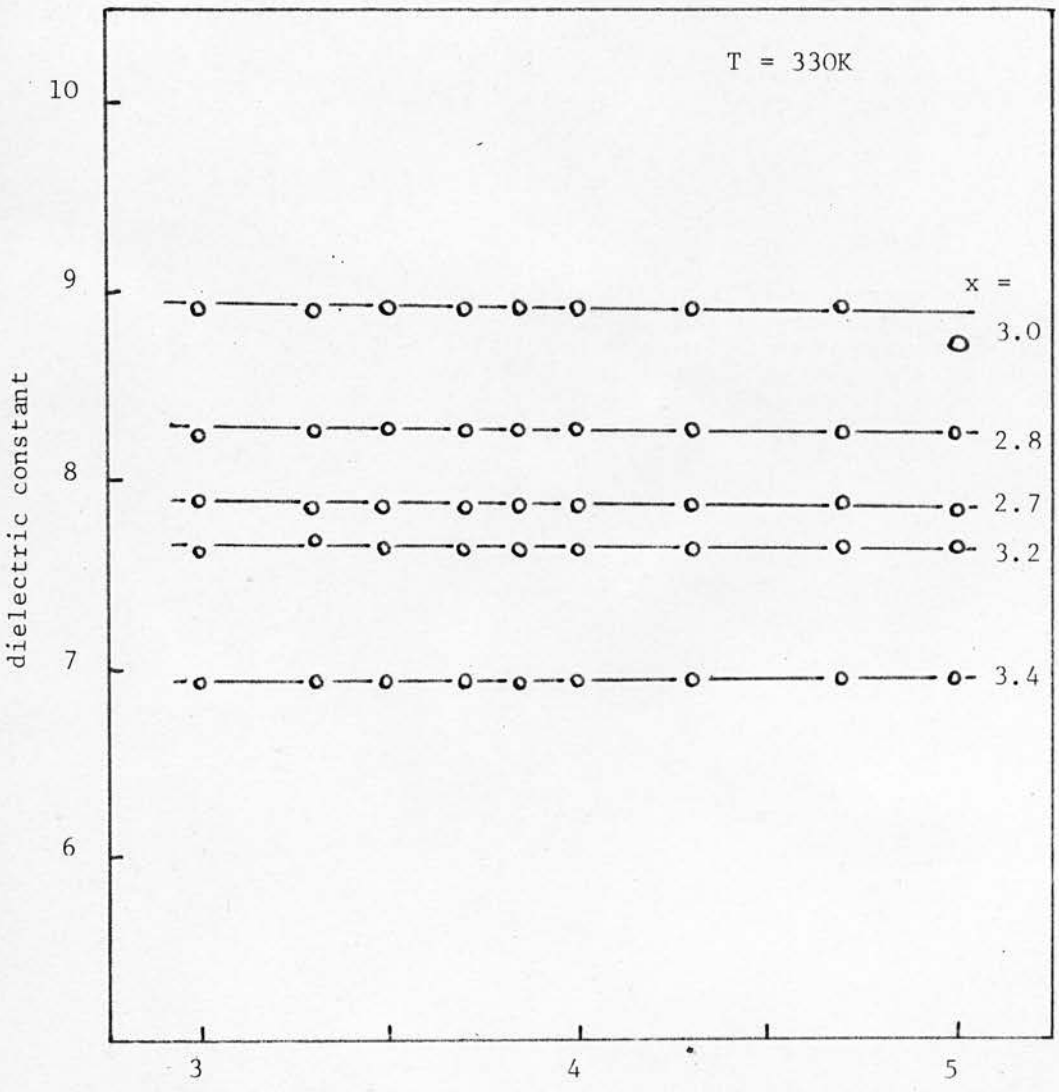

Figure (8.20)

Dielectric constants of As_2S_x

The same series of measurements performed on the As - S system was repeated on the As - Se system. Again evaporated gold electrodes were used.

6.5.4.1 D.C. conductivity

The d.c. conductivity of the As - Se glasses is described by equation (8.5) and the temperature dependence is shown in figure (8.21). In this case the temperature range was 50^{o} C to 110^{o} C. As - Se glasses have a lower glass transformation temperature than As - S glasses[65].

The activation energies and pre-exponential constants found are:

Nominal Se content As_2Se_x	E eV	C ohm^{-1} cm^{-1}
x = 2·6	0·882	540
2·8	0·886	710
3·0	0·882	845
3·2	0·878	840
3·4	0·870	640

The behaviour of the constant C and the conductivity for two temperatures is shown in figures (8.22) and (8.23). From these results it is apparent that the behaviour of the As - S and As - Se systems is quite different. The maximum in C and σ near stoichiometry in the As - Se system agrees well

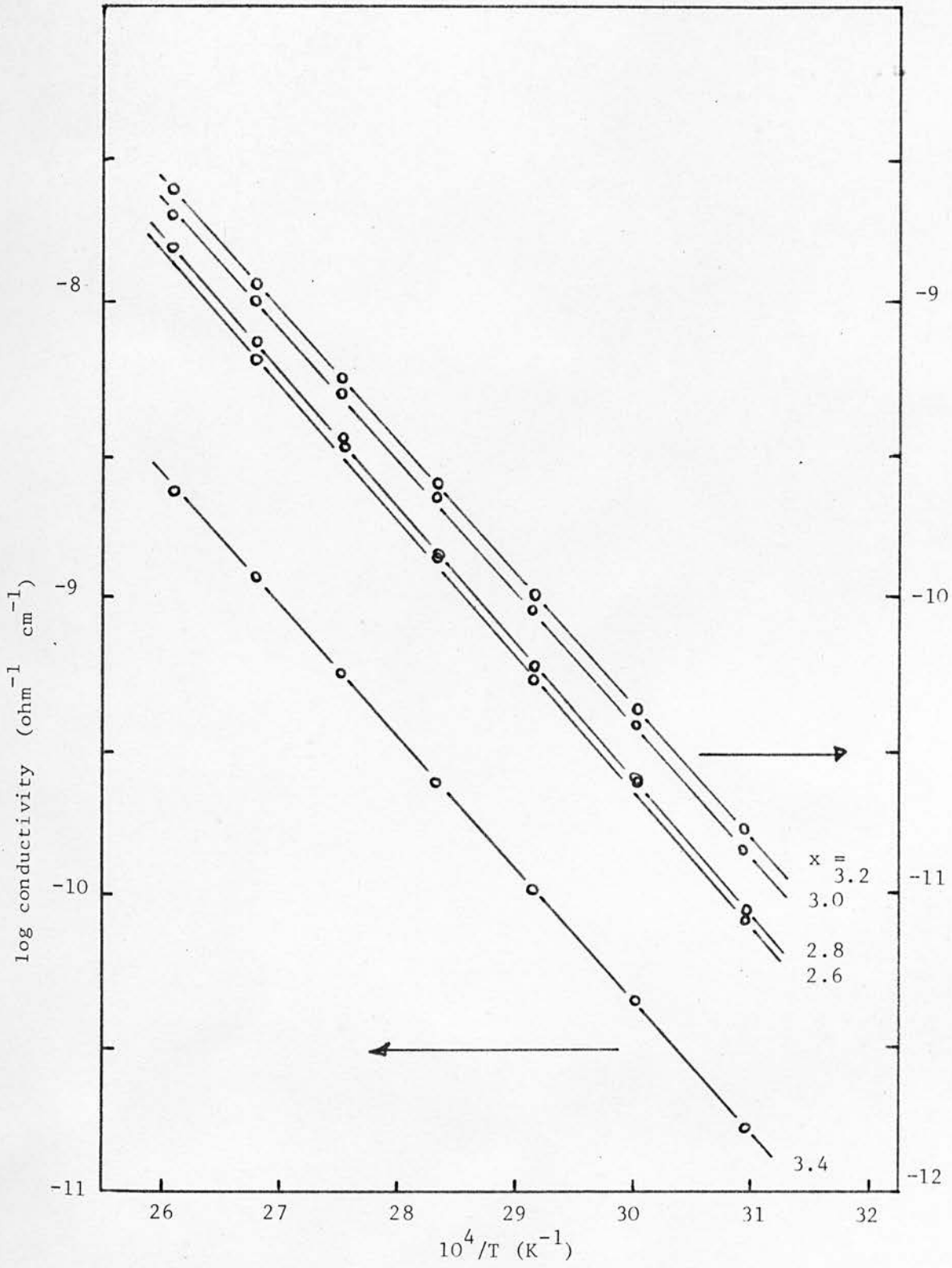

Figure (8.21)

D.c. conductivity of As_2Se_x

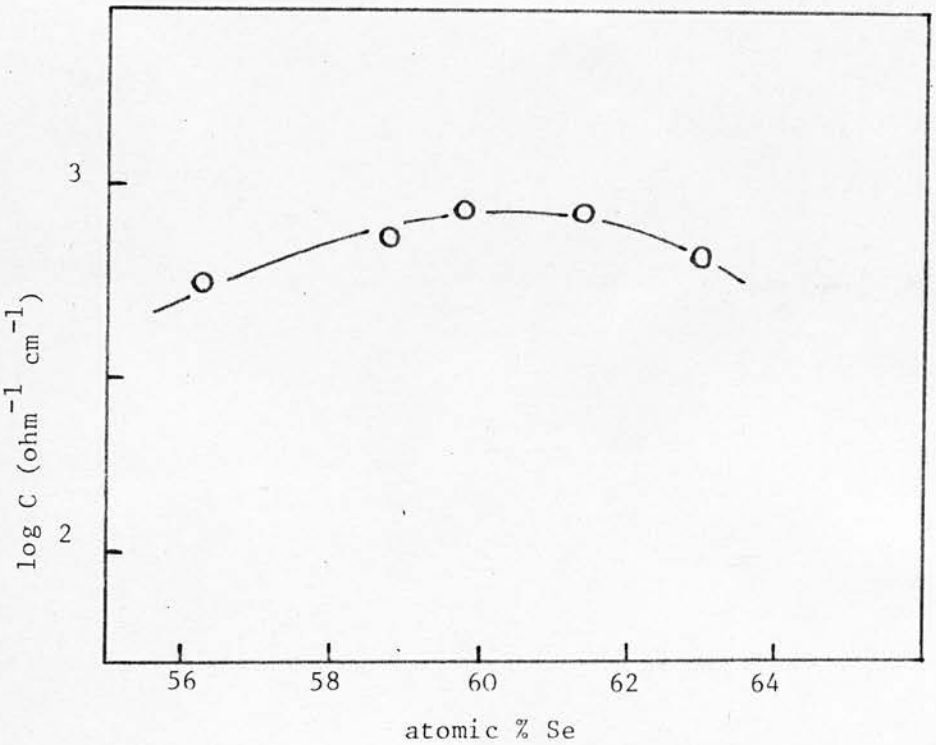

Figure (8.22)

Pre-exponential constant of the As-Se system

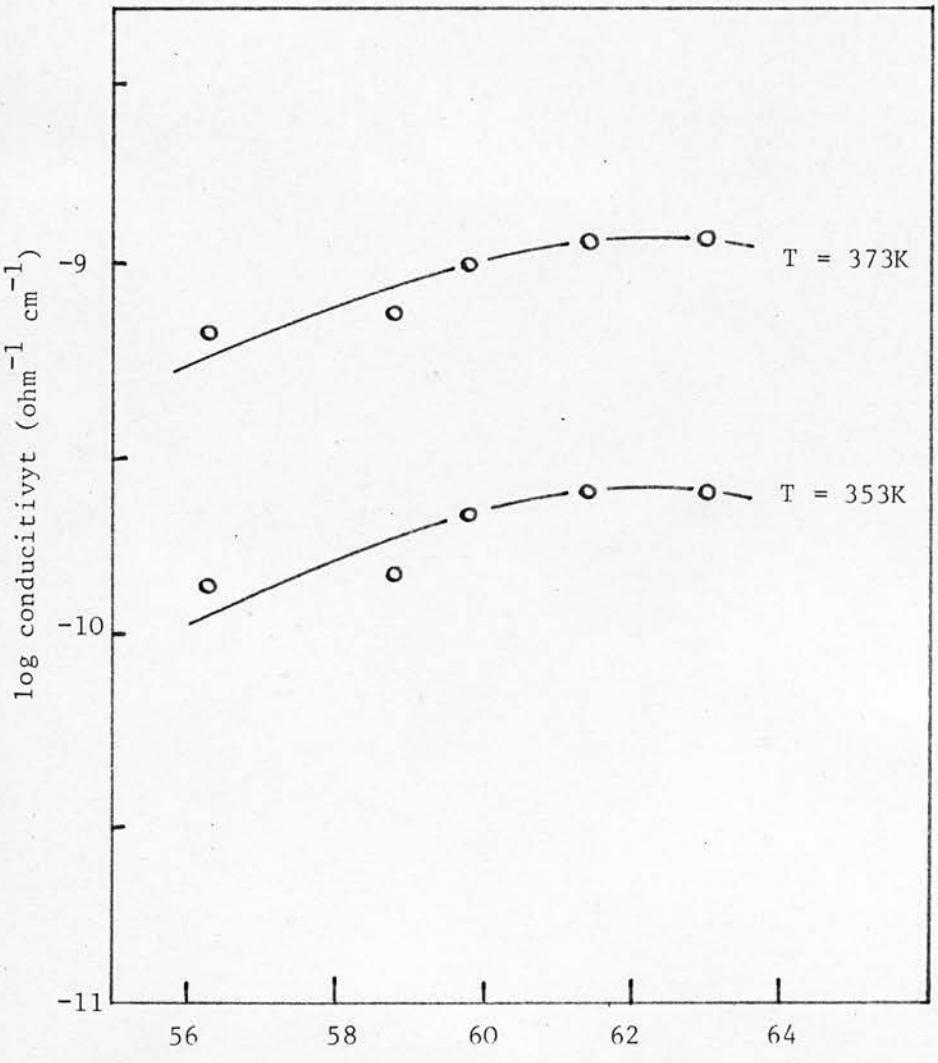

Figure (8.23)

D.c. conductivity of the As-Se system

with the results of Edmond[57].

6.5.4.2 A.C. Conductivity

The frequency dependence for various temperatures is illustrated in figures (8.24) to (8.28).

The conductivity at low frequencies can be seen to be dominated by the d.c. component so that the measured conductivity is

$$\sigma_m = \sigma_{DC} + \sigma_{AC} \qquad (8.7)$$

The frequency range covered is not great enough to allow a temperature variation of the slope s of the logarithm of the a.c. component to be determined, but at 315 K the slopes are:

Nominal Se content	slope
$As_2 Se_x$	s
x = 2·6	1·10
2·8	0·94
3·0	1·10
3·2	0·93
3·4	0·92

The errors on the slopes are fairly large (about ± 0·1) as

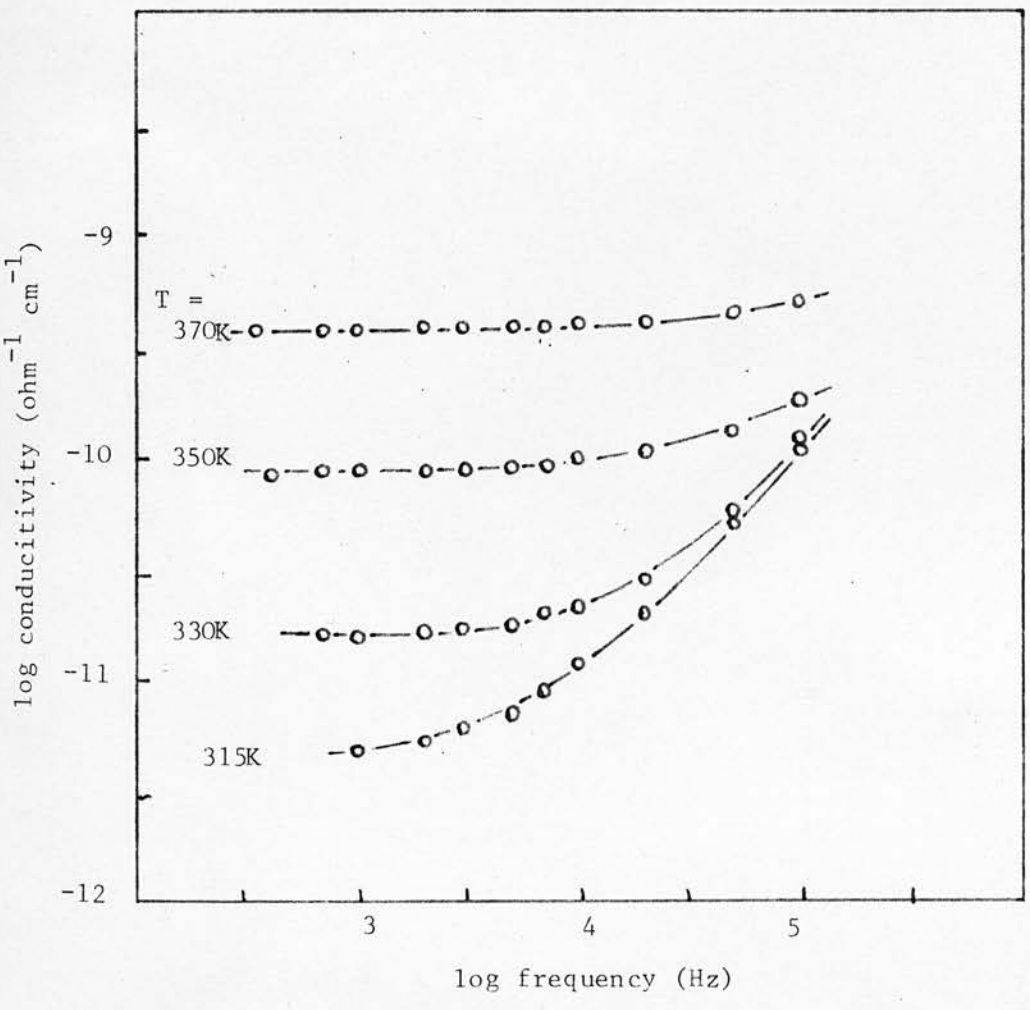

Figure (8.24)

A.c. conductivity of $As_2Se_{2.6}$

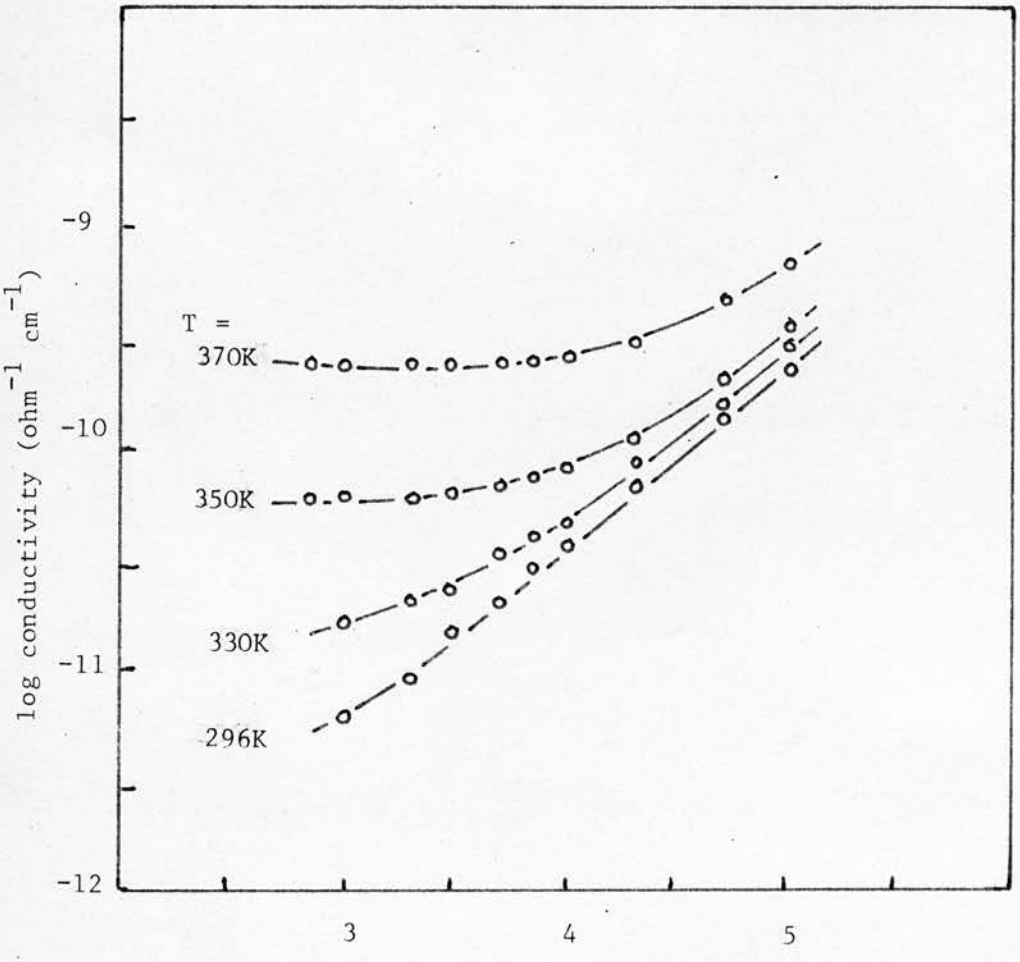

Figure (8.25)

A.c. conductivity of $As_2Se_{2.8}$

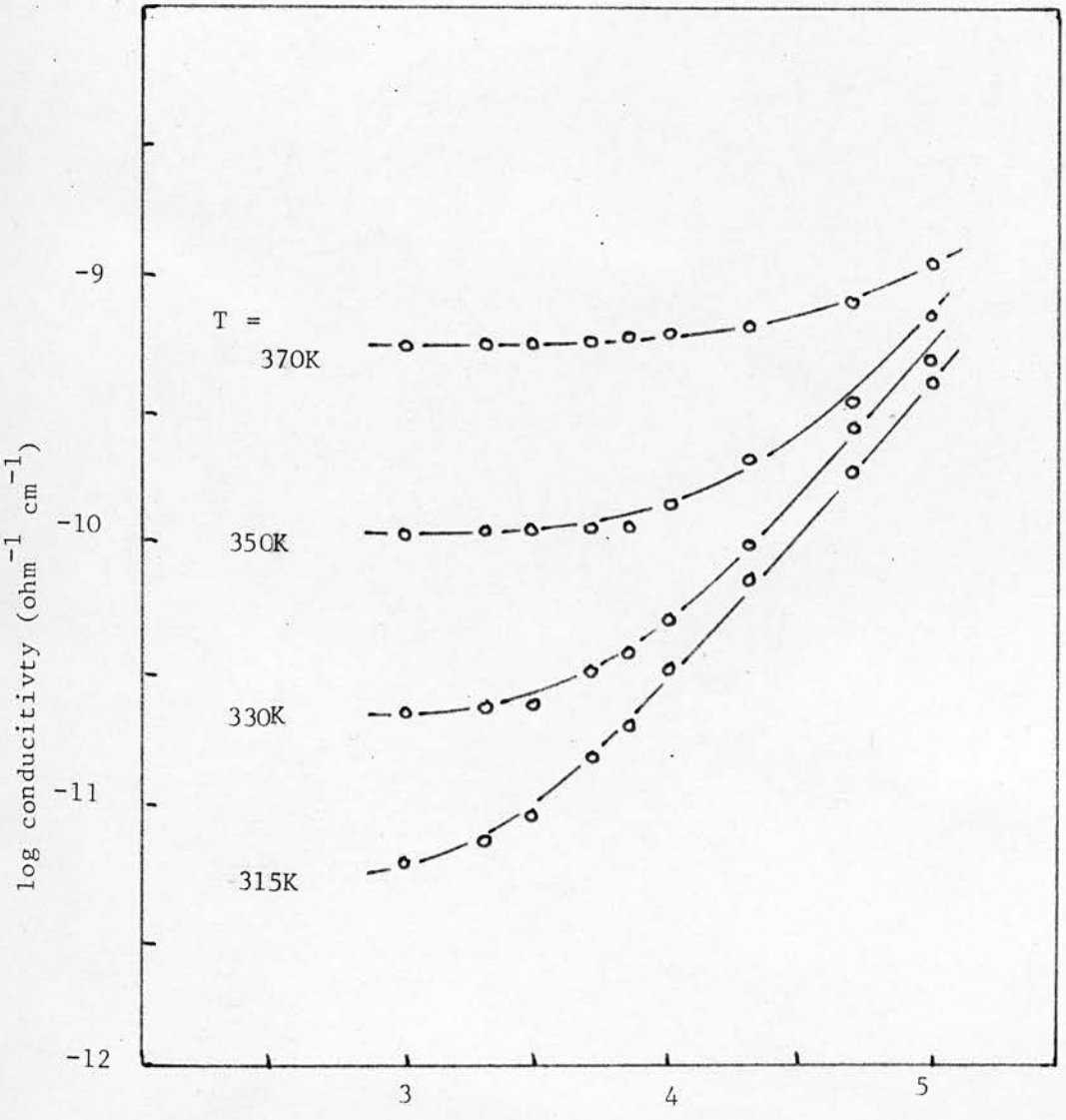

Figure (8.26)

A.c. conducitivty of $As_2Se_{3.0}$

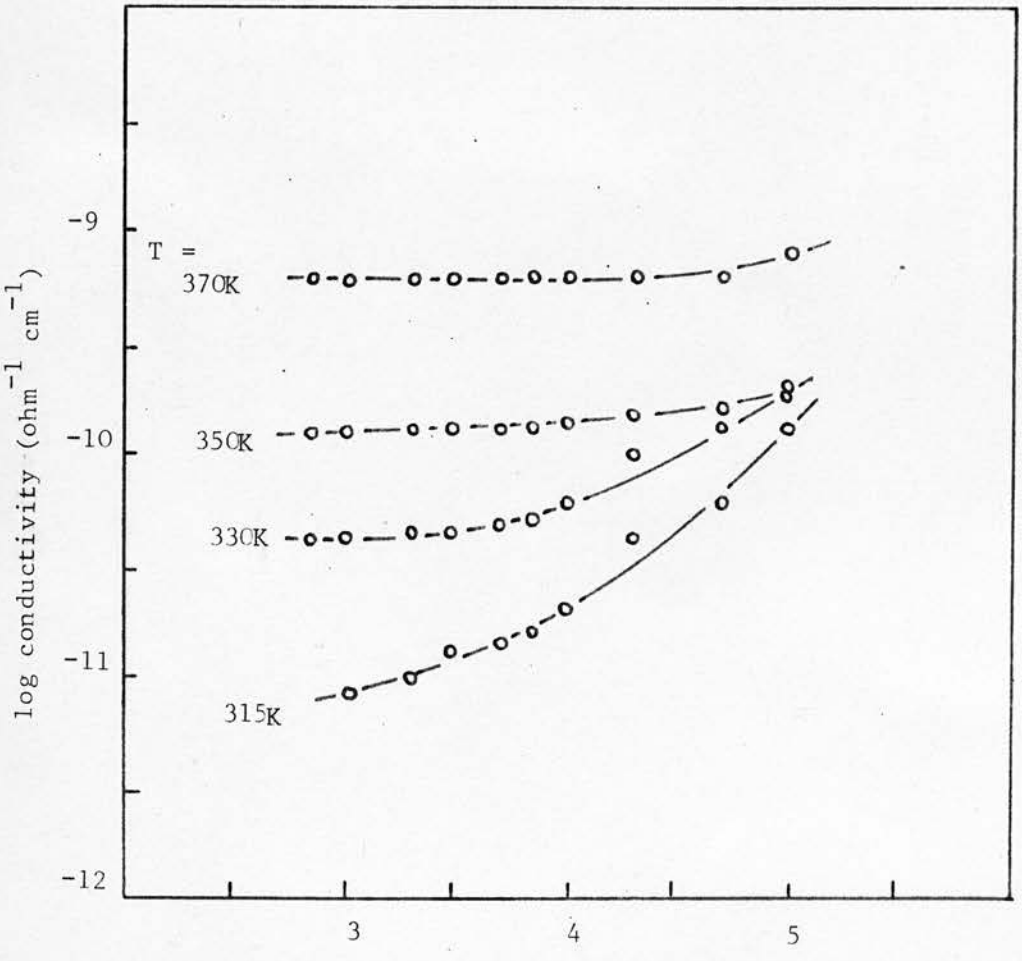

Figure (8.27)

A.c. conducitivty of $As_2Se_{3.2}$

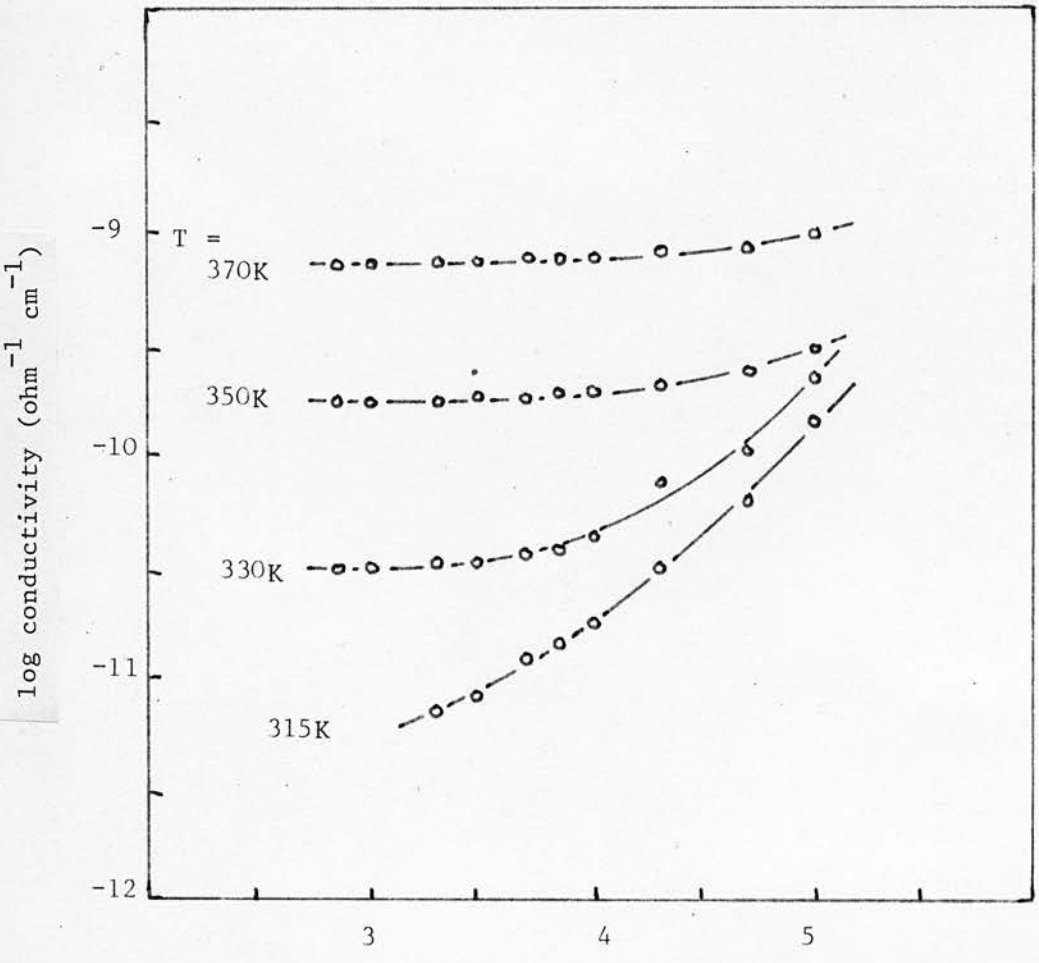

Figure (8.28)

A.c. conductivity of $As_2Se_{3.4}$

there was some scatter in the measured points and the a.c. conductivity was dominated by the d.c. component. Nevertheless, as in the As - S system, the slope s appears to decrease with decreasing As concentration.

Figure (8.29) shows the a.c. and d.c. conductivities as a function of Se content at 330 K: a convenient temperature to show the transition from the d.c. to the a.c. conductivity. Again there is a contrast with the a.c. measurements of the As - S system, a maximum in the conductivity at stoichiometry is indicated.

The measurements on the As - Se system were in general more difficult to make consistently than those of the As - S system. There was more scatter in the conductivity points and the values of the dielectric constants varied quite considerably on repeating a series of measurements, sometimes on the same sample as well as on the same material. In the majority of measurements the dielectric constants lay between 9 and 10·5 but the materials $As_2 Se_{2.8}$ and $As_2 Se_{3.0}$ sometimes gave values between 11·8 and 13·9. The mean values are given in figure (8.30) and the spread is indicated by the bars. These two ranges are not outside those reported in the literature[16] [38] [44]. Unless there was an intermittent fault in the sample holder or measuring bridge, the most probable reason for these results would seem to be the existence of bad contacts to the material.

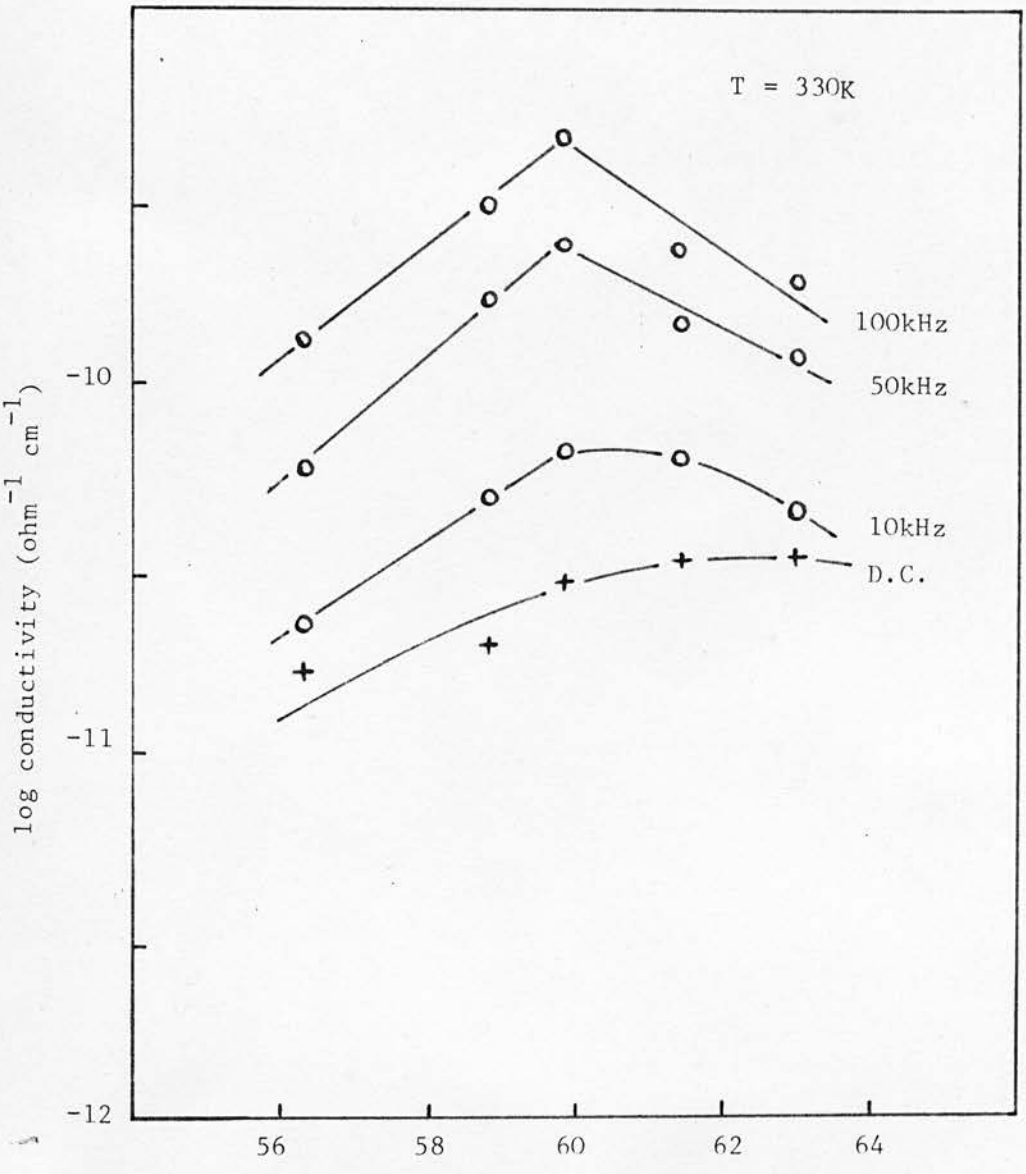

Figure (8.29)

Conductivity of the As-Se system

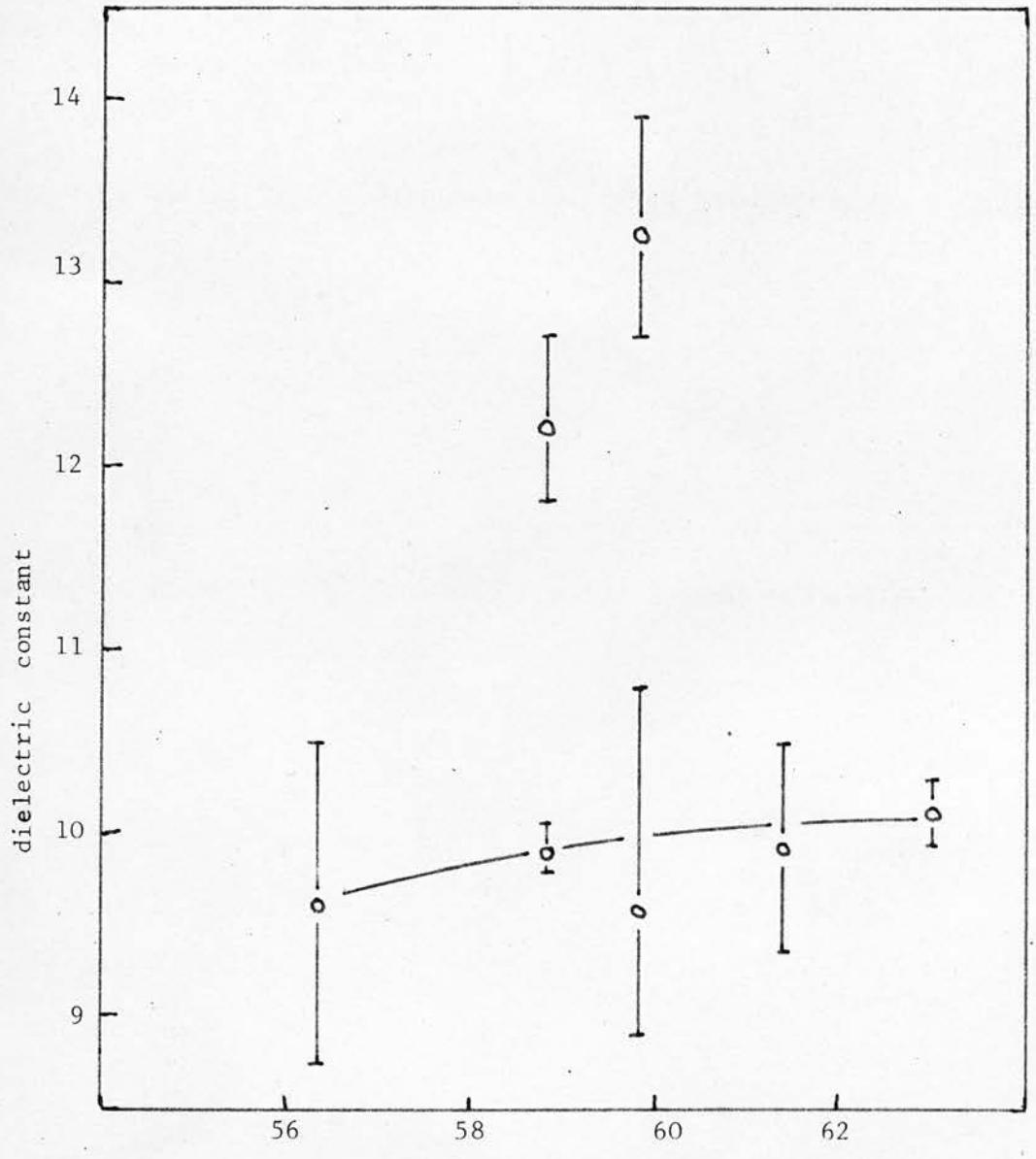

Figure (8.30)

Average values of the dielectric constant of the As-Se system.

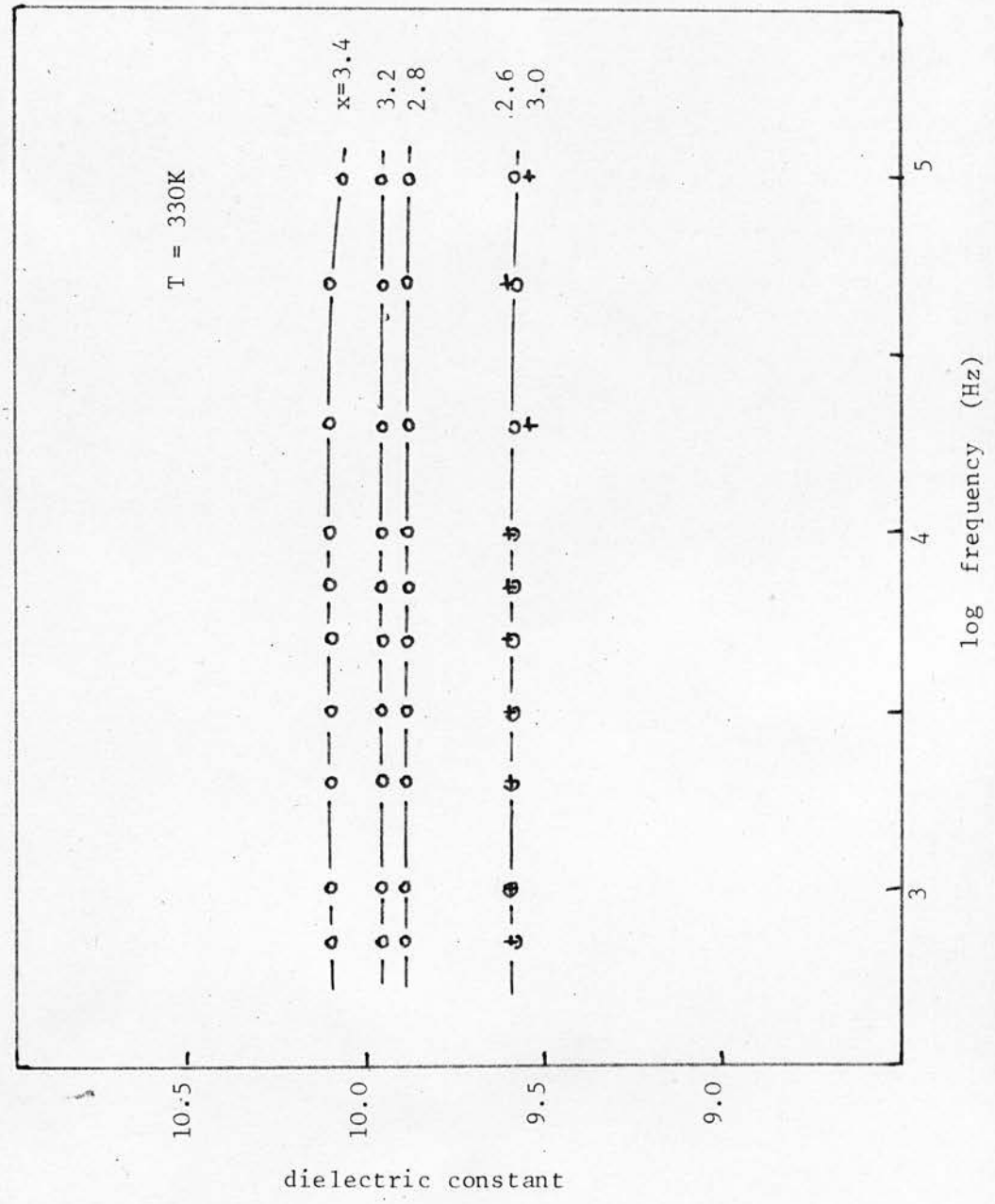

Figure (8.31)

Dielectric constant of As_2Se_x

The frequency dependence of the dielectric constants of samples near the average is shown in figure (8.31). Measurements which give high dielectric constants did not show any more variation with frequency than the lower results.

8.6 Microwave results

8.6.1 Arsenic sulphide

Measurements were made on several small ring resonators (mean radius 9·67 mm) and one of mean radius 16·4 mm. The latter was prepared by the slow melting technique described in section (6.3.3). The results were calculated using the computer program described in section (7.5) and appendix (A.2).

8.6.1.1 Dielectric constant

The frequency of each microstrip resonance enabled the effective dielectric constant to be determined using equation (6.45). To arrive at the true dielectric constant the expression of Jain et al[75] (i.e. equation (6.19)) was used. Figure (8.32) shows the variation of the effective dielectric constant (ϵ'_e) with frequency for two of the smaller resonators. The solid and dashed lines on the graph show the theoretical values for ϵ'_e calculated from equation (6.19) using the dimensions of the two resonators. These were: strip width, w, 1·5 mm; mean ring radius, r, 9·67 mm; and thicknesses, h, 1·54 mm and 1·30 mm. It can

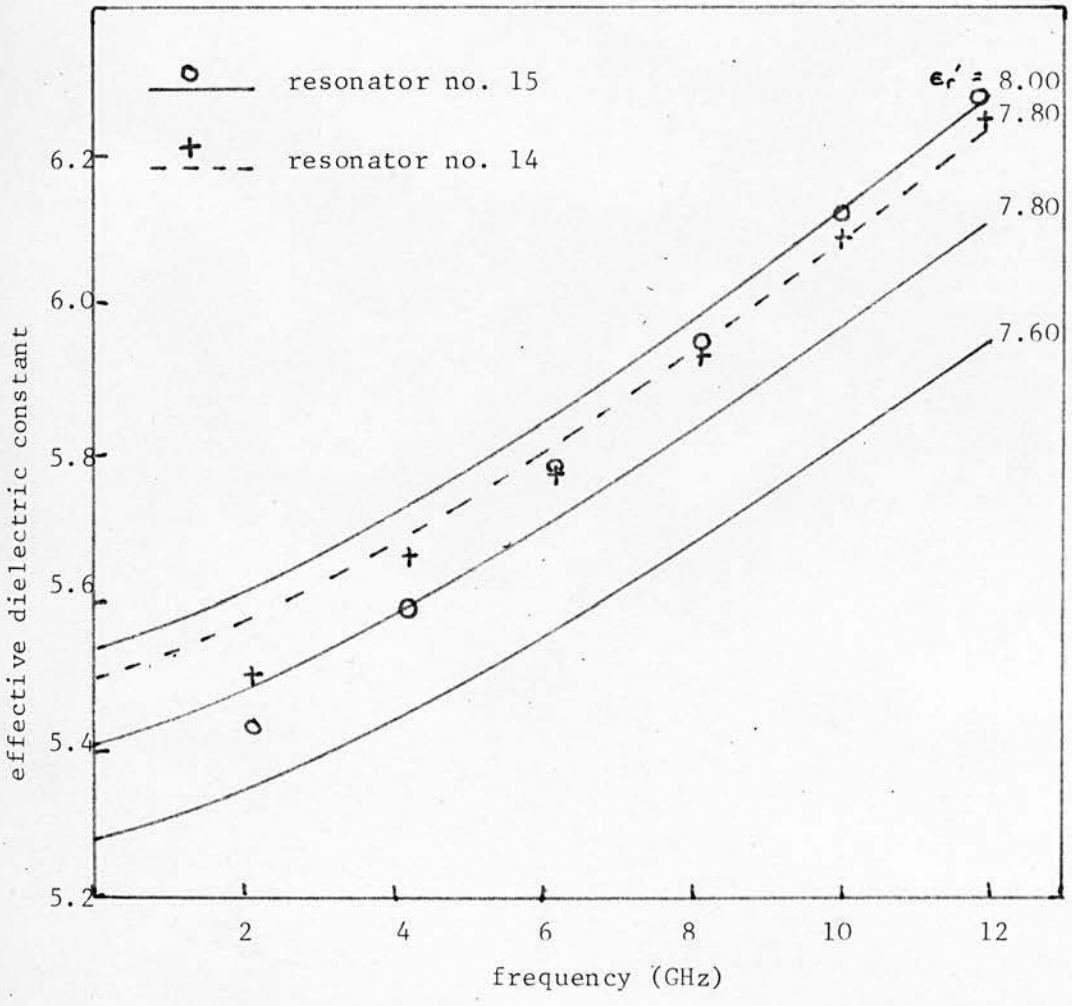

Figure (8.32)

Microstrip effective dielectric constant of two As_2S_3 resonators

be seen that the difference in substrate thickness has little effect on the effective dielectric constant. Assuming the permittivity is constant (or decreasing) over the frequency range (0 to 12 G Hz) the agreement with theory is not as good as for the alumina substrate (figure (7.4)). However, the deviation is small and probably not significant.

Figure (8.33) shows the dielectric constant as a function of frequency for both the small and large resonators. The agreement between them is good over the whole range of frequencies.

8.6.1.2 Dielectric loss

The dielectric loss was difficult to determine accurately for the reasons given in sections (6.4) and (7.4.1) and the same uncertainty about the results exists as for the alumina resonator.

For the smaller ring resonators the unloaded Q factors typically varied from 150 at 2·1 G Hz to 270 at 11·8 G Hz. Figure (8.34) illustrates the resulting loss tangent for each resonance calculated by the equations of Schneider (equations (6.34), (6.35) and (6.8)) for the conductor attenuation and using the correction indicated by figure (6.2) for radiation losses; also included are calculations made using the "wide strip" equation for the conductor attenuation

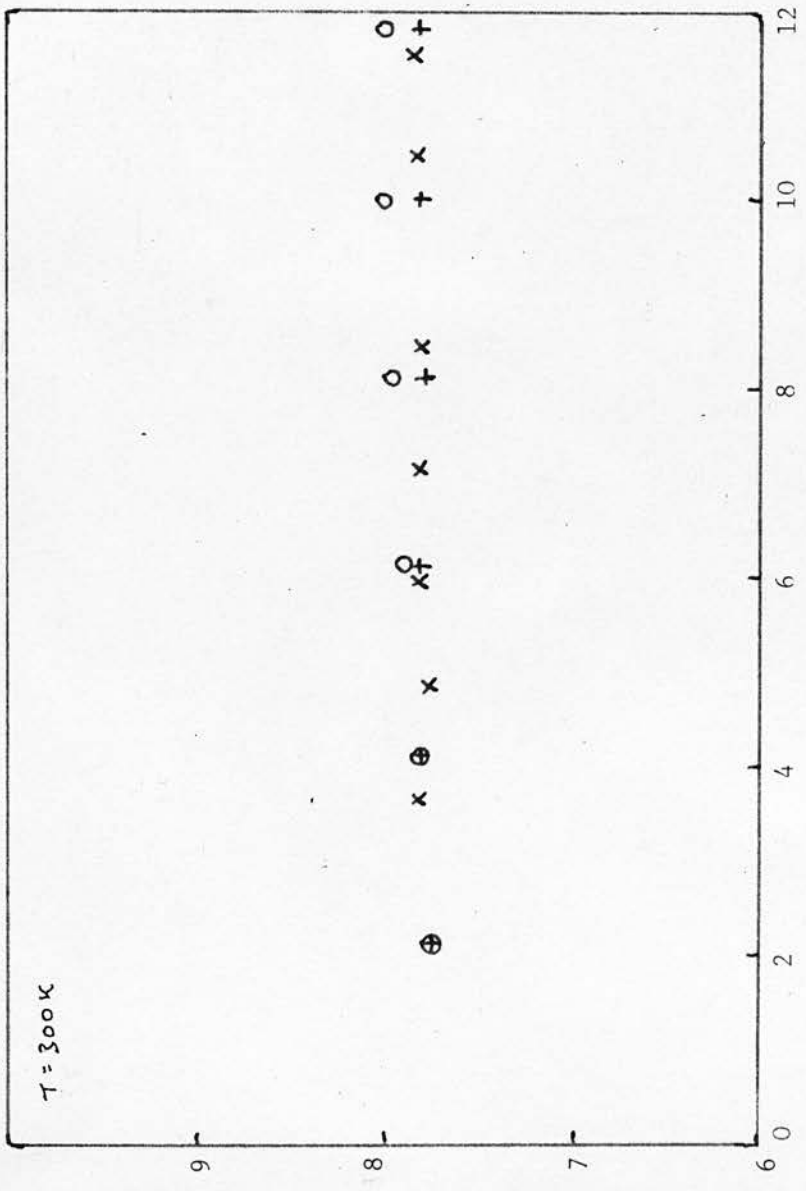

dielectric constant

Figure (8.33)

Dielectric constant of As_2S_3

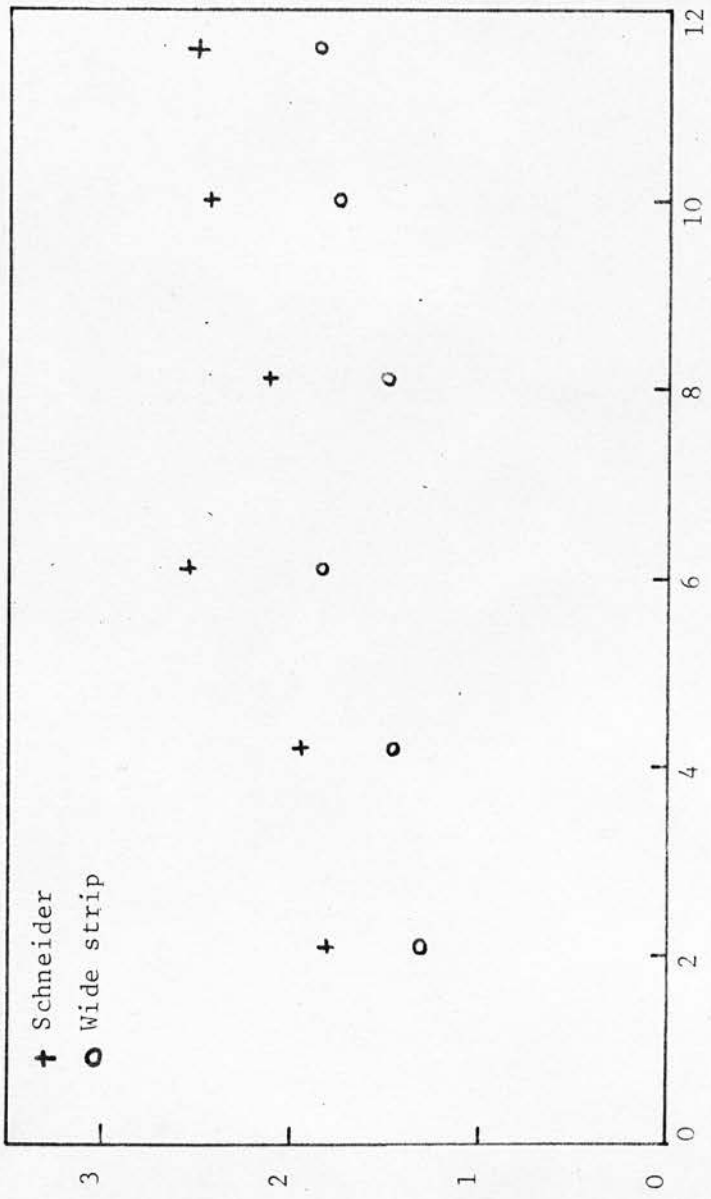

Figure (8.34)

Loss tangent of As_2S_3

$$\alpha_c = \frac{R_s}{Z_0 W} \qquad \text{(equation (6.24))}$$

which is often found to give good agreement with experiment. A comparison with figure (7.5) shows that the loss tangent for $As_2 S_3$ is probably a little greater than that for alumina, noting that the most accurate results will be those at the higher frequencies (between 8 and 12 G Hz). The resonator with the larger radius produced resonances of higher Q (228 at 3·66 G Hz to 554 at 11·51 G Hz) but the resulting loss tangents were again close to $2 \cdot 10^{-3}$ (i.e. within $\pm 0 \cdot 5 \cdot 10^{-3}$ over the whole frequency range) and the higher Q factors can be attributed to a decrease in the radiated power. These values for the loss tangents probably indicate the maximum losses in the materials because of the uncertainty of the magnitudes of conductor resistivity, radiation losses and the effect of conductor thickness, as discussed in section (6.4).

Figure (8.35) compares the conductivity measured by the microstrip technique with the low frequency conductivity. Included in the diagram are the results of Hayatee[16] which show an apparent loss peak close to $5 \cdot 10^8$ Hz. The present microwave results are not inconsistent if the difference in the low frequency results is considered, but it should be remembered that (as pointed out in chapter 4) there are often large differences in the magnitudes of the a.c. conductivity measured by different experiments on different samples. The

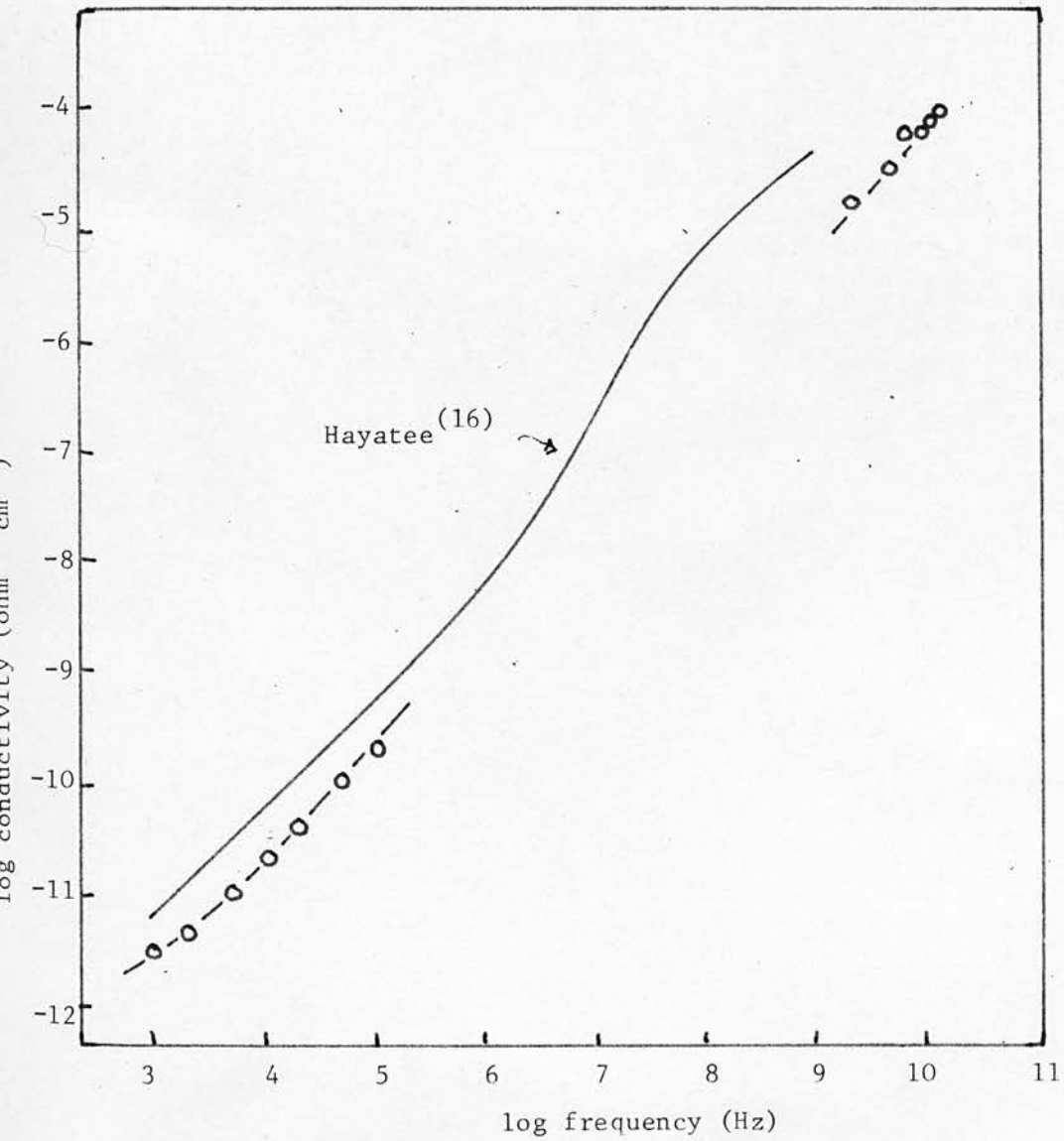

Figure (8.35)

A.c. conductiivty of As_2S_3

different samples used for the low and high frequency measurements in this work make a firm conclusion over the whole frequency range difficult but the present results indicate that the microwave results are an extension of those at low frequencies. An important point to note is that the conductivity shows no sign of saturating.

8.6.1.3 Temperature variation

The temperature was varied between 90 K and 380 K as described in section (7.2.2). Because the frequency variation involved plug-in units to change from band to band (i.e. 1·8 to 4·2 G Hz ; 3·8 to 8·2 G Hz ; and 8 to 12·4 G Hz) the measurements were made at fixed frequency and complete runs performed at 2·12 and 9·97 G Hz on a small resonator and 7·12 G Hz on the large resonator.

The results for the dielectric constant are shown in figure (8.36). The differences in the values for each frequency are not significant and probably arise from measurement errors or the inaccuracy of the theoretical equations for the dispersion of the effective dielectric constant.

The variation with temperature is very small (less than 0·1 over the whole range). The temperature and frequency variation of the dielectric parameters should bear a correlation if the relaxation time depends on temperature.

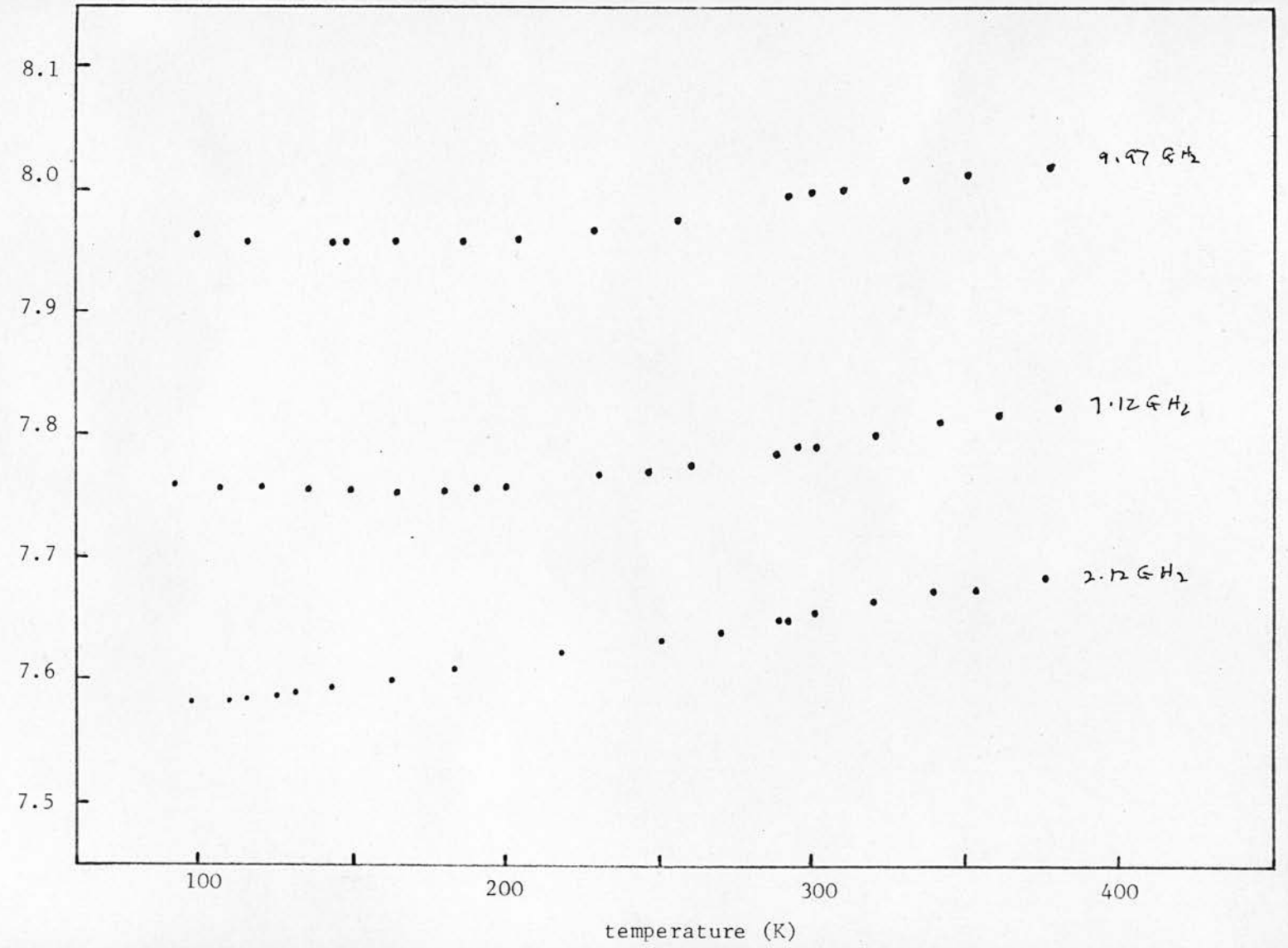

Figure (8.36)

Dielectric constant of As_2S_3

In the simple Debye case with the relaxation time given by

$$\tau = \tau_0 \exp \frac{U}{kT}$$

the equivalent frequency range (for the 10 G Hz resonance) is very approximately 5 G Hz (380 K) to 10^{12} Hz (100 K) for $U \sim 0{\cdot}05$ e V . The results therefore imply a continuing decrease in the dielectric constant as the frequency increases through the microwave region, though without a knowledge of the distribution function for relaxation times the extent of the increase cannot be estimated. The fact that the increase of ϵ'_r with T is very small may mean that the measurement frequency is far from a region of dielectric dispersion or that there is a broad distribution of relaxation times for the mechanism involved as at lower frequencies.

The variation of loss tangent with temperature is complicated by the temperature coefficient of resistance of the gold conductors. As the temperature drops the resistivity falls and the conductor losses also fall. This results in a higher conductor Q factor. At the three frequencies used the highest Q factors measured were generally at low temperatures and this may have been caused, at least partly, by the resistivity change.

Taking the temperature coefficient of resistivity of gold as $3{\cdot}4.10^{-3}$ per degree Celsius[102] the resistivity changes to a third of its room temperature value at 100 K;

this adds $1 \cdot 8 \cdot 10^{-3}$ at 2·12 G Hz, $6 \cdot 10^{-4}$ at 7·12 G Hz and $5 \cdot 10^{-4}$ at 9·97 G Hz to the loss tangents. The uncorrected values of $1/Q_D$ are shown in figure (8.37). To provide a clearer view of the trend of $1/Q_D$ with increasing temperature the points showing large scatter were omitted and those remaining corrected for the changing resistivity with the results shown in figure (8.38). The loss tangent is proportional to $1/Q_D$ by a factor close to 1·05 for the three frequencies. There is very little change in $\tan\delta$ with temperature which is consistant with the low frequency results and the model of Pollak described in chapter 3.

8.6.2 Arsenic selenide results.

Only two resonators were made using arsenic selenide as the substrate. Both of these suffered from defects.

The first made was a straight line resonator of length 14·0 mm and conductor width 1·50 mm. This form suffers from the fringing of the electric field at the ends of the strip giving rise to a larger effective length, but it is still possible to calculate the conductivity.

From an unloaded Q factor of 221 at 9·14 G Hz the loss tangent is approximately $3 \cdot 10^{-3}$ giving a conductivity of $1 \cdot 6 \cdot 10^{-4}$ ohm^{-1} cm^{-1} assuming a dielectric constant of 10[38].

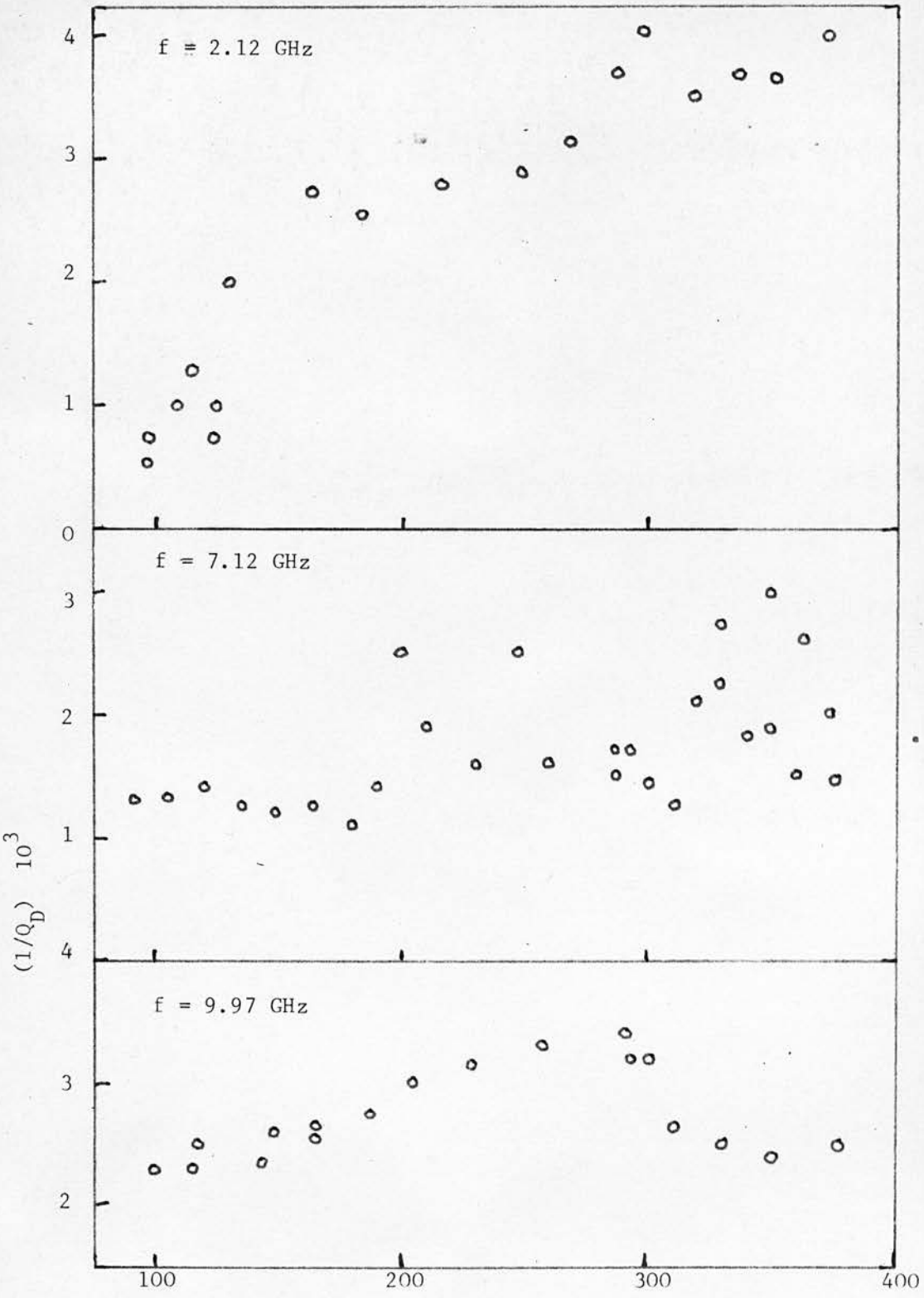

Figure (8.37)

Dielectric losses $(1/Q_b)$ of As_2S_3 resonators

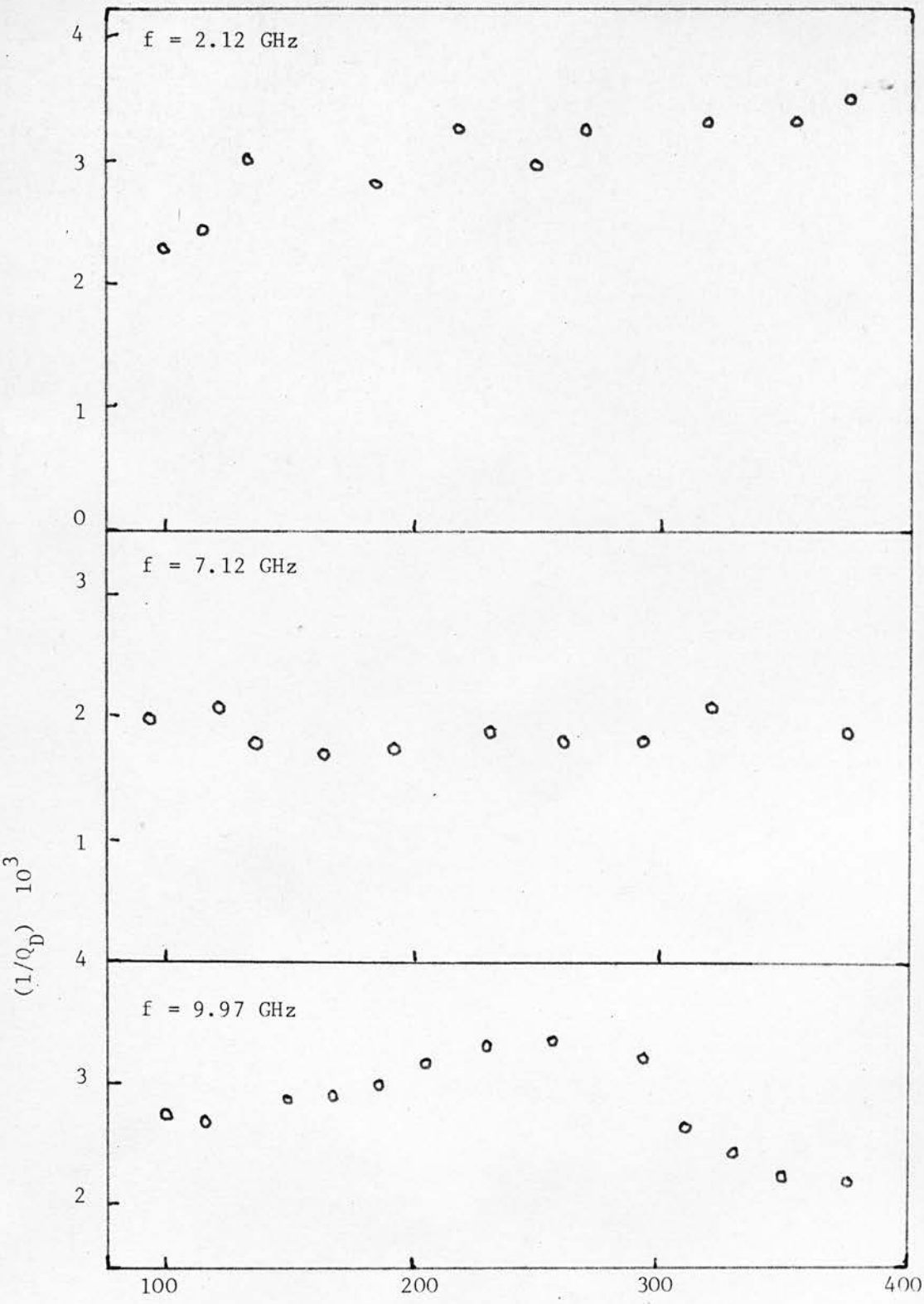

Figure (8.38)

Dielectric losses of As_2S_3 resonators corrected for temperature coefficient of resistance of gold

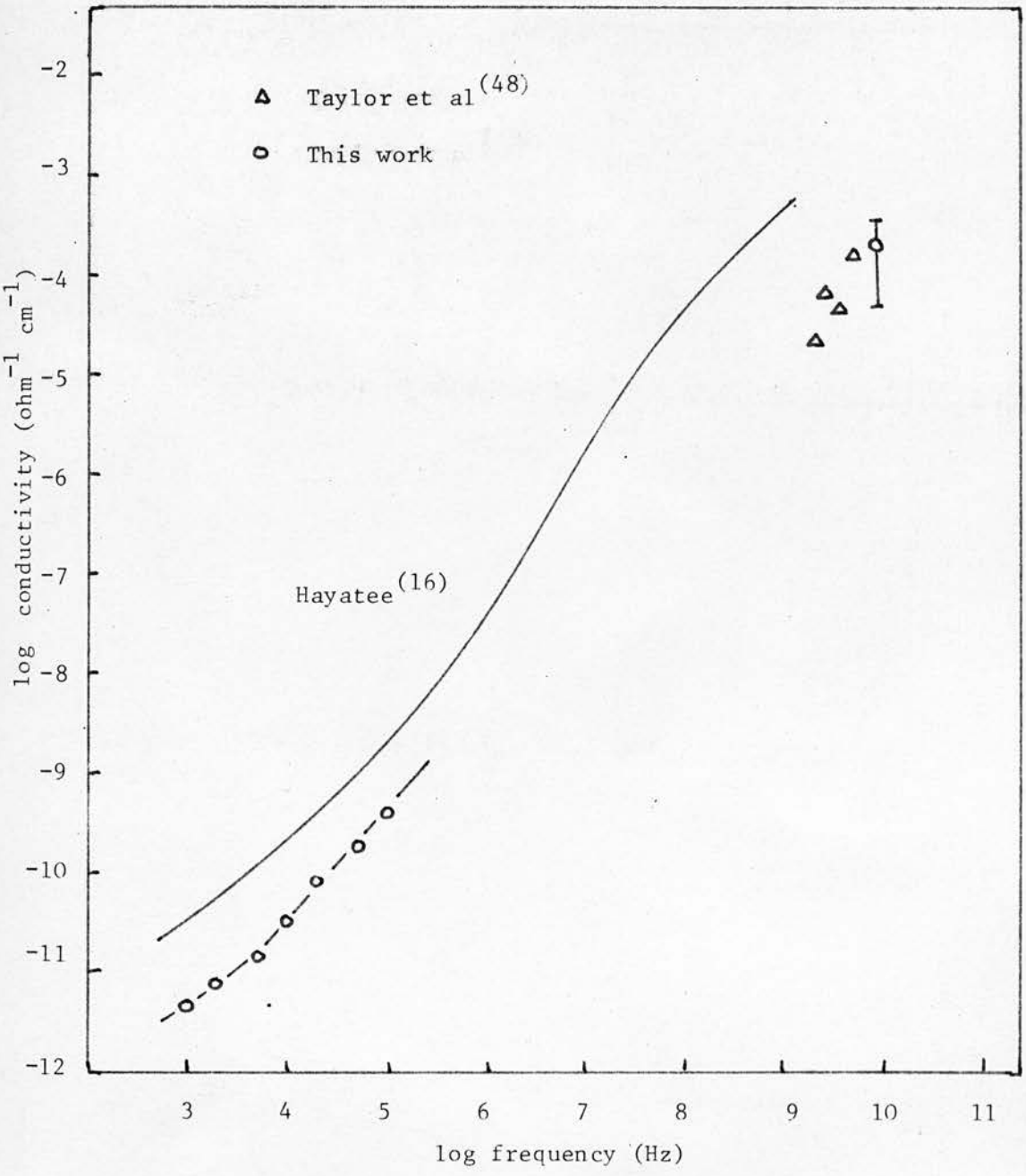

Figure (8.39)

A.c. conductivity of As_2Se_3

A ring resonator of radius 9·67 mm was prepared but during the evaporation of the ground plane a crack appeared from excess heating and broke the conducting ring. Nevertheless five resonances were found over the range 1·8 to 12·4 G Hz. The resulting dielectric constants ranged from 7·0 to 7·8 which is below the square of the refractive index[103] and therefore unreliable. The resonator had Q factors of less than 100 indicating high losses; this was probably the result of the crack.

Figure (8.39) compares the audio and microwave frequency results and includes the results of Hayatee[16] and Taylor, Bishop and Mitchell[48]. As with $As_2 S_3$ these results indicate that the conductivity increases linearly with frequency at least as far as the microwave region.

CHAPTER 9

Discussion

In this final chapter the results are discussed in terms of the theoretical formulations for the a.c. and d.c. conductivities of amorphous semiconductors, and, more qualitatively, with reference to the structure of glasses in the As - S and As - Se systems.

9.1 Review of conductivity equations.

The relevant equations describing the d.c. and a.c. conductivities of amorphous semiconductors are (see chapters 2 and 3):

$$\sigma_{DC} = C \exp - \frac{E}{kT} \tag{9.1}$$

and

$$\sigma_{AC} = \frac{\pi^3}{96} \left[N(E_F)\right]^2 e^2 kT a^5 \omega \left[\ln \frac{\omega_0}{\omega}\right]^4 \tag{9.2}$$

These expressions describe, at least qualitatively, the observed temperature and frequency dependences for a hopping mechanism in amorphous semiconductors.

9.2 Microwave conductivity.

In view of the several possible explanations for the low frequency behaviour of the a.c. conductivity in

amorphous semiconductors it was important to obtain results in the microwave region. At a high enough frequency (i.e. when the period of oscillation becomes comparable to or shorter than the relaxation time of the dielectric relaxation mechanism) it should be possible to distinguish between the proposed mechanisms. As the frequency is increased a saturation of the conductivity may indicate hopping conduction or Maxwell-Wagner polarisation whereas a further increase of the conductivity, not necessarily proportional to the first power of frequency, may show that the conductivity is dominated by a tail from the infra-red vibration band.

A comparison with the low frequency results for As_2S_3 and As_2Se_3 (figures (8.35) and (8.39) respectively) shows a continuation of the $\sigma = A\omega^s$ dependence with $s \approx 1$. However, care should be exercised in this conclusion because of the gap in the measurements between 10^5 and 10^9Hz (the region where increased frequency dependences have been reported[16][42]) and also because of the differing magnitudes of the conductivity found by different authors.

The results are more useful for providing an indication of any possible saturation in the conductivity at high frequencies. The present results show no sign of this though this may mean that the measurement frequency was still too low. It thus appears that the most likely mechanisms at these frequencies are either a low frequency extension of the

far infra-red absorption as first put forward by Austin and Garbett[46], or a continuation of the low frequency electronic hopping. The tail of a phonon absorption band would be expected to have a temperature dependence of T^{n-1} for an n -phonon process[46], whereas phonon assisted hopping has a dependence between T^0 and T^1 [31]. Unlike some situations in crystalline materials a single phonon process is allowed when the lattice is disordered[46] and this will give rise to a temperature independent conductivity.

It is not possible to be precise about the temperature dependence of the microwave conductivity owing to the numerous corrections needed to be made to the microstrip results, but there is no indication that it is strong in arsenic sulphide (figure (8.38)). The evidence for this is supported by the small variation of the dielectric constant with temperature (figure (8.36)). Pollak's[31] model for the a.c. hopping conductivity describes the results found with reasonable accuracy if it is assumed that the mechanism will still be applicable at high frequencies. The small temperature dependence can be explained as resulting from an increasing need for correlation between the hopping events as the mean hopping distance decreases. In this case the appropriate equation for the conductivity is (equation (3.85))

$$\sigma = \frac{\pi^2}{4} \alpha \omega \frac{r_\omega^3}{r_s} \epsilon N_c \qquad (9.3)$$

in which the temperature dependence has disappeared. At a

frequency of 10 GHz the average hopping distance r_ω $(\approx a \ln \frac{\omega_0}{\omega})$ has decreased to about 3a and if this represents the average distance between localised states implies that the density of such states is close to 10^{21} cm^{-3}. This is probably too high and leads to a carrier concentration, N_c, of approximately 3.10^{19} cm^{-3} using equation (9.3) with $a = 3\,\text{Å}$ and $\omega_0 = 10^{12}$ sec^{-1}.

With the absence of any other explanation for the a.c. conductivity at microwave frequencies and the decreasing hopping distance, it seems likely that the loss process in this region in amorphous As_2S_3 is due to the tail of the phonon absorption region. This view is re-enforced by the indication of a slight temperature dependence at a frequency at which the degree of correlation should be high because the mean hopping distance is small.

A conductivity with an ω^1 and weak temperature dependence can be described by the assumption of a wide distribution of relaxation times[17] for the relevant physical process. Using the very general formalism of Gevers and Du Pré[24] it is possible to extract a magnitude for the conductivity. In section (3.5.1) it was shown how the variation of the dielectric constant with temperature was related to the loss tangent and the coefficient of thermal expansion, α_L, starting with the assumption that there existed a wide distribution of relaxation times. The resulting equation was

$$\frac{1}{\epsilon'_r} \cdot \frac{\delta \epsilon'_r}{\delta T} = A \tan\delta - \alpha_l \left(1 + \epsilon_\infty - \frac{2}{\epsilon_\infty}\right) \qquad (9.4)$$

where

$$A = \frac{2}{\pi T} \cdot \ln \frac{\omega'_o}{\omega} \qquad (9.5)$$

For many amorphous dielectrics the value of about $0{\cdot}06 K^{-1}$ was found for A at room temperature.

In some cases the right hand side of equation (9.4) can be simplified by neglecting one or other of the two terms but for $As_2 S_3$ the expansion coefficient is too high ($2{\cdot}37.10^{-5}\ K^{-1}$ (104)) for this.

Taking ϵ_∞ as $6{\cdot}4$ (53) and the temperature variation of ϵ'_r from figure (8.36) results in

$$A \tan\delta \approx 2{\cdot}2 . 10^{-4}\ K^{-1}$$

Figure (8.38) shows that $\tan\delta$ at 300K is close to 3.10^{-3} and thus

$$A \approx 0{\cdot}075\ K^{-1}$$

This value is probably a minimum because of the likely errors in the loss tangent but it is close to the average value of $0{\cdot}06\ K^{-1}$.

Equation (9.4) shows that the temperature coefficient of the dielectric constant ($\frac{1}{\epsilon'_r} \frac{\delta \epsilon'_r}{\delta T}$) could be negative for low values of the loss tangent, assuming that A does

not vary much from the value of $0{\cdot}06\ K^{-1}$. The positive temperature coefficient found therefore indicates that

$$A \tan\delta > \alpha_L' \left(1 + \epsilon_\infty - \frac{2}{\epsilon_\infty}\right)$$

i.e. $A \tan\delta > 1{\cdot}8.10^{-4}\ K^{-1}$ approximately.

Taking a value of $0{\cdot}1\ K^{-1}$ for A shows that $\tan\delta > 1{\cdot}8.10^{-3}$. This corresponds to a minimum conductivity of 8.10^{-5} ohm^{-1}.cm^{-1} at 10 GHz which is close to that found for arsenic sulphide (see figure (8.35)).

Equations (9.4) and (9.5) can be used to form a general expression for the a.c. conductivity:

$$\sigma = \frac{\pi}{2} \epsilon_o T\omega \left[\ln \frac{\omega_o'}{\omega}\right]^{-1} \left[\frac{\delta\epsilon_r'}{\delta T} + \epsilon_r' \alpha_L \left(1 + \epsilon_\infty - \frac{2}{\epsilon_\infty}\right)\right] \qquad (9.6)$$

This equation has a similar explicit temperature dependence to the equations of Pollak[31] and Austin and Mott[32] although the frequency dependence is close to $\omega^{1{\cdot}1}$ rather than $\omega^{0{\cdot}8}$. These two frequency dependences agree well with the audio-frequency conductivity data described in section (8.5.3.2), where it was found that for glasses of the As - S and As - Se systems the conductivity depended on composition and temperature such that if it was proportional to ω^s, then $0{\cdot}8 < s < 1{\cdot}1$.

It should be stated that at microwave frequencies

the relaxation times may not have a uniform distribution for a particular process as it is likely that the contribution due to thermally assisted hopping is decreasing and the phonon tail component increasing. However, the concept of a distribution of relaxation times is largely a mathematical device to describe a broad dielectric loss peak and because of this may not be affected by a change of conduction process provided it is smooth: thus the work of Gevers and Du Pré[24] may still be valid.

9.3 D.c. and low frequency conductivity in the As - S and As - Se systems.

The d.c. conductivities of all materials studied obeyed equation (9.1). However, there are major differences between the As - Se and As - S systems. Firstly, the values of the pre-exponential constants, C, varied quite considerably in magnitude. For the stoichiometric compounds values of 840 ohm^{-1} cm^{-1} for As_2Se_3 and 28·3 ohm^{-1} cm^{-1} for As_2S_3 were found. Mott and Davis[13] conclude that high values of C imply conduction in the extended states whereas low values originate from conduction in the localised states. This immediately separates the two glass systems from their position as very similar "prototype" amorphous semiconductors in which they are often regarded. The second difference is in the variation of the constant C (and therefore the conductivity) as the composition is changed: the As - Se system has a broad maximum in conductivity at or close to the

stoichiometric composition but the As - S system shows a sharp minimum at $As_2 S_3$. These differences reflect differing conduction mechanisms.

The activation energies for the two systems (see sections (8.5.3.1) and (8.5.4.1)) change slowly and uniformly with composition so that it is likely that the conduction mechanisms in each system are the same throughout the composition ranges studied. Writing the activation energy as

$$E = E_F - E_v \simeq \gamma T \qquad (9.7)$$

where γ is a temperature coefficient gives

$$C = \sigma_0 \exp \frac{\gamma}{k} \qquad (9.8)$$

The coefficient, γ , is expected to be roughly half the coefficient of the optical energy gap[13]. For $As_2 Se_3$ and $As_2 S_3$ this implies values of $3{\cdot}5.10^{-4}$ eV K^{-1}[107] and $2{\cdot}5.10^{-4}$ eV K^{-1}[61] for the two glasses respectively. Substituting these values in equation (9.8) gives the magnitudes of σ_0 as 15 Ohm^{-1} cm^{-1} for $As_2 Se_3$ and $1{\cdot}5$ ohm^{-1} cm^{-1} for $As_2 S_3$. These values are probably rather low ($As_2 Se_3$) and high ($As_2 S_3$) for definitely classifying the conduction as either occuring in the non-localised or localised states, but there is no certainty as to what the correct limits should be and the errors in the calculation of

σ_o could be fairly large. It is possible to calculate the values for γ of the compositions in the two systems by assuming that the constant σ_o is the same over each range of materials. This gives

$As_2 Se_x$		$As_2 S_x$	
x	γ (eV K^{-1})	x	γ (eV K^{-1})
2·6	$3·1.10^{-4}$	2·7	$3·9.10^{-4}$
2·8	$3·3.10^{-4}$	2·8	$3·6.10^{-4}$
3·0	$3·5.10^{-4}$	3·0	$2·5.10^{-4}$
3·2	$3·5.10^{-4}$	3·2	$4·2.10^{-4}$
3·4	$3·2.10^{-4}$	3·4	$4·7.10^{-4}$

where x is the nominal composition.

The value for $As_2 S_{3·4}$ ($4·7.10^{-4}$ eVK^{-1}) is greater than that found by Koseck and Tauc[61] for $As_2 S_5$ ($3·4.10^{-4}$ eVK^{-1}) so it seems likely that σ_o changes in the range close to stoichiometry (at least for the As - S system) provided nothing unusual happens between $As_2 S_{3·4}$ and $As_2 S_5$: e.g. a peak in γ at an intermediate composition. The increase in γ away from stoichiometry appears to show the correct trend indicating that this is an additional factor which needs to be considered as contributing to the magnitude of the conductivity. Hurst[106], as a result of thermopower measurements, finds that there is a minimum in γ at the stoichiometric composition in the As - Se system and this shows that the variation of σ_o dominates in this case.

For a comparison between these two glass systems

the d.c. conductivities are replotted in figure (9.1). Also shown are the results of Edmond[57] (As - Se) and Minami et al[56] (As - S). The As - Se conductivity is shown in greater detail in figure (9.2) and again compared with Edmond's work to emphasise that the maximum does not occur at the composition $As_2 Se_3$ but slightly on the Se rich (or As depleted) side.

The conduction in the As - Se system, probably being in the extended states, will be trap limited and the addition of excess As or Se is likely to increase the density of localised states by increasing the disorder. The increase in the density of traps will decrease the conductivity. Viewed in this way the maximum in the conductivity should occur at the most ordered composition which at first sight would appear to be $As_2 Se_3$. This was found by Hurst[106].

The structure of $As_2 S_3$ and $As_2 Se_3$ is similar: two-dimensional layers of 6 membered rings of As $X_{3/2}$ units[2][3] (X = S or Se). In the amorphous state variations in the bond angles and folding of the layers eliminate the long range order. If the most "ordered" material is not $As_2 Se_3$ but a composition with a slight depletion of As then the conductivity will be a maximum at this composition. This could be achieved if the glass is based on large units of $(As_2Se_3)_n$ in which the continuity of the layer network requires the elimination of a small amount of As[105]. It should be noted that this contradicts the conclusion of

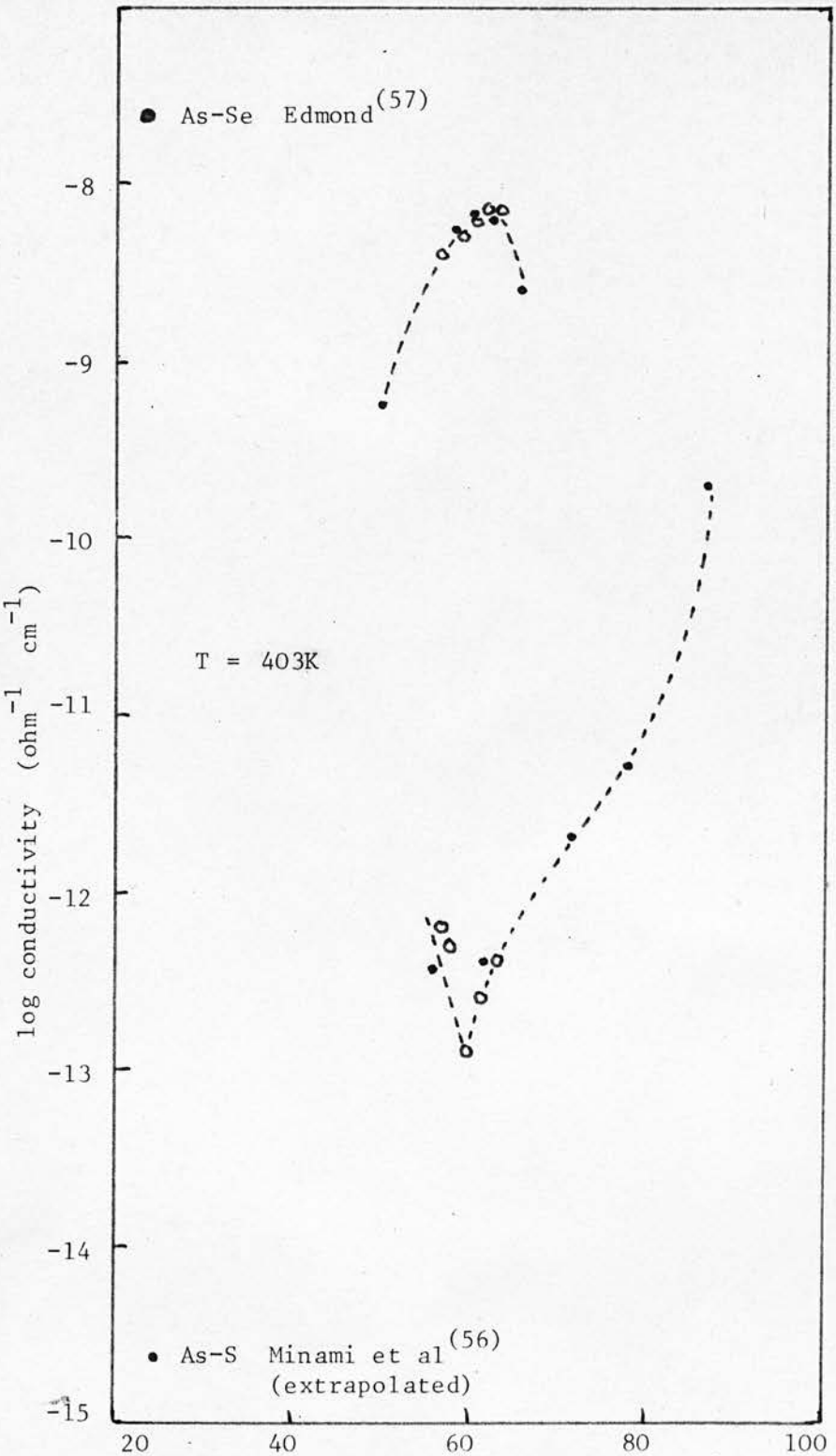

Figure (9.1)

D.C. conductivity of the As-S and As-Se systems

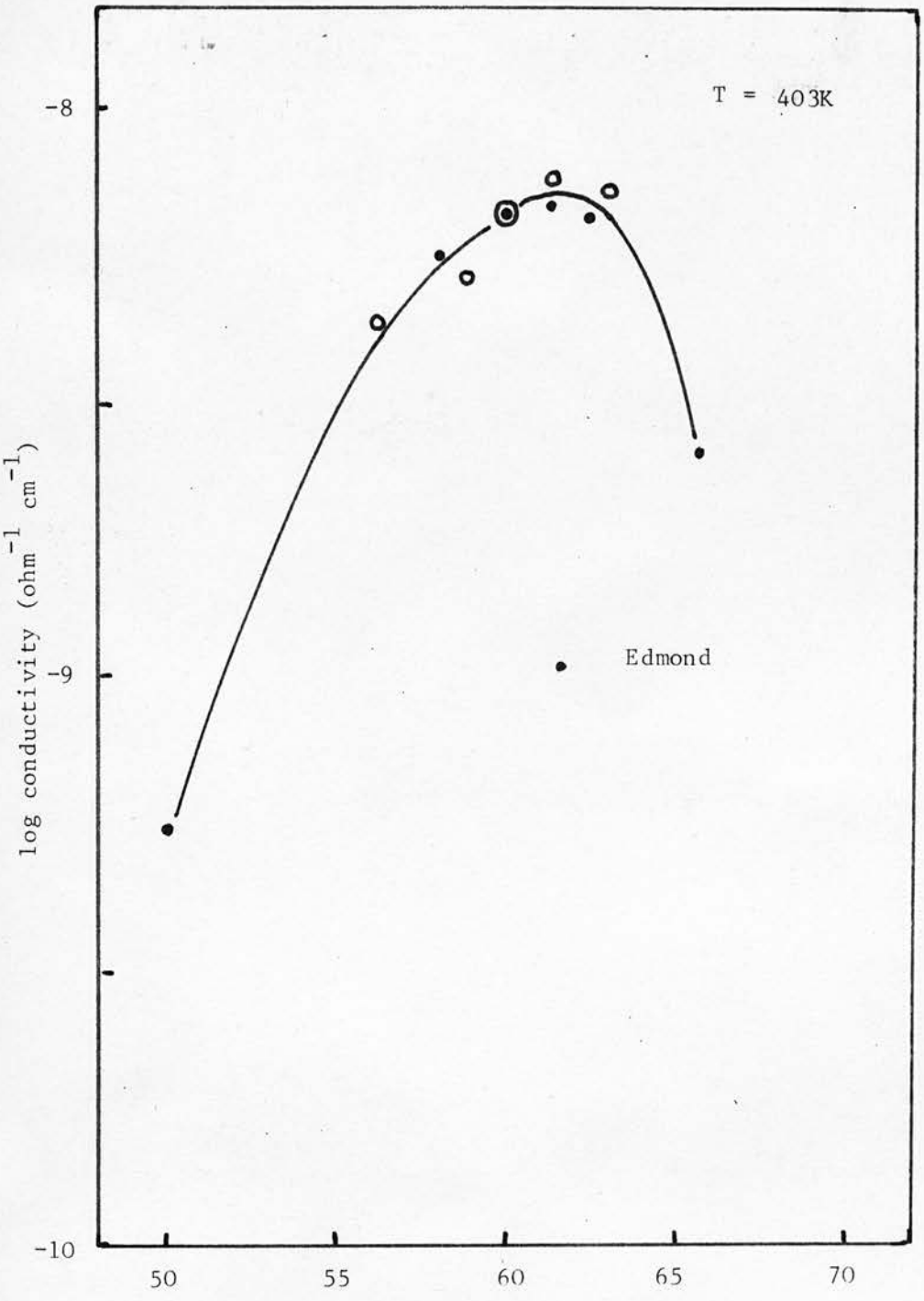

Figure (9.2)

D.C. conductivity of the As-Se system

Myers and Felty[2] that 57 at.% Se is the composition with the most extensive network formation as deduced from a broad maximum in the glass transformation temperature at that composition.

The addition of As to $As_2 S_3$ causes units of $As_4 S_4$ to be formed[2][3] and excess S is incorporated by the forming of S linkages in the layers[3]. The study of the glass transformation temperature by Myers and Felty[2] shows that the structure of As - S glasses breaks down more rapidly than that of As - Se glasses. This conclusion is supported by the observation of Hurst[106] that the bond strengths in the two systems differ: As - As, Se - Se and As - Se have similar strengths but As - S is strong compared with As - As or S - S. The more rapid breakdown of "order" will lead to a sharper increase in the density of localised states and the d.c. conductivity, which probably occurs by the hopping of carriers between localised states, will be increased. This is observed in the present work (figures (8.11) and (9.1)). In this system the minimum would be expected at the stoichiometric composition.

The a.c. conductivities (figures (8.16) to (8.18) and (8.29)) follow the d.c. conductivities in that there is a maximum in the As - Se system and a minimum in the As - S system, but again there are further differences. Figure (8.29) shows that as the relative magnitude of the d.c. component

of the conductivity decreases (as the frequency increases) the conductivity maximum in the As - Se system moves towards the stoichiometric composition. This would be expected to occur in a material of large $(As_2 Se_3)_n$ units where the more resistive linking of the layers would become less effective as the frequency was increased. It is worth noting that in the a.c. hopping model of Pollak[31] and Austin and Mott[32] the conductivity is proportional to the square of the density of states at the Fermi energy, so that, if it is applicable to As - Se glasses, the increase in disorder must be small enough for the resulting increase in $N(E_F)$ to be overwhelmed by a decrease in some other factor. It is possible that the density of states at the energy at which the electrons are contributing to the conductivity is unaffected by the addition of small amounts of As or Se and the density of states at the mobility edges only are increased. In this way the d.c. conductivity is likely to be more affected than the a.c. conductivity if it depends on a trap limiting process. This implies that it is not meaningful to use equation (9.2) to deduce values for $N(E_F)$ from the a.c. conductivity of different compositions of the As - Se system without altering the values of the other factors in the equation.

In the As - S system the rapid breakdown of the structure with the addition of excess As or S leading to a rapid increase in the density of localised states leads to

an increase in the a.c. conductivity away from stoichiometry. This is found (figures (8.16) to (8.18)) but, again in contrast to the As - Se compounds, the conductivity minimum is frequency and temperature dependent and moves away from the $As_2 S_3$ composition as the frequency increases. This is a reflection of a change in the index s of the equation $\sigma = A\omega^s$ and indicates the differing frequency dependences between glasses with excess As and those with excess S . The values of s are tabulated in section (8.5.3.2).

The differing frequency dependences may result from the dependence of the conductivity on a factor N which is the concentration of singly occupied pairs of localised states[33]. For weak correlation Pollak[33] lets

$$N^2 = N(E_F)\, k\, T\, N_s \qquad (9.9)$$

and for strong correlation

$$N^2 = N_c\, N_s \qquad (9.10)$$

where N_s is the density of localised states and N_c is the carrier concentration. If the electron hopping is occuring in a region where (9.9) applies and as the frequency increases (9.10) becomes increasingly important, then N will be frequency dependent. This can lead to a higher value for the index s (of $\sigma = A\omega^s$) than that predicted by equation (9.2). The disorder existing in the different As - S compositions is likely to cause differing densities of localised states and thus alter the frequency at which the change from weak to strong correlation occurs.

If this is the case then materials with excess As in the As - S system would be closer to the change-over than those with excess S as the conductivity in the former materials is increasing more rapidly with frequency. This is true at all temperatures used (see section (8.5.3.2.)). The more rapidly increasing conductivity in the excess As compounds would then show that these were relatively more disordered than those with excess S. The apparent change of the minimum with frequency can be easily described by the different frequency dependences. Assume that there are three compounds A, B and C in which the frequency dependences of the conductivity of A and B are similar but C has a weaker dependence. If the conductivities are of the form $\sigma = A\omega^s$ and the magnitudes of the conductivities are similar then over some frequency the situation will be as shown in figure (9.3a). Plotting the logarithm of the conductivity as a function of composition then leads to the situation illustrated in figure (9.3b). As the frequency has increased the conductivity minimum has moved to a different composition: therefore there may be no particular significance in the apparent move of the minimum of the conductivity with increasing frequency in the As - S system. The important factors are the frequency dependence, magnitude and the temperature variation.

The temperature variation of the conductivity of the As - S compounds illustrated in figure (8.13) shows that only materials with excess S have a measurable temperature dependence. This supports the supposition that correlation

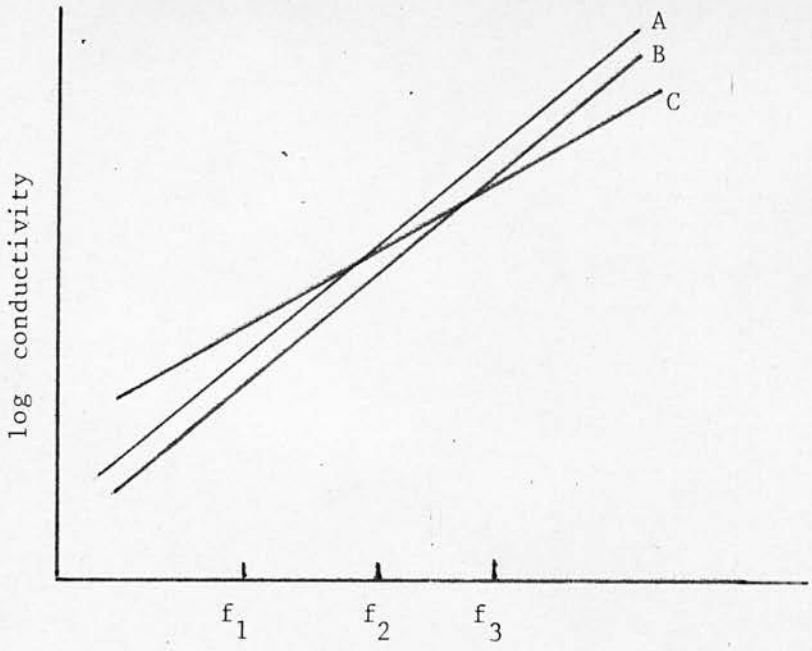

Figure (9.3a)

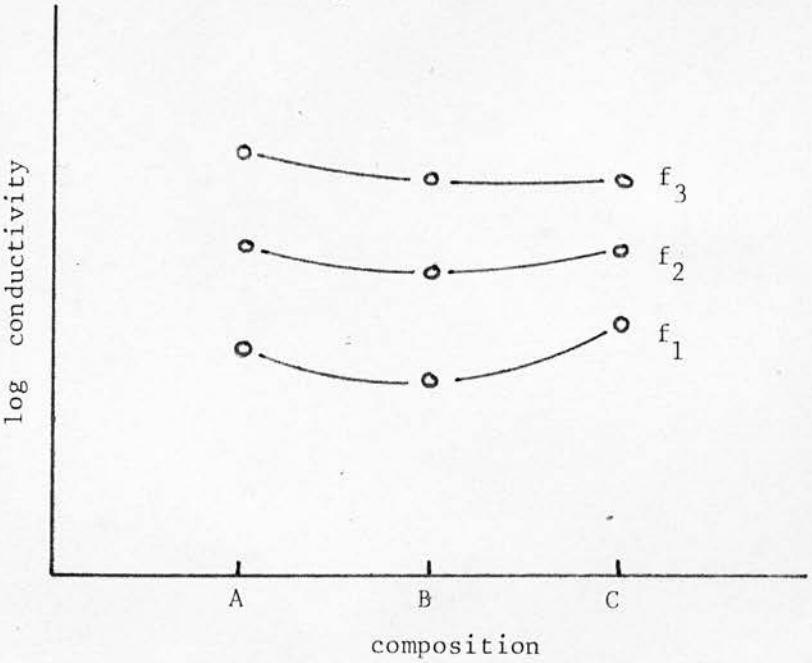

Figure (9.3b)

effects were more important in the compositions with excess As as there is theoretically no temperature dependence in this case[31]. This situation is described by equation (9.3). The linear increase (for frequencies up to 10 k Hz) found in the remaining materials corresponds to equation (9.2).

The information that can be inferred from the measurements of the a.c. and d.c. conductivities is mainly qualitative. The density of localised states in the mobility gap seems to increase as the material departs from stoichiometry. The increase is such that the effect on the As - S system is greater than that on the As - Se system and the result is the contrasting behaviour of the a.c. conductivities. The d.c. activation energy shows that the mobility gap is not very dependent on composition in both systems and the d.c. conductivity shows that the density of states at the band edges is increased. The trap limited conductivity of the As - Se glasses is thus reduced and the hopping conductivity of the As - S system increased. Provided the electron hopping model of Pollak[31] does describe the conductivity then equation (9.2) can be used to estimate the density of states at the Fermi energy $N(E_F)$. At a frequency of 1 k Hz and a temperature of 330 K this gives:

$$N(E_F) \approx 6.10^{17}\ cm^{-3}.eV^{-1} \quad \text{for } As_2S_3$$

and $$N(E_F) \approx 10^{18}\ cm^{-3}.eV^{-1} \quad \text{for } As_2Se_3.$$

when values of 3 Å for a and $10^{12}\ sec^{-1}$ for ω_o are

used. These values are probably maxima considering the likely errors (particularly the estimation of a). If they represent a true value for the density at E_F then, as Davis and Mott have suggested[14], there may be a peak in the density of states at this energy.

9.4 Inhomogeneity and contact effects.

It was pointed out in section (3.6) that a dielectric loss that is independent of frequency can be explained by the assumption of the existence of conductive regions dispersed in a resistive matrix in the material giving rise to interfacial polarisation. Such a situation is a possibility in an amorphous material and is more likely when the compound is non-stoichiometric. The addition of As or Se (or S) to $As_2 Se_3$ (or $As_2 S_3$) may well have caused some phase separation which has produced, or at least affected, the results. The majority of the scanning electron micrographs (figures (8.3a) and (8.3b)) show no evidence of this although features as small as 0·1μm could be resolved. The materials which did show some separation of the components were those of the As - S system with excess As but this was estimated to be less than 1% by volume.

If the measurements are a result of the Maxwell-Wagner effect then no conclusions can be made as to the physical processes involved because the extent and physical properties of the components are unknown. Sample preparation and

structural studies then become of vital importance when used in conjunction with electrical measurements on amorphous materials. This is underlined by the effect on the conductivity of annealing the samples shown in figure (8.8).

The results of using gold and aluminium contacts on samples of $As_2 S_3$ shown in figures (8.4) to (8.7) provide evidence that caution is needed when analysing a.c. conductivity measurements. The different electrode materials produced different values of the conductivity (at a given frequency) and different slopes when the logarithm of the conductivity was plotted against the logarithm of the frequency. Figure (8.6) shows that at 5 k Hz the conductivity is $1{\cdot}5.10^{-11}$ ohm^{-1} cm^{-1} for gold electrodes and $10^{-11} ohm^{-1} cm^{-1}$ for aluminium electrodes. The slopes are 1·06 (gold) and 1·13 (aluminium). Figures (8.4) and (8.5), which show the sample resistance as being proportional to the sample thickness for both types of electrode and an apparant zero resistance for zero thickness, are not consistent with the different conductivities. If one electrode was blocking then the conductivity would be decreased and this would show as a resistance at zero sample thickness[108]. There is obviously a need for more extensive work to be done in this area to characterise the effect of different electrodes on a.c. measurements. This can only be done on samples free from defects (such as component separation) and impurities.

9.5 Concluding remarks.

The a.c. and d.c. conductivities of the glasses investigated in the As - S and As -Se systems are consistent with the general ideas of phonon assisted hopping in the localised states and conduction in the extended states above the mobility edge proposed by Pollak[31] and Mott and Davis[13].

The method of preparation of amorphous semiconductors is, however, an important factor in determining the final structure of the bulk material (this alone may be the cause of the widely differing magnitudes found for the a.c. conductivity on the same material) it is perhaps premature to reach any definite conclusions as to the precise physical mechanism for the dielectric properties of the two glass systems. The use of truly homogeneous glasses with electrodes of known reliability is necessary for acceptable results.

It is clear that the a.c. conductivity of amorphous semiconductors obeys a relation similar to

$$\sigma = A\omega^{s}$$

for $s \approx 1$, and importance should be focussed of the behaviour of the index s for different glasses with a view to determining the effect of structure on the conduction process. As the ideal case of a wide flat distribution of relaxation times leads to $s \approx 1{\cdot}1$ (Gevers and Du Pré[24] and equation (9.6)) this value could be regarded as the ideal limit and deviations from this value will depend on the

material and the mechanism.

The temperature dependence also needs more precise determination. In the hopping model this is of importance because of the differing dependences predicted[31] for correlated and uncorrelated hopping. The present results for $As_2 S_3$ are consistent with the predicted temperature dependences: the conductivity at low frequencies (1 k Hz) is proportional to temperature and at higher frequencies ($>$ 10 k Hz) is temperature independent (figure (8.13)). At microwave frequencies there appears to be a slight increase of the conductivity with temperature (figure (8.38)) showing that the conductivity may become temperature independent at intermediate frequencies only.

The microstrip technique for dielectric measurements has proved to be useful for the general determination of the permittivity and loss over a wide frequency and temperature range. The main drawbacks to its use lie in the incomplete theoretical formulation for the microstrip losses and dispersion of the dielectric constant. This has meant that the results have been dependent on some semi-empirical equations and thus are not as accurate as they might be. Nevertheless the results achieved are consistent with those of other work[37] and can be used to provide an indication of the trend of the conductivity and dielectric constant when the frequency and temperature were varied.

The argument as to the correct a.c. conduction mechanism will not be resolved until the existence of the "omega squared" region between 10^6 and 10^9 Hz is either proved or disproved and measurements have been made at even higher frequencies. The loss peak sometimes found between 10^8 and 10^9 Hz[16] may be the result of the dielectric relaxation of large molecular groups in the solid which can be eliminated by careful sample preparation. With this in view it might be possible to create the loss peak by making measurements on non-stoichiometric materials at these frequencies when, for example in the As - S system, the existence of S rings or chains (excess S) or units of $As_4 S_4$ (excess As) may produce the dielectric relaxation sometimes found.

APPENDIX A1

Electromagnetic Theory

A1.1 Derivation of cavity modes in cylindrical coordinates.

Maxwell's equations for electromagnetic fields are:

$$\nabla \times \underline{E} = -\frac{\partial \underline{B}}{\partial t} \tag{A.1}$$

$$\nabla \cdot \underline{D} = \rho \tag{A.2}$$

$$\nabla \times \underline{H} = \underline{J} + \frac{\partial \underline{D}}{\partial t} \tag{A.3}$$

$$\nabla \cdot \underline{B} = 0 \tag{A.4}$$

where $\underline{E}$ is the electric field, $\underline{D}$ is the electric flux density, ρ is the free charge density, $\underline{H}$ is the magnetic field, $\underline{J}$ is the current density and $\underline{B}$ is the magnetic flux density.

For isotropic, linear media the relations

$$\underline{D} = \epsilon' \underline{E}$$

$$\underline{B} = \mu \underline{H}$$

and

$$\underline{J} = \sigma \underline{E}$$

can be used for permittivity ϵ' and permeability μ .

The modes of propagation in a waveguide must satisfy equations (A.1) to (A.4) with the appropriate boundary conditions. Away from any regions of free charge Maxwell's equations are

$$\nabla \times \underline{E} = \mu_o \frac{\partial \underline{H}}{\partial t} \tag{A.5}$$

$$\nabla \cdot \underline{E} = 0 \tag{A.6}$$

$$\nabla \times \underline{H} = \sigma \underline{E} + \epsilon' \frac{\partial \underline{E}}{\partial t} \tag{A.7}$$

$$\nabla \cdot \underline{H} = 0 \tag{A.8}$$

for a nonmagnetic medium.

If the electric and magnetic fields are alternating, the resulting wave equations are

$$\nabla^2 \underline{E} = (i\omega\sigma - \omega^2\epsilon')\mu_o \underline{E} = -k^2 \underline{E} \tag{A.9}$$

and

$$\nabla^2 \underline{H} = (i\omega\sigma - \omega^2\epsilon')\mu_o \underline{H} = -k^2 \underline{H} \tag{A.10}$$

where

$$k^2 = \omega^2 \epsilon' \mu_o - i\omega\sigma\mu_o$$

which may also be written

$$k^2 = \omega^2 \mu_0 \left(\epsilon' - i\frac{\sigma}{\omega}\right) \qquad (A.11)$$

and thus the expression in brackets can be called the complex permittivity ϵ^* so that

$$\epsilon^* = \epsilon' - i\epsilon'' \qquad (A.12)$$

where $\epsilon'' = \frac{\sigma}{\omega}$

If waves propagating in the Z direction are considered then let the solutions be

$$\underline{E} = \underline{E}'_0 \exp(i\omega t + \gamma z) \qquad (A.13)$$

$$\underline{H} = \underline{H}'_0 \exp(i\omega t + \gamma z) \qquad (A.14)$$

where γ is the propagation constant in the dielectric. In general

$$\gamma = i\omega \sqrt{\mu_0 \epsilon^*} \qquad (A.15)$$

and the intrinsic impedance is

$$Z = \frac{E}{H} = \frac{i\omega\mu_0}{\gamma} \qquad (A.16)$$

For a cylindrical waveguide of radius a a transverse electric (TE) mode will be described in detail as this

configuration is often used in dielectric measurements. The equation for the Z component of the magnetic field is

$$\nabla^2 H_z = -\omega^2 \mu_0 \epsilon^* H_z \qquad (A.17)$$

Using a cylindrical coordinate system this gives

$$\frac{1}{r}\frac{\partial}{\partial r}\left(r\frac{\partial H_z}{\partial r}\right) + \frac{1}{r^2}\frac{\partial^2 H_z}{\partial \phi^2} + \frac{\partial^2 H_z}{\partial z^2} = -\omega^2 \mu_0 \epsilon^* H_z = -k^2 H_z \qquad (A.18)$$

Let $H_z = R(r)\,\Phi(\phi)\,Z(z)$

then equation (A.18) reduces to

$$\frac{r^2}{R}\left(R'' + \frac{R'}{r}\right) + \frac{\Phi''}{\Phi} + r^2\left(\frac{Z''}{Z} + k^2\right) = 0 \qquad (A.19)$$

where the dashes refer to differentiation with respect to the arguments.

If $H_z = H_1 \exp(i\omega t + \gamma z)$ then (A.19) becomes

$$\frac{r^2}{R}\left(R'' + \frac{R'}{r}\right) + \frac{\Phi''}{\Phi} + r^2\left(\gamma^2 + k^2\right) = 0$$

As r and ϕ are independent variables let $\Phi''/\Phi = -m^2$ (a constant); this has the solution

$$\Phi(\phi) = C\cos m\phi + D\sin m\phi \qquad (A.20)$$

Writing $k_c^2 = \gamma^2 + k^2$ results in

$$R'' + \frac{R'}{r} + \left(k_c^2 - \frac{m^2}{r^2}\right) R = 0 \qquad (A.21)$$

which is Bessel's equation for the m th order and has the solution

$$R(r) = AJ_m(k_c r) + BY_m(k_c r) \qquad (A.22)$$

where J_m is Bessel's function of the first kind of order m and Y_m is Bessel's function of the second kind of order m .

The general solution for H_z is

$$H_z = [AJ_m(k_c r) + BY_m(k_c r)][C\cos m\phi + D\sin m\phi].e^{i\omega t + \gamma z} \qquad (A.23)$$

The other field components are H_r , H_ϕ , E_r and E_ϕ for a TE mode, and these may be derived from H_z by the relations

$$\nabla \times \underline{E} = -i\omega\mu_o \underline{H}$$

$$\nabla \times \underline{H} = i\omega\epsilon^* \underline{E}$$

giving

$$H_r = \frac{\gamma}{k_c^2} \cdot \frac{\partial H_z}{\partial r} \qquad (A.24)$$

$$H_\phi = \frac{\gamma}{k_c^2} \cdot \frac{1}{r} \cdot \frac{\partial H_z}{\partial \phi} \qquad (A.25)$$

$$E_r = \frac{-i\omega\mu_o}{k_c^2} \cdot \frac{1}{r} \cdot \frac{\partial H_z}{\partial \phi} \qquad (A.26)$$

$$\frac{E}{\phi} = \frac{i\omega\mu_o}{k_c^2} \cdot \frac{\partial H_z}{\partial \phi} \qquad (A.27)$$

If the waveguide includes the axis $r = 0$ then as $Y_m(0)$ is infinite $B = 0$. By a suitable rotation the expression for H_z can be simplified to

$$H_z = A J_m(k_c r)\cos m\phi \cdot \exp(i\omega t + \gamma z) \qquad (A.28)$$

A cylindrical cavity can be considered as a waveguide with short circuiting planes at each end. A standing wave is formed from the two travelling waves propagating in opposite directions. i.e.

$$H_z = A_1 J_m(k_c r)\cos m\phi \cdot \exp(i\omega t + \gamma z) + A_2 J_m(k_c r)\cos m\phi \cdot \exp(i\omega t - \gamma z) \qquad (A.29)$$

Let $\gamma = \alpha + i\beta$ where α is the attenuation constant and β is a phase factor. Neglecting conductor attenuation (i.e. $|\alpha| \ll |\beta|$) gives

$$H_z = J_m(k_c r)\cos m\phi \left[A_1 \exp \beta z + A_2 \exp -\beta z\right] \exp i\omega t \qquad (A.30)$$

and $k_c = \omega^2\mu_o \varepsilon' - \beta^2$ is real.

The boundary conditions for a cavity of length d are that at $r = a$ (the cavity radius) the electric field is tangential to the conductor and also $H_z = 0$ at $z = 0$ and $z = d$. The first condition gives that

$$J'_m(k_c a) = 0 \qquad (A.31)$$

(where the prime refers to differentiation with respect to $k_c r$) and the second is satisfied by taking $A_2 = -A_1$ and $\beta = n\pi/d$.

The resulting expression for the axial magnetic field is

$$H_z = A_1 J_m(k_c r)\cos m\phi \sin \beta z \exp i\omega t \qquad (A.32)$$

This with the relations (A . 24) - (A . 27), defines the TE_{mln} mode for a cylindrical cavity. The integer l refers to the solution of equation (A.31) and is the number of half-period variations of E_ϕ with respect to r.

A mode commonly used for dielectric measurements is the TE_{01n} mode and the non-zero field components are

$$H_z = A J_0(k_c r)\sin \beta z \qquad (A.33)$$

$$H_r = -A\frac{\beta}{k_c^2} \cdot J'_0(k_c r)\cos \beta z \qquad (A.34)$$

and

$$E_\phi = A\frac{i\omega\mu_0}{k_c^2} \cdot J'_0(k_c r)\sin \beta z \qquad (A.35)$$

where $\beta = n\pi/d$ and the time dependence (exp $i\omega t$) has been omitted.

APPENDIX A2

Computer Programs

Two computer programs using the Fortran 1V language were developed, both concerning the calculations involved in the microstrip measurements (Chapters 6 and 7).

The first program is a test of the theoretical model of the ring resonator and is essentially solving equation (6.50) by reading the resonant frequency, radii of the annulus and an approximate starting value for the quantity kr_1 ($= \frac{2\pi f}{c} \sqrt{\epsilon'_e} \cdot r_1$). The solutions for k (and thus ϵ'_e) are found by a method of successive approximations. The program also generates its own Bessel functions and their first derivatives.

The second program was used to calculate the dielectric parameters resulting from measurements of the frequencies and Q factors of the microstrip resonators. In order to achieve the maximum accuracy the effects of temperature have been included. These are contained in the thermal expansion coefficient of $As_2 S_3$ ($2{\cdot}4 \cdot 10^{-5}/^{\circ}C$ [104]) and the temperature coefficient of resistance of gold ($3{\cdot}4 \cdot 10^{-3}/^{\circ}C$ [102]). Also, as an empirical adjustment to the conductor losses, the resistivity of gold has been doubled in accordance with the findings of several authors [95][96][97], to arrive at a more realistic value for the dielectric conductivity. This point is explained in greater detail in chapter 7.

The main parameters of the programs are defined immediately following the programs.

PROGRAM 1: Theoretical Ring Resonator.

```
      INTEGER R
      DIMENSION X1(6,101), X2(6,101)
      DIMENSION FR(12),FREQ(12),RAD(2)
      READ(5,20)(X1(N,1),N=1,6)
   20 FORMAT(6F3.1)
C                              K IS NO OF RESONANCES
      READ(5,21)K
   21 FORMAT(12)
      READ(5,22)(RAD(J),J=1,2)
   22 FORMAT(2F3.2)
      READ(5,23)(FR(J),J=1,K)
   23 FORMAT(15F6.4)
       WRITE(6,70)RAD(1),RAD(2)
   70 FORMAT('0','RING RESONATOR WITH RADII',F5.2,'AND',
     5        F5.2,'CM.')
      WRITE(6,69)
   69 FORMAT('0',3X,'ORDER',6X,'FREQUENCY',4X,'EFF D CONST', 6X,
     9   'SQRT(EFF)',10X,'INDEX')
      C=2.998E10
      PI=3.14159
      DO30 N=1,K
      FREQ(N)=FR(N)*1.E9
    6 R=1
    5  X2(N,R)=RAD(2)*X1(N,R)/RAD(1)
      SL=DBJ(N,X1(N,R))/DBJ(N,X2(N,R))
      SR=DBY(N,X1(N,R))/DBY(N,X2(N,R))
```

CONTINUED

```
C                    SIMPLE X2=F+X1 CONVERGENCE
      FN=SR-SL
      X1(N,R+1)=FN+X1(N,R)
      DIF=ABS(X1(N,R+1)-X1(N,R))
      IF(DIF-1.E-5)7,8,8
    7 RTEFF=C*X1(N,R)/(2.*PI*FREQ(N)*RAD(1))
      EFF=RTEFF**2.
      WRITE(6,71)N,FR(N),EFF,RTEFF,R
   71 FORMAT('0',6X,12,3(8X,F7.4),12X,13)
      GOTO 30
    8 R=R+1
      IF(R-100)5,30,30
   30 CONTINUE
      STOP
      END
```

SUBFUNCTIONS

(a) BESSEL FUNCTION $J_n(x)$

```
      FUNCTION BJ(N,X)
      SUM1=((X/2.)**N)/GAMMA(N+1.)
        DO1 J=1,0000
      SUM2=SUM1+((-1.)**J)*((X/2.)**(N+2.*J))/(GAMMA(J+1.)*
     8  GAMMA(N+J+1.))
      IF(ABS(SUM2-SUM1).LT.1.E-5)GOTO 2
    1 SUM1=SUM2
    2 BJ=SUM2
      RETURN
      END
```

(b) FIRST DERIVATIVE OF $J_n(x)$

```
      FUNCTION DBJ(N,X)
      M=N+1
      DBJ=N*BJ(N,X)/X-BJ(M,X)
      RETURN
      END
```

(c) BESSEL FUNCTION $Y_n(x)$

```
      FUNCTION BY(N,X)
      GAM=.5772157
      O1=-GAM
      DO1 I=1,N
      O2=O1+1./I
    1 O1=O2
      SUM1=((X/2.)**N)*(2.*ALOG(X/2.)+GAM-O1)/GAMMA(N+1.)
      DO2 K=1,10000
      P1=-GAM
      DO3 L=1,K
      P2=P1+1./L
    3 P1=P2
      NN=N+K
      Q1=-GAM
      DO4 M=1,NN
      Q2=Q1+1./M
    4 Q1=Q2
      SUM2=SUM1+((-1.)**K)*((X/2.)**(N+2.*K))*(2.*ALOG
     5  (X/2.)-P1-Q1)/(GAMMA(K+1.)*GAMMA(N+K+1.))
      IF(ABS(SUM2-SUM1).LT.1.E-5)GOTO 5
    2 SUM1=SUM2
    5 CONTINUE
      IF(N.EQ.O) SUM4=O.
      IF(N.EQ.O) GOTO 7
      G=N
      SUM3=GAMMA(G)/((X/2.)**N)
```

CONTINUED

```
      IF(N.EQ.1)SUM4=SUM3
      IF(N.EQ.1)GOTO 7
      MM=N-1
      DO6 J=1,MM
      H=N-J
      SUM4=SUM3+GAMMA(H)*((X/2.)**(2.*J-N))/GAMMA(J+1.)
      IF(ABS(SUM4-SUM3).LT.1.E-5)GOTO 7
    6 SUM3=SUM4
    7 BY=(SUM2-SUM4)/3.14159
      RETURN
      END
```

(d) FIRST DERIVATIVE OF $Y_n(x)$

```
      FUNCTION DBY(N,X)
      M=N+1
      DBY=N*BY(N,X)/X-BY(M,X)
      RETURN
      END
```

The parameters of interest are:

X1(N,1) = initial estimated value of kr_1 for the N th resonance

X2(N,2) = corresponding value of kr_2

RAD(J) = radius of circle

FR(N) = frequency of the N th resonance

EFF = effective dielectric constant

PROGRAM 2: Microstrip calculations

```
C               MICROSTRIP RESONATOR PROGRAM
C               RING RESONATORS
      INTEGER TEMP
      C=2.998E1Ø
      PI=3.14159
      RES=2.4
      RES=RES*2.
      AA=12Ø.*PI
      CEX=2.4E-5
      CRES=3.4E-3
      WRITE(6,11)
   11 FORMAT('Ø','MICROSTRIP DIELECTRIC CONSTANTS AND
     9  CONDUCTIVITY', ' OF ARSENIC SULPHIDE (AS2S3)')
      WRITE(6,12)
   12 FORMAT(' ','GOLD CONDUCTORS')
C               READ RADIUS DIELECTRIC THICKNESS CONDUCTOR
C               THICKNESS AND WIDTH AND SAMPLE NUMBER
    1 READ(5,98)RAD,H,W,THI,NO
   98 FORMAT(F4.3,2X,F4.3,2X,F4.3,2X,F3.2,2X,I2)
      IF (NO.EQ.Ø)GOTO 8
      WRITE(6,13)NO
   13 FORMAT('Ø','SAMPLE NUMBER ',I2)
      WA=W*1Ø.
      HA=H*1Ø.
      TH=THI*1.E-4
      BA=W/H
```

CONTINUED

```
      DA=H/W
      B=1./SQRT(1.+10.*H/W)
      WRITE(6,22)HA
   22 FORMAT('0',6X,'DIELECTRIC THICKNESS(H)  = ',F4.2,'MM')
      WRITE(6,33)WA
   33 FORMAT(' ',6X,'CONDUCTOR WIDTH(W)  = ',F4.2,'MM')
      WRITE(6,44)THI
   44 FORMAT(' ',6X,'CONDUCTOR THICKNESS(T)  = ',F3.1,
     9  'MICRONS')
      WRITE(6,55)
   55 FORMAT('0','N',4X,'W/H',6X,'Z',5X,'QM',5X,'QU',5X,'QR'
     9  6X,'QC',6X,'QD',6X,'EFF',12X'FR',6X,'ER',5X,'DLOSS',
     8  6X,'TAND',6X,'COND',3X,'TEMP')
      WRITE(6,77)
   77 FORMAT(' ',11X,'OHMS',57X,'GHZ',31X,'/OHM.CM',5X,'K')
C              READ FREQUENCY MEASURED Q
C              INSERTION LOSS AND TEMPERATURE
    5 READ(5,99)FR,QM,DP,TEMP
   99 FORMAT(F6.4,2X,F3.0,2X,F3.1,2X,I3)
      IF(FR.EQ.0.0)GOTO 1
C              CALCULATE RADIUS (INCLUDING THERMAL EXPANSION)
      RES=RES*(1.+CRES*(TEMP-295.))
      RIE=RAD*(1.+CEX*(TEMP-295.))
      FLE=PI*RIE
      F=FR*1.E9
      XLO=C/F
      AKO=2.*PI*F/C
```

CONTINUED

```
C                CALCULATE EFFECTIVE DIELECTRIC CONSTANT
C                FROM FREQUENCY AND RADIUS
C                WITHIN REASONABLE LIMITS
      N=Ø
    6 N=N+1
      EFF=((N*XLO)/(2.*FLE))**2
      IF(EFF.GT.8.Ø.OR.EFF.LT.4.7)GOTO 6
C                FIND TRUE DIELECTRIC CONSTANT
C                USE COUPLED MODE MODEL (JAIN ET AL.)
C                FIND EFFECTIVE DIELECTRIC CONSTANT CLOSE
C                TO MEASURED DIELECTRIC CONSTANT
      DO31 J=65ØØ,85ØØ,1
      ER=J/1ØØØ.
      E=(ER+1.)/2.+(ER-1.)/(2.*SQRT(1.+1Ø.*H/W))
      CC=(ER-1.)*(AKO*H)**2.
      PT=(SQRT(ER**2.+4.*CC)-ER)/2.
      ETM=1.+(PT/(H*AKO))**2.
      A=SQRT(2./(ER-1.))
      CX=ATAN(ER*SQRT((1.+B)/(1.-B)))
      FL=2.998E1Ø*A*CX/(2.*PI*SQRT(1.-B)*H)
      EE=Ø.22*(SQRT(ER)-1.)**2.*(W/H)**(3./4.)*(F/FL)**(4./3.)
      D=(SQRT(E)+SQRT(ETM))/2.
      G=SQRT(EE+((SQRT(E)-SQRT(ETM))/2.)**2.)
      EFC=(D+G)**2
      IF(ABS(EFC-EFF).LT.Ø.ØØ1)GOTO 7
   31 CONTINUE
```

CONTINUED

```
C               CALCULATE IMPEDANCE AND ATTENUATION
C               (SCHNEIDER)
    7 R=SQRT(4.*(PI**2)*FR*RES)*1.E-3
      S=(ALOG((2.*H)/TH))/PI
      IF(BA-1.)2,3,3
    2 ZO=6Ø.*ALOG(8.*DA+BA/4.)
      T=(1Ø.*R)/(PI*ALOG(1Ø.))
      U=8.*DA-BA/4.
      V=1.+DA+DA*S
      BW=H*ZO*EXP(ZO/6Ø.)
      ATTO=T*U*V/BW
      GOTO 4
    3 E=BA+2.42-.44*DA+(1.-DA)**6
      ZO=AA/E
      FA=R*ZO/(72Ø.*H*(PI**2)*ALOG(1Ø.))
      GA=1.+.44*(DA**2)+6.*(DA**2)*((1.-DA)**5)
      ATTO=FA*GA*(1.+BA+S)
    4 ATT=ATTO*(SQRT(EFF))
      Z=ZO/SQRT(EFF)
C               CALCULATE CONDUCTOR Q AND RADIATION Q
C               (SCHNEIDER AND ROBERTS AND EASTER)
      QO=(2Ø.*PI)/(ALOG(1Ø.)*XLO*ATTO)
      TP=1./1Ø.**(DP/1Ø.)
      QU=QM/(1.-SQRT(TP))
      IF(N.EQ.1)P=6.ØE-1
      IF(N.EQ.2)P=1.2E-1
      IF(N.EQ.3)P=2.4E-2
```

CONTINUED

```
      IF(N.EQ.4)P=6.ØE-3
      IF(N.EQ.5)P=1.5E-3
      IF(N.GT.5)P=1.ØE-4
      PN=45Ø.*P*(HA**2)/((.25*XLO)**2*Z)
      QR=2ØØ.*PI/PN
C              CALCULATE DIELECTRIC Q DIELECTRIC LOSS
C              LOSS TANGENT AND CONDUCTIVITY
      QD=1./(1./QU-1./QO-1./QR)
      TAND=(1./ER-1.)/(QD*(1./EFF-1.))
      ERR=ER*TAND
      COND=2.*PI*FR*8.854*ERR*1.E-5
      WRITE(6,111)N,BA,Z,QM,QU,QR,QO,QD,EFF,FR,ER,ERR,TAND,
     5  COND,TEMP
  111 FORMAT('Ø',I1,3X,F4.2,3X,F4.Ø,3X,F4.Ø,3X,F4.Ø,3X,F5,Ø,
     9  3X,F5.Ø,3X,F5.Ø,3X,F5.3,3X,'**',3X,F7.4,3X,F5.3,3X,
     8  E7.2,3X,E7.2,3X,E7.2,3X,I3)
      GOTO 5
      STOP
      END
```

The parameters of interest are:

RES = resistivity of gold (μ ohm.cm.)

CEX = coefficient of expansion of $As_2 S_3$

CRES = coefficient of resistance of gold

RAD = mean radius of the ring

H = dielectric thickness (mm)

W = conductor width (mm)

THI = conductor thickness (μm)

FR = frequency (GHz)

QM = measured Q factor

DP = insertion power loss (db)

TEMP = temperature (K)

EFF = effective dielectric constant

ER = true dielectric constant

Z = microstrip impedance

QO = QC = conductor Q factor

QU = unloaded Q factor

P = percentage power radiated (Roberts and Easter(90))

QR = radiation Q factor

QD = dielectric Q factor

TAND = dielectric loss tangent

ERR = dielectric loss

COND = conductivity

APPENDIX A3

Tabulated Results

In these results the following symbols are used:

l	=	sample thickness
A	=	sample area (of faces)
f	=	frequency
σ	=	conductivity
ε'_r	=	dielectric constant
T	=	temperature (degrees Kelvin)
h	=	dielectric thickness
w	=	conductor width
t	=	conductor thickness
r	=	resonator radius
R	=	resistance
C	=	capacitance
Q_L	=	loaded Q factor
α	=	insertion loss

A3.1 Microstrip measurements - Alumina Substrates (section 7.4.1)

Alumina type Deranox 975 obtained from Messrs. Andermann and Ryder.

Manufacturers quoted values: $\varepsilon'_r = 9{\cdot}49$, $\tan\delta = 4{\cdot}3\ 10^{-4}$ at $25^{\circ}C$ and 9·368 GHz.

ring resonator parameters:

dielectric thickness, h = 1·00 mm

conductor width, w = 1·50 mm

conductor thickness, t = 1·78 microns

mean resonator radius, r = 9·67 mm

resonant frequency (GHz)	1·91	3·81	5·65	7·47	9·25	10·97
loaded Q factor, Q_L	172	202	292	332	398	438
transmitted power loss (db), α	13	10	10	12	17	12
conductor Q factor (equations (6.34) and (6.35) and figure (6.1))	250	428	581	706	784	851
conductor Q factor (equation (6.24))	232	328	400	461	512	555
effective dielectric constant	6·63	6·77	6·87	6·98	7·12	7·28
loss tangent ($x10^3$) (equations (6.34) and (6.35) used)	1·43	2·40	1·20	1·61	1·27	1·15
loss tangent ($x10^3$) (equation (6.24) used)	1·10	1·65	0·81	0·82	0·57	0·50

A3.2 Electrode/thickness dependence of $As_2 S_3$ at audio frequencies.

(a) Gold electrodes

A = 0·71 cm^2 (all samples), T = 315K

no.6 l = 1·88 mm

f	R	C
kHz	ohm	arbitrary units
1	$7·7.10^{10}$	4·10
5	2.10^{10}	4·10
10	9.10^{9}	4·10

no.8 l = 1·30 mm

f	R	C
1	$4·8.10^{10}$	5·75
5	$9·7.10^{9}$	5·75
10	$3·3.10^{9}$	5·75

no.10 l = 1·02 mm

f	R	C
1	$3·8.10^{10}$	7·40
5	$8·0.10^{9}$	7·40
10	$3·4.10^{9}$	7·40

no.12 l = 0·83 mm

f	R	C
1	$2·5.10^{10}$	9·10
5	$6·0.10^{9}$	9·10
10	$2·6.10^{9}$	9·10

no.14 l = 0·650 mm

f	R	C
1	$3{\cdot}3.10^{10}$	11·85
5	$6{\cdot}5.10^{9}$	11·85
10	$4{\cdot}0.10^{9}$	11·85

no.16 l = 0·504 mm

f	R	C
1	$2{\cdot}9.10^{10}$	15·35
5	$5{\cdot}4.10^{9}$	15·35
10	$2{\cdot}1.10^{9}$	15·35

note: for l = 2·30 mm C = 3·10 (f = 5 kHz)
and l = 2·17 mm C = 3·35 (f = 5 kHz)
The conductivity was too small to measure accurately.

(b) Aluminium electrodes.
A = 0·71 cm^2 (all samples), T = 315 K

no.7 l = 1·50 mm

f	R	C
1	$1{\cdot}0.10^{11}$	4·90
5	$2{\cdot}0.10^{10}$	4·90
10	$8{\cdot}5.10^{9}$	4·90

no.9 l = 1·10 mm

f	R	C
1	$7 \cdot 7 \cdot 10^{10}$	6·80
5	$1 \cdot 45 \cdot 10^{10}$	6·80
10	$6 \cdot 25 \cdot 10^{9}$	6·80

no.11 l = 0·90 mm

f	R	C
1	$6 \cdot 37 \cdot 10^{10}$	8·10
5	$1 \cdot 11 \cdot 10^{10}$	8·10
10	$4 \cdot 54 \cdot 10^{9}$	8·10

no.13 l = 0·744 mm

f	R	C
1	$7 \cdot 29 \cdot 10^{10}$	10·15
5	$1 \cdot 14 \cdot 10^{10}$	10·15
10	$5 \cdot 30 \cdot 10^{9}$	10·15

no.15 l = 0·576 mm

f	R	C
1	$8 \cdot 00 \cdot 10^{10}$	13·25
5	$8 \cdot 10 \cdot 10^{9}$	13·25
10	$3 \cdot 66 \cdot 10^{9}$	13·25

no.17 $l = 0.446$ mm

f	R	C
1	$4.16.10^{10}$	17.20
5	$6.25.10^{9}$	17.20
10	$2.66.10^{9}$	17.20

note: for $l = 2.04$ mm , $C = 3.65$ (5kHz)

and $l = 2.86$ mm , $C = 2.45$ (5kHz)

The conductivity was too low to measure accurately.

A3.3 Annealing of $As_2 S_3$

before annealing: $l = 1.37$ mm, $A = 0.786$ cm^2

after annealing: $l = 1.33$ mm, $A = 0.786$ cm^2

f	before annealing		after annealing	
Hz	σ	ϵ'_r	σ	ϵ'_r
	ohm^{-1} cm^{-1}		ohm^{-1} cm^{-1}	
10^3	$3.3.10^{-12}$	8.20	$2.00.10^{-12}$	8.26
2.10^3	$5.5.10^{-12}$	8.20	$3.9.10^{-12}$	8.26
3.10^3	$7.5.10^{-12}$	8.20	$5.7.10^{-12}$	8.26
5.10^3	$1.20.10^{-11}$	8.20	$9.2.10^{-12}$	8.26
7.10^3	$1.65.10^{-11}$	8.20	$1.36.10^{-11}$	8.26
10^4	$2.23.10^{-11}$	8.13	$2.04.10^{-11}$	8.20
2.10^4	$4.30.10^{-11}$	8.13	$3.91.10^{-11}$	8.26
5.10^4	$1.02.10^{-10}$	8.13	$1.12.10^{-10}$	8.26
1.10^5	$2.41.10^{-10}$	8.13	$2.21.10^{-10}$	8.26

error in dielectric constant: $\pm$ 0.07

annealing time: 4 hours

annealing temperature: 180° C

A3.4 D.c. conductivity of As - S system.

(a) $As_2 S_{2.7}$ l = 0·775 mm A = 1·24 cm^2

(b) $As_2 S_{2.8}$ l = 0·534 mm A = 1·27 cm^2

(c) $As_2 S_{3.0}$ l = 1·49 mm A = 0·50 cm^2

(d) $As_2 S_{3.2}$ l = 1·65 mm A = 1·29 cm^2

(e) $As_2 S_{3.4}$ l = 1·26 mm A = 1·23 cm^2

Temperature	σ $ohm^{-1}.cm^{-1}.10^{14}$				
°C	(a)	(b)	(c)	(d)	(e)
150	295	233	54·0	133	180
140	142	112	26·4	57·5	84·0
130	62·7	49·3	1·20	27·5	38·8
120	27·0	22·6	5·22	10·4	15·0
110	12·9	8·65	2·10	4·24	5·90
100	5·65	3·66	0·835	1·64	2·32
90	2·38	1·36	0·290	0·576	0·836
80	-	0·475	-	0·199	0·290

electrodes: evaporated gold.

A3.5 A.c. conductivity of the As - S system.

electrodes: evaporated gold.

(a) $As_2 S_{2.7}$ l = 0·775 mm A = 1·24 cm^2

(i) T = 370 K

f	σ	ϵ'_r
Hz	$ohm^{-1}\ cm^{-1}$	
700	$3{\cdot}8.10^{-12}$	7·85
10^3	$4{\cdot}7.10^{-12}$	7·85
2.10^3	$6{\cdot}6.10^{-12}$	7·88
3.10^3	$1{\cdot}00.10^{-11}$	7·85
5.10^3	$1{\cdot}91.10^{-11}$	7·85
7.10^3	$2{\cdot}76.10^{-11}$	7·85
10^4	$3{\cdot}95.10^{-11}$	7·85
2.10^4	$8{\cdot}95.10^{-11}$	7·85
5.10^4	$2{\cdot}26.10^{-10}$	7·85
10^5	$5{\cdot}58.10^{-10}$	7·80

(ii) T = 350 K

f	σ	ϵ'_r
Hz	$ohm^{-1}\ cm^{-1}$	
700	$\approx 4{\cdot}5.10^{-12}$	7·88
10^3	$3{\cdot}80.10^{-12}$	7·85
2.10^3	$7{\cdot}80.10^{-12}$	7·85
3.10^3	$1{\cdot}16.10^{-11}$	7·88
5.10^3	$1{\cdot}85.10^{-11}$	7·85
7.10^3	$3{\cdot}07.10^{-11}$	7·85
10^4	$4{\cdot}00.10^{-11}$	7·85
2.10^4	$9{\cdot}10.10^{-11}$	7·80
5.10^4	$2{\cdot}48.10^{-10}$	7·85
10^5	$5{\cdot}60.10^{-10}$	7·80

(iii) T = 330 K

f	σ	ϵ'_r
Hz	$ohm^{-1}\ cm^{-1}$	
700	-	-
10^3	$3{\cdot}6.10^{-12}$	7·88
2.10^3	$7{\cdot}5.10^{-12}$	7·85
3.10^3	$1{\cdot}13.10^{-11}$	7·85
5.10^3	$1{\cdot}95.10^{-11}$	7·85
7.10^3	$2{\cdot}80.10^{-11}$	7·85
10^4	$4{\cdot}60.10^{-11}$	7·85
2.10^4	$8{\cdot}70.10^{-11}$	7·85
5.10^4	$2{\cdot}35.10^{-10}$	7·85
10^5	$5{\cdot}55.10^{-10}$	7·80

(iv) T = 315 K

f	σ	ϵ'_r
Hz	$ohm^{-1}\ cm^{-1}$	
700	-	-
10^3	$3{\cdot}8.10^{-12}$	7·85
2.10^3	$8{\cdot}1.10^{-12}$	7·85
3.10^3	$1{\cdot}19.10^{-11}$	7·85
5.10^3	$1{\cdot}97.10^{-11}$	7·85
7.10^3	$2{\cdot}88.10^{-11}$	7·85
10^4	$4{\cdot}40.10^{-11}$	7·85
2.10^4	$9{\cdot}90.10^{-11}$	7·80
5.10^4	$2{\cdot}6.10^{-10}$	7·85
10^5	$5{\cdot}5.10^{-10}$	7·80

(b) $As_2 S_{2.8}$ l = 0·534 mm A = 1·27 cm^2

(i) T = 370 K

f	σ	ϵ'_r
Hz	$ohm^{-1}\ cm^{-1}$	
700	$3{\cdot}4.10^{-12}$	8·18
10^3	$3{\cdot}0.10^{-12}$	8·21
2.10^3	$5{\cdot}9.10^{-12}$	8·25
3.10^3	$8{\cdot}8.10^{-12}$	8·25
5.10^3	$1{\cdot}52.10^{-11}$	8·25
7.10^3	$2{\cdot}15.10^{-11}$	8·28
10^4	$3{\cdot}60.10^{-11}$	8·28
2.10^4	$6{\cdot}53.10^{-11}$	8·25
5.10^4	$1{\cdot}70.10^{-10}$	8·25
10^5	$4{\cdot}38.10^{-10}$	8·21

(ii) T = 350 K

f	σ	ϵ'_r
Hz	$ohm^{-1}\ cm^{-1}$	
700	-	-
10^3	3.10^{-12}	8·18
2.10^3	$5{\cdot}9.10^{-12}$	8·25
3.10^3	$9{\cdot}1.10^{-12}$	8·25
5.10^3	$1{\cdot}5.10^{-11}$	8·25
7.10^3	$1{\cdot}86.10^{-11}$	8·25
10^4	$2{\cdot}90.10^{-11}$	8·21
2.10^4	$6{\cdot}07.10^{-11}$	8·18
5.10^4	$1{\cdot}67.10^{-10}$	8·21
10^5	$3{\cdot}84.10^{-10}$	8·21

(iii) T = 330 K

f	σ	ϵ'_r
Hz	$ohm^{-1}\ cm^{-1}$	
10^3	3.10^{-12}	8·21
2.10^3	$6·1.10^{-12}$	8·25
3.10^3	$8·4.10^{-12}$	8·28
5.10^3	$1·43.10^{-11}$	8·25
7.10^3	$1·96.10^{-11}$	8·25
10^4	$2·82.10^{-11}$	8·25
2.10^4	$6·27.10^{-11}$	8·25
5.10^4	$1·69.10^{-10}$	8·21
10^5	$3·70.10^{-10}$	8·21

(iv) T = 315 K

f	σ	ϵ'_r
Hz	$ohm^{-1}\ cm^{-1}$	
10^3	$2·5.10^{-12}$	8·28
2.10^3	$5·7.10^{-12}$	8·25
3.10^3	$8·8.10^{-12}$	8·25
5.10^3	$1·47.10^{-11}$	8·21
7.10^3	$2·17.10^{-11}$	8·21
10^4	$3·45.10^{-11}$	8·21
2.10^4	$7·19.10^{-11}$	8·21
5.10^4	$2·21.10^{-10}$	8·25
10^5	$5·67.10^{-10}$	8·21

(c) $As_2 S_{3\cdot0}$ l = 1·33 mm A = 0·785 cm^2

(i) T = 370 K

f	σ	ϵ'_r
Hz	$ohm^{-1}\ cm^{-1}$	
700	$1\cdot35.10^{-12}$	8·26
10^3	$5\cdot1.10^{-12}$	8·26
2.10^3	$7\cdot3.10^{-12}$	8·15
3.10^3	$9\cdot3.10^{-12}$	8·15
5.10^3	$1\cdot33.10^{-11}$	8·21
7.10^3	$1\cdot77.10^{-11}$	8·21
10^4	$2\cdot21.10^{-11}$	8·21
2.10^4	$4\cdot27.10^{-11}$	8·26
5.10^4	$1\cdot02.10^{-10}$	8·26
10^5	$2\cdot56.10^{-10}$	8·26

(ii) T = 350 K

f	σ	ϵ'_r
Hz	$ohm^{-1}\ cm^{-1}$	
700	$2\cdot7.10^{-12}$	8·21
10^3	$3\cdot4.10^{-12}$	8·26
2.10^3	$5\cdot1.10^{-12}$	8·26
3.10^3	$6\cdot80.10^{-12}$	8·26
5.10^3	$9\cdot18.10^{-12}$	8·26
7.10^3	$1\cdot36.10^{-11}$	8·26
10^4	$2\cdot04.10^{-11}$	8·21
2.10^4	$3\cdot91.10^{-11}$	8·26
5.10^4	$1\cdot12.10^{-10}$	8·26
10^5	$2\cdot21.10^{-10}$	8·26

(iii) T = 330 K

f	σ	ϵ'_r
Hz	$ohm^{-1}\ cm^{-1}$	
700	$1 \cdot 7 \cdot 10^{-12}$	8·21
10^3	$2 \cdot 2 \cdot 10^{-12}$	8·13
$2 \cdot 10^3$	$3 \cdot 9 \cdot 10^{-12}$	8·13
$3 \cdot 10^3$	$5 \cdot 6 \cdot 10^{-12}$	8·13
$5 \cdot 10^3$	$9 \cdot 3 \cdot 10^{-12}$	8·13
$7 \cdot 10^3$	$1 \cdot 36 \cdot 10^{-11}$	8·13
10^4	$1 \cdot 53 \cdot 10^{-11}$	8·13
$2 \cdot 10^4$	$3 \cdot 91 \cdot 10^{-11}$	8·13
$5 \cdot 10^4$	$9 \cdot 36 \cdot 10^{-11}$	8·13
10^5	$1 \cdot 53 \cdot 10^{-10}$	8·13

(d) $As_2 S_{3\cdot2}$ $l = 1\cdot65$ mm $A = 1\cdot29$ cm^2

(i) T = 370 K

f	σ	ϵ'_r
Hz	ohm^{-1} cm^{-1}	
10^3	$5\cdot1\cdot10^{-12}$	7·67
$2\cdot10^3$	$8\cdot3\cdot10^{-12}$	7·61
$3\cdot10^3$	$9\cdot0\cdot10^{-12}$	7·67
$5\cdot10^3$	$1\cdot21\cdot10^{-11}$	7·61
$7\cdot10^3$	$1\cdot60\cdot10^{-11}$	7·61
10^4	$2\cdot05\cdot10^{-11}$	7·61
$2\cdot10^4$	$4\cdot08\cdot10^{-11}$	7·61
$5\cdot10^4$	$8\cdot56\cdot10^{-11}$	7·61
10^5	$1\cdot41\cdot10^{-10}$	7·61

(ii) T = 350 K

f	σ	ϵ'_r
Hz	ohm^{-1} cm^{-1}	
10^3	$4\cdot10^{-12}$	7·67
$2\cdot10^3$	$3\cdot8\cdot10^{-12}$	7·61
$3\cdot10^3$	$5\cdot1\cdot10^{-12}$	7·61
$5\cdot10^3$	$8\cdot9\cdot10^{-12}$	7·61
$7\cdot10^3$	$1\cdot34\cdot10^{-11}$	7·61
10^4	$1\cdot79\cdot10^{-11}$	7·61
$2\cdot10^4$	$3\cdot38\cdot10^{-11}$	7·61
$5\cdot10^4$	$8\cdot36\cdot10^{-11}$	7·61
10^5	$1\cdot60\cdot10^{-10}$	7·61

(iii) T = 330 K

f	σ	ϵ'_r
Hz	$ohm^{-1}\ cm^{-1}$	
10^3	$2{\cdot}6.10^{-12}$	7·61
2.10^3	$3{\cdot}8.10^{-12}$	7·67
3.10^3	$5{\cdot}1.10^{-12}$	7·61
5.10^3	$8{\cdot}3.10^{-12}$	7·61
7.10^3	$1{\cdot}35.10^{-11}$	7·61
10^4	$1{\cdot}66.10^{-11}$	7·61
2.10^4	$3{\cdot}25.10^{-11}$	7·61
5.10^4	$7{\cdot}00.10^{-11}$	7·61
10^5	$1{\cdot}58.10^{-10}$	7·67

(iv) T = 315 K

f	σ	ϵ'_r
Hz	$ohm^{-1}\ cm^{-1}$	
10^3	$2{\cdot}6.10^{-12}$	7·56
2.10^3	$3{\cdot}9.10^{-12}$	7·61
3.10^3	$5{\cdot}1.10^{-12}$	7·67
5.10^3	$8{\cdot}5.10^{-12}$	7·61
7.10^3	$1{\cdot}08.10^{-11}$	7·61
10^4	$1{\cdot}40.10^{-11}$	7·61
2.10^4	$3{\cdot}19.10^{-11}$	7·61
5.10^4	$6{\cdot}90.10^{-11}$	7·56
10^5	$1{\cdot}49.10^{-10}$	7·61

(e) $As_2 S_{3.4}$ l = 1·26 mm A = 1·23 cm^2

(i) T = 370 K

f	σ	ϵ'_r
Hz	$ohm^{-1}\ cm^{-1}$	
10^3	$4{\cdot}5.10^{-12}$	6·83
2.10^3	$6{\cdot}5.10^{-12}$	6·83
3.10^3	$8{\cdot}6.10^{-12}$	6·87
5.10^3	$1{\cdot}31.10^{-11}$	6·87
7.10^3	$1{\cdot}82.10^{-11}$	6·87
10^4	$2{\cdot}22.10^{-11}$	6·83
2.10^4	$3{\cdot}74.10^{-11}$	6·87
5.10^4	$9{\cdot}09.10^{-11}$	6·87
10^5	$1{\cdot}62.10^{-10}$	6·87

(ii) T = 350 K

f	σ	ϵ'_r
Hz	$ohm^{-1}\ cm^{-1}$	
10^3	$3{\cdot}1.10^{-12}$	6·83
2.10^3	$5{\cdot}1.10^{-12}$	6·87
3.10^3	$6{\cdot}1.10^{-12}$	6·87
5.10^3	$9{\cdot}9.10^{-12}$	6·83
7.10^3	$1{\cdot}48.10^{-11}$	6·87
10^4	$1{\cdot}99.10^{-11}$	6·87
2.10^4	$3{\cdot}88.10^{-11}$	6·83
5.10^4	$9{\cdot}68.10^{-11}$	6·83
10^5	$1{\cdot}80.10^{-10}$	6·87

(iii) T = 330 K

f	σ	ϵ'_r
Hz	$ohm^{-1}\ cm^{-1}$	
10^3	$3{\cdot}1.10^{-12}$	6·84
2.10^3	$4{\cdot}1.10^{-12}$	6·84
3.10^3	$5{\cdot}6.10^{-12}$	6·84
5.10^3	$9{\cdot}7.10^{-12}$	6·84
7.10^3	$1{\cdot}22.10^{-11}$	6·84
10^4	$1{\cdot}95.10^{-11}$	6·84
2.10^4	$3{\cdot}36.10^{-11}$	6·84
5.10^4	$8{\cdot}46.10^{-11}$	6·84
10^5	$1{\cdot}68.10^{-10}$	6·84

(iv) T = 315 K

f	σ	ϵ'_r
Hz	$ohm^{-1}\ cm^{-1}$	
10^3	$3{\cdot}1.10^{-12}$	6·84
2.10^3	$4{\cdot}1.10^{-12}$	6·84
3.10^3	$5{\cdot}6.10^{-12}$	6·80
5.10^3	$8{\cdot}7.10^{-12}$	6·80
7.10^3	$1{\cdot}33.10^{-11}$	6·84
10^4	$1{\cdot}64.10^{-11}$	6·80
2.10^4	$3{\cdot}06.10^{-11}$	6·84
5.10^4	$7{\cdot}84.10^{-11}$	6·84
10^5	$1{\cdot}49.10^{-10}$	6·80

A3.6 $As_2 S_{2.6}$ - phase separated sample.

electrodes: evaporated gold.

$l = 0.91$ mm $\quad A = 1.12$ cm^2

(a) d.c. conductivity.

temperature °C	σ ohm^{-1} cm^{-1}
150	$8.28.10^{-12}$
140	$4.07.10^{-12}$
130	$2.04.10^{-12}$
120	$8.46.10^{-13}$
110	$3.62.10^{-13}$
100	$1.50.10^{-13}$
90	$5.45.10^{-14}$
80	$2.08.10^{-14}$
70	$7.65.10^{-15}$
60	$2.61.10^{-15}$

(b) a.c. conductivity

(i) T = 370 K

f Hz	σ ohm^{-1} cm^{-1}	ε'_r
500	$5.93.10^{-11}$	7.44
700	$6.09.10^{-11}$	7.36
10^3	$6.90.10^{-11}$	7.28
2.10^3	$8.20.10^{-11}$	7.21
3.10^3	$8.95.10^{-11}$	7.28
5.10^3	$1.03.10^{-10}$	7.21

7.10^3	$1{\cdot}09.10^{-10}$	7·21
10^4	$1{\cdot}31.10^{-10}$	7·21
2.10^4	$1{\cdot}85.10^{-10}$	7·21
5.10^4	$3{\cdot}22.10^{-10}$	7·21
10^5	$6{\cdot}58.10^{-10}$	7·18

(ii) T = 350 K

f	σ	ε'_r
Hz	$ohm^{-1}\ cm^{-1}$	
500	$2{\cdot}28.10^{-11}$	7·28
700	$2{\cdot}36.10^{-11}$	7·25
10^3	$2{\cdot}52.10^{-11}$	7·18
2.10^3	$3{\cdot}17.10^{-11}$	7·18
3.10^3	$3{\cdot}74.10^{-11}$	7·25
5.10^3	$4{\cdot}56.10^{-11}$	7·21
7.10^3	$5{\cdot}33.10^{-11}$	7·21
10^4	$7{\cdot}81.10^{-11}$	7·18
2.10^4	$9{\cdot}76.10^{-11}$	7·21
5.10^4	$2{\cdot}64.10^{-10}$	7·21
10^5	$5{\cdot}53.10^{-10}$	7·16

(iii) T = 330 K

f	σ	e'_r
Hz	$ohm^{-1}\ cm^{-1}$	
500	$5{\cdot}7.10^{-12}$	7·25
700	$7{\cdot}3.10^{-12}$	7·21
10^3	$9{\cdot}0.10^{-12}$	7·21
2.10^3	$1{\cdot}22.10^{-11}$	7·21
3.10^3	$1{\cdot}71.10^{-11}$	7·25
5.10^3	$2{\cdot}52.10^{-11}$	7·18
7.10^3	$3{\cdot}41.10^{-11}$	7·18
10^4	$5{\cdot}20.10^{-11}$	7·18
2.10^4	$9{\cdot}60.10^{-11}$	7·21
5.10^4	$2{\cdot}44.10^{-10}$	7·18
10^5	$5{\cdot}74.10^{-10}$	7·25

(iv) T = 315 K

f	σ	e'_r
Hz	$ohm^{-1}\ cm^{-1}$	
500	$4{\cdot}5.10^{-12}$	7·28
700	$3{\cdot}2.10^{-12}$	7·25
10^3	$4{\cdot}7.10^{-12}$	7·28
2.10^3	$8{\cdot}5.10^{-12}$	7·28
3.10^3	$1{\cdot}30.10^{-11}$	7·28
5.10^3	$2{\cdot}08.10^{-11}$	7·25
7.10^3	$3{\cdot}04.10^{-11}$	7·18
10^4	$4{\cdot}19.10^{-11}$	7·18
2.10^4	$8{\cdot}9.10^{-11}$	7·18
5.10^4	$2{\cdot}22.10^{-10}$	7·18
10^5	$4{\cdot}99.10^{-10}$	7·18

A3.7 D.c. conductivity of the As - Se system.

(a) $As_2 Se_{2.6}$ l = 1·63 mm A = 0·909 cm^2

(b) $As_2 Se_{2.8}$ l = 1·41 mm A = 0·710 cm^2

(c) $As_2 Se_{3.0}$ l = 3·25 mm A = 0·866 cm^2

(d) $As_2 Se_{3.2}$ l = 1·28 mm A = 0·801 cm^2

(e) $As_2 Se_{3.4}$ l = 1·73 mm A = 0·740 cm^2

temperature	σ $ohm^{-1}.cm^{-1}.10^{11}$				
°C	(a)	(b)	(c)	(d)	(e)
110	-	153	201	242	234
100	65·6	73·6	102	117	119
90	32·9	34·8	50·6	55·7	56·6
80	14·1	14·6	22·5	24·6	24·6
70	5·40	5·97	9·20	10·4	10·7
60	2·46	2·49	3·86	4·32	4·46
50	0·891	0·816	1·43	1·68	1·65

electrodes: evaporated gold, except $As_2 Se_{2.8}$ (aluminium)

A3.8 A.c. conductivity of the As - Se system.

electrodes: evaporated gold.

(a) $As_2 Se_{2.6}$ $l = 1.63$ mm $A = 0.909$ cm^2

(i) $T = 370$ K

f	σ	ε'_r
Hz	ohm^{-1} cm^{-1}	
500	$3.60.10^{-10}$	9.68
700	$3.69.10^{-10}$	9.68
10^3	$3.74.10^{-10}$	9.68
2.10^3	$3.78.10^{-10}$	9.68
3.10^3	$3.81.10^{-10}$	9.60
5.10^3	$3.96.10^{-10}$	9.60
7.10^3	$3.96.10^{-10}$	9.60
10^4	$4.05.10^{-10}$	9.60
2.10^4	$4.14.10^{-10}$	9.60
5.10^4	$4.43.10^{-10}$	9.60
10^5	$5.13.10^{-10}$	9.60

(ii) $T = 350$ K

f	σ	ε'_r
Hz	ohm^{-1} cm^{-1}	
500	$8.81.10^{-11}$	9.60
700	$8.72.10^{-11}$	9.60
10^3	$8.81.10^{-11}$	9.60
2.10^3	$8.72.10^{-11}$	9.60
3.10^3	$8.81.10^{-11}$	9.60

5.10^3	$9{\cdot}17.10^{-11}$	9·60
7.10^3	$9{\cdot}17.10^{-11}$	9·60
10^4	$9{\cdot}62.10^{-11}$	9·60
2.10^4	$1{\cdot}06.10^{-10}$	9·60
5.10^4	$1{\cdot}33.10^{-10}$	9·60
10^5	$1{\cdot}80.10^{-10}$	9·60

(iii) T = 330 K

f	σ	ϵ'_r
Hz	$ohm^{-1}\ cm^{-1}$	
500	$1{\cdot}26.10^{-11}$	9·40
700	$1{\cdot}53.10^{-11}$	9·60
10^3	$1{\cdot}62.10^{-11}$	9·60
2.10^3	$1{\cdot}62.10^{-11}$	9·60
3.10^3	$1{\cdot}69.10^{-11}$	9·60
5.10^3	$1{\cdot}76.10^{-11}$	9·60
7.10^3	$2{\cdot}10.10^{-11}$	9·60
10^4	$2{\cdot}16.10^{-11}$	9·60
2.10^4	$2{\cdot}88.10^{-11}$	9·54
5.10^4	$5{\cdot}75.10^{-11}$	9·60
10^5	$1{\cdot}26.10^{-10}$	9·54

(iv) T = 315 K

f	σ	ϵ'_r
Hz	$ohm^{-1}\ cm^{-1}$	
10^3	$4{\cdot}9.10^{-12}$	9·60
2.10^3	$5{\cdot}4.10^{-12}$	9·60

3.10^3	$6{\cdot}3.10^{-12}$	9·54
5.10^3	$7{\cdot}0.10^{-12}$	9·60
7.10^3	$8{\cdot}1.10^{-12}$	9·60
10^4	$1{\cdot}20.10^{-11}$	9·54
2.10^4	$1{\cdot}98.10^{-11}$	9·60
5.10^4	$5{\cdot}22.10^{-11}$	9·60
10^5	$1{\cdot}10.10^{-10}$	9·60

(b) $As_2 Se_{2.8}$ l = 0·762 mm A = 0·240 cm^2

(i) T = 370 K

f	σ	ϵ'_r
Hz	$ohm^{-1}\ cm^{-1}$	
500	$2{\cdot}37.10^{-10}$	11·9
10^3	$2{\cdot}37.10^{-10}$	11·9
2.10^3	$2{\cdot}43.10^{-10}$	11·9
3.10^3	$2{\cdot}46.10^{-10}$	11·9
5.10^3	$3{\cdot}52.10^{-10}$	11·8
7.10^3	$2{\cdot}55.10^{-10}$	11·8
10^4	$2{\cdot}67.10^{-10}$	11·9
2.10^4	$3{\cdot}02.10^{-10}$	11·9
5.10^4	$4{\cdot}83.10^{-10}$	11·9
10^5	$7{\cdot}00.10^{-10}$	11·9

(ii) T = 350 K

f	σ	ϵ'_r
Hz	$ohm^{-1}\ cm^{-1}$	
500	$5 \cdot 81 \cdot 10^{-11}$	12·4
700	$5 \cdot 86 \cdot 10^{-11}$	12·4
10^3	$6 \cdot 28 \cdot 10^{-11}$	12·5
$2 \cdot 10^3$	$5 \cdot 86 \cdot 10^{-11}$	12·4
$3 \cdot 10^3$	$6 \cdot 50 \cdot 10^{-11}$	12·4
$5 \cdot 10^3$	$6 \cdot 82 \cdot 10^{-11}$	12·4
$7 \cdot 10^3$	$7 \cdot 61 \cdot 10^{-11}$	12·4
10^4	$8 \cdot 60 \cdot 10^{-11}$	12·4
$2 \cdot 10^4$	$1 \cdot 14 \cdot 10^{-10}$	12·5
$5 \cdot 10^4$	$1 \cdot 98 \cdot 10^{-10}$	12·4
10^5	$3 \cdot 78 \cdot 10^{-10}$	12·5

(iii) T = 330 K

f	σ	ϵ'_r
Hz	$ohm^{-1}\ cm^{-1}$	
10^3	$1 \cdot 59 \cdot 10^{-11}$	12·1
$2 \cdot 10^3$	$2 \cdot 22 \cdot 10^{-11}$	12·1
$3 \cdot 10^3$	$2 \cdot 20 \cdot 10^{-11}$	12·1
$5 \cdot 10^3$	$3 \cdot 28 \cdot 10^{-11}$	12·1
$7 \cdot 10^3$	$4 \cdot 46 \cdot 10^{-11}$	12·1
10^4	$4 \cdot 50 \cdot 10^{-11}$	12·1
$2 \cdot 10^4$	$7 \cdot 64 \cdot 10^{-11}$	12·1
$5 \cdot 10^4$	$1 \cdot 27 \cdot 10^{-10}$	12·1
10^5	$2 \cdot 86 \cdot 10^{-10}$	12·1

(iv) T = 296 K

f	σ	ϵ'_r
Hz	$ohm^{-1}\ cm^{-1}$	
10^3	$6{\cdot}4.10^{-12}$	12·1
2.10^3	$9{\cdot}5.10^{-12}$	12·3
3.10^3	$1{\cdot}6.10^{-11}$	12·3
5.10^3	$2{\cdot}07.10^{-11}$	12·3
7.10^3	$3{\cdot}02.10^{-11}$	12·3
10^4	$3{\cdot}67.10^{-11}$	12·3
2.10^4	$6{\cdot}68.10^{-11}$	12·3
5.10^4	$1{\cdot}43.10^{-10}$	12·4
10^5	$2{\cdot}13.10^{-10}$	12·4

(c) $As_2 Se_{3\cdot0}$ l = 3·25 mm A = 0·866 cm^2

(i) T = 370 K

f	σ	ϵ'_r
Hz	$ohm^{-1}\ cm^{-1}$	
10^3	$5{\cdot}44.10^{-10}$	9·49
2.10^3	$5{\cdot}50.10^{-10}$	9·64
3.10^3	$5{\cdot}63.10^{-10}$	9·49
5.10^3	$5{\cdot}74.10^{-10}$	9·35
7.10^3	$5{\cdot}82.10^{-10}$	9·35
10^4	$6{\cdot}01.10^{-10}$	9·35
2.10^4	$6{\cdot}49.10^{-10}$	9·35
5.10^4	$7{\cdot}80.10^{-10}$	9·35
10^5	$1{\cdot}11.10^{-9}$	9·49

(ii) T = 350 K

f	σ	ϵ'_r
Hz	$ohm^{-1}\ cm^{-1}$	
10^3	$1 \cdot 05 \cdot 10^{-10}$	9·20
$2 \cdot 10^3$	$1 \cdot 08 \cdot 10^{-10}$	9·35
$3 \cdot 10^3$	$1 \cdot 13 \cdot 10^{-10}$	9·20
$5 \cdot 10^3$	$1 \cdot 25 \cdot 10^{-10}$	9·20
$7 \cdot 10^3$	$1 \cdot 26 \cdot 10^{-10}$	9·20
10^4	$1 \cdot 43 \cdot 10^{-10}$	9·20
$2 \cdot 10^4$	$1 \cdot 99 \cdot 10^{-10}$	9·35
$5 \cdot 10^4$	$3 \cdot 28 \cdot 10^{-10}$	9·07
10^5	$7 \cdot 31 \cdot 10^{-10}$	9·20

(iii) T = 330 K

f	σ	ϵ'_r
Hz	$ohm^{-1}\ cm^{-1}$	
10^3	$2 \cdot 25 \cdot 10^{-11}$	9·20
$2 \cdot 10^3$	$2 \cdot 29 \cdot 10^{-11}$	9·20
$3 \cdot 10^3$	$2 \cdot 44 \cdot 10^{-11}$	9·20
$5 \cdot 10^3$	$3 \cdot 18 \cdot 10^{-11}$	9·20
$7 \cdot 10^3$	$3 \cdot 75 \cdot 10^{-11}$	9·20
10^4	$5 \cdot 00 \cdot 10^{-11}$	9·35
$2 \cdot 10^4$	$9 \cdot 46 \cdot 10^{-11}$	9·20
$5 \cdot 10^4$	$2 \cdot 64 \cdot 10^{-10}$	9·20
10^5	$4 \cdot 83 \cdot 10^{-10}$	9·20

(iv) T = 315 K

f	σ	ϵ'_r
Hz	$ohm^{-1}\ cm^{-1}$	
10^3	$6{\cdot}00.10^{-12}$	8·91
2.10^3	$7{\cdot}12.10^{-12}$	9·06
3.10^3	$9{\cdot}0.10^{-12}$	8·91
5.10^3	$1{\cdot}54.10^{-11}$	8·91
7.10^3	$1{\cdot}87.10^{-11}$	8·91
10^4	$3{\cdot}49.10^{-11}$	8·91
2.10^4	$7{\cdot}5.10^{-11}$	8·91
5.10^4	$2{\cdot}70.10^{-10}$	8·91
10^5	$5{\cdot}36.10^{-10}$	9·20

(d) $As_2 Se_{3\cdot2}$ l = 1·28 mm A = 0·801 cm^2

(i) T = 370 K

f	σ	ϵ'_r
Hz	$ohm^{-1}\ cm^{-1}$	
500	$6{\cdot}08.10^{-10}$	9·99
700	$6{\cdot}08.10^{-10}$	9·99
10^3	$5{\cdot}92.10^{-10}$	9·99
2.10^3	$5{\cdot}96.10^{-10}$	9·93
3.10^3	$5{\cdot}98.10^{-10}$	9·79
5.10^3	$6{\cdot}04.10^{-10}$	9·79
7.10^3	$6{\cdot}14.10^{-10}$	9·84
10^4	$6{\cdot}19.10^{-10}$	9·93
2.10^4	$6{\cdot}40.10^{-10}$	9·99
5.10^4	$6{\cdot}91.10^{-10}$	9·93
10^5	$8{\cdot}40.10^{-10}$	9·93

(ii) T = 350 K

f	σ	ϵ'_r
Hz	$ohm^{-1}\ cm^{-1}$	
500	$1 \cdot 20 . 10^{-10}$	9·93
700	$1 \cdot 28 . 10^{-10}$	9·84
10^3	$1 \cdot 28 . 10^{-10}$	9·93
$2 . 10^3$	$1 \cdot 25 . 10^{-10}$	9·93
$3 . 10^3$	$1 \cdot 24 . 10^{-10}$	9·84
$5 . 10^3$	$1 \cdot 28 . 10^{-10}$	9·93
$7 . 10^3$	$1 \cdot 32 . 10^{-10}$	9·93
10^4	$1 \cdot 33 . 10^{-10}$	9·99
$2 . 10^4$	$1 \cdot 44 . 10^{-10}$	9·93
$5 . 10^4$	$1 \cdot 84 . 10^{-10}$	9·93
10^5	$2 \cdot 59 . 10^{-10}$	9·93

(iii) T = 330 K

f	σ	ϵ'_r
Hz	$ohm^{-1}\ cm^{-1}$	
700	$4 \cdot 0 . 10^{-11}$	9·79
10^3	$4 \cdot 25 . 10^{-11}$	9·79
$2 . 10^3$	$4 \cdot 48 . 10^{-11}$	9·86
$3 . 10^3$	$4 \cdot 48 . 10^{-11}$	9·93
$5 . 10^3$	$4 \cdot 81 . 10^{-11}$	9·98
$7 . 10^3$	$5 \cdot 20 . 10^{-11}$	9·98
10^4	$6 \cdot 10 . 10^{-11}$	9·98
$2 . 10^4$	$1 \cdot 0 . 10^{-10}$	9·93
$5 . 10^4$	$1 \cdot 35 . 10^{-10}$	9·93
10^5	$1 \cdot 90 . 10^{-10}$	9·93

(iv) T = 315 K

f	σ	ϵ'_r
Hz	$ohm^{-1}\ cm^{-1}$	
10^3	$8{\cdot}8.10^{-12}$	9·79
2.10^3	$9{\cdot}6.10^{-11}$	9·74
3.10^3	$1{\cdot}28.10^{-11}$	9·74
5.10^3	$1{\cdot}44.10^{-11}$	9·68
7.10^3	$1{\cdot}60.10^{-11}$	9·74
10^4	$2{\cdot}00.10^{-11}$	9·74
2.10^4	$4{\cdot}32.10^{-11}$	9·68
5.10^4	$6{\cdot}10.10^{-11}$	9·74
10^5	$1{\cdot}30.10^{-10}$	9·68

(e) $As_2 Se_{3{\cdot}4}$ l = 1·73 mm A = 0·74 cm^2

(i) T = 370 K

f	σ	ϵ'_r
Hz	$ohm^{-1}\ cm^{-1}$	
500	$6{\cdot}91.10^{-10}$	10·3
700	$7{\cdot}02.10^{-10}$	10·1
10^3	$7{\cdot}14.10^{-10}$	10·2
2.10^3	$7{\cdot}26.10^{-10}$	10·3
3.10^3	$7{\cdot}33.10^{-10}$	10·3
5.10^3	$7{\cdot}54.10^{-10}$	10·3
7.10^3	$7{\cdot}49.10^{-10}$	10·1
10^4	$7{\cdot}56.10^{-10}$	10·1
2.10^4	$7{\cdot}84.10^{-10}$	10·0
5.10^4	$8{\cdot}12.10^{-10}$	10·1
10^5	$9{\cdot}71.10^{-10}$	10·1

(ii) T = 350 K

f	σ	ϵ'_r
Hz	$ohm^{-1}\ cm^{-1}$	
500	$1 \cdot 73 . 10^{-10}$	10·5
700	$1 \cdot 71 . 10^{-10}$	10·1
10^3	$1 \cdot 76 . 10^{-10}$	10·3
$2 . 10^3$	$1 \cdot 73 . 10^{-10}$	10·2
$3 . 10^3$	$1 \cdot 81 . 10^{-10}$	10·2
$5 . 10^3$	$1 \cdot 75 . 10^{-10}$	10·2
$7 . 10^3$	$1 \cdot 83 . 10^{-10}$	10·1
10^4	$1 \cdot 87 . 10^{-10}$	10·0
$2 . 10^4$	$1 \cdot 96 . 10^{-10}$	10·1
$5 . 10^4$	$2 \cdot 34 . 10^{-10}$	10·0
10^5	$2 \cdot 58 . 10^{-10}$	10·0

(iii) T = 330 K

f	σ	ϵ'_r
Hz	$ohm^{-1}\ cm^{-1}$	
700	$3 \cdot 0 . 10^{-11}$	10·1
10^3	$2 \cdot 81 . 10^{-11}$	10·1
$2 . 10^3$	$3 \cdot 16 . 10^{-11}$	10·2
$3 . 10^3$	$3 \cdot 15 . 10^{-11}$	10·2
$5 . 10^3$	$3 \cdot 27 . 10^{-11}$	10·1
$7 . 10^3$	$3 \cdot 63 . 10^{-11}$	10·0
10^4	$4 \cdot 21 . 10^{-11}$	10·0
$2 . 10^4$	$7 \cdot 61 . 10^{-11}$	10·0
$5 . 10^4$	$1 \cdot 01 . 10^{-11}$	10·1
10^5	$2 \cdot 22 . 10^{-11}$	10·0

(iv) T = 315 K

f	σ	ε'_r
Hz	$ohm^{-1}\ cm^{-1}$	
2.10^3	$7{\cdot}0.10^{-12}$	10·1
3.10^3	$8{\cdot}2.10^{-12}$	10·0
5.10^3	$1{\cdot}17.10^{-11}$	9·9
7.10^3	$1{\cdot}40.10^{-11}$	10·0
10^4	$1{\cdot}75.10^{-11}$	10·0
2.10^4	$3{\cdot}04.10^{-11}$	9·9
5.10^4	$5{\cdot}86.10^{-11}$	9·9
10^5	$1{\cdot}40.10^{-10}$	9·9

A3.9 Dielectric constants of the As - Se system.

frequency: 5 kHz

(a) $As_2 Se_{2.6}$

Temperature K	electrode material	ϵ'_r
295	none	10·2
370	none	8·76
350	none	8·79
330	none	8·89
315	none	8·89
370	Au	9·68
350	Au	9·60
330	Au	9·60
315	Au	9·60
370	Au	9·53
350	Au	9·53
330	Au	9·53
295	Au	9·74

(b) $As_2 Se_{2.8}$

temperature K	electrode material	ϵ'_r
325	Au	9·86
295	Al	9·84
325	Al	9·89
295	Al	12·0

295	Al	12·2
330	none	12·2
370	none	11·8
295	none	12·3
350	none	12·2
295	Al	10·0

(c) $As_2 Se_{3\cdot0}$

temperature K	electrode material	ϵ'_r
295	none	9·16
330	none	9·28
350	none	9·28
370	none	9·35
313	none	8·91
350	Au	9·58
370	Au	9·58
330	Au	12·7
315	Au	9·64
330	Al	9·91
330	Au	10·5
330	Al	9·96
330	Au	9·56
330	Au	13·2
330	Al	13·2
330	Au	13·9
330	none	9·35
330	Au	10·8

(d) $As_2 Se_{3.2}$

temperature K	electrode material	ϵ'_r
350	none	9·71
370	none	9·65
330	none	9·77
315	none	9·65
370	Au	9·77
350	Au	9·90
330	Au	9·96
315	Au	9·35
295	Au	10·5

(e) $As_2 Se_{3.4}$

temperature K	electrode material	ϵ'_r
370	Au	10·3
350	Au	10·2
330	Au	10·1
315	Au	9·95
295	Au	9·95

A3.10 $As_2 S_3$ microstrip results. (room temperature)

(a) Sample number 11

h = 1·75 mm w = 1·50 mm t = 2·6 μm

ring resonator, r = 9·67 mm

f GHz	Q_L
8·52	213
10·33	258
11·86	297

(b) Sample No. 9

h = 1·56 mm w = 1·50 mm t = 1·6 μm

ring resonator, r = 9·67 mm

f GHz	Q_L
8·85	221

(c) Sample No. 14

h = 1·30 mm w = 1·50 mm t = 1·3 μm

ring resonator, r = 9·67 mm

f GHz	Q_L
2·099	54
4·155	90
6·160	-

8·108	-
10.009	157
11·873	-

poor sample: low Q factors.

(d) Sample No. 15

h = 1·54 mm w = 1·54 mm t = 1·6 μm

ring resonator, r = 9·67 mm

f GHz	Q_L	insertion loss, α db
2·125	89	15
2·1256	116	11
2·1262	118	12
2·1269	105	13
2·1150	110	12
2·1264	155	-
2·1160	86	-
4·1773	122	13
4·21	140	-
4·1838	138	10
6·17	155	-
6·1552	142	13
6·1539	154	-
6·23	171	-
8·12	180	-
8·0910	142	14
8·0852	252	-

8•0913	213	-
9•96	262	12
9•9708	197	5
9•9767	212	12
9•9713	200	13
9•9778	168	-
9•9736	177	-
9•9793	227	-
11•8146	163	12
11•8274	250	12

(e) Sample No. 21

h = 2•05 mm w = 2•0 mm t = 0•9 μm

ring resonator, r = 16•4 mm

f GHz	Q_L	α db
3•6591	146	13
4•8495	160	12
5•9869	230	10
7•1253	240	12
8•2406	275	9
10•4464	262	10
11•5123	271	14

A3.11 Temperature variation of the $As_2 S_3$ microstrip.

(a) Sample No. 15 (10GHz resonance)

h = 1·54 mm w = 1·50 mm t = 1·6 μm

ring resonator, r = 9·67 mm (at T = 295 K)

T	f	Q_L
K	GHz	
290	9·9778	168
256	9·9921	173
228	10·0010	178
204	10·0152	184
186	10·0208	196
164	10·0265	209
143	10·0315	221
115	10·0356	223
99	10·0379	224
147	10·0304	206
164	10·0268	203
113	10·0358	211
300	9·9724	177
330	9·9583	212
350	9·9506	217
377	9·9410	212
292	9·9744	177
310	9·9671	203

(b) Sample No. 15 (2GHz resonance)

T	f	Q_L
K	GHz	
289	2·1264	155
270	2·1286	98
250	2·1307	101
218	2·1335	102
183	2·1371	106
162	2·1394	178
143	2·1412	145
97	2·1451	148
98	2·1450	142
110	2·1441	136
126	2·1421	136
125	2·1427	143
131	2·1421	123
115	2·1437	129
165	2·1385	103
291	2·1290	91
300	2·1278	87
320	2·1267	93
339	2·1249	91
353	2·1237	92
376	2·1213	89

(c) Sample No. 21 (7GHz resonance)

h = 2·05 mm w = 2·00 mm t = 0·9 μm

ring resonator, r = 16·4 mm (at T = 295K)

T K	f	Q_L
294	7·1290	236
314	7·1209	272
330	7·1146	201
350	7·1129	222
376	7·1007	256
288	7·1316	235
260	7·1402	239
230	7·1487	240
200	7·1580	189
180	7·1630	288
149	7·1673	278
135	7·1715	273
120	7·1715	256
106	7·1737	262
92	7·1748	269
164	7·1654	272
190	7·1601	260
210	7·1541	222
247	7·1446	186
350	7·1127	169
363	7·1076	184
375	7·1022	216

330	7·1198	177
288	7·1327	250
301	7·1266	256
320	7·1195	210
341	7·1112	225
360	7·1062	250

Note: In the calculation of the conductivity of the above an insertion loss of 12 db was assumed.

A3.12 $As_2 Se_3$ microstrip results (room temperature)

(a) Sample No. 1

h = 1·40 mm w = 1·50 mm t = 1·7 μm

straight line resonator, length = 14 mm

f GHz	Q_L
9·14	166
12·18	-

(b) Sample No. 3

h = 1·76 mm w = 1·50 mm t = 1·1 μm

ring resonator, r = 9·67 mm

f GHz	Q_L
4·42	-
6·422	41
8·165	-
10·398	76
12·319	-

cracked substrate, resonances difficult to find.

REFERENCES

1.	Hopkins, T.E. et al.	J. Phys. Chem.	66	(1962)	733
2.	Myers, M.B. and Felty, E.J.	Mat. Res. Bull.	2	(1967)	535
3.	Tsuchihashi, S. and Kawamoto, Y.	J. Non-Cryst. Sol.	5	(1971)	286
4.	Kolomiets, B.J.	Phys. Stat. Sol.	7	(1964)	359
5.	Owen, A.E.	Phys.Education	5	(1970)	97
6.	Owen, A.E.	Progress in Ceramic Sc.	3	(1963)	78
7.	Pollack, M.	Int. Conf. Phys. Semiconductors, Exeter		(1962)	p.86
8.	Mott, N.F.	Phil. Mag.	17	(1968)	1259
9.	Cohen, M.H.	J. Non-Cryst. Sol.	4	(1970)	391
10.	Mott, N.F.	Adv. in Phys.	16	(1967)	49
11.	Cohen, M.H. et al.	Phys. Rev. Letts.	22	(1969)	1065
12.	Mott, N.F.	Phil. Mag.	22	(1970)	1
13.	Mott, N.F. and Davis, E.A.	"Electronic Processes in Non-Crystalline Materials"		O.U.P. 1971	
14.	Davis, E.A. and Mott, N.F.	Phil. Mag.	22	(1970)	903
15.	Mott, N.F.	Phil. Mag.	19	(1969)	835
16.	Hayatee, F.G.M.	Ph.D.Thesis University of Edinburgh		1971	

17.	Gevers, M.	Philips Res. Reports	1	(1946)	197
18.	Debye, P.	"Polar Molecules"	Chemical Catalog 1929		
19.	O'Dwyer, J.J. and Harting, C.E.	Prog. in Diel.	7	(1967)	1
20.	Frohlich, H.	"Theory of Dielectrics"	O.U.P. 1963		
21.	Pollack, M. and Geballe, T.H.	Phys. Rev.	122	(1961)	1742
22.	Fuchs, R. and Von Hippel, A.	J. Chem.Phys.	34	(1961)	2165
23.	von Schweidler, E.	Ann. d. Phys.	24	(1907)	711
24.	Gevers, M. and du Pré, F.K.	Disc. Faraday Soc.	42A	(1946)	47
25.	Cole, K.S. and Cole, R.H.	J.Chem. Phys.	9	(1941)	341
26.	Garton, C.G.	Disc. Faraday Soc.	42A	(1946)	56
27.	Jonscher, A.K.	J. Non-Cryst. Sol.	8-10	(1972)	293
28.	Frohlich, H. et al.	Phys. Kondens. Mat.	1	(1963)	359
29.	Sussman, J.A.	Proc.Phys.Soc.	79	(1962)	758
30.	Sewell, G.L.	Phys. Rev.	129	(1963)	597
31.	Pollack, M.	Phil. Mag.	23	(1971)	519
32.	Austin, I.G. and Mott, N.F.	Adv. Phys.	18	(1969)	41
33.	Pollack, M.	to be published			

34.	Pike, G.E.	Phys. Rev. B.	6	(1972)	6
35.	van Beek, L.K.H.	Prog. in Diel.	7	(1967)	64
36.	Sillars, R.W.	J. I. E. E.	80	(1937)	378
37.	Mitchell, D.L. et al.	J. Non-Cryst. Sol.	8-10	(1972)	231
38.	Lakatos, A.I. and Abkowitz, M.	Phys. Rev. B.	3	(1971)	3
39.	Crevecoeur, C. and de Wit, H.J.	Sol.St.Comms.	9	(1971)	445
40.	Polanco, J.I. et al.	Phil. Mag.	25	(1972)	117
41.	Street, R.A. and Yoffe, A.D.	J. Non-Cryst. Sol.	8-10	(1972)	745
42.	Kitao, M.	Jap.J. Appl. Phys.	11	(1972)	1472
43.	Rockstad, H.K.	J. Non-Cryst. Sol.	2	(1970)	192
44.	Ivkin, E.B. and Kolomiets, B.J.	J. Non-Cryst. Sol.	3	(1970)	41
45.	Kitao, M. et al.	Phys.Stat.Sol.	37	(1970)	K119
46.	Austin, I.G. and Garbett, E.S.	Phil. Mag.	23	(1971)	17
47.	Amrhein, E.M.	Phys. Letts.	29A	(1969)	329
48.	Taylor, P.C. et al.	Sol.St.Comms.	8	(1970)	1783
49.	Lilja, R. and Stubb, T.	Acta Polytech. Scandanavica	28	(1964)	
50.	Gebbie, H.A. and Kiely, D.G.	Proc.Phys.Soc.	65B	(1952)	553
51.	Klinger, Y. and Saker, E.W.	Proc.Phys.Soc.	66B	(1953)	1117

52.	Bishop, S.G. et al.	J. Non-Cryst. Sol.	5	(1971)	351
53.	Young, P.A.	J. Phys. C.	4	(1971)	93
54.	Kawamoto, Y. and Tsuchihashi, S.	J. Am. Ceramic Soc.	54	(1971)	131
55.	Myuller, R.L. et al.	Solid State Chemistry		(1966)	168
56.	Minami, T. et al.	J. Non-Cryst. Sol.	3	(1970)	327
57.	Edmond, J.T.	J. Non-Cryst. Sol.	1	(1968)	39
58.	Lezal, D. et al.	Slaboproudy Obzor	31	(1971)	277
59.	Arai, K. et al.	Jap. J.Appl. Phys.	11	(1972)	1080
60.	Minami, T. et al.	J. Ceramic Soc. Japan	78	(1970)	299
61.	Kosek, F. and Tauc, J.	Czech.J. Phys.	B20	(1970)	94
62.	Maruno, S.	Jap. J.Appl. Phys.	6	(1967)	1474
63.	Sutton, P.M.	Prog. in Diel.	2	(1960)	113
64.	Tanaka, M. and Minami, T.	Jap. J.Appl. Phys.	4	(1965)	939
65.	Arai, K. and Saito, S.	Jap. J.Appl. Phys.	10	(1971)	1669
66.	Tanaka, M. et al.	Jap. J.Appl. Phys.	5	(1966)	185
67.	Lynch, A.C.	Proc. I.E.E.	104B	(1957)	363

68. Sucher, M. and Fox, J. "Handbook of Microwave Measurements" Vol II. Wiley and Sons. 1963

69. Von Hippel, A.R. "Dielectric Materials and Applications" Wiley and Sons. 1962

70. Horner, F. et al. J.I.E.E. 93 III(1946) 53

71. Wheeler, H.A. I.E.E.E. Trans. M.T.T. MTT-12 (1964) 280

72. Schneider, M.V. Bell. Syst. Tech. J. 48 (1969) 1421

73. Troughton, P. I.E.E. Conf. Publ. 58 (1970) 1703

74. Kell, R.C. et al. Elect. Letts. 6 (1970) 614

75. Jain, O.P. et al. Elect. Letts. 7 (1971) 405

76. Deutsch, J. and Jung, H.J. Nachrichtentech. Zeit. 23 (1970) 620

77. Arnold, S. Elect. Letts. 5 (1969) 673

78. Chudobiak, W.J. et al. I.E.E.E. Trans. M.T.T. MTT-19 (1971) 783

79. Schneider, M.V. Proc. I.E.E. 60 (1972) 144

80. Vendeln, G.D. Microwave J. 13 (1970) 63

81. Collin, R.E. "Field Theory of Guided Waves" McGraw-Hill 1960

82. Pucel, R.A. et al. I.E.E.E. Trans. M.T.T. MTT-16 (1968) 342

83. Caulton, M. et al. R.C.A. Rev. 27 (1966) 377

84. Wheeler, H.A. I.E.E.E. Trans. M.T.T. MTT-13 (1965) 172

85. Welch, J.D. and Pratt, H.J. — Herem Record (1966) 100

86. Horton, R. et al. — Elect. Letts 7 (1971) 490

87. "Microwave Engineers' Handbook" — Horizon House 1964 p.66

88. Lewin, L. — Proc. I.E.E. 107C (1960) 163

89. Denlinger, E.J. — I.E.E.E. Trans. M.T.T. MTT-17 (1969) 235

90. Roberts, R.J. and Easter, B. — Elect. Letts. 7 (1971) 191

91. Schneider, M.V. — Bell Syst. Tech. J. 48 (1969) 2325

92. Olyphant, M. and Bell, J.H. — I.E.E.E. Trans. E.I. EI-5 (1970) 26

93. Wolff, I. and Knoppik, N. — Elect. Letts. 7 (1971) 779

94. King, D.D. — I.R.E. Trans. M.T.T. MTT-3 (1955) 75

95. Schneider, M.V. et al. — Bell Syst. Tech. J. 48 (1969) 1703

96. Patel, R.N. — Elect. Letts. 6 (1970) 455

97. Corkhill, J.R. and O'Donnell, E.R. — Elect. Letts. 8 (1972) 500

98. Keister, F.Z. — I.E.E.E. Trans.M.T.T. MTT-16 (1968) 469

99. Garton, C.G. — J.I.E.E. 93 (1946) 398

100. Maruno, S. et al — Jap. J.Appl. Phys. 10 (1971) 653

101. Lynch, A.C. Proc. I.E.E. 104B (1952) 359

102. "Handbook of Thermophysical Properties of Solid Materials" Vol. 1 McMillan 1961

103. Bock, J. and Su, G.J. J. Chem. Phys. 57 (1972) 1464

104. Glaze, F.W. et al. J. Res. N.B.S. 59 (1957) 83

105. Owen, A.E. Private communications

106. Hurst, C.H. Ph.D. Thesis, Cambridge 1973

107. Edmund, J.T. Br.J. Appl. Phys. 17 (1966) 979

108. Tsugame, S. et al. Jap. J. Appl. Phys. 4 (1965) 77